SCUOLA NORMALE SUPERIORE

PISA

and

THE INTERNATIONAL CENTRE for GENETIC ENGINEERING and BIOTECHNOLOGY (ICGEB)

TRIESTE

Analysis of the β-adducin gene: new insights into gene structure and function

Thesis submitted for the Degree of Doctor of Philosophy

Perfezionamento in Genetica Molecolare e Biotecnologie

Candidate: **Luisa Costessi**

Supervisor: **Andrés F. Muro, Ph.D**

Accademic Year: **2007-2008**

Acknowledgments

At the end of more than four years of work I want to take this opportunity to express my gratitude to everyone who has shared this important period of my life with me: this thesis is not a reflection of my efforts alone.

First of all, I would like to thank my supervisor, Andrès, for his tireless enthusiasm and wide research outlook. I am very grateful for his constant presence, guidance and support in my PhD project which allowed me to learn many useful things and to improve my scientific knowledge.

My special thanks go to all the members of Mouse Molecular Genetics group, especially to Faby and Sandra for their great friendship and sympathy, constant help and precious suggestions in any situation. Also to Fede, who worked with me everyday, side by side, sharing all the adventures of this period and becoming not only my "nearest" PhD colleague but a special and good friend.

I would also like to remember all the people of the former Molecular Pathology group who shared with me these years. Thanks to Maury and Yuna, for their precious help and support in numerous situations, and also to Cri, Erica, and Michy for their friendship. To my extraordinary friend Ely, for all the wonderful time that we have spent together in the lab and outside the institute, my PhD period would not have been the same without you.

I would like to express my gratitude to Prof. Baralle for giving me the opportunity to begin my scientific career in his group, and for his special quality of being "ever present for everyone".

Many thanks go also to everyone in the ICGEB components, for their collaboration and for the fantastic atmosphere that they create in the institute. In particular, to Giulia, for allowing me to include a part of her work in this dissertation, and to Wendy, for her help in polishing my English.

In addition, I would like to take this chance to express my gratitude to my external collaborators, Dr. Chishti (University of Illinois College of Medicine, Chicago, USA.) and Dr. Tongiorgi (University of Trieste, Trieste, Italy), and to extend it to all the members of their groups.

A tender thank you is also deserving of my mother and father, the guiding lights in my life, and to Francesco and Martina for their constant presence, support and trust during my study.

And last, but not least, all my love and gratitude to Emy, particularly for his patience, and for everything he has said and done to help and encourage me.

ABSTRACT

Adducins are a family of membrane skeleton proteins encoded by three related genes (*ADD1*, *ADD2* and *ADD3* or α-, β- and γ-adducin genes). Both *ADD1* and *ADD3* are ubiquitously expressed, while the β-adducin gene shows a pattern of expression restricted to brain and haematopoietic tissues. Adducin is found as either a heterodimer or heterotetramer of α/β or α/γ subunit composition in most tissues. Human erythrocytes mainly contain α/β heterodimers, whereas the γ-subunit is also found at low levels in mouse red blood cells (RBCs). In erythrocytes, adducin is localised at the actin-spectrin junctions (junctional complexes), where it promotes the association of actin to spectrin, and bundles and caps the fast-growing ends of actin filaments. The junctional complexes comprise of other proteins, such as tropomodulin, tropomyosin, Protein 4.1, p55 and dematin, promoting and modulating spectrin–actin interactions, forming membrane associations, and regulating actin filament length. A mouse strain bearing a targeted mutation in the β-adducin gene was previously created in our lab and it was demonstrated that the mutant mice had abnormal erythrocytes, developing mild spherocytic hereditary elliptocytosis. These abnormalities were associated with alterations in the levels of several erythrocyte skeletal proteins: α-adducin, α-tropomyosin and actin were down-regulated, while the levels of γ-adducin and tropomodulin were increased. In addition, α- and β-subunits of the dimeric CapZ, the main muscle actin-capping protein of actin filaments barbed-ends, and which is mainly found in the cytoplasm of normal erythrocytes (ECapZ), were ~9-fold upregulated in RBC mutant skeletons, suggesting the existence of a compensatory mechanism. Moreover, purified adducin was re-incorporated into adducin deficient ghosts partially displacing ECapZ. The erythrocyte skeletal composition of dematin-adducin double knock-out mice (DAKOs) was also analysed. Despite their stronger phenotype and the presence of more significant alterations in red cell skeletons than those observed in the single mutants, the levels of ECapZ α- and β-subunits remained unaltered in the RBC skeleton of DAKOs. These results reflect the severe haemolytic anaemia manifested by the double mutant mice, and suggest the importance of adducin and dematin in the maintenance of the shape and mechanical properties of the erythrocyte membrane skeleton. Other actin-rich structures were also analysed, such as that of lens eye fibre cells, and showed analogous variations of most cytoskeletal proteins (except for CapZ

which showed no changes) suggesting different skeletal organisation between erythrocytes and lens fibre cells.

In addition to its presence in erythrocytes and eye lens cells, β-adducin is also very abundant in the brain where it is detected as a protein of similar size to the versions found in spleen, but it is translated from a peculiar brain-specific mRNA of 8-9 kb, instead of 3.5–4.5 kb of that detected in spleen. The molecular basis of this difference was discerned by determining the structure of the brain-specific β-adducin transcript in rats, mice and humans. Brain- and spleen-specific promoters and first exons, apparently not conserved in humans, were identified in rodents. It was demonstrated that β-adducin brain mRNAs are processed in all three species by a common mechanism utilising tissue-specific alternative polyadenylation sites (denominated A_4 in the brain), which generates an unusually long 3'-untranslated region (3'-UTR) of about 5-6 kb. Proximal erythroid-specific polyadenylation regions in rodents (A_1 and A_{2-3}) and humans (A_1, A_2 and A_3) were also identified. In all of these regions, the elements defining the core polyadenylation signals were identified: the hexanucleotide motif, the U-rich and GU-rich elements, and the cleavage site itself, known as the poly(A) site. A study of the β-adducin tissue-specific alternative polyadenylation mechanism was initiated by performing transient transfection assays of chimeric minigenes mimicking the structure and the arrangement of the polyadenylation sites in the β-adducin gene. It was shown that minigene-derived β-adducin transcripts were correctly polyadenylated at the A_4 brain-specific site in HeLa cells. Using a deletion strategy to analyse the contribution of the core polyadenylation elements to poly(A) site selection by the chimeric minigenes, it was observed that the lack of the U-rich region of the A_4 site directly decreased the efficiency of pre-mRNA processing, and that the use of an upstream cryptic poly(A)site is trigged by the absence of the A_4 site hexanucleotide motif. In addition, the long brain-specific β-adducin mRNA is localised with dendrites, highlighting the importance of the 5-6 kb 3'-UTR in the subcellular localisation of the β-adducin transcript in the brain, and probably in other regulatory functions not yet addressed.

To summarise, the molecular alterations underlying the red cell shape and structure abnormalities found in mutant β-adducin mice, in double adducin-dematin KO mice, and also those found in other actin-rich structures, such as eye lens fibre cells, were characterised. Additionally, the molecular basis of the size differences in the mRNAs from brain and spleen in humans, rats and mice was determined. Preliminary experiments aimed to characterise the tissue-specific mechanisms regulating those differences were also performed.

TABLE of CONTENTS

LIST of FIGURES and TABLES

ABBREVIATIONS

The standard abbreviations used in this dissertation follow IUPAC rules. All abbreviations are defined also in the text when they are introduced for the first time. Abbreviations mentioned only once are not included in this table.

ABBREVIATION	
DNA	Deoxyribonucleic acid
cDNA	Copy DNA
RNA	Ribonucleic acid
nt	Nucleotides
dNTPs	Deoxynucleoside triphosphates (A, C, G and T)
N	Nucleotide (A or C or G or T)
R or Pu	Purine (G or A)
Y or Pyr	Pyrimidine (T or C)
bp	Base pairs
kb	Kilobase
aa	Amino acid
kDa	Kilodalton
MW	Molecular weight
+/+	β-adducin homozygote wild type (controls)
+/-	β-adducin heterozygote
-/-	β-adducin homozygote mutant, knockout, or β-adducin deficient
KO	Knockout
DAKO	Dematin headpiece domain and β-adducin double knockout
RBC	Red blood cell
HS	Hereditary spherocytosis
HE	Hereditary elliptocytosis
SphHE	Spherocytic HE
HSt	Hereditary stomatocytosis
BP	Blood pressure
OF	Osmotic fragility
GPA/GPB/GPC/GPD	Glycophorins A, B, C and D
DHP	Dematin headpiece domain
PKC	Protein kinase C
PKA	Protein kinase A (cAMP dependent)
CBC	Cap-binding complex
snRNA	Small nuclear RNA

snRNP	Small nuclear ribonucleoprotein particles
hnRNP	Heterogenous ribonuclear protein
SR	Arginine-serine rich protein
USE	Upstream element
DSE	Downstream element
CPSF	Cleavage/polyadenylation specificity factor
CstF	Cleavage stimulation factor
CF	Cleavage factor
Pol II	RNA polymerase II
CTD	C-terminal domain of Pol II
PAP	Poly(A) polymerase
PABP	Poly(A)-binding protein
TSS	Transcription start site
PIC	Transcription pre-initiation complex
Inr	Initiator element
ORF	Open reading frame
UTR	Untranslated region
EST	Expressed sequence tag
ARE	AU-rich element
miRNA	microRNA
LS	mRNA localisation signal
mN1	First brain-specific exon of mouse β-adducin
mE1	First erythroid-specific exon of mouse β-adducin
hE1	Erythroid-specific exon of human β-adducin
Rpm	Revolutions per minute
DTT	Dithiothreitol
EDTA	Ethylenediamine tetra-acetic acid
IPTG	Isopropyl-β-d-thiogalactopyranoside
TBE	Tris-borate-EDTA (buffer)
SDS	N-lauroylsarcosine sodium salt
Tris	Tris (hydroxyethyl) amino-ethane
PBS	Phosphate buffer saline
IPTG	Isopropyl-d-thiogalactopyranoside
ddH_20	Double-distilled water
ATP	Adenosine triphosphate
ADP	Adenosine diphosphate
c-AMP	Cyclic adenosine monophosphate
R.T.	Room temperature
O.N.	Over night

1 INTRODUCTION

1.1 Cells membrane cytoskeleton

The cytoplasm of eukaryotic cells is spatially organised by a network of protein filaments known as the cytoskeleton. This network contains three principal types of filaments: microtubules, intermediate filaments and actin filaments (Figure 1.1 A, B, and C). They connect organelles in different regions of the cell and are used as tracks for the transport between them. In addition, filament networks provide mechanical support, which is especially important for animal cells, which do not have rigid external walls. The cytoskeleton forms an internal scaffold for the large volume of cytoplasm, holding it like a framework of girders supporting a building. Each of the three types of protein filaments is a helical polymer that has a different arrangement and function in the cell. By themselves, however, the three types of filaments could provide neither shape nor strength to the cell. Their functions depend on accessory proteins that link the filaments among them and to other cell components. Accessory proteins are also essential for the controlled assembly of the protein filaments in particular locations, and they provide the motors that either move organelles along the filaments or move the filaments themselves (Lodish, 2003).

1.1.1 - Microtubules -

Microtubules are long and stiff cylindrical structures (diameter of 25 nm) (Figure 1.1 A), and usually have one end anchored in the centrosome and the other free and extend throughout the cytoplasm. They govern the location of membrane-bounded organelles and other cell components and during the M phase of the cell cycle they create the mitotic spindle. Microtubules comprise tubulin molecules, each of which is a heterodimer consisting of two closely related and tightly linked globular polypeptides called *α- and β-tubulin*. The microtubule structure is built of 13 linear protofilaments, each composed of alternating α- and β-tubulin subunits and bundled in parallel to form a cylinder. Since the 13 protofilaments are aligned in parallel with the same polarity, the microtubule itself is a polar structure which has both a *plus* (fast-growing) and a *minus* (slow-growing) end. The minus-ends of microtubules are stabilised due to being embedded in the centrosome while the fast-growing ends are free to add tubulin molecules. Therefore, each microtubule is a highly dynamic structure that alternately

grows by the addition (polymerisation) or shrinks by the loss (depolymerisation) of tubulin subunits: this behaviour is called *dynamic instability*. Their polymerisation and depolymerisation are controlled by the presence of the GTP bounds to the β-tubulin and Mg^{2+} ions, and GTP-hydrolysis, respectively (Kreis and Vale, 1999).

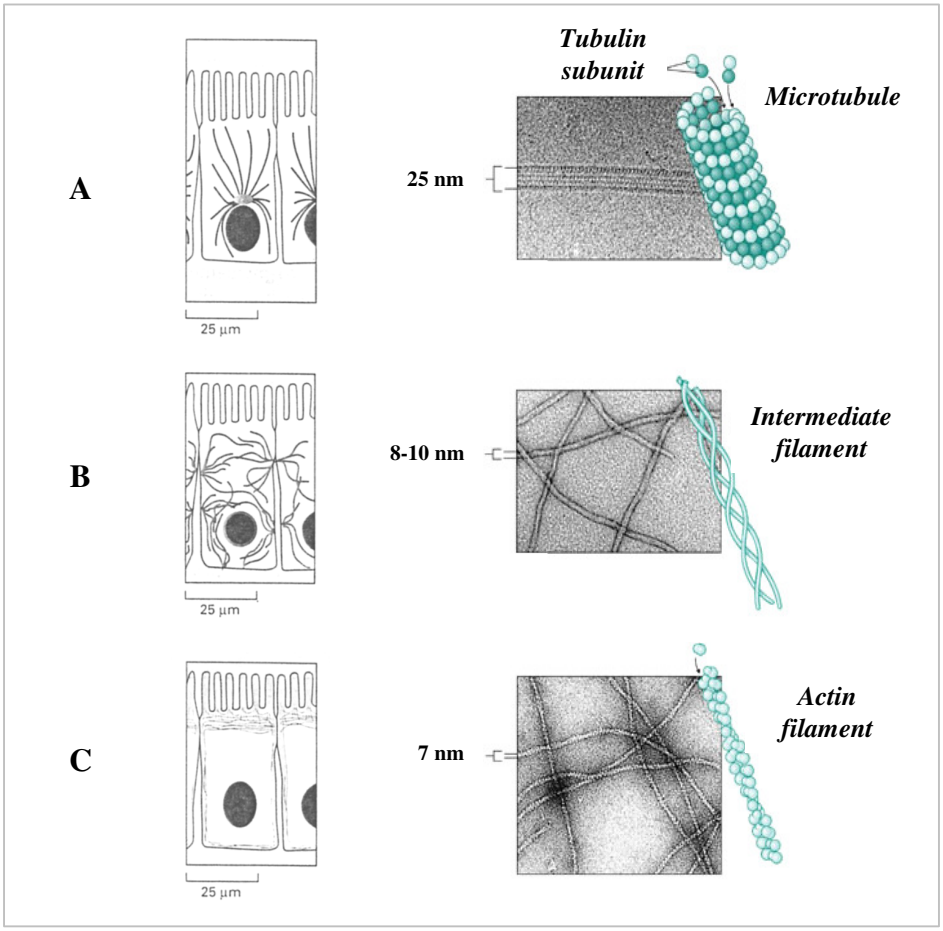

Figure 1.1: Cytoskeletal filaments. The three major types of filaments that form the cytoskeleton: microtubules, intermediate filaments and actin filaments are represented in Panels A, B, and C, respectively.

1.1.2 - Intermediate filaments -

Intermediate filaments are tough, rope-like polymers of fibrous polypeptides that resist stretch and play a structural or tension-bearing role providing mechanical stability to cells and tissues. They are called "intermediate" because they have a diameter of 8-10 nm, between that of actin filaments and microtubules (Figure 1.1 B). In most animal cells an extensive network of intermediate filaments surrounds the nucleus and extends towards the cell periphery, where they interact with the plasma membrane. In addition, a tightly woven basketwork of intermediate filaments, the *nuclear lamina*, underlies the internal side of the nuclear envelope. Intermediate filaments are particularly prominent in the cytoplasm of cells that are subject to mechanical stress (for example, in epithelia, neuronal and muscle cells. A variety of tissue-specific forms are known to differ in the

type of polypeptide they comprise: the *keratin filaments* of epithelial cells, the *neurofilaments* of nerve cells, the *glial filaments* of astrocytes and Schwann cells, the *desmin filaments* of muscle cells, and the *vimentin filaments* of fibroblasts and many other cell types. Nuclear *lamins*, which form the nuclear lamina, are a separate family of intermediate filament proteins. The monomers of the different types of intermediate filaments differ in sequence and molecular weights, but they all comprise a homologous structure: two globular domains (N- and C- terminus) linked by a central rod domain that forms a coiled-coil structure when the protein (Kreis and Vale, 1999)

1.1.3 - Actin filaments -

Actin filaments (F-actin) are flexible helicoidal polymers with a diameter of 5-8 nm (Figure 1.1 C). They consist of a tight helix of uniformly oriented globular actin, or *G actin*. Actin is the most abundant protein in many eukaryotic cells, often constituting up to 5% of total cell protein (in skeletal muscle cells it reaches about 10% of their mass). Each actin molecule is a single polypeptide of 42 kDa folded to create two structural domains divided by a central cleft where ATP and Mg^{2+} are bound. All higher eukaryotes have several isoforms of the protein encoded by a highly conserved family of genes that reside in different chromosomes. Four different α-actins are found in muscle cells and are associated with contractile structures. Instead, β- and γ-actins are the principal constituents of non-muscle cells, where γ-actin accounts for stress filaments and β-actin is in the front (or leading edge) of moving cells when actin filaments polymerise. Although there are subtle differences in the properties and functions of different forms of actin, their primary structures are highly conserved and all assemble into filaments that are essentially identical (Kreis and Vale, 1999). Like microtubules, actin filaments are polar structures, with two structurally different ends: a relatively inert and slow-growing *minus-end* (or pointed-end) and a fast-growing *plus-end* (or darbed-end). The difference in elongation rates at the opposite ends of actin filaments is caused by a different G-actin critical concentration (C_c) values at the two ends. C_c is the concentration of G-actin where equilibrium between polymerisation and depolymerisation reactions is reached: C_c at the minus-end is higher than that of the plus-end. At G-actin concentration between the C_c of the two ends a particular dynamic behaviour, called *treadmilling,* occurs: actin molecules are added continually to the plus-end of the filament and are lost continually from the minus one, with no net change in filament length. Polymerisation of actin requires ATP as well as cations, (K^+ and

Mg^{2+}), while ATP hydrolysis weakens the bonds in the polymer and thereby promote de-polymerisation. Several actin binding proteins influence the polymerisation of actin filaments, and thus their length and stability. Capping proteins, such as *tropomodulin*, *CapZ* and *adducin* bind to the ends of the filaments preventing monomer association and dissociation, while *tropomyosin*, stabilises F-actin interacting along its length. Other filament-binding severing and capping proteins are *cofilin, severin* and *gelsolin*: they bind to F-actin, break them into shorter filaments and remain attached at the plus-end preventing further addition or exchange of actin subunits. In addition, *thymosin* and *actin-depolymerising factor (ADF)* inhibit the assembly of actin into filaments, while *profilin* has a role in stimulating the polymerisation of actin by accelerating the exchange of ATP for ADP (Fowler, 1996; Fowler, 1997; Pollard et al., 2000). Section 1.2.2 analyses in details several of these proteins.

The dynamic modulation of the polymerisation and depolymerisation processes implies that actin filaments can form both stable and labile structures in cells. Stable actin filaments are a crucial component of the contractile apparatus of muscle cells (sarcomere) and membrane skeleton of erythrocytes, and form the core of particular cellular cell-surface protrusions such as microvilli, lamellipodia, microspikes, stereocilia, etc. Many cellular activities such as locomotion, chemotaxis, phagocytosis, and cytokinesis depend on labile structures constructed from actin filaments (Fowler, 1996; Pollard et al., 2000).

Actin filaments normally exist in different arrangements (linear bundles, two and three dimensional networks) maintained essentially by *actin filament cross-linking proteins* (*fimbrin, α-actinin, filamin*, *spectrin* and *dystrophin*). Because these proteins also bind integral membrane proteins, these networks are generally located in the cortical region adjacent to the plasma membrane: actin filaments lying just beneath the plasma membrane form the *cell cortex*. It is mainly this actin-rich layer that gives the cell mechanical strength, and controls the shape and surface movements of cells in accordance to the cell environment (Kreis and Vale, 1999).

The cell cortex network is attached to the plasma membrane in numerous ways:

- *Direct connections between actin filaments and membrane:* integral membrane proteins directly interact with actin filaments;
- *Indirect connections between actin filaments and membrane:* more complex and common complex linkages that connect actin filaments to integral membrane proteins

through peripheral membrane proteins, like *filamin* in platelets, *dystrophin* in muscle cells, *ERM proteins* (ezrin-radixin-moesin) in epithelial cells, etc.

1.2 Plasma membrane and cytoskeleton of erythrocytes

The plasma membrane of the red blood cells (RBCs) has been extensively studied more than any other eukaryotic membrane for a number of reasons: a) RBCs are available in large numbers relatively uncontaminated by other cell types; b) since these highly specialised cells lack transcellular filaments system, nucleus and internal organelles, the plasma membrane is their only cellular structure; C) it can be easily isolated and studied avoiding the serious problem of contamination by internal membranes (in other cell types the cytoplasmic membrane typically constitutes less than 5% of the cell's membrane). The RBC membrane is basically comprised of a lipid bilayer with its associated proteins (Bennett and Gilligan, 1993).

The *erythrocyte cytoskeleton* is the filamentous network of proteins that underlies the cytoplasmic surface of the membrane and is anchored to it. It is composed of proteins that are structurally homologous to those participating in the formation of eukaryotic cell cytoskeleton, being a similar but less elaborated filamentous network of proteins. The main components of the RBC skeleton are spectrin and actin that are organised as a hexagonal spectrin network linked to short actin filaments. The spectrin-actin junctions comprise a group of accessory proteins that promote and modulate spectrin-actin interactions, regulate the actin filament length and form membrane associations. The most important members of these junctions are tropomyosin, tropomodulin, adducin, Protein 4.1, p55, Protein 4.2 and dematin. The junctions that create the vertexes of the polygonal structure of the skeleton are known as *junctional complexes* (Figure 1.2) (Bennett and Gilligan, 1993).

SDS-PAGE analysis of the proteins of red cell ghosts (a product obtained during the RBC protein purification process that contains skeletal and membrane constituents) indicates the presence of a dozen of distinct species (often identified as "Band" proteins) (Fairbanks et al., 1971). By contrast, two dimensional separation employing isoelectrofocusing and SDS-PAGE demonstrated the membrane to be composed of more than a hundred different proteins (Low et al., 2002; Rosenblum et al., 1982).

According to their location, the proteins of the RBC membranes can be divided into two general groups: *integral RBC membrane proteins* and *peripheral RBC membrane proteins* (Figures 1.2 and 1.3).

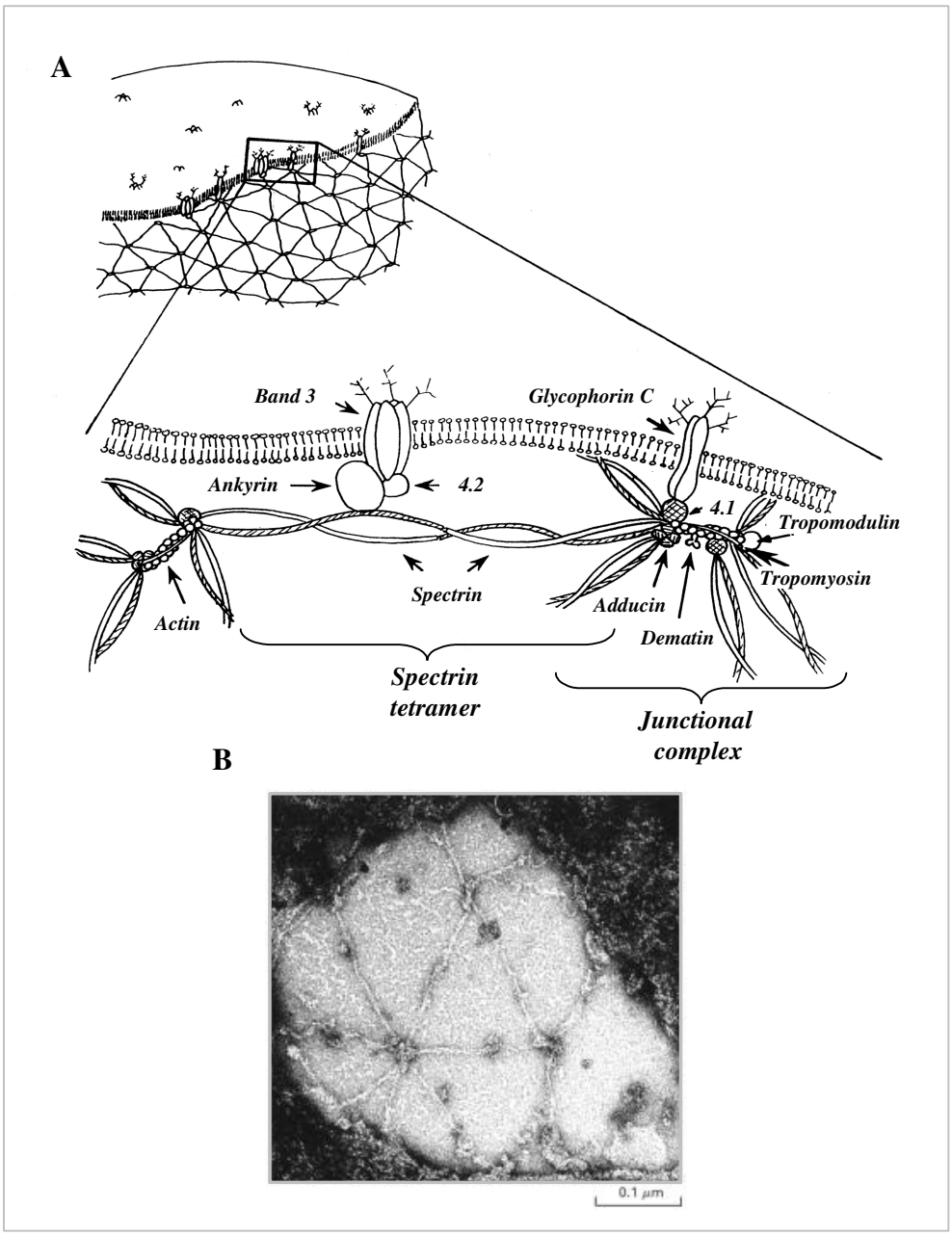

Figure 1.2: Erythrocyte cytoskeleton. Panel A shows a schematic model of protein organisation of erythrocyte membranes. The scheme is adapted from Bennett and Gilligan, 1993. A RBC membrane electron microscopic image is shown in Panel B. The structural organisation of the cytoskeleton is clearly visible: spectrin tetramers appear as spokes and interact with junctional complexes (hubs) generating a hexagonal network. Ankyrin molecules are detectable as dark spots located along the spokes of spectrin. The image in Panel B is from Lodish et al., 2003.

1.2.1 - *Integral RBC membrane proteins* -

The integrals proteins are tightly bound to the RBC membrane through hydrophobic interactions with lipids in the bilayer (Figures 1.2 and 1.3). These proteins span the membrane and have distinct structural and functional domains, both within the bilayer and on either side of the membrane. The most abundant and well characterised proteins that belong to this group are (Tanner, 1993):

- *Band 3 (anion exanger-1):* is a member of a family of anion transporters. It is the major transmembrane protein of the RBCs (~10^6 copies of polypeptide chains per RBC arranged as dimers), constituting about 25% of total membrane proteins. It is encoded by the *AE1* gene whose expression is largely restricted to erythrocytes. In addition to RBCs, Band 3 is expressed in both mouse and human kidneys as different isoforms. In RBC membranes Band 3 has a structural function in RBC membranes: it acts as an anchor site to the membrane of the skeleton, primarily through its interaction with ankyrin and secondarily binding to Proteins 4.1 or 4.2 (Bennett and Gilligan, 1993). In addition, it is as a membrane anion transporter, AE1 mediates Cl-/HCO3- exchange, thus enhancing the blood capacity for carrying CO_2 from tissues to the lung, and for acid-base homeostasis (Jennings, 1989).

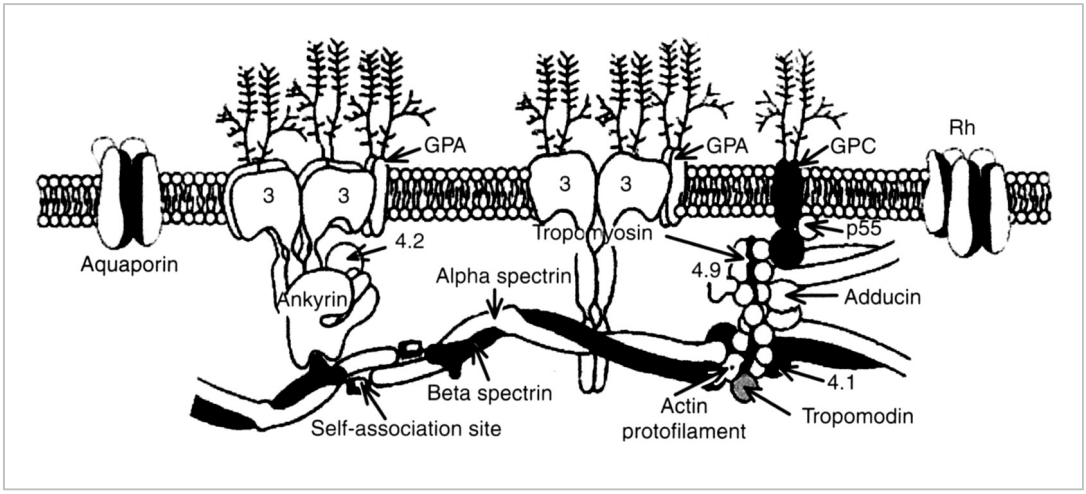

Figure 1.3: Peripheral and integral RBC membrane proteins. The figure shows a schematic representation of the erythrocyte plasma membrane and of the cytoskeletal network located on its cytoplasmic surface. The integral proteins, Band 3, glycophorins A and C (GPA and GPC, respectively) aquaporin and palmitoylated protein Rh are represented. Spectrin tetramers, actin filaments and the protein that constitute the junctional complex creating the skeletal network, such as tropomyosin, tropomodulin, adducin, Protein 4.2 and dematin (Protein 4.9) are indicated. The direct (between skeletal and membrane proteins) and indirect (mediated by ankyrin) interactions between the skeleton and the membrane are shown. The scheme is adapted from Lux et al. 1995.

- *Glycophorins*: are sialic acid-rich small transmembrane glycoproteins divided into four groups: glycophorin A -GPA-, B -GPB-, C -GPC- and D -GPD- (Figures 1.2 and 1.3). They constitute ~2% of the total RBC membrane protein. Glocophorins A, B, C and D are different polypeptides (36, 20, 32, and 23 kDa, respectively; GPD is a truncated form of GPC) and are the products of three distinct genes. The majority of the carbohydrates on the RBC surface (90% sialic acids) are anchored to these proteins and impart a strong net negative charge to the cell surface. This is functionally important in reducing the interactions of erythrocytes with one another as well as with other cells,

including vascular endothelium. In RBCs, GPA is the major component present at 5-9 x 10^6 copies per cell. GPC is also present anchoring the red cell skeleton to the membrane through the binding of Protein 4.1 and of p55 (Marfatia et al., 1995; Marfatia et al., 1997). GPC, unlike GPA and GPB, has a pattern of expression that is not limited to the erythroid lineage suggesting that it probably also has a role in cytoskeletal interactions in many other tissues (Chasis and Mohandas, 1992).

Other two abundant RBC integral-membrane proteins are *Aquaporins* (such as Aquaporin-1) and *Palmitoylated proteins* (Rh30 and Rh50) (Tanner, 1993).

1.2.2 - ***Peripheral RBC membrane proteins: the erythrocyte cytoskeleton*** -

The cytoskeletal network located on the cytoplasmic surface of the lipid bilayer of RBCs is generated by the interactions between peripheral membrane proteins (frequently called *horizontal interactions*). The RBC skeleton appears as a regular network in which the basic unit is composed of a hexagonal spectrin lattice. The sides of this structure consist of long, flexible spectrin tetramers, while the vertexes are formed by the attachment of the tail ends of spectrin with the short actin filaments and a group of accessory proteins that promote and modulate spectrin-actin interactions, regulate the actin filament length and form membrane associations. All the molecules that interact at the vertexes create the junctional complex (Figure 1.2 and 1.3) (Bennett, 1989; Gilligan and Bennett, 1993; Shen et al., 1986). This structural model of the erythrocytes skeleton organisation has been confirmed by high resolution electron microscopy of isolated membranes (Figure 1.2 B) (Liu et al., 1987; Shen et al., 1986). The most important members of these junctions are tropomyosin, tropomodulin, adducin, protein 4.1, p55, protein 4.2 and dematin. A brief description of the most important components of the membrane skeleton is below:

- *Spectrin:* is the most abundant and principal component of the cytoskeleton, in fact, it constitutes about 25% of the membrane-associated protein mass (~ 2.5 x 10^5 copies per cell). Spectrin is a heterodimer formed by two large, structurally similar subunits encoded by two genes at different chromosomal location: α and β subunits (260 and 246 kDa, respectively). Each polypeptide is a long, thin, flexible rod (~100 nm in length) organised into a number of independently folded domains. The two antiparallel polypeptide chains, loosely intertwine and attach noncovalently to each other at multiple points. The heterodimers self-associate “head-to-head” to form ~200 nm-long tetramers. Tetrameric species of spectrin appear to predominate in the

membrane skeleton (Bennett and Gilligan, 1993). The "tail" ends of six tetramers are linked together by binding to short actin filaments and to other cytoskeletal proteins at the *junctional complex* (Bennett, 1989; Shen et al., 1986) (Figure 1.2).

- *Actin filaments:* as opposed to the actin filaments observed in nonmuscle cells which are generally long and vary in length, erythrocytes actin filaments (or protofilaments) are relatively short and uniform (Figure 1.4): they are composed of 12-18 monomeric units of G-actin and have an approximatelength of 33-37 or ~67 nm, depending on experimental conditions (Coleman et al., 1989; Shen et al., 1986). In each red blood cell there are approximately 3-4 x 10^4 of these short structures (Fowler, 1996). Different mechanisms have been proposed to describe how such short actin protofilaments are generated. According to the "ruler" mechanism, several actin binding proteins regulate the assembly, the stability and especially the length of the short F-actin in RBCs: an external "molecular ruler," made out of actin-binding proteins such as tropomodulin and tropomyosin, protect a segment of the short actin filament of about 37 nm consisting of ~12 G-actin preventing elongation and depolymerisation (Sung et al., 2000), while capping and bundling by adducin can stabilise the protofilaments (Fowler, 1996). Confoundingly, the recently discovered "helix" mechanism affirms that the intrinsic properties of actin filaments, for example turns, chemical bonds, and dimensions of the helix, may favour its fragmentation into short protofilaments under mechanical stress (Sung and Vera, 2003). Each short actin filament is linked by about six spectrin tetramers tails at the junctional complex: these interactions create the hexagonal lattice that composes the basic units of the cytoskeleton. Other skeletal proteins, such as tropomyosin, adducin tropomodulin, bind and stabilise the short protofilaments (Bennett and Gilligan, 1993).

- *Adducin:* is a heterodimeric protein composed by the association of α, β and γ subunits. Oligomers in human erythrocytes comprise α/β subunits (Gardner and Bennett, 1986), while α/γ as well as α/β combinations of subunits are detectable in mouse RBC (Gilligan et al., 1999; Muro et al., 2000). These heterodimers are present in erythrocytes at ~3 x 10^5 copies/cell (Gardner and Bennett, 1986).Adducin has several functions: it recruits spectrin to actin filaments (Bennett et al., 1988; Gardner and Bennett, 1987; Hughes and Bennett, 1995), bundles actin filaments (Mische et al., 1987; Taylor and Taylor, 1994), and caps the fast-growing ends of actin filaments (Kuhlman et al., 1996) (Figure 1.4). These activities indicate that adducin promotes the formation

of spectrin-actin junctions and increases their stability. More information about this protein can be found in Section 1.7.

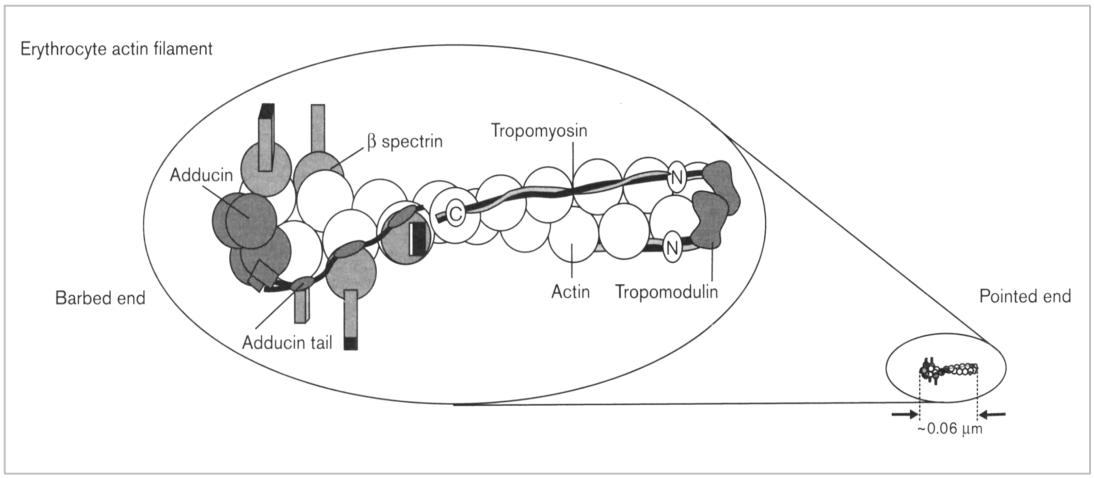

Figure 1.4: The short erythrocyte actin filament. The figure shows a molecular model of the RBC protofilament. Two molecules of tropomyosin are localised along each of the two grooves of the actin filament. Two tropomodulin molecules are associated with the terminal actin subunit of the F-actin pointed-ends and to the N-terminus of each of the two tropomyosin dimers. The C-terminal tail domains of adducin are associated with β subunits of spectrin along the actin filaments, whereas its N-terminal head domains cap the darbed-end of the protofilament. The scheme is adapted from Fowler et al., 1996.

- *CapZ:* is a capping protein for the barbed-end of actin filaments in non-erythroid cells. Its main function is to prevent monomer association and dissociation by capping F-actin barbed ends, but it also facilitates actin polymerisation by binding to and stabilising monomers or oligomers of actin forming nuclei for filaments assembly and elongation (Casella et al., 1986; Schafer and Cooper, 1995). It is a highly conserved heterodimer formed by the association of α and β subunits (36 kDa and 32 kDa, respectively). Different isoforms of the subunits are present in a wide variety of tissues and organisms. C-terminal ends of both subunits are required for effective barbed-end capping of filaments (Casella and Torres, 1994; Schafer et al., 1994). Erythrocytes contain abundant amounts of a non-muscular isoform of CapZ (ECapZ) composed mainly by the $\alpha_1\beta_2$ subunits, as described for CapZ from many other non-muscle cells (platelets, neutrophils, etc) (DiNubile et al., 1995). Despite purified ECapZ is fully functional in blocking actin elongation from barbed filament ends, as well as in nucleating actin polymerisation, this erythroid capping protein is mainly located in the cytoplasm and is not associated with protofilaments in the RBC membrane skeleton (Kuhlman and Fowler, 1997). This contrasts with what is observed in platelets, where the same CapZ is located in the cytosol and sometimes in association with actin filaments (Barkalow et al., 1996), or in striate muscle, where all the capping protein is associated with the filament at the Z disks of the sarcomere (Rybicki et al., 1988).

Therefore, erythrocytes contain two actin filament barbed-end capping proteins: ECapZ with a high affinity (K_{cap} ~1-5 nM) and adducin with a lower affinity (K_{cap} ~100 nM) for the end of actin filaments, but of the two, adducin caps and stabilises the protofilament barbed-ends. How adducin can outcompete ECapZ with its apparently higher affinity (20-100 fold) is unclear. The absence of ECapZ from the F-actin in the RBC skeleton is not due to a defect of the protein, nor to a cytosolic inhibitor factor, or even to its insufficient concentration in the cytoplasm. It was hypothesised that this peculiar phenomena is determined by the presence of additional co-factors or specific cellular conditions in the RBC that could induce (Kuhlman and Fowler, 1997):

a) an increase of adducin affinity for the protofilaments. For example, it binds more tightly to spectrin-actin complexes than to pure actin filaments (Gardner and Bennett, 1987), thus interactions with spectrin and actin in the junctional complex may increase its affinity for actin filament darbed-ends. Adducin capping activity my also be regulated by specific phosphorylation or dephosphorylation reactions(Matsuoka et al., 2000);

b) a reduction of the apparent high affinity of ECapZ for F-actin. High concentrations of ECapZ in the cytoplasm could induce its overcrowding and consequently might reduce the apparent high affinity of the capping protein for the protofilaments (Kuhlman and Fowler, 1997).

- *Tropomodulin:* is a globular protein (~40 kDa) present as approximately 3 x 10^4 copies per RBC. It is a capping protein that binds to the pointed-end of the actin protofilaments (Fowler, 1996) (Figure 1.4). The C-terminal end of the protein contains an actin binding domain, important for capping activity, while the N-terminal portion contains the binding sites for the N-terminal ends of the two tropomyosin molecules that are associated with actin filament (Kostyukova et al., 2006; Sung and Lin, 1994). The presence of tropomyosin is required for tight capping of F-actin pointed-ends. In fact, in the absence of tropomyosin, tropomodulin only partially inhibits monomer association and dissociation at the minus-end of filaments (Weber et al., 1994). Therefore, the tropomodulin/tropomyosin complex blocks the elongation and depolymerisation of the actin filaments at the pointed-end contributing to the stability and length determination of the actin filament (Fowler, 1996). Tropomodulin is a highly conserved protein among species and tissues. It's abundant in striated muscule cells where it plays an essential role in the assembly of the sarcomere and it is also a fundamental cytoskeleton component in erythrocyte membranes and eye lens cells (Fowler, 1996; Woo and

Fowler, 1994). The function of tropomodulin in other non-muscle and non-erythroid cells is still not well understood.

- *Tropomyosin:* is a rigid rod-like fibrous molecule composed of two small polypeptides (35 kDa) associated to form a coiled-coil structure (~33-35 nm) (Figure 1.4). RBC skeletons each contain ~7 x 10^4 dimeric molecules of tropomyosin and they correspond to approximatelly 1% of the membrane protein (Fowler and Bennett, 1984; Shen et al., 1986). Tropomyosin exists in a large number of isoforms [high and low molecular weight (MW) isoforms] which are generated in different tissues by the alternative use of promoters and the alternative RNA processing of different genes (at least 4 distinct genes have been characterised in mammalians: α, β, γ, and δ) (Lin et al., 1997), suggesting that the different isoforms are not functionally equivalent (Gunning et al., 2005). Among the different tropomyosin isoforms, TM5 and TM5b (29 and 28.7 kDa, respectively) are the 2 major forms expressed in human erythrocytes. Although they are products of 2 different genes (γ-TM and α-TM genes, respectively), they share several common features, including molecular weight (both are low MW isoforms), the presence of similar binding domains, and a high affinity for actin and tropomyosin (Sung et al., 2000; Sung and Lin, 1994). The rod-like structure and the actin-binding ability of dimeric tropomyosin allow it to localise, polymerised end-to-end, along each of the two grooves of the actin filament, providing structural stability and modulating the filament length (Figure 1.4). In RBCs, two dimeric tropomyosin molecules are associated with the short protofilament protecting 6-7 actin monomers in one strand (or 12-14 G-actin in the double helix) (Cooper, 2002; Fowler and Bennett, 1984). The tropomyosin ability to bind and reduce depolymerisation of actin filaments is improved when tropomodulin simultaneously interacts with both the pointed-end of the actin filament and to the terminal tropomyosin molecule: in fact, tropomodulin seems to strengthen the binding of the terminal tropomyosin molecule to the pointed-end of the protofilament (Weber et al., 1994). In erythrocytes, the binding of tropomodulin to tropomyosin also seems also to block the ability of the tropomyosin dimer to self-associate in a head-to-tail structure (Fowler, 1990; Sung and Lin, 1994). In non-erythroid cells, tropomyosin can regulate many properties of F-actin: increase filament stiffness, protect filaments from the depolymerising effects of severing and depolymerising factors (cofilin, gelsolin, ADF, etc), enhancing F-actin stability and, moreover, influence myosin mechanochemistry (Cooper, 2002; Gunning et al., 2005).

In conclusion, the combined action of tropomyosin and tropomodulin strongly influences the length and increases stability of the actin filaments.

- *Protein 4.1:* is a complex family of erythroid (4.1R) and non-erythroid protein 4.1 isoforms generated by the involvement of both multiple genes and alternative splicing pathways (Conboy et al., 1991; Takakuwa, 2000). Interestingly, several 4.1R pre-mRNA splicing events exhibit developmental switches in their expression patterns, implying that distinct 4.1R functions are critical at different stages of cell differentiation (Baklouti et al., 1996). Moreover, in RBCs alternative splicing regulates the expression of alternative translation initiation sites in exon 2 (AUG1) and exon 4 (AUG2) generating 135 kDa and 80 kDa isoforms of the protein, respectively (Baklouti et al., 1996; Chasis et al., 1996). Among the different 4.1R isoforms the 80 kDa one is the best characterised. It was estimated that each RBC contains ~2 x 10^5 copies of this molecule (Bennett and Gilligan, 1993). By multiple protein-protein interactions, 4.1R promotes the formation of two ternary protein complexes in the erythrocyte membrane: spectrin-actin-4.1R and GPC-4.1R-p55 complexes (Figures 1.2 and 1.3). They are critical to the structural integrity of the skeleton and to its attachment to the membrane lipid bilayer (Bennett and Gilligan, 1993; Marfatia et al., 1994). Thus, by lateral interactions with the spectrin/actin network and vertical interactions with the cytoplasmic domain of transmembrane proteins GPC and Band 3, 4.1R is essential for maintaining erythrocyte shape and membrane mechanical properties (deformability and stability) (Chang and Low, 2001).

- *p55:* is the major palmitoylated phosphoprotein associated with the cytoplasmic side of the erythrocyte membrane (Bennett and Gilligan, 1993; Ruff et al., 1991). Approximately 8 x 10^5 molecules of p55 are detectable in each mature erythrocyte. It is a member of a family of cytoskeletal and signalling proteins termed membrane-associated guanylate kinase homologues (MAGUKs). As a component of the GPC-4.1R-p55 ternary complex, p55 modulates the interactions between Protein 4.1 and GPC, regulating the stability and mechanical properties of RBC plasma membrane (Marfatia et al., 1995; Marfatia et al., 1994).

- *Dematin (or Band 4.9):* is an actin-bundling protein that was originally identified as a component of the junctional complex of the human erythroid membrane skeleton (Siegel and Branton, 1985) (Figure 1.2 A). It is also abundantly expressed in the human brain, heart, skeletal muscle, kidney, and lung (Kim et al., 1998). Dematin is a trimeric protein composed of two copies of a 48 kDa polypeptide and one copy of a 52 kDa

polypeptide, generated by alternative splicing by the same pre-mRNA (Azim et al., 1995). Both subunits of dematin consist of a N-terminal core domain that includes one actin binding site and a highly conserved protease-resistant C-terminal headpiece domain (DHP) (75 residues) which is homologous to the headpiece domain of villin (an actin-binding protein of the brush border cytoskeleton of absorptive epithelia cells) and contains an actin-binding site, a cAMP-kinase phosphorylation site, and the residue involved in trimer formation (Azim et al., 1995; Rana et al., 1993). DHP is essential for dematin actin bundling activity *in vitro* (Siegel and Branton, 1985) and allows the correct maintenance of the mechanical proprieties of the erythrocyte skeleton (Khanna et al., 2002). Dematin is also a substrate for multiple protein kinases: phosphorylation of dematin (in the DHP) by cAMP-dependent protein kinase is known to abolish its actin-bundling activity *in vitro* (Husain-Chishti et al., 1988) but not eliminate actin binding activity (Azim et al., 1995). Because actin bundles appear to be absent in mature red cells, the role of dematin in actin bundling events remains unclear. Therefore, the physiological function of dematin might be accounted for its actin-binding activity or by as yet unknown binding functions in mature erythrocytes. In this context, dematin stoichiometry in human erythrocytes is significant: a quantitative assay revealed ~4,3 x 10^4 copies of trimeric dematin (Husain-Chishti et al., 1988). Because there are 3-4 x 10^4 actin oligomers per erythrocyte (Fowler, 1996), it is likely that one dematin trimer is associated with one actin oligomer *in vivo*. It has recently been postulated that dematin could function as a molecular bridge between the junctional complexes and the plasma membrane by an actin-independent mechanism (Chen et al., 2007).

- *Protein 4.2:* is a 72 kDa peripheral membrane protein. Approximatelly 2 x 10^5 copies of this component are detectable in each RBC. Isoforms of the protein exist also in many non-erythroid cells. In RBCs, Protein 4.2 binds to the cytoplasmic domain of Band 3. In solution, it can also bind directly to ankyrin and Protein 4.1. Interaction with Band 3 and ankyrin may promote and stabilise the vertical interactions between the skeleton network and the plasma membrane *in vivo* (Bennett and Gilligan, 1993) (Figures 1.2 and 1.3).

RBC cytoskeleton is connected to the overlying lipid bilayer membrane by multiple interaction mechanisms (*vertical interactions*) (Figures 1.2 and 1.3 A):

- *Direct linkages between skeleton and membrane*: are mainly mediated by skeletal Protein 4.1. It binds spectrin (N-terminus) and actin at the junctional complex as well as the cytoplasmic domain of both Band 3 and GPC (Bennett and Gilligan,

1993; Marfatia et al., 1994). Another direct interaction is the GPC-p55-4.1R ternary complex, which is constituted by three binary protein-protein interactions, GPC-4.1R, GPC-p55, and 4.1R-p55. In the complex, p55 stabilises the interaction between the two GPC in a Ca^{2+}-dependent manner (Nunomura et al., 2000). Since isoforms of Protein 4.1, p55 and GPC are present in many non-erythroid cells, their interactions may be prototypical of similar associations between cytoskeleton and membrane in other cells.

- *Indirect linkages between skeleton and membrane*: are mediated by *ankyrin.*

Ankyrine is a large intracellular protein (210 kDa) that comprises three independent domains: a N-terminal Band 3-binding domain, followed by a β-spectrin-binding domain and a C-terminal regulatory domain. By simultaneously connecting the β subunit of spectrin (C-terminus) with the cytoplasmic domain of the transmembrane protein Band 3, ankyrin links the spectrin network to the membrane. This interaction is the major site of attachment between the membrane skeleton and the plasma membrane (Bennett, 1982).

Ankyrin deficiency results in severe changes in red cells morphology and a markedly shortened RBC lifespan (Delaunay, 2007), whereas the absence of GPC causes only a slight change in RBC shape and survival (Chasis and Mohandas, 1992), together suggests that the GPC–4.1 linkage is functionally less significant than the Band 3–ankyrin–spectrin linkage. Moreover, Protein 4.2, which binds ankyrin *in vitro*, may help stabilise the ankyrin–Band 3 interaction (Bennett and Gilligan, 1993).

1.3 Membrane skeleton role: deformability, stability and shape

During their 120-day life span in circulation, erythrocytes are constantly subjected to the flow dynamics of the cardiovascular system and frequently undergo extensive passive deformation by passing through narrow capillaries. The survival of the erythrocytes depends on the capacity of the plasma membrane and membrane skeleton to resist to forces of pressure in order to avoid cell fragmentation.

Therefore, the fundamental role of the RBC cytoskeleton is to confer an elastic behaviour to membrane. The elasticity allows for a degree of the membrane deformation and, consequently, increases membrane stability by maintaining overall the structural integrity and biconcave shape of erythrocytes (Chasis and Mohandas, 1986). Other distinct cellular features, such as erythrocyte shape and cytoplasmic viscosity, can also influenced the elasticicity of RBCs (Mohandas and Chasis, 1993).

1.3.1 - <u>Membrane deformability and stability</u> -

Deformability determines the extent of membrane deformation that can be induced by a defined level of applied force, whilst *stability* is the maximum extent of deformation that a membrane can undergo, beyond which it cannot completely recover its initial shape and thereby undergoes fragmentation. Normal levels of membrane deformability and stability allow RBCs to circulate without fragmenting, whilst a decrease in these mechanical properties leads to a collapse of the membrane under normal physiological circulatory stresses. These membrane properties are correlated to:

1) *Spectrin tetramers conformational state*: deformability derives from the reversible conformational changes from the folded and unfolded state of spectrin (Chasis and Mohandas, 1986; Mohandas and Chasis, 1993).

2) *The strength degree (the avidity) of the intra- or inter-molecular interactions at junctional complexes and/or of the associations between integral membrane proteins and skeletal network:* a decrease in these connections induces a reduction in membrane stability and *vice versa*. The grade of association of the mentioned proteins can be regulated by several mechanisms such as phosphorylation and the intracellular concentration of some molecules or ions (e.g. 2,3-diphosphoglycerate, Ca^{2+}) (Mohandas and Chasis, 1993; Mohandas and Evans, 1994).

In the erythrocyte non-deformed state, spectrin molecules exist in a folded conformation. During a reversible deformation of the RBC membrane, where changes in shape occur but the surface area remains constant, a rearrangement of the skeletal network takes place in which some spectrin molecules become uncoiled and extended whilst others become more compressed and folded. In this condition, the membrane behaves as a visco-elastic solid: after undergoing elastic extensions, it is capable of completely recovering its initial shape. Should external forces increase further, the membrane becomes increasingly extended and some of the spectrin molecules attain their maximal extension resulting in the interaction between the other skeletal proteins becoming weaker. When the limit of reversible deformability is achieved, a continued application of fluid force induces an increase in surface area and the break of junctional complexes, leading to permanent, “plastic”, deformation and membrane fragmentation (Mohandas and Evans, 1994).

Whereas normal erythrocytes completely recover their shape following repeated cycles of deformation during circulation, pathologic RBCs with weakened junctions between skeletal proteins fail to recover their initial shape and undergo “plastic”

deformation generating elliptocytes, spherocytes and other RBC shapes in haemolytic anaemia (Delaunay, 2007; Hoffman, 2000).

1.3.2 - Cell shape -

The distinctive biconcave disk shape of erythrocytes is acquired during reticulocyte maturation and is generated by the reorganisation of membrane phospholipids, skeletal components and membrane integral proteins (Chasis et al., 1989). These reorganisations include the loss of membrane lipids and integral proteins (such as transferrin, insulin and fibronectin receptors), and a major reorganisation of the skeletal protein network (Mohandas and Chasis, 1993).

The biconcave disk shape of normal erythrocytes creates an advantageous surface area-volume relationship, allowing the RBC to undergo marked deformation while maintaining a constant surface area. The normal human adult red cell has a volume of 90 fl and a surface area of 140 μm^2. If the erythrocyte were a sphere of identical volume, it would have a surface area of only 98 μm^2. The excess surface area, provided by the discoid shape, allows the RBC to undergo extensive deformation. The erythrocyte must maintain this favourable surface area-volume relationship during its circulating life span. Either membrane loss (leading to reduction in surface area) or an increase in cell water content (leading to increase in cell volume) will create a more spherical shape with less redundant surface area. This loss of surface area redundancy leads to decreased cellular deformability, compromised red cell function and reduced survival (Mohandas and Chasis, 1993).

So, derangements in the structural organisation as a result of changes in any of the individual components of the membrane, be they either lipid or protein, lead to altered cell deformability, stability and shape that are the cause of many RBC disorders.

1.3.3 - Cytoplasmic viscosity -

Cytoplasmic viscosity is regulated by haemoglobin concentration and cell water content of the cell. In the range of physiological RBC haemoglobin concentration (27-35 g/dl), the contribution of cytoplasmic viscosity to cellular deformability is negligible. Concentrations greater than 37 g/dl, however, increase viscosity exponentially. When cytoplasmic viscosity arrives to high levels, its contribution to cell deformability begins to dominate. Thus, the failure of normal volume homeostasis mechanisms, which results in cellular dehydratation, can limit cell deformability owing to increased cytoplasmic viscosity.

1.4 Disorders of the red blood cell membrane

Progress in the characterisation of the structure and function of erythrocyte membrane proteins and their genes has provided considerable advances in the understanding of the molecular pathology of RBC membrane disorders such as the characterisation of mutations or deficiencies in membrane proteins as a well-defined cause of hereditary haemolytic disease (Table 1.1).

Band	Protein	MW (gel) (kd)	MW (calc) (kd)	Copies per Cell (10^{-3})	Total (%)	Gene Symbol	Chromosomal Localization	Amino Acids	Gene Size (kb)	No. of Exons	Involvement in Hemolytic Anemias
1	α-Spectrin	240	280	240	16	SPTA1	1q22–q23	2,429	80	52	HE, HS
2	β-Spectrin	220	246	240	14	SPTB	14q23–q24.2	2,137	>100	32	HE, HS
2.1	Ankyrin	210	206	120	405	ANK1	8p11.2	1,881	>100	40	HS
2.9	α-Adducin	103	81	30	2	ADDA	4p16.3	737	85	16	N
2.9	β-Adducin	97	80	30	2	ADDB	2p13–2p14	726	~100	17	N
3	Anion exchanger 1	90–100	102	1,200	27	EPB3	17q21–qter	911	17	20	HS, SAO, HAc
4.1	Protein 4.1	80	66	200	5	EL11	1p33–p34.2	588	>100	23	HE
4.2	Pallidin	72	77	200	5	EB42	15q15–q21	691	20	13	HS
4.9	Dematin	48 + 52	43	140	1	—	8p21.1	383	—	—	N
4.9	p55	55	53	80	—	MPP1	Xq28	466	—	—	N
5	β-Actin	43	42	400–500	5.5	ACTB	7pter–q22	375	>4	6	N
5	Tropomodulin	43	41	30		TMOD	9q22	359	—	—	N
6	G3PD	35	37	500	3.5	GAPD	12p13.31–p13.1	335	5	9	N
7	Stomatin	31	32	—	2.5	EPB72	9q33–q34	288	12	7	HSt
7	Tropomyosin	27 + 29	28	80	1	TPM3	1q31	239	—	—	N
PAS-1	Glycophorin A	36		500–1,000	85	GYPA	4q28–q31	131	>40	7	HE
PAS-2	Glycophorin C	32	14	50–100	4	GYPC	2q14–q21	128	14	4	HE
PAS-3	Glycophorin B	20		100–300	10	GYPB	4q28–q31	72	>30	5	N
	Glycophorin D	23		20	1	GYPC	2q14–q21	107	14	4	N
	Glycophorin E	—		—	—	GYPE	4q28–q31	59	>30	4	N

Table 1.1: Major RBC membrane proteins and their involvement in hereditary haemolytic anaemias. Abbreviations: HE, hereditary elliptocytosis; HS, hereditary spherocytosis; H, no haematological abnormalities reported; SAO, Southeast Asian ovalocytosis; Hac, hereditary acanthocytosis; HSt, hereditary stomatocytosis; G3PD, glyceraldehyde-3-phosphate dehydrogenase. The table is from Hoffman et al., 2000.

According to morphological and clinical phenotypes, RBC membrane disorders can be classified into three general groups: hereditary spherocytosis, hereditary elliptocytosis or hereditary stomatocytosis (Delaunay, 2007; Hoffman, 2000).

1.4.1 - Hereditary spherocytosis (HS) -

This disorder is the most common cause of non-immune haemolytic anaemia in people of Northern European ancestry.

HS is characterised by the presence of spherical erythrocytes or spherocytes in the peripheral blood. These pathological RBCs are generated by molecular defects that lead to the deficiency or dysfunction of the skeletal and integral membrane proteins that participate in the vertical interactions: spectrin, ankyrin, Band 3 and Protein 4.2. Consequently, those erythrocytes having weak connections between the skeleton and the overlying lipid bilayer membrane are susceptible to release skeleton-free lipid microvesicles from the cells resulting in the loss of membrane surface area. This produces spherocytosis with a strong reduction in cell deformability and stability, leading to a faster lysis of the RBC.

A typical HS patient is relatively asymptomatic: mild jaundice may be the only symptom. Only uncommon cases have a life-threatening haemolysis. Anaemia, which is usually mild to moderate, may be absent in some cases because of the compensatory bone marrow hyperplasia. Splenomegaly is present in most HS patients and is produced by the increased removal of abnormally shaped erythrocytes by the spleen.

1.4.2 - Hereditary elliptocytosis (HE) and related disorders -

HE is a heterogeneous group of red cell membrane disorders with a wide spectrum of clinical presentations, ranging from asymptomatic elliptocytosis to life-threatening haemolytic anaemia with poikilocytosis and red cell fragmentation.

HE and related disorders commonly exhibit the presence of elliptical red cells in peripheral blood. These altered erythrocyte result from molecular defects that lead to the deficiency or dysfunction of the skeletal proteins that participate in the horizontal membrane protein associations: spectrin, protein 4.1 and GPC. These defects induce the assembly of a disrupted and unstable skeletal lattice in RBC precursors which allow the cells to undergo "plastic" deformations and to permanently acquire the elliptical shape. On the basis of erythrocytes morphology, HE can be divided into three major groups:

- *Common HE:* is characterised by biconcave elliptocytes and, in some patients, rod-shaped cells. The clinical severity of common HE is highly variable, ranging from an asymptomatic condition to a severe recessively inherited haemolytic anaemia, designated *hereditary pyropoikilocytosis* (HPP), in which numerous red cell fragments, microspherocytes, and poikilocytes are revealed in circulation.
- *Spherocytic HE (SphHE):* is a rare condition (5-10 % of all HE cases), also called haemolytic ovalocytosis, and it is characterised by the presence of round "fat" ovalocytes (elliptocytes that are less prominent and less elongated than in mild HE), spherocytes and some microspherocytes and microelliptocytes in the blood. Thus, it is a phenotypic hybrid of HE and HS. This disorder is usually mild to moderate and is often incompletely compensated. The molecular bases of SphHE are not completely known.
- *South Asian Ovalocytosis (SAO):* is highly prevalent in the malaria-infested countries. It is characterised by the presence of typical ovalocytes in the peripheral blood: rigid, spoon-shaped cells that have either a longitudinal slit or a transverse ridge. A remarkable feature of these cells is their resistance to infection and invasion by several strains of the malaria parasite (including *Plasmodium falciparum* and *knowleis*). The heterozygote is asymptomatic but the homozygote form is lethal *in utero*.

1.4.3 - Hereditary stomatocytosis (HSt) -

HSt designates a heterogeneous group of hereditary haemolytic anaemias. The disorder is characterised by the presence of stomatocytes: RBCs with a three-dimensional shape of a cup or a bowl. These cells show abnormalities in cation permeability (Na^+ and K^+) that lead to changes in red cell volume: increase (*Hydrocytosis*) or decrease (*Xerocytosis*) volume of stomatocytes.

Deformability of the overhydrated erythrocytes is decreased and their osmotic fragility is markedly increased, inducing haemolysis and leading to a moderate-severe anaemia. The molecular basis of this permeability defect is not completely unknown. Decrease or absence of the integral membrane protein Band 7.2b (stomatin) has been found in erythrocyte membranes of affected patients. However, targeted disruption of the stomatin gene in mouse does not result in stomatocytosis unequivocally demonstrating that Band 7.2b does not play a direct role in red cell cation transport and suggesting that stomatocytosis is most probably the result of an abnormality in an erythrocyte membrane protein that is involved in the insertion and retention of Band 7.2b in the red cell membrane. The mechanism of cellular dehydratation is unclear and complex, involving a net intracellular loss of cation content and cell water decrease. Opposite to the overhydrated cells, dehydrated RBCs have a decreased fragility, even if the disorder is characterised by a moderate to severe haemolysis.

Considering that isoforms of RBC membrane skeletal proteins are also expressed in non-erythroid tissues, mutations in their genes have also the potentiality to cause non-erythroid defects. In some cases mutations of skeleton proteins induce clear pathological states in other systems: for instance, Protein 4.1R and ankyrin defects are able to cause neurological deficits. In other cases, such as the β-adducin null mutation, other adducin isoforms are upregulated to partially compensate for the primary deficiency. In such situations, the effects may be subtle but could increase under stress or with age(Birkenmeier and Barker, 2004).

1.5 Knock-out mouse models of erythrocyte membrane proteins

The mouse is a very valuable system for the study of mammalian RBC structure and function for the following reasons: a) both fetal and adult erythropoiesis proceed in a similar manner in humans and mice; b) the structural components and organisation of the human and mouse erythrocyte membranes are similar; c) genetically engineered mice provide useful insights of the function of RBC membrane proteins , and also in

non-erythroid cells (Mohandas and Gascard, 1999). Therefore, engineered mouse strains of erythrocyte membrane proteins provide a tool for addressing questions regarding the specific etiology of red cell defects and expand our ability to more precisely define the specific contribution of the various membrane proteins to the erythroid and non-erythroid membrane structure and function.

1.5.1 - Targeted disruption of Band 3 -

Two knockouts models of mouse Band 3 have been developed, one in which both the erythroid and kidney isoforms were deleted (Peters et al., 1996) and another in which only the erythroid isoform was selectively inactivated, leaving the kidney Band 3 intact (Southgate et al., 1996). Both Band 3-null mice were severely anaemic, neonatal mortality was extremely high and erythropoiesis was accelerated as reflected by splenomegaly/hepatomegaly and extensive reticulocyte production. Identical red cell phenotypes were noted in both KO strains: RBCs were spherocytic with an extensive loss of surface area. Remarkably, spectrin was incorporated in normal amounts, although with slower kinetics, whilst the levels of other major skeletal components (actin, Protein 4.1, GPC, p55, adducin and dematin) and the skeletal architecture were normal. In contrast, ankyrin was synthesised in normal amounts but its assembly was reduced by 50 % due to rapid turnover, while both Protein 4.2 and GPA were completely devoid in the Band 3 null red cell membranes. These data imply that Band 3 provides the critical binding site for Protein 4.2 assembly onto the membrane and that it may be a chaperon partner for GPA trafficking to the membrane. Moreover, these results indicate that Band 3 is not required for proper RBC skeleton assembly *in vivo* but is essential for membrane stability (Hassoun et al., 1998; Peters et al., 1996; Southgate et al., 1996).

1.5.2 - Targeted disruption of Protein 4.1 -

The Protein 4.1-null mice have been reported to be viable and did not exhibit any gross abnormalities. Moderate haemolytic anaemia was detected and the RBC were mycrocytic and dehydrated (Shi et al., 1999). In contrast to the elliptocytic morphology seen in human 4.1R deficiency (Hoffman, 2000), Protein 4.1-null red cells were spherocytic and presented also fragmented cells. Mouse null erythrocytes membranes contained no p55 and had reduced amounts of spectrin, ankyrin and GPC. Abnormal erythrocyte morphology, lower membrane stability, and reduced expression of some skeletal proteins detected in mutant mice together indicated that the loss of 4.1R

compromises membrane skeleton assembly in erythroid progenitors and its attachment to the membrane (Shi et al., 1999). These findings not only reinforce the key role of Protein 4.1 in modulating the mechanical integrity of the RBC membrane, but they also enable the identification of an important function of 4.1 in assembly of the full complement of membrane skeleton during erythroid differentiation.

1.5.3 - Targeted disruption of tropomodulin -

Two knockout models of tropomodulin have been generated (Chu et al., 2003; Fritz-Six et al., 2003). In both cases, tropomodulin null embryos died around embryonic day 10 due to abnormalities in cardiac contractility, vascular morphogenesis and haematopoiesis. The absence of tropomodulin led to a primary defect in *de novo* myofibril assembly, resulting in aborted heart development, and induced the formation of mechanically weakened primitive erythroid cells. These defects reflect the essential role of erythrocyte tropomodulin in the assembly of both cardiac sarcomeres and the membrane skeleton in erythroid cells.

1.5.4 - Targeted disruption of tropomyosin -

Two different groups have shown that target disruption of α-tropomyosin gene leads to embryonic lethality (Blanchard et al., 1997; Rethinasamy et al., 1998). They reported that heterozygous mice were viable and reproduced normally, and cardiac morphology, histology and function remained unaltered (sarcomeres had normal morphology and contractility). No viable homozygous mice were obtained after the targeted deletion of the γ-tropomyosin gene, which eliminates all the non-muscle isoforms generated from it (Hook et al., 2004). These data demonstrate that total α- or γ tropomyosin deficiencies are incompatible with life. No studies were caaied out on potential alterations of RBC and their membrane components induced by the deletion of a single allele in viable heterozygous α and γ tropomyosin mutant animals.

1.5.5 - Skeletal and cardiac actin-deficient mice -

Of the four muscle actin genes (skeletal, cardiac, vascular, and enteric), only the skeletal and cardiac ones have been disrupted to date (Crawford et al., 2002; Kumar et al., 1997). The two animal models died in the early neonatal period. Newborn skeletal muscles from skeletal-actin deficient mice were similar to those of wt mice in size, fibre type, and ultrastructural organisation although they showed a marked reduction in force production compared to that of controls. Homozygous null animals at birth showed an increase in cardiac and vascular smooth-muscle actin mRNA in skeletal muscle. Thus,

while this increase can partially compensate for the lack of skeletal actin in null mice, it is not sufficient to support adequate skeletal muscle growth and/or function (Crawford et al., 2002). A similar partial compensation mechanism was also observed in cardiac actin-null mice: increased expression of vascular smooth muscle and skeletal actins was detected in the hearts of newborn homozygous mutants but apparently it was insufficient to maintain myofibrillar integrity and to prevent the severe structural and functional heart perturbations induced by the cardiac actin deficiency (Kumar et al., 1997). No animal models lacking non-muscular actin have been generated to date.

1.5.6 - Targeted disruption of Protein 4.2 -

Deficiency of Protein 4.2 in mice resulted in mild spherocytosis. The membrane skeleton architecture was intact, and the content of spectrin, ankyrin, Protein 4.1, adducin and p55 in deficient RBC membrane was normal. However, Band 3 and Band 3–mediated anion transport were decreased. Mutant RBCs showed significant changes in membrane cation transporter activities that induced altered cation content (K^+/Na^+) resulting in cell dehydration (Peters et al., 1999). These results show that Protein 4.2 is important for the maintenance of the normal surface area of erythrocytes by stabilising Band 3 mediated interactions and is required for normal RBC cation transport.

1.5.7 - Targeedt disruption of dematin headpiece domain -

Targeted deletion of the headpiece domain (DHP) of both 48-kDa and 52-kDa subunits of dematin generated viable mice that developed compensated anaemia with spherocytosis and microcytosis (Khanna et al., 2002). The headpiece null RBCs were osmotically fragile and exhibited a marked reduction in deformability and stability. The headpiece deletion induced a loss of spectrin and actin from the RBC membrane skeleton and GPC from the lipid bilayer of erythrocytes, with the consequent formation of a weakened membrane skeleton that was weakly anchored to the bilayer. No any other detectable alterations of the main membrane proteins were detected in dematin headpiece mutant animals (DKO). In addition, atomic force microscopy revealed that the mutant appears to lack specific vertical interactions between the cytoskeleton and the plasma membrane (Chen et al., 2007). The absence of the DHP did not influence the dimer-tetramer equilibrium of spectrin, which is consistent with the model supporting a role of dematin at the tail end of spectrin where actin oligomers cross-link spectrin into the membrane skeleton. Finally, DKO revealed the importance of the headpiece domain in dematin trimer formation. Together, these results provide evidence for the

physiological significance of dematin and demonstrate a role for the DHP in the maintenance of structural integrity and mechanical properties of erythrocytes *in vivo* (Chen et al., 2007; Khanna et al., 2002).

The effects of β-adducin target deletion and that of the double inactivation of dematin and β-adducin will be described in Sections 1.8 and 1.9.

1.6 The skeleton of the eye lens fibres membranes

The vertebrate ocular lens is an optically dense, bi-convex, flexible living lens, located between the reflecting surface of the cornea and the retina, and is composed of cells that, similarly to RBC, are very rich in skeletal components (Woo et al., 2000).

It is an encapsulated and avascular tissue comprising a single cell type originally derived from the surface ectoderm. In the mature lens, a *monolayer* of *epithelial cells* underlies the anterior *capsule*, which acts as a thick basement membrane of these epithelial cells. The rest of the lens mass comprises *lens fibre cells* that are derived by differentiation from the most proximal of the epithelial cells located near the equator of the lens. This differentiation process continues throughout the lifespan of the host with new lens fibre cells laid down over pre-existing fibre cells. Thus, lens fibre cells are arranged as concentric layers, with the oldest fibre cells (*nuclear fibre cells*) at the centre, or *nucleus*, and the youngest at the lens surface (Menko, 2002) (Figure 1.5).

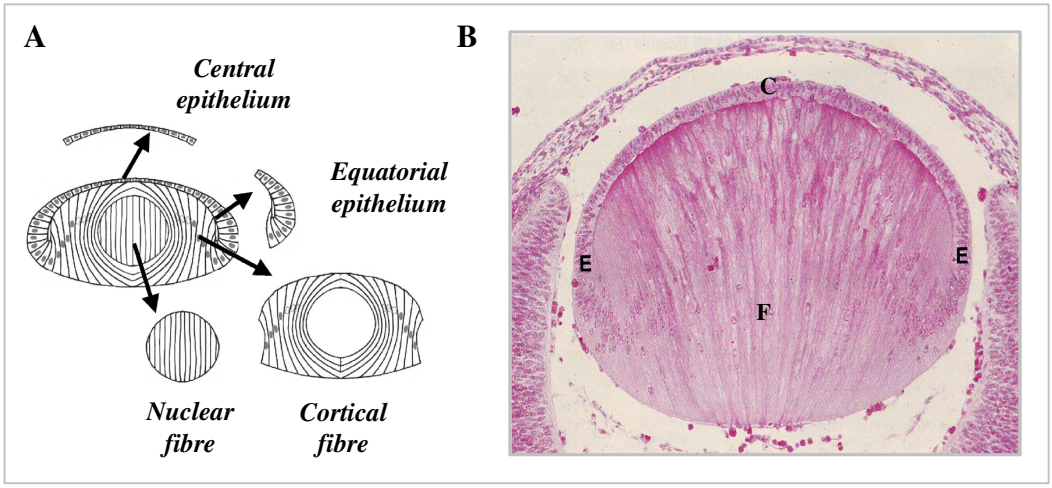

Figure 1.5: Histology of ocular lens. Panel A shows a schematic representation of the four distinct regions of differentiation present in eye lens: the *central epithelium* composed of epithelial cells committed to the lens lineage; the *equatorial epithelium* comprised of two distinct regions, the zone of proliferation in its most anterior aspect followed by the transition zone where the lens epithelial cells withdraw from the cell cycle and initiate their differential program; the *cortical fibre* zone in which the distinctive morphogenesis that characterise lens fibre cells differentiation occurs; and the *nuclear fibre* region, where the fibre region became mature. The scheme is adapted from Menko, 2002. A histological image of a hematoxylin (purple) stained lens sagittal section is shown in Panel B. *Central epithelium, equatorial epithelium* and *fibres* are indicated with letters "C", "E" and "F", respectively.

During differentiation, cuboidal epithelial cells at the equator first exit from the cell cycle then elongate progressively to form highly elongated, polarised epithelial cells, called *cortical fibre cells*. Concomitant with these morphological changes, differentiating epithelial cells also initiate the expression of fibre cell-specific proteins including the crystallin and intermediate filament proteins. This process is also accompanied by an increase in the ratio of filamentous actin and is characterised by the reorganisation of actin and lens-specific intermediate filaments networks. Finally, lens fibres lose most of their cellular organelles including the nuclei, and some cytoskeletal components, such as microtubules and vimentin intermediate filaments, are also degraded. During fibre elongation, the cells migrate along the epithelium and detach at the suture where they form contacts with their counterparts from the opposite side of the lens. The continuous addition of new fibre cells at the lens periphery leads to a gradual inward movement of older and mature cells to the centre of the lens to form the nucleus. This process created the ocular lens: a fascinating and unique tissue that grows continuously throughout the lifespan of the host (Menko, 2002).

The main functions of the lens are to transmit and focus visible light on the retina. The optical proprieties required to do this are transparency, reflection power (high reflective index and curvature or symmetrical shape) and properties of accommodation. The transparency and the reflective power of the lens are due to its symmetrical shape and optical homogeneity. Transmission of light to the retina is allowed by the tightly ordered packing of small soluble proteins (like crystallin) in the cytoplasm, the absence of organelles and the arrangement of lens fibre in layers approximately perpendicular to the light entering the eye thereby reducing to a minimum the light absorption and scattering. Essential for the maintenance of the transparency are those cytoskeletal structures that are able to interact with cytoplasmic soluble proteins and to control their distribution and orientation in the lens fibres (Clark et al., 1999). Visual accommodation principally derives from the lens fibres deformability which is correlated to the structural organisation of actin filaments (Yeh et al., 1986).

In common with other non-erythroid cells of mammals, lens fibres possess:

- *Microtubules:* they increase in number as the epithelial cell starts to elongate, and orientate along the axis of the future fibre. They have been found in epithelial cells and cortical fibres but not in the nuclear fibres: in fact, they are lost completely during the fibre cells maturation. Microtubules in association with motor proteins play an

important role in transporting lens proteins in vesicles during fibre cell differentiation and elongation (Lo et al., 2003).

- *Intermediate filamenst:* are the major cytoskeletal elements of the eye lens and are present as unique beaded filaments. Two specific proteins, *CP49* and *filensin*, constitute the intermediate filaments that are synthesised during lens differentiation. They possess unique structural features and unusual assembly characteristics, which distinguish them from canonical intermediate filament proteins (Prescott et al., 1996). Lens-specific intermediate filaments are the key cytoskeletal elements in organising and maintaining lens fibre cell architecture and are essential in determining the optical properties (transparency) of the lens as they appear to provide attachment sites for crystalline (Clark et al., 1999; Perng and Quinlan, 2005).
- *Actin filaments:* actin is one of the major cytoskeletal proteins in the lens and has been purified and characterised in the lens fibres of several species. Besides actin, the lens also contains isoforms of most erythrocyte membrane skeleton components (Aster et al., 1984; Faquin et al., 1988; Ireland et al., 1983; Repasky et al., 1982; Woo and Fowler, 1994). Unlike the RBC skeleton, the lens contains approximately 2000 actin monomers per tropomodulin molecule (in RBCs the ratio is ~12-18:1), suggesting that the majority of actin is assembled into long filaments, and not into short, actin filaments (Woo et al., 2000). Ultrastructural analysis also confirmed the presence of relatively long actin filaments extending into the cytoplasm of lens fibre. In the lens, actin filaments have several roles. Most of the events that occur during the process of differentiation of lens epithelial cells into fibre cells are highly coordinated through the reorganisation of actin filaments (Rao and Maddala, 2006). In mature nuclear fibres, the actin skeleton provides stability to cells, maintaining the membrane integrity and the overall elongated shape. Moreover, it supports an important scaffolding function for the organisation of cytosolic and membrane-bound proteins in the lens fibres. All these roles are essential to maintain the transparency of the elongated, long-lived cells of the lens. The membrane skeleton also plays a role in conferring deformability during visual accommodation (Clark et al., 1999; Rao and Maddala, 2006).

The main skeleton components (actin, tropomyosin, and spectrin) are expressed and membrane-associated in all lens cells (both undifferentiated and differentiated). In contrast, tropomodulin is expressed concomitantly with lens fibre cell differentiation and assembles onto the membrane skeleton only after fibre cells have begun to elongate (Lee et al., 2000; Sussman et al., 1996). As in erythrocyte skeletons, both tropomodulin

and tropomyosin co-localise with actin filaments on fibre cell plasma membranes (Woo et al., 2000). Furthermore, actin filaments, tropomyosin and tropomodulin, once assembled, remain membrane-associated and are not proteolysed during fibre cell maturation and aging, despite degradation of α-spectrin and other cytoskeletal filament systems such as microtubules and canonical intermediate filaments (Lee et al., 2000; Prescott et al., 1996). This seems to indicate that tropomodulin may be required for actin filament stabilisation and/or determination of filament length in the membrane skeleton of lens fibre cells, as it is in the sarcomeres of cardiac myofibrils and in the membrane skeleton of RBC (Lee et al., 2000). It was demonstrated that tropomodulin-actin complexes do not contain spectrin in lens cells. Instead, spectrin is associated with actin in different complexes that do not contain tropomodulin. These results suggest that tropomodulin-capped actin filaments and spectrin-cross-linked actin filaments are assembled in distinct structures in the lens fibre cells skeleton creating a membrane-network organisation that is different from that of erythrocytes (Woo et al., 2000). In addition, a large soluble pool of actin, tropomodulin and spectrin, which does not exist in erythrocytes, was identified in lenses. This difference implies the presence of distinct pools of cytoskeletal components in the lens: membrane-bound (forming the membrane skeleton) and soluble pools (constituting precursors necessary for rapid assembly of the membrane skeleton during fibre cell elongation) (Woo and Fowler, 1994). In conclusion, the molecular organisation of the membrane skeleton along the lateral membranes of the lens fibre cells may be qualitatively different from erythrocytes, despite the fact that many of the components are identical isoforms in both cell types.

1.7 Adducin

As we previously introduced (Section 1.2) adducin is one of the components of cytoskeletal network. Next paragraphs will focus on all the details about this protein.

1.7.1 - Adducin genes and their expression -

Adducin is encoded by three closely related genes termed α, β and γ adducins (*ADD1*, *ADD2*, and *ADD3*, respectively in humans), which have a different chromosomal location in humans, rats and mice. The primary transcripts of all three adducin genes undergo alternative splicing, generating a wide variety of mRNAs. Most encode truncated isoforms compared with the originally described ones, although there is no evidence that all the alternatively spliced forms are translated into proteins (Citterio et al., 1999; Gilligan et al., 1997; Lin et al., 1995; Tisminetzky et al., 1995;

Tripodi et al., 1991). Both α– and γ-adducins are expressed ubiquitously, while β-adducin expression is mainly restricted to brain and haematopoietic tissues, suggesting a different transcriptional regulation and function for all three genes (Gilligan et al., 1999; Muro et al., 2000; Tripodi et al., 1991).

1.7.2 - β-adducin gene -

The human β–adducin gene spans over 100 kb and comprises 17 exons. Its primary transcript undergoes a complex pattern of alternative splicing generating the β–Add97 and β–Add63 mRNAs families (Figure 1.6). A splicing event at the junction of exon 13a/intron generates the mRNAs belonging to β–Add97 family. On the other hand, if the splicing does not occur, and the intron 13 is retained the β-Add63 is generated. In this case, an in-frame stop codon 87 bp downstream from the 5'-splice junction of exon 13a should be used to eventually translated a truncated form of the protein belonging to β–Add63 family (Gilligan et al., 1997; Tisminetzky et al., 1995).

β-Add97 family. The β-1 form (or ADD97) is the main variant present in human red cells and brain. It comprises all exons (coding for 726 amino acids), except for exon 15, and is the most abundant and best characterised one. Alternative exclusion of different combinations of internal exons (from exon 3 to 10) gives rise to different isoforms of ADD97 lacking the central regions of β–adducin (Gilligan et al., 1997; Sinard et al., 1998; Tisminetzky et al., 1995).

β-Add63 family. The β-2 form (also called ADD63), is generated upon utilisation of a polyadenylation site found in the unspliced intron that follows exon 13. It has been identified as a clone from a mouse (then rat) spleen cDNA library and its protein product has not yet been characterised (the proteins should share 531 N-terminal amino acids with β-1 form, but diverge to a novel 30 amino acid C-terminus). Similarly to the ADD97 family, various isoforms generated by alternative splicing that lack the same groups of exons constitute the ADD63 family (Figure 1.6) (Gilligan et al., 1997; Tisminetzky et al., 1995; Tripodi et al., 1991)

A peculiar mRNA of approximately 8-9 kb was found in brain of rats and mice (Gilligan et al., 1999; Joshi et al., 1991; Tripodi et al., 1991). In this tissue, the long β-adducin transcript is the most abundant mRNA form detected. None of the previously described β-adducin mRNA isoforms has been able to account for the presence of this long transcript. However, the translated product of this long mRNA in brain is approximately 110 kDa, roughly similar to the 97 kDa β-adducin isoform of erythroid

tissues. This small difference is not explained by the huge size difference between the brain 8-9 kb transcript and the 3-4 kb mRNA found in haematopoietic tissues(Bennett et al., 1988; Muro et al., 2000).

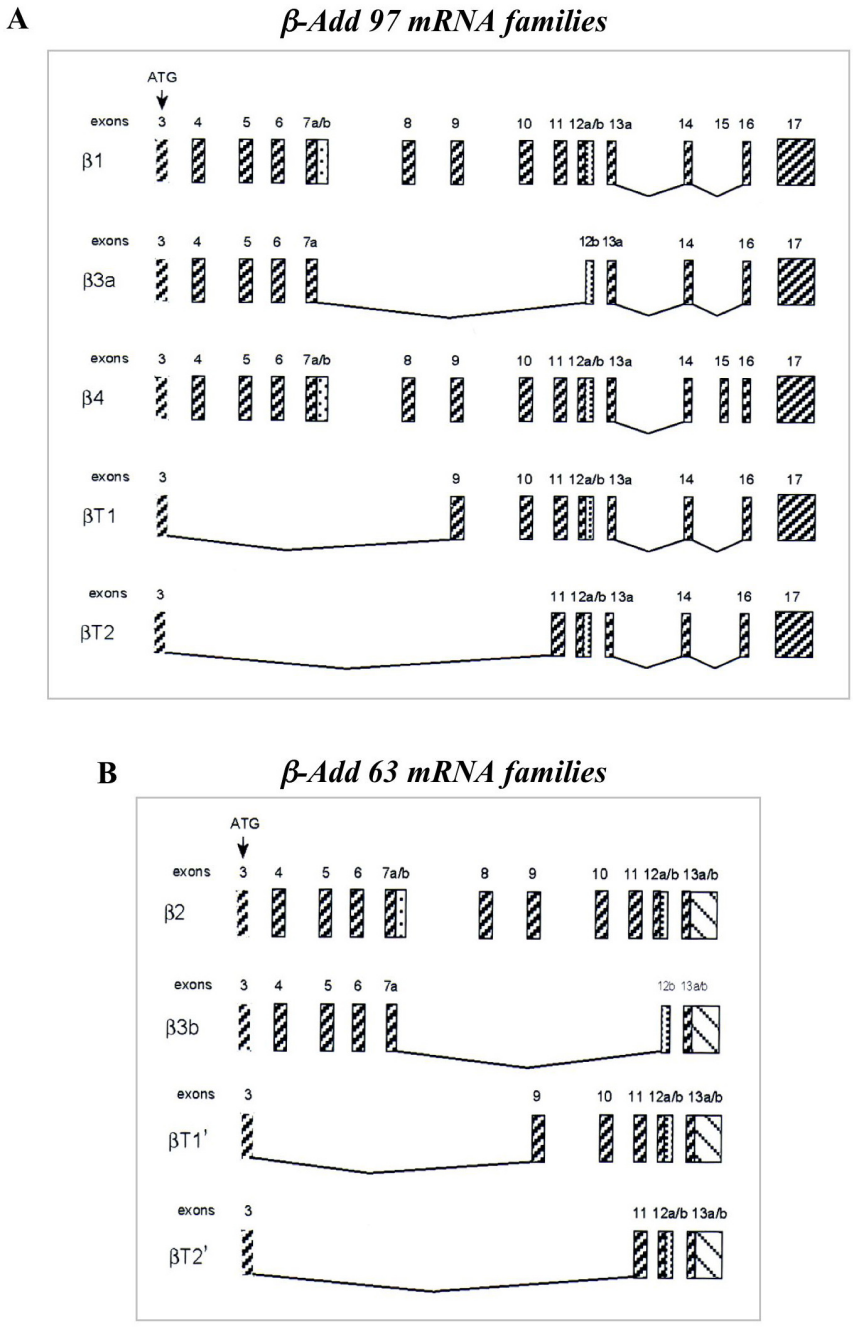

Figure 1.6: Alternative splicing of human β-adducin pre-mRNA. A scheme of the alternative spliced mRNA forms belonging either β-Add97 or β-Add63 families is presented in Panel A and B, respectively. Lines connecting exons are indicated whenever a coding sequence is bypassed and alternative splicing occurs. The initiation of translation occurs in exon 3. Alternative stop codons and 3'-UTRs are found within exons 13b and 17 in β-Add63 and β-Add97, respectively. Exons 9, 11 and 12 can function as acceptor of splicing for both the β−Add97 and β−Add63 mRNAs families (Tripodi et al. 1991; Tisminetzky et al. 1995; Gilligan et al. 1997; Sinard et al. 1998).

In humans, the β−Add97 mRNAs family is detected in all neuronal tissues (with highest expression in the cerebellum), bone marrow, fetal brain, and fetal liver. Similarly, β-Add63 mRNAs are detectable in all neuronal and haematopoietic tissues, although the level of expression is lower than that of β-Add97 family. Surprisingly, only the β-Add97 mRNAs family shows expression in adult and fetal lung. Expression of β-Add mRNAs families in the mouse is similar to that of human with high levels in brain and spleen (Gilligan et al., 1999).

It was observed that the level of expression of β-adducin transcript in brain seems to be linked to cellular density. The highest expression of β-adducin mRNA is seen in the stratum pyramidale of all of the hippocampal regions and in the molecular, Purkinje, and granular layers of the cerebellum. Other areas of high cellular density also show high levels of β-adducin mRNA, including the granule layer of the olfactory bulb, piriform cortex, layer 2 of the tenia tecta, bed nucleus of the stria terminalis, and several hypothalamic nuclei. Lower levels of expression are observed in the cortex and striatum (Rabenstein et al., 2005).

1.7.3 - Adducin protein structure -

Adducin was isolated from human erythrocytes as a mixture of heterodimers and heterotetramers, and no monomeric adducin has been observed in all types of cells tested so far. In human RBC oligomers comprise α/β subunits, and in other cells include α/γ as well as α/β combinations of subunits (Dong et al., 1995; Gardner and Bennett, 1986; Hughes and Bennett, 1995). In reticulocytes, the striking difference in the amount of the α- and β-adducin mRNAs, being α-adducin mRNA abundant and β-adducin mRNA rare, suggests that synthesis of the β subunit may be the limiting factor in assembly of adducin heteromers (Joshi et al., 1991).

The primary sequences of α and β adducin display 49 % identity and 66% similarity at the amino acid level in humans, while γ subunit shares 60-70% sequence similarity with either α– or β–adducin. Moreover, α, β and γ subunits have shown a very high homology among humans, rats and mice (approximately 90%) at amino acid level. The identity is almost complete for the functional domains suggesting a total conservation of adducin functions across species (Muro et al., 2000).

All adducin subunits contain the following three domains (Figure 1.7) (Matsuoka et al., 2000):

- N-terminal protease-resistant head domain: is the globular portion of the molecule and the most conserved region among adducin subunits. There is little information regarding functions of this domain, even though it seems to contain oligomerisation sites;
- The neck domain: contains oligomerisation sites and therefore is required for oligomerisation. It is also involved in promoting the interactions of adducin with spectrin and actin;
- C-terminal protease-sensitive tail domain: is highly conserved among the three adducin subunits. At the C-terminal end at the domain is localised a 22-residue MARCKS-related domain, having high homology to the myristoylated alanine-rich C kinase substrate (MARCKS) protein. In addition, the domain has clusters of lysine residues that confers polybasic nature to the region and contains the major sites for protein kinase C and A, and calmodulin binding. This domain is able to mediate contact between adducin and spectrin-actin complexes.

In conclusion, dimers or tetramers of adducin are formed by two or four head domains in contact one another to form a globular core, and interacting neck domains and tail domains extending away from the core (Hughes and Bennett, 1995; Matsuoka et al., 2000).

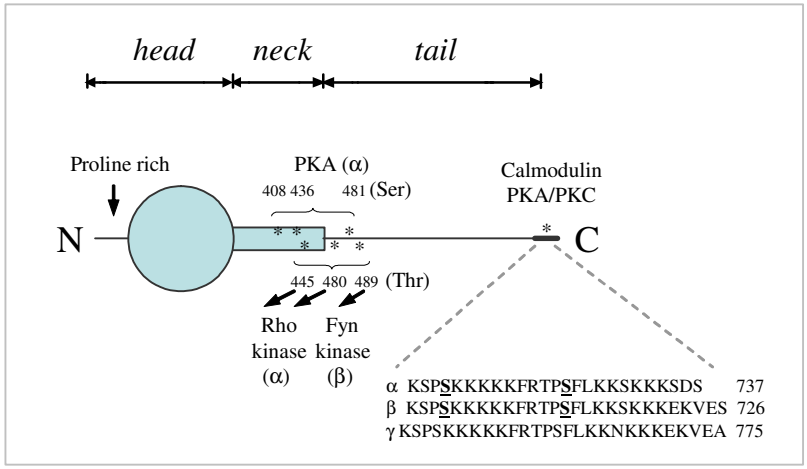

Figure 1.7: A model of human adducin monomer. The figure shows a scheme of the adducin monomer structure. A sphere, a box and a line are used to represent the head, neck and tail domain, respectively. The calmodulin-binding region is indicated as a solid black box, and the amino acid sequences of the C-terminal MARCKS-related domain of α, β and γ adducin are presented. The major phosphorylation sites of PKA, PKC and Rho-kinase are indicated by asterisks. The phosphorylation sites of PKC identified in MARCKS-related domain are underlined. PKA and Rho-kinase preferentially phosphorylated the Ser/Thr residues present in and close to the neck domain (indicated with their residue numbers). The figure is adapted from Motsuoka et al., 2000.

1.7.4 - Adducin in vitro activities -

In vitro assays have shown that adducin recruits spectrin to actin filaments (Bennett et al., 1988; Gardner and Bennett, 1987; Hughes and Bennett, 1995), bundles actin filaments (Mische et al., 1987; Taylor and Taylor, 1994) and caps the fast-growing ends of actin filaments (Kuhlman et al., 1996) (Figure 1.8). Each of these individual activities may reflect different aspects of adducin function in living cells. Adducin is the first example of an actin-capping protein that recruits other proteins to actin filament and that have the ability not only to associate with the end of the actin filament but also with the its sides. The single MARCKS-related and the neck domains are necessary but not sufficient for the mentioned activities of adducin: in fact, each single domain itself exhibits minimal spectrin-recruiting, actin-capping and actin-binding activities or almost completely lost them (Matsuoka et al., 2000).

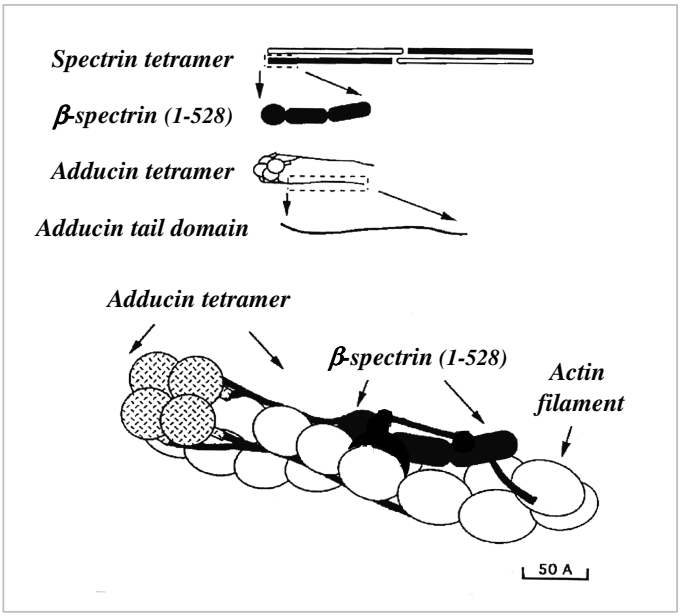

Figure 1.8: A schematic model of adducin association with actin filament and spectrin. In the figure the actin filament appears as two steep helices twining slowly round each other. A single spectrin repeat domain is a three-helix bundle. The adducin head domains cap the fast-growing end of F-actin. Adducin C-terminal tail domains bind spectrin and actin filament to form the ternary complex. The figure is adapted from Liet al., 1998.

1.7.5 - Regulation of adducin functions -

Adducin activities are regulated by phosphorylation in serine and threonine residues and by the Ca^{2+}-calmodulin binding (adducin was originally purified based on its calmodulin binding activity). Protein kinase C (PKC) and cAMP-dependent protein kinase (PKA) phosphorylation inhibits and down-regulates, respectively, both the adducin actin-capping and spectrin-recruiting activities. By contrary, Rho-kinase

phosphorylation (Rho-kinase) enhances adducin-actin interactions. In addition, Fyn kinase (a Src-family tyrosine kinase involved in neuronal development, transmission, and plasticity in mammalian central nervous system) phosphorylation seems to slightly increase the capping activity. Finally,Ca^{2+}-calmodulin inhibits adducin activities (Gotoh et al., 2006; Matsuoka et al., 2000).

The major phosphorylation sites common for PKA and PKC and the main calmodulin-binding site are localised in the MARCKS-related domain. Other PKA, Rho- and Fyn-kinase phosphorylation sites are present in the neck and tail domains (Gotoh et al., 2006; Matsuoka et al., 2000) (Figure 1.7). Interestingly, calmodulin-binding of β-adducin is inhibited by PKA and PKC phosphorylation of the MARCKS-related domain. Calmodulin in turn inhibits the rate of PKA and PKC phosphorylation of β-adducin (but not α-adducin). These findings suggest a complex reciprocal relationship between the regulation mechanisms of adducin functions (Matsuoka et al., 2000).

1.7.6 - *Adducin cellular localisation and in vivo activities* -

Adducin is localised at junctional complexes of the cytoskeleton in mature erythrocytes (Derick et al., 1992) and is expressed in early erythropoiesis when the spectrin-actin network is forming (Nehls et al., 1991). In epithelial tissues, adducin and spectrin are both concentrated at sites of cell-cell contact (Kaiser et al., 1989). In brain adducin is expressed at high levels and it is identified as a constituent of synaptic structures (Bennett et al., 1988; Seidel et al., 1995). In rat, α-adducin is found to be highly enriched in regions with high synapse densities of the hippocampus (CA1 and CA3 regions), corpus striatum, cerebral cortex and cerebellum and in particular, it is localised at distinct sub-cellular structures. It is present in a subset of dendrites, dendritic spines, growth cones and pre-synaptic terminals, suggesting the possibility that adducin plays some role in dynamic assembly-disassembly underlying synaptic plasticity (Matsuoka et al., 1998; Seidel et al., 1995).

In vivo studies showed that adducin phosphorylation by different kinases, such as PKC and Rho-kinase, can have different effects in its subcellular localisation. For instance, PKC induces the redistribution of adducin away from cell contact sites of epithelial cells and its concentration in dendritic spines of hippocampal neurons. Rho and Fyn kinase produce adducin translocation and accumulation in the membrane area and in the leading edge of cells. These results indicate that the phosphorylation of

adducin by Rho-kinase, Fyn as well as PKC plays crucial roles in the regulation of synaptic plasticity, membrane ruffling and cell motility (Matsuoka et al., 2000).

1.7.7 - Adducin and hypertension -

Extensive studies have demonstrated a link between adducin and hypertension in rats and humans. Human α-adducin gene polymorphisms (Cusi et al., 1997) were found to be significantly associated with hypertension although this observation was dependent in the ethnical origin of the populations (Bianchi et al., 2005). In addition, adducin polymorphisms associated to abnormal cell sodium reabsorption have been found in a congenital rat strains after having been selected for high and low blood pressure (BP) [Milan hypertensive (MHS) and normotensive (MNS) rat strains, respectively] (Bianchi et al., 2005).

The direct involvement of the adducin gene family in the modulation of BP is supported by the detection of hypertension in β-adducin deficient mice (Section 1.8) (Marro et al., 2000)

A long series of parallel studies in the MHS model and hypertensive patient indicate that an altered adducin function may cause hypertension through enhanced constitutive tubular sodium reabsorption. In human or rat renal cells, mutated α-adducin causes a rearrangement of the actin cytoskeleton impairing the Na-K pump endocytosis and increasing its activity (Bianchi et al., 2005).

1.8 β-adducin knock-out mice

To elucidate the *in vivo* function of β−adducin our group carried out a targeted disruption of the β subunit gene generating β-adducin knockout (KO) mice model by replacing exons 9 to 13 with a NeoR cassette (Muro et al., 2000). This deletion ensured the elimination of all β-adducin mRNA isoforms and the exons that encompass the most important functional domains: the oligomerisation domain, the calmodulin-binding domain of the neck region, PKA phosphorylation sites, the region containing the Q529R polymorphism associated with hypertension in rats, and a major part of the tail domain responsible for modulating adducin activity. Deletion of exons 9 to 13 corresponded to a reduction of 744 bases of the β-Add97 mRNA and the elimination of all the 3' coding and noncoding end of β-Add63. Although a deleted mRNA form was present in the brain, spleen and other tissues of mutant mice, no protein (normal or deleted forms) was

detected either in these tissues nor in RBC skeleton and cytoplasm of β-adducin null mice.

Mutant mice reached adulthood without showing any obvious phenotypical abnormality, and they reproduced at the same rate as their wild-type littermates. Except splenomegaly, no differences by gross histological and pathological analysis of mouse organs from KO mice were detected. Haematological analysis showed a significant decrease in the hematocrit, mean corpuscular haemoglobin (MCH), and haemoglobin values in -/- mice. Erythrocytes of mutant animals evidence a marked increase in the osmotic fragility (OF) (Figure 1.9), they were significantly smaller (decrease in mean corpuscular volume -MCV-) and had an increase in mean corpuscular haemoglobin concentration (MCHC) values. These modifications were due to a loss of membrane surface and dehydration that resulted in the observed increase in OF. Higher levels of bilirubin were detected and reticulocyte count was increased. All these haematological evidences indicate that β-adducin mutant mice suffer from a mild anaemia with compensated haemolysis.

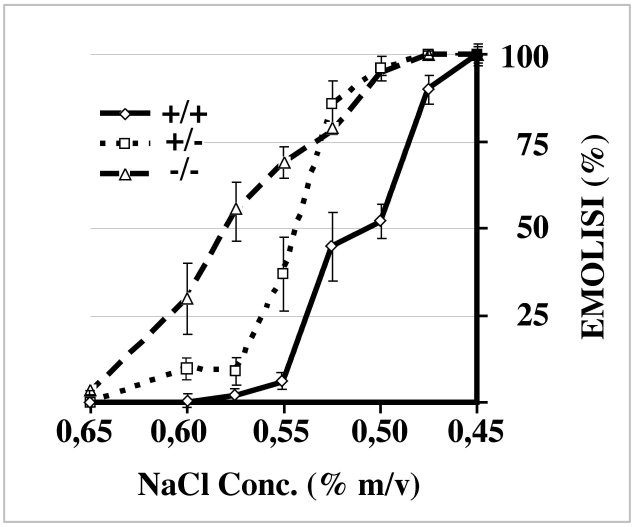

Figure 1.9: Osmotic fragility of RBCs. The graph shows the data obtained testing the OF of erythrocytes from +/+ (◇), +/− (□), and −/− (△) mice. Results (mean ± standard error) are expressed as percentage of lysis in graded salt concentrations. C_{50} values were determined by logarithmic linearization of the OF curve. The figure is from Muro et al., 2000.

In addition, the peripheral blood smears of β-adducin -/- mice showed heterogeneity of the erythrocyte shapes, including normal erythrocytes, elliptocytes, rounded elliptocytes, and occasional spherocytes (Figure 1.10).

The observed RBCs osmotic fragility and mild elliptocytosis defined a phenotype in mutant mice similar to that present in the human disorder denominated spherocytic hereditary elliptocytosis (SphHE) (Section 1.4.2) (Hoffman, 2000).

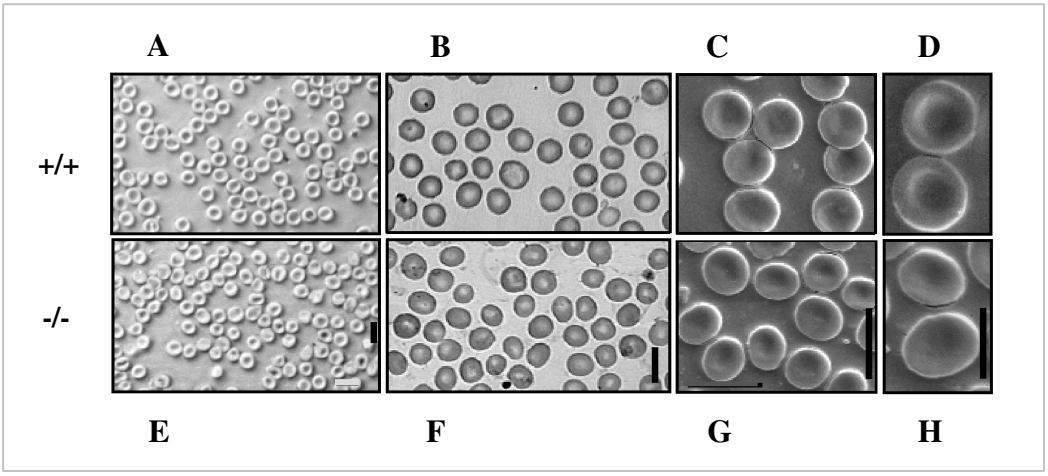

Figure 1.10: Morphology of RBCs. Native (A and E Panels) and May-Gruenwald Giemsa stained (B and F Panels) light microscopy and scanning electron (C, D, G, and H Panels) microscopy of peripheral blood smears of wild-type (A, B, and C Panels) and mutant mice (D, E, and F Panels) are shown. The abnormal morphology and the decrease in the concavity of erythrocytes of mutant mice are visible. [Bar 10 µm (A, B, C, E, F, and G Panels), 5 µm (D and H Panels)]. The figure is from Muro et al., 2000.

Quantification of the relative amounts of RBC skeletal proteins in β-adducin ghosts and skeletons showed normal levels of α- and β-spectrin, ankyrin, Band 3, Protein 4.2, and Protein 4.1 (Figure 1.11 A). However, a 15% reduction in actin levels, a threefold increase in Hb retention and the lack of an unidentified 65 kDa protein were observed in RBCs ghosts and skeletons from mutant mice. The levels of various unknown proteins were slightly increased in the region of 18-40 kDa in the -/- skeletal preparations (Figure 1.11 A). Moreover, the levels of the α-adducin subunit was reduced to about 20% of that of the wild-type mice (Figure 1.11 B) and a fourfold upregulation of the γ-adducin subunit levels was observed in mutants (Figure 1.11 C).

The molecular analyses indicated that the absence of β-adducin and consequent altered levels of the α- and γ-adducin subunits and others erythrocyte skeletal proteins may produce defective junctional complexes affecting the normal structure of the membrane skeleton, producing a marked increase in OF, altered haematological parameters, erythrocyte dysmorphology and inducing the pathological condition in the β-adducin deficient mice.

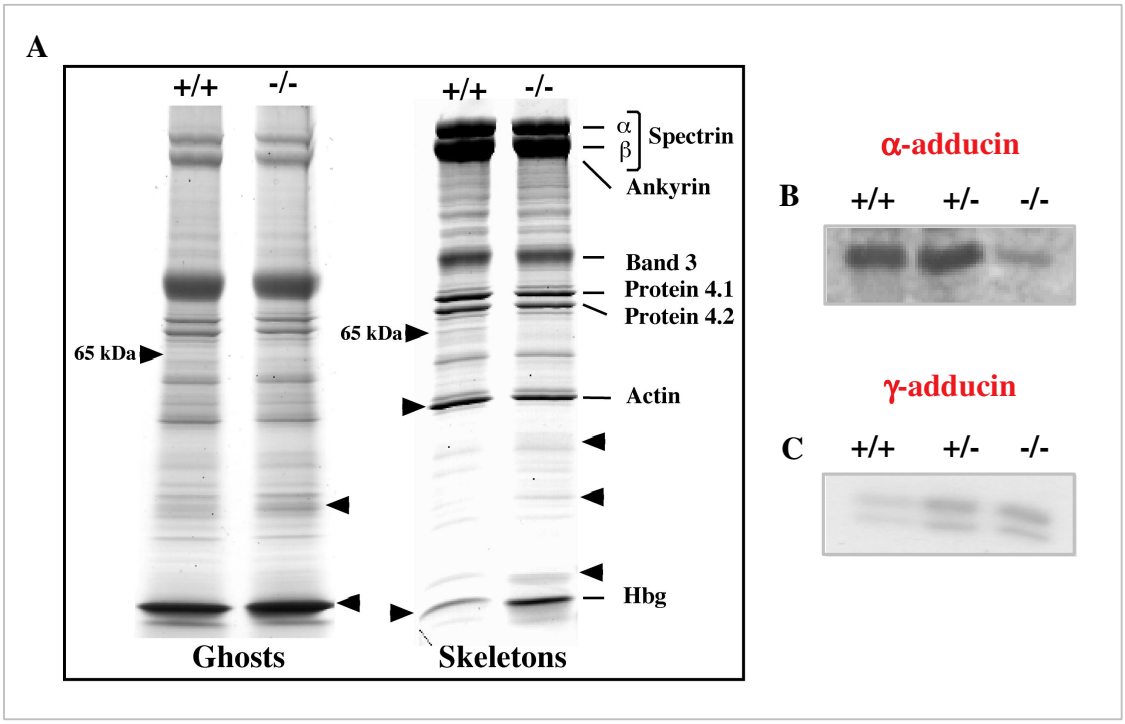

Figure 1.11: Analysis of ghost and skeletal proteins in β–adducin mutant mice. Panel A shows Coomassie blue stained gels (SDS-PAGE) of ghosts and membrane skeletons from normal (+/+) and mutant (−/−) mice. The major proteins are indicated on the right. Variations between normal and mutant animals are indicated by arrows. Western blot analysis of ghost proteins of adult wild-type (+/+), heterozygous (+/−), and homozygous mutant (−/−) mice using anti α-adducin and anti γ-adducin antibodies are shown in Panels B and C, respectively.

In parallel to our β-adducin knock-out mouse, Gilligan's group created a mouse model deficient for adducin β subunit (AKO) (Gilligan et al., 1999)and minor differences between both models were observed. We see predominance of elliptocytes, whereas their predominant feature is spherocytosis. Erythrocytes from both animal models are osmotically fragile and have smaller MCV, and all other haematological parameters are similar. Regarding the amount of the erythrocyte skeleton components, a slightly reduction of spectrin and a significant decrease in GPC level were detected in the mutant ghosts when compared with the control, while no significant alterations were shown in the amounts of GPA, ankyrin, protein 4.2, and p55 between erythrocyte ghosts of mutant and control mice (Chen et al., 2007; Gilligan et al., 1999). Both models were analysed in different genetic backgrounds: our mouse mutants were backcrossed for 5 generations, being at least 98% identical to the C57Bl/6 genetic background, whereas Gilligan et al. studied the β-adducin mutation phenotype within a mixed 50% SvC129 and 50% C57Bl/6 genetic background. It has been previously reported for other gene knockout models that the phenotype may vary with different genetic backgrounds. This

observation could be the cause of the differences seen between our mutant animals and those of Gilligan's group.

1.8.1 - β-adducin deficient mice and hypertension

The knockout model also gave us the opportunity to study the direct association between β-adducin and hypertension in a well-defined genetic background(Marro et al., 2000). We found that mutant animals developed hypertension, with no changes in the heart rate. A sharp decrease of α-adducin (70%) levels and a lesser reduction in γ-adducin levels (50%) was observed in the heart of mutant animals. Despite the observed marked changes in adducin expression, no alterations of heart morphological, mechanical, or electric properties have been detected in the KO animal, suggesting a lack of involvement of these proteins in heart function. Although altered kidney events seem to connect adducin polymorphisms to the development and maintenance of hypertension in rats and humans (Bianchi et al., 2005), preliminary studies of kidneys of β-adducin deficient mice showed normal gross histological analysis and serum creatinine levels suggesting a normal kidney function (Marro et al., 2000).

In conclusion, the development of hypertension in β-adducin mutant mice strongly and directly evidences that hypertension is triggered by a mutation in the adducin gene family although the precise mechanism remains uncertain. Anyhow, the absence of β–adducin and concomitant modification of α– and γ–adducin levels in heart and other tissues, together with previous data on rat adducin polymorphisms (Bianchi et al., 2005) support the hypothesis that the abnormal adducin complex assembly might be an important determinant of BP.

1.8.2 - AKO mice and synaptic plasticity underlying learning and memory -

The expression of α and γ subunits in the brain of β-adducin deficient mice have changes similar to those detected in RBC: decrease in α-adducin and increase in γ-adducin levels (Gilligan et al., 1999). Neurophysiologic analyses revealed that mutant mice exhibit deficits in both short- and long-term synaptic plasticity. Moreover, behavioural analyses evidenced that learning (spatial and general) and memory were impaired in AKO animals(Rabenstein et al., 2005). These data together with the observation that α- and β–adducin mRNAs are found to be highly enriched in regions with high synapse density thought to be critically involved in learning and memory suggest that adducin is involved in setting synaptic strength, as well as synaptic plasticity associated with learning and memory. Therefore, the loss of adducin seem to

result in synapses that are less responsive to stimulation and therefore may impair normal processes underlying learning and memory (Gilligan et al., 1999; Rabenstein et al., 2005; Seidel et al., 1995).

1.9 Dematin-adducin double knock-out mice

Stoichiometrically, dematin and adducin are major constituents of the junctional complex and, by virtue of their actin binding and bundling properties, they are believed to regulate the dynamics of actin protofilaments in the erythrocyte membrane. To test whether they perform a redundant function at the RBC, the double knock-out mouse strain lacking β-adducin and the headpiece domain of dematin (DAKO) was generated(Chen et al., 2007). DAKO was created by crossing of DKO (Khanna et al., 2002) and AKO (Gilligan et al., 1999).

DAKO mice showed that the combined mutations resulted in more severe haematological alterations. A significant decrease was observed in the erythrocyte counts, haemoglobin and hematocrit content. The high reticulocyte counts (12-fold increase) and the increased total serum bilirubin levels in the peripheral blood of double mutant mice indicated the presence of a regenerative anaemia and explained the severe splenomegaly observed in mutant animals. The double mutant mice exhibited marked spherocytes, acanthocytes, fragmented erythrocytes and ghosts, and these altered erythrocytes showed increased osmotic fragility. All this data indicated that the DAKO mice develop a severe haemolytic but regenerative anaemia.

The analyses of the protein expression profile of double mutant ghosts and skeletons revealed some alterations in the levels of the RBC cytoskeletal components. About 15% reduction of both spectrin and actin, and a modest decrease in Protein 4.1 were evidenced in the DAKO ghosts and skeletons. No significant alterations were observed in the amounts of GPC and, like in the single mutants, in the levels of GPA, ankyrin, Protein 4.2, and p55 in DAKO erythrocyte ghosts. Atomic force microscopy revealed differences in the skeletal structures between wt and DAKO erythrocytes: large protein aggregates and a decrease in filament number were evidenced in the mutant membrane cytoskeleton. These observations seem to indicate the presence of cytoskeletal network damages and suggest that both vertical and horizontal associations of the cytoskeleton appear to be broken in the double mutant.

In conclusion, the inability to maintain the membrane stability and to regulate cell shape, which induce the erythrocyte reduced life span and the severe haemolytic

anaemia in DAKO animals, are caused by alterations of the erythrocyte cytoskeleton architecture and probably by the fact that the linkage of the spectrin-actin network to the membrane is compromised. Together, these results reveal the essential role of dematin and adducin in the maintenance of an efficient erythrocyte skeleton, and suggest the functional redundancy of the two proteins at the junctional complex (Chen et al., 2007).

1.10 mRNA processing reactions

For eukaryotes coding genes, simply copying the genetic information from a DNA template into a RNA transcript by RNA Polymerase II does not result in the completion of mRNA synthesis. Before a gene transcript is ready to be transported out of the nucleus, it has to undergo three major processing events to produce the fully translatable mRNA. These comprise the acquisition of a cap structure at the 5′ terminus, the splicing out of introns within the body of the pre-mRNA, and the generation of a 3′ end, usually modified by the addition of a poly(A) tail. When pre-mRNAs are not processed efficiently, they are rapidly degraded in the nucleus. These modifications of the primary RNA (in particular 5'-capping and 3' polyadenylation) are necessary not only for the protection of mature transcripts but also for the regulation of translation. Therefore, small changes in overall RNA processing efficiency in a particular cell or the effective strength of a particular splicing or polyadenylation site can serve as an important control point for gene expression in a tissue or developmental stage-specific manner (Rio, 1993; Shatkin and Manley, 2000; Zhao et al., 1999).

1.10.1 - Capping -

The first pre-mRNA processing step occurs as soon as ~20–30 nt have been synthesised by RNA Polymerase II. A three-step reaction adds a cap structure to the 5′ end of all the transcripts. This structure consists of a guanine nucleotide connected to the mRNA via an unusual 5′-5′ triphosphate linkage. In the nucleus, the 5'cap is recognised by the cap-binding complex (CBC) which mediates the mRNA nuclear export. In the cytoplasm, the cap structure bound to CBC plays an important role in the stabilisation of the mRNA, since it represents an obstacle for 5′-3′ exonucleases(Meyer et al., 2004). In addition, in the cytoplasm the nuclear cap binding proteins are replaced by the translation initiation factor, eIF-4E. The cap bound to eIF-4E and other translation initiation factors enhances translation by promoting the engagement of the ribosomal subunits with the mRNA (Shatkin and Manley, 2000). This is at least partly

achieved by the interaction of eIF4G with poly(A)-binding protein (PABP), resulting in a translationally competent circular mRNA-protein complex (Mangus et al., 2003).

1.10.2 - Splicing -

With a few exceptions mammalian genes are interrupted by noncoding sequences (introns) and to generate a functional message from the DNA template, mRNA splicing must occur. The transcribed pre-mRNA contains several consensus elements, which are essential for the splicing reaction. The 5′ exon-intron junction or splice site is marked by the consensus sequence AG/***GU****RAGU* (R, purine; Y, pyrimidine). The end of the intron, the 3′ splice site, is defined by $(Y)_nNYAG$/RNNN. About 20-50 nt upstream of the 3′ splice site lies the branchpoint $CURA^{2OH}Y$ with a highly conserved adenosine followed by the pyrimidine-rich track.

Splicing event occurs in two transesterification reactions whose net result is the fusion of two exon sequences and the release of the intervening intron as a loop-shaped structure. Five U-rich small nuclear RNAs (snRNAs) U1, U2, U4, U5, and U6 associated with proteins in small nuclear ribonucleoprotein particles (snRNPs), together with many other proteins, assemble over the intron to form the spliceosome, the ribonucleoprotein complex that catalyzes the splicing events. Interaction of the U1 snRNA with the 5′ splice site initiates spliceosome assembly. The 3′ splice site and adjacent pyrimidine tract are identified through interactions with a dimeric splicing factor U2AF35/65. This in turn, helps recruits U2 snRNP to the branchpoint. After U1 and U2 snRNPs associate with the pre-mRNA, the trimeric snRNP complex of U4, U5 and U6 join the initial complex to form the spliceosome. After formation of the spliceosome, extensive rearrangements in the pairing of snRNPs and the pre-mRNA lead to the release of the U1 and U4 snRNPs and convert the spliceosome into a catalytically active conformation which mediates the first transesterification reaction. Following further rearrangements between the snRNPs, the second transesterification bonds the two exons releasing the intron associated with the snRNPs (Rio, 1993).

1.10.3 - 3' end formation: polyadenylation signals and machinery -

An essential step in protein encoding mRNAs maturation and transcription termination is posttranscriptional cleavage of mRNA precursor. After cleavage, most eukaryotic mRNAs, with the exception of replication-dependent histone transcripts (in higher eukaryotes), acquire a poly(A) tract that in mammalian consists of 150-250 adenosine residues at their 3′ ends. The formation of this poly(A) tail is directed by

sequences present in the pre-mRNA, the *polyadenylation signals* (*cis*-regulatory elements), and by the polyadenylation machinery, consisting of at least six multimeric proteins, the *cleavage and polyadenylation factors* (*trans*-acting factors) (Wahle and Kuhn, 1997; Wahle and Ruegsegger, 1999; Zhao et al., 1999).

- *Mammalian polyadenylation signals* -

The 3'-end processing consisting in the cleavage of a eukaryotic transcript and the poly(A) tail addition occurs at specific *polyadenylation sites* [poly(A) sites] (also called cleavage sites) located downstream from stop codons in the 3'-untranslated region (UTR). The genomic sequence surrounding a poly(A) site is referred to as the poly(A) region.

A

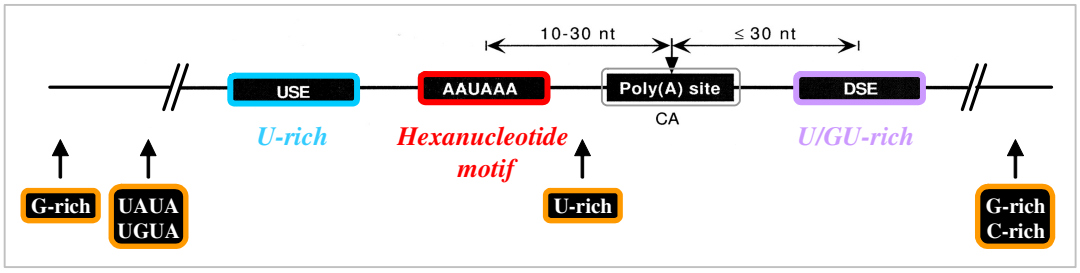

B

	Frequency (%) Hs	Mm	Hs.B
AAUAAA	53.18	59.16	58.2
AUUAAA	16.78	16.11	14.9
UAUAAA	4.37	3.79	3.2
AGUAAA	3.72	3.28	2.7
AAGAAA	2.99	2.15	1.1
AAUAUA	2.13	1.71	1.7
AAUACA	2.03	1.65	1.2
CAUAAA	1.92	1.80	1.3
GAUAAA	1.75	1.16	1.3
AAUGAA	1.56	0.90	0.8
UUUAAA	1.20	1.08	1.2
ACUAAA	0.93	0.64	0.6
AAUAGA	0.60	0.36	0.7

Figure 1.12: Elements of mammalian polyadenylation signals. Panel A shows a schematic representation of the positions and sequence features of the elements that define a mammalian polyadenylation signal. The hexanucleotide motif, polyadenylation or cleavage site (frequently defined by the CA dinucleotide), USE (upstream element) and DSE (downstream element) are evidenced with red, gray, blue and violet boxes, respectively. In orange boxes are indicated some putative auxiliary elements identified by *in silico* analyses. The scheme of Panel A is adapted from Zhao et al., 1999 and Hu et al., 2005. The table in Panel B indicates the frequency of the hexanucleotide motif variants in the humans (Hs) and mice transcriptomes (Mm) reported by Tian et al., 2005 and identified in humans one by Beaudoing et al., 2000 (Hs.B).

In mammalian poly(A) regions, several elements define the core *polyadenylation signal* determining the use of a specific poly(A) site: the highly conserved hexanucleotide AAUAAA motif found 10-30 nt upstream of the poly(A) site and the less conserved elements located upstream and downstream it (upstream and downstream elements, USE and DSE, respectively) and the poly(A) site itself. Additional sequences outside of this core recruit regulatory factors or maintain the core signal in an open and accessible structure (Zhao et al., 1999) (Figure 1.12 A). Some features of these *cis*-regulatory elements are described below:

- *Hexanucleotide or AAUAAA motif*. The consensus sequence AAUAAA was initially revealed by a comparison of nucleotide sequences preceding the poly(A) sites in several mRNAs (Proudfoot and Brownlee, 1976) and then has been found in most polyadenylated mRNAs of animal cells (Zhao et al., 1999). Extensive mutagenesis studies and the analysis of naturally occurring mutations have conclusively established that this hexanucleotide is essential for both cleavage and poly(A) addition (Manley, 1988; Wahle and Keller, 1992). The sequence AAUAAA is one of the most highly conserved sequence elements known (Proudfoot, 1991). Several groups, analysing human ESTs and UTRdb using different algorithms, estimated AAUAAA incidences varying from 48.1 to 59% and identified numerous single-base variants of the canonical AAUAAA hexamer (Figure 1.12 B) (Beaudoing et al., 2000; Beaudoing and Gautheret, 2001; Gautheret et al., 1998; Graber et al., 1999; Tabaska and Zhang, 1999; Tian et al., 2005). In all the hexanucleotide signal variants positions 3, 4, and 6 are highly conserved, while positions 1, 2 and 5 are tolerant to point mutations. They are described by an NNUANA consensus (where N is any nucleotide). This suggests a model where an unique polyadenylation machinery is tolerant to a limited level of mutation in its regular signal. The most frequent variant is AUUAAA (incidence from 10.9 to 17%) (Figure 1.12 B), whose activity is comparable to that of the canonical sequence: it directs cleavage *in vitro* with an efficiency of 66%, relative to the wild-type level (Sheets et al., 1990). Mutations of any other nucleotide strongly reduce the cleavage and polyadenylation efficiencies *in vitro* (Conway and Wickens, 1987; Sheets et al., 1990) and *in vivo* (Wickens and Stephenson, 1984). The abundance of single-base variants of AAUAAA correlates with their measured processing efficiencies (Graber et al., 1999). In addition, the reduced processing efficiency correlated to the hexanucleotide variants is also confirmed by the evidence that the number of ESTs associated with the canonical AAUAAA hexamer is higher than that associated with any other variant of the signal

(Beaudoing et al., 2000; Tian et al., 2005). However, polyadenylation efficiency does not strictly depend on the hexameric signal: “strong” sites may contain variant signals while “weak” sites may comprise canonical AAUAAA hexamers. In fact, the flanking USE, DSE and in auxiliary sequences also affect polyadenylation efficiency (Legendre and Gautheret, 2003). In addition, polyadenylation signals with hexamer motif variants are usually associated with alternative or tissue-specific polyadenylation (Edwalds-Gilbert et al., 1997).

- *Downstream element (DSE)*. The second element of the core polyadenylation signal is within approximately 30 nt downstream of the poly(A) site (Figure 13 A). This element is observed in a large portion of genes and is poorly conserved. Two main types of DSEs have been described, a U-rich element and a GU-rich element (Figure 1.12 A). The U-rich element is a short run of U residues (Chou et al., 1994; Gil and Proudfoot, 1987). The GU-rich type has the consensus like YGUGUUYY (Y = pyrimidine) in several genes(McLauchlan et al., 1985). A polyadenylation signal may have only one DSE (Chou et al., 1994; McDevitt et al., 1986) or may have both a U-rich element and a GU-rich element working together synergistically (Gil and Proudfoot, 1987). However, some DSEs contain no matches to either the canonical U- or GU-rich motif (Sittler et al., 1994). The proximity of the DSE to the poly(A) site can affect the cleavage site position (Mason et al., 1986) and the efficiency of cleavage (Gil and Proudfoot, 1987; McDevitt et al., 1986). Point mutations or small deletions in the DSE have only weak effects, while larger deletions are required to abolish polyadenylation process: this is in agreement with the idea that the DSE is poorly defined and possibly redundant (Zarkower and Wickens, 1988) and evidenced that this element is required for an efficient processing of the mRNA 3’-end.

- *Poly(A) site*. The selection of the cleavage site is determined mainly by the distance between the upstream AAUAAA sequence and the DSE (Chen et al., 1995). The local sequence surrounding the cleavage site is not conserved, although adenosine is found at the cleavage site of 70% of vertebrate mRNAs(Sheets et al., 1990). Thus, the first nucleotide of the poly(A) tail in most mRNAs is probably template encoded(Moore et al., 1986; Sheets et al., 1990). A study involving saturation mutagenesis demonstrated that the order of preference for the cleavage site nucleotide follows the order of A > U > C ≫G (Chen et al., 1995). The penultimate nucleotide is most often a C residue (in 59% of all genes analysed) (Sheets et al., 1990). Thus, a CA dinucleotide defines the poly(A) site for most genes (Figure 1.12 A).

- *Upstream element (USE)*. This sequence element is common among viral polyadenylation signals, such as adenovirus (E3, L1, L3 and L4), Epstein-Barr virus, simian virus 40 (SV40) late, ground squirrel hepatitis virus, and retroviruses such as human immunodeficiency virus type 1 (HIV-1) (Zhao et al., 1999). More recently, functional USEs have also been identified in the poly(A) regions of many cellular genes such as complement factor C2 (Moreira et al., 1995), lamin B2 (Brackenridge et al., 1997), collagen (Natalizio et al., 2002), cyclooxygenase isoenzymes-2(Hall-Pogar et al., 2005), etc. The position and sequence of the USE are poorly defined. It is often a U-rich sequence, in which a consensus sequence has not emerged, located within the 100 nt upstream the AAUAAA element (Hu et al., 2005) (Figure 1.12 A). Its role in both viral and cellular genes is to enhance the polyadenylation process: it improves the cleavage efficiency by acting as recognition site for 3'-end processing factors (Carswell and Alwine, 1989; Hall-Pogar et al., 2007; Moreira et al., 1998).
- *Auxiliary sequences*. In addition to the above mentioned core polyadenylation signal sequences, some auxiliary elements localised upstream and/or downstream the poly(A) site that can generally enhance polyadenylation efficiency in both viral and cellular systems have been characterised. G-rich sequences (GRS) located downstream of the DSE are common positive auxiliary elements in mammalian polyadenylation signals. The SV40 late pre-mRNA contains a GRS in its polyadenylation site downstream of U-rich element that is able to enhance processing efficiency (Bagga et al., 1995; Chen and Wilusz, 1998). More recent studies revealed that ~34% of mammalian polyadenylation signal contain short GRS in the region downstream the DSE. All the analysed GRS bind hnRNP H/H' stimulating polyadenylation events (Arhin et al., 2002). Recently, a bioinformatic analysis of human cDNA/ESTs sequences revealed that poly(A) sites may have an additional set of *cis*-acting elements that were conserved among yeast and plants and may be involved in the regulation of mRNA polyadenylation. These novel elements include upstream and downstream G-rich and C-rich elements, as well as other upstream elements (Figure 1.12 A). The functions of all these sequences remain to be validated (Hu et al., 2005). Moreover, other sequences which are binding sites for splicing factors can positively or negatively modulate the efficiency of 3′ processing (Section 1.11.2)

The elements described above are thought to work by acting as sequence recognition sites for factors that stabilise the polyadenylation complex. However, it was evidenced that the secondary structure of these elements influences polyadenylation.

For instance, secondary structure downstream of the murine secretory immunoglobulin M poly(A) site is critical for positively regulating the use of this site (Phillips et al., 1999), while a stem-loop containing the HIV-1 core poly(A) signal (Klasens et al., 1999) and base-pairing in HDV mRNA (Hsieh et al., 1994) reduce 3'-end processing.

Three possible mechanisms by which auxiliary elements and USE enhance *in vitro* 3'-end processing have been proposed. First, these sequences can promote processing efficiency by maintaining the core elements in an unstructured domain, which allows the general polyadenylation factors to efficiently assemble on the RNA substrate. Second, they can enhance processing by forming a stable structure, which helps focus binding of cleavage stimulation factor (CstF) to the core elements of polyadenylation signal preventing the factor from sliding along the pre-mRNA. Finally, the interaction of specific proteins with these sequences may play an active role in stimulating 3'-end processing, probably increasing or stabilising the association of the polyadenylation factors with the RNA substrate. Therefore, these sequences serve as an integral part of the polyadenylation signal affecting signal strength and possibly regulations (Chen and Wilusz, 1998).

Although critical, the mechanisms of polyadenylation site selection are not yet fully understood. In particular, it is not completely clear how the polyadenylation machinery is able to distinguish *bona fide* polyadenylation signals from the multiple look-alikes interspersed along the 3'-UTR. It seems that among the potential polyadenylation sites it is selected the one that allows a stable assembly of the polyadenylation machinery (Weiss et al., 1991). In fact, the strength of *cis*-regulatory elements for binding *trans*-acting factors can determine the efficiency of the polyadenylation reaction in a specific site. Therefore, not strictly the presence of a "strong" (efficiently processed) hexanucleotide motif but also the sequences flanking it, DSE, USE and auxiliary sequences contribute to the definition of *bona fide* polyadenylation sites from randomly occurring hexamer motifs (Legendre and Gautheret, 2003). This is demonstrated by the evidence that alterations of the 3' regions of genes induce variations in polyadenylation site selection and processing of transcripts causing a number of diseases (Chen et al., 2006).

- *Cleavage and polyadenylation factors* -

Multiple protein factors, generally highly conserved, are required for the formation of mRNA 3'-ends. The main factor involved in cleavage and polyadenylation in mammals are described below (Zhao et al., 1999).

- *Cleavage/polyadenylation specificity factor (CPSF)*: is required for both the cleavage and poly(A) addition reactions and, consistent with this function, recognises AAUAAA, a signal also essential for both reactions. The binding of purified CPSF is very weak but can be greatly enhanced by a cooperative interaction with cleavage stimulating factor (CstF) bound to the downstream signal sequences (DSE). It is a large protein complex containing basically160, 100, 70, and 30 kDa subunits, referred to as CPSF-160, CPSF-100, CPSF-73, and CPSF-30, respectively. The largest subunit (160 kDa) is crucial for AAUAAA recognition even if the participation of other CPSF subunits facilitates the recognition of the motif. CPSF-160 interacts specifically with the 77-kDa subunit of CstF and with Poly(A) polymerase (PAP), which is consistent with the cooperative interactions of CPSF with CstF or PAP in forming stable complexes on the RNA precursor. Interestingly, the 160 kDa subunit inhibits the activity of PAP in nonspecific assays, implying that CPSF may facilitate both poly(A) synthesis and termination. The 100 and 73 kDa subunits of CPSF are closely related and possess endonuleolytic activity. CPSF-73 seems to catalyze the cleavage reaction. The role of CPSF-30 is most probably to cooperate with CPSF-160 in the recognition of RNA substrates and, through an interaction with Poly(A)-binding protein (PABP) to stabilise the polyadenylation complex.

- *Cleavage stimulation factor (CstF)*: interacting with the DSE it is necessary for mRNA cleavage. It can also stimulate poly(A) addition on substrates binding to the USE. It consists of three polypeptides of 77, 64, and 50 kDa. CstF-77 was shown to be the middle subunit bridging CstF-64 and CstF-55 and its direct interaction with CPSF-160 probably contributes to stabilisation of the CPSF-CstF-RNA complex. CstF-64 binds the DSE of pre-mRNAs, while the 50-kDa subunit interacts with the C-terminus of CTD of RNA polymerase II.

- *Cleavage factors (CF) I_m and II_m*: are needed only for cleavage as they are supposed to form the endonuclease responsible for the cleavage of pre-mRNAs. CF I_m consists of fourth polypeptides and increases the stability of the CPSF-RNA complex, suggesting that this factor may also interact with CPSF and contribute to the overall stability of the 3'-end-processing complex. The interaction of CF I_m with RNA substrate seems to be an early step in the assembly of the 3'-end-processing complex, which facilitates the recruitment of other processing factors. CF II_m has not been purified and its function has not yet been clarified, but it is essential for cleavage.

- *RNA polymerase II (Pol II)*: the conserved C-terminal domain (CTD) of Pol II largest subunit has properties that make it an authentic cleavage factor. On the contrary, Pol II does not appear to be involved in the poly(A) addition step. CTD interacts with CPSF and CstF, this probably stabilise the cleavage complex or induce allosteric effects on it. The involvement of Pol II in cleavage is consistent with studies showing that protein-encoding mRNAs transcribed by Pol I and Pol III were mostly not polyadenylated, and that CstF colocalises with phosphorylated Pol II *in vivo*.
- *Poly(A) polymerase (PAP)*: is the key polypeptide in the process of polyadenylation. It catalyzes the addition of the poly (A) tail (activity which adds adenosine residues to the 3'-ends of RNAs), but also participates in the cleavage of pre-mRNA by stimulating or actively participating in the process. It is a polymorphic enzyme and exists in two active forms: PAP I and PAP II. In AAUAAA-dependent polyadenylation, PAP is recruited to the processing complex by interaction with CPSF-160. PAP, differently to the other polymerases, does not require a template strand: in fact, it. catalyzes the addition of adenosine to the 3'-end of mRNA in a sequence-independent manner
- *Poly(A)-binding protein (PABP)*: tends to form oligomers binding specifically to the poly(A) tail. It is required for the rapid elongation of the poly(A) tail and to control its length.

1.10.4 - Steps in processing: assembly, cleavage, and polyadenylation -

The mutually cooperative interactions of CPSF, CstF, CF I_m, PAP, and PABP in catalyzing accurate and efficient cleavage and polyadenylation have been well documented (Wahle and Kuhn, 1997; Wahle and Ruegsegger, 1999; Zhao et al., 1999). Figure 1.13 shows the model of mRNA 3'-end formation in mammalian cells. The initiating step in the assembly of a functional cleavage/polyadenylation complex is the recognition of signals on the pre-mRNA by CPSF and CstF in a process assisted by CF I_m. CPSF binds to AAUAAA element through CPSF-160 with the help of the others CPSF subunits, and CstF binds to the DSE via CstF-64. The individual interactions of CPSF and CstF with their cognate sequences are weak but are stabilised by the cross-factor interaction of CPSF-160 and CstF-77. A final component of the initiation complex is Pol II. The CPSF-CstF interactions define the region in which cleavage site must lie. The formation of a cleavage-competent complex requires the additional recruitment of CF II_m and PAP. The contacts of CF I_m and CF II_m with the other factors

and RNA are not known, but PAP at this point probably interacts with CPSF-160. The assembly of all of these factors may be sufficient to enable cleavage to occur.

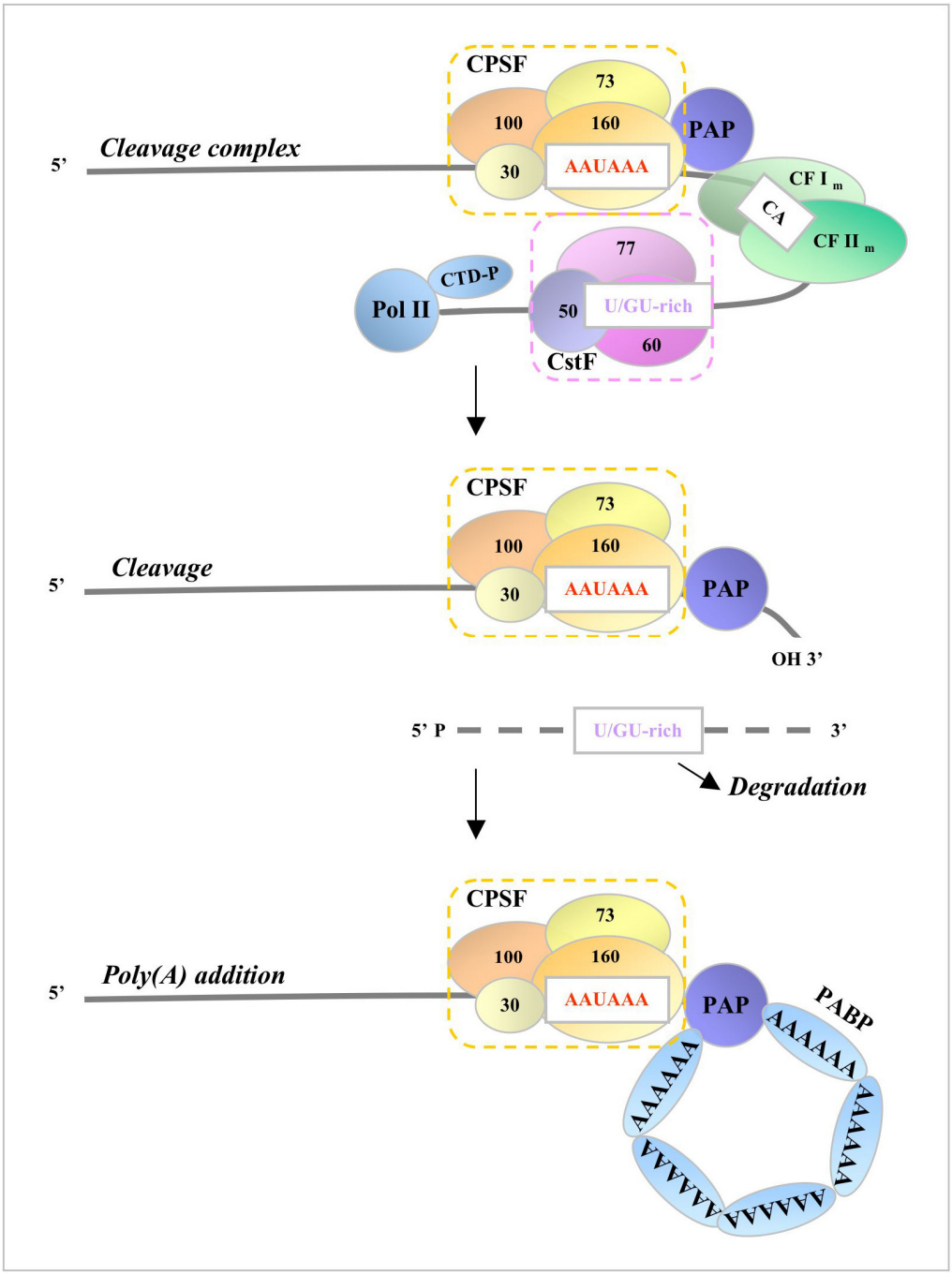

Figure 1.13: Schematic representation of mammalian mRNA 3'-end processing. The cleavage complex formation, cleavage and poly(A) tail synthesis steps are indicated. The scheme is adapted from Zhao et al., 1999.

There is no indication of a reorganisation of the complex before catalysis, as occurs during the splicing reaction. However, since it seems that reconstitution of polyadenylation *in vitro* requires only CPSF and PAP, significant changes probably take place after cleavage, with release and degradation of the 3'-cleavage product and

dissociation of the CstF, Pol II, CF I_m, and CF II_m cleavage factors. The situation may be different in the cell, with some factors remaining in the processing complex. This possibility is supported by evidences that CstF can stimulate polyadenylation if a CstF-binding site is present upstream of the hexanucleotide motif. Assembly and cleavage are followed by polyadenylation. The interaction with CPSF serves to recruit PAP to the AAUAAA-containing substrate. A complex of CPSF and PAP is adequate for a slow polymerisation of an adenosine tract, but full processive activity requires PABP. In fact, the poly(A) addition is slow (distributive synthesis) for the first 11-14 adenosine residues until a binding site for PABP has been created. Then, when PABP binds to this initial tail, it increases the stability and processivity of the PAP-CPSF complex and therefore stimulates the rapid elongation of the poly(A) tail to the final 150-250 adenosine residues found on nuclear poly(A) mRNA. When the tails reach this length, processive elongation switches to a slow and distributive mode again. PABP is necessary to terminate poly(A) addition at this point, but the mechanism to regulate the length of the added tail is not yet clear.

Poly(A) tail synthesis termination seems to be coupled with the disruption of the critical interaction between CPSF and PAP and their release from the finished product. The dissociation of the polyadenylation complex is followed by the release of the final product. It is very important to notice that cleavage and polyadenylation are closely coupled. The fact that PAP and CPSF are in involved in both the reactions indicates that cleavage is immediately followed by the release of the final product.

1.10.5 - Role of the poly(A) tail -

Poly(A) tails are essential structural and functional elements of eukaryotic mRNAs. They are important for the regulation of mRNA export from the nucleus to the cytoplasm, mRNA stability, translation initiation and efficiency. Transcripts which are not polyadenylated, or cleaved in the case of histone mRNAs, are degraded or not transported efficiently into the cytoplasm, and the amount of protein expressed from that gene decreases (Huang and Carmichael, 1996; Sachs and Wahle, 1993).

The role of poly(A) tail in nuclear export is probably attributable to PABP. In fact, there is evidence that the yeast equivalent of PABP interacts with nucleoporines and nuclear pore associated proteins. This view is consistent with the observed nucleocytoplasmic shuttling of yeast and mammalian PABPs (Mangus et al., 2003).

The poly(A) tail of mRNA promotes translation in synergy with the cap. This function is mediated by the interaction of the PABP with a number of translation

factors, including the initiation factors eIF4G and the termination factor eRF-3 (Mangus et al., 2003; Sachs et al., 1997). The interaction of the scaffold factor eIF4G with both the cap-binding factor eIF4E and PABP circularises the mRNA into the "closed loop" complex. This complex is thought both to stabilise the association of the cap-binding initiation factors and to facilitate the recycling of ribosomes that have terminated their translation of the mRNA. In addition, the regulation of poly(A) tail length controls mRNAs translation in the oogenesis and early development of many animal species. In most cases, long poly(A) tails (80–500 adenine residues) correlate with translation, and short tails (20–50 A) with repression of translation. Many of these regulated mRNAs are maternal, which are stored in an translationally inactive form in the growing oocyte and are translationally activated at specific stages of oocyte or early embryo development (Sonenberg and Dever, 2003).

The mRNA stability is mainly regulated by the presence of the PABP at the level of the poly(A) tail (Mangus et al., 2003). In the two general processes of mRNA degradation, decapping and deadenylation pathways, poly(A) tail removal occurs before the transcripts is degraded (Meyer et al., 2004). PABP can be an antagonist of poly(A) shortening: in fact, its presence on the poly(A) tail provides a protective effect, which is, in part, attributable to physical hindrance of the deadenylase and in part to inhibition of deadenylase activity. Moreover, PABP can facilitate and stabilise the binding of additional factors to their target sequence in the 3'-UTR, which mainly retard rapid mRNA decay precluding access of endonuclease to their recognition site (for example, αCP proteins in the 3'-UTR of α-globin mRNA). As noted above, PABP also interacts with the termination factor eRF3, a consequence of which is a decrease in the number of PABP multimers associated with the poly(A) tail. This observation links translation termination to poly(A) shortening and suggests one mechanism for orchestrating a standardized 'clock' that limits the lifetime of a poly(A) tail and, in turn, the mRNA to which it is appended (Mangus et al., 2003).

1.11 Crosstalk between mRNA processing events

Although each of the reactions above described -capping, splicing and polyadenylation- can be analysed biochemically as distinct processes, they are interlinked and they influence one another's specificity and efficiency (Figure 1.14) (Proudfoot et al., 2002).

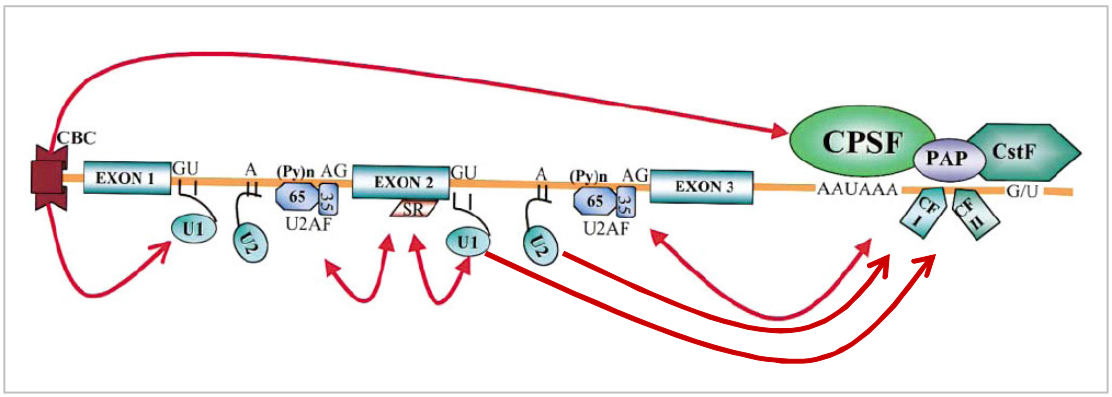

Figure 1.14: Molecular inter-connections between mRNA processing reactions. A schematic representation of the eukaryotic pre-mRNA structure is shown in the figure. Some of the main sequence elements and protein factors involved in capping, splicing and polyadenylation are indicated. Red arrows specify the interconnections between the mRNA processing reactions. The scheme is adapted from Proudfoot et al., 2002.

1.11.1 - Capping interactions with splicing and polyadenylation -

The capping process plays an important role in splicing significantly enhancing the formation of spliced mRNA. In fact, it was demonstrated that the cap structure enhanced the excision of the first, cap-proximal intron, but had a lesser effect on the splicing efficiency of the second intron. Depletion of the 80 kDa subunit of the cap-binding complex (CBC) resulted in significant inhibition of splicing. Furthermore, CBC positively influences the interaction of U1 and U6 snRNAs with the 5′ splice site. However, especially in mammalian systems, the question of how the cap and splicing components interacts remains unsolved. hnRNP F has been identified as a potential candidate that links the CBC with the splicing machinery. It can specifically interact with both CBC subunits and, moreover, hnRNP F-depleted extracts show a reduced splicing efficiency (Proudfoot et al., 2002).

Around the same time that the cap-splicing interconnection was discovered, a similar efficiency dependence of polyadenylation on the cap structure was showed. The cap structure has been shown to enhance the efficiency of 3' processing *in vitro* (Cooke and Alwine, 1996; Gilmartin et al., 1988; Hart et al., 1985). The addition of a cap analogue to HeLa cell nuclear extract resulted in a reduction in poly(A) site cleavage. Moreover, uncapped pre-mRNAs were found to be poorly processed by nuclear extracts, and to compete less efficiently for 3' processing factors than capped pre-mRNAs. It was discovered that CBC plays a key role in pre-mRNA recognition and 3'-end processing. It enhanced the cleavage reaction significantly, but showed only a modest effect on the poly(A) addition reaction. Similar to splicing, CBC appeared to have a stabilising effect on the polyadenylation complex with its target pre-mRNA. It

was also evidenced that the communication between the 5'-and 3'-ends of the pre-mRNA during processing is mediated by the physical association of the CBC with 3' processing factors bound at the poly(A) region. These data provides further support for the hypothesis that pre-mRNAs and mRNAs may exist and be functional in the form of "closed-loops," due to interactions between factors bound at their 5'-and 3'-ends (Flaherty et al., 1997).

1.11.2 - Connections between splicing and polyadenylation –

Several evidences have been accumulated in support of a physical connection between the splicing and the polyadenylation machinery (Figure 1.14). Depending on the context, splicing factors can stimulate or inhibit cleavage and poly(A) addition. Moreover, some of the interactions between splicing and polyadenylation factors appear to have evolved into regulatory mechanisms, and there are several cases in which the cell uses splicing factors to influence the decision of how or when to polyadenylate an mRNA precursor (Proudfoot et al., 2002). Splicing and polyadenylation cooperate in:

- *Recognition of constitutive 3'-terminal exons or 3'-terminal exon definition.*

Experiments that revealed the process of exon definition in RNA splicing evidenced that an interaction of splicing and polyadenylation factors could bridge the last exon and define its 3'-splice site and its poly(A) site (Niwa et al., 1992).

In higher eukaryotes the 3′ and 5′ splice sites are recognised synergistically through interactions stretching across the exon. SR proteins are the key players in this process. They are recruited to the exon through interactions between their RNA binding domains and specific exon enhancer sequences (exonic splicing enhancers). SR proteins also interact through serine arginine-rich (RS) domains with other RS domain containing proteins in U1 and U2 snRNPs. Considering that U1 snRNP contacts the 5'-splice site and the U2 snRNP defines the 3'splice site (the larger 65 kDa subunit of U2 snRNP interacts with the pyrimidine tract while the 35 kDa subunit directly contacts the 3′ splice site AG sequence, their interactions with the bridging SR proteins permit precise identification of the exon in the pre-mRNA (Konarska, 1998). This exon definition mechanism is also applied to the terminal exon of pre-mRNA, although in this case the end of the exon is defined by the poly(A) signal. Consequently, both splicing and polyadenylation factors interact to define the last exon affecting the efficiency of both the polyadenylation and last intron removal (Niwa et al., 1992). The cross talk of these two processes across a terminal exon involves factors such as U2AF U2 snRNP, which are associated with early recognition of the 3'-splice site. In fact,

U2AF65 is able to interact with the C-terminal domain of PAP and the 59 kDa subunit of CF I_m (Kyburz et al., 2006; Millevoi et al., 2006; Vagner et al., 2000). U2AF65/CF I_m complex stimulates *in vitro* cleavage and polyadenylation (Millevoi et al., 2006). Moreover, it was demonstrated that CPSF is necessary for efficient splicing activity and that mutations in the pre-mRNA binding site of the U2 snRNP resulted in impaired splicing and in more reduced cleavage efficiency (Kyburz et al., 2006).

In addition, alsoU1 snRNP and its components seem to be involved in the 3'-terminal exon definition and polyadenylation processes. For instance, 3'-end processing was stimulated at the SV40 late polyadenylation site by the interaction between snRNP-free U1A protein to USE (Lutz and Alwine, 1994). Moreover, the direct contact of U1A with the CPSF 160-kDa subunit stabilised the interaction of CPSF with its substrate stimulating polyadenylation process (Lutz et al., 1996). It was also demonstrated that snRNP-free U1A interacts with the polypyrimidine tract-binding protein-associated factor (PTB) forming a complex that was hypothesised to be involved in the recognition of the 3'-terminal exons (Lutz et al., 1998). Moreover, U1A and PTB were USE-specific factors able to promote the COX-2 alternative polyadenylation (Hall-Pogar et al., 2005). Finally, interaction between the U1 snRNP, PAP and CF I_m were also documented even though their functional role have to be determined (Awasthi and Alwine, 2003; Raju and Jacob, 1988).

Interestingly, terminal exon definition also appears to be employed in a negative way, as a number of studies demonstrate that poly(A) site recognition is inhibited by the proximity of a 5′ splice site (Proudfoot, 1996). This inhibition will not normally occur in the terminal exon of a gene but it may arise when a poly(A) site is positioned within the body of a gene. In papillomaviruses, which again maximize their gene expression repertoire by employing internal poly(A) signals, U1 snRNP 70 kDa subunit binding to the 5'-splice site results in inhibition of polyadenylation via a direct interaction with PAP (Gunderson et al., 1998). Examples of a similar type of regulation are well documented in retroviruses, where functional poly(A) signals may exist in the transcribed portion of the 5′ LTR sequence: promoter-proximal poly(A) site is repressed by interaction of the U1 snRNP with a downstream 5'splice site localised (Ashe et al., 1997).

- *Recognition of alternative 3'terminal exons.*

Another example of splicing and polyadenylation crosstalk comes from genes where alternative polyadenylation leads to the expression of different gene products. In

these genes poly(A) sites are located in different exons and the formation of the 3'-end is mediated by alternative splicing (Edwalds-Gilbert et al., 1997). Section 1.13.3 is focused on this topic.

1.12 Transcription and mRNA processing of protein-encoding gene

Despite capping, splicing and polyadenylation have traditionally been viewed as posttranscriptional processing events, in more recent years it has emerged that these reactions are not only capable of influencing each other but are also tightly linked to transcription therefore, it is now believed that most mRNA processing reactions occur cotranscriptionally. Much of this linkage involves the transcribing enzyme itself, RNA polymerase II (Pol II), and specifically the C-terminal domain of its largest subunit (CTD). A large body of evidence indicates that the CTD has a significant role in enhancing the efficiency of all three of the mRNA processing reactions (Bentley, 2005; Calvo and Manley, 2003; Proudfoot et al., 2002). The findings that evidence the association of polyadenylation and the different stages of gene transcription are elucidated below.

1.12.1 - Transcription initiation and elongation -

Experimental data evidence that certain polyadenylation factors can interact with the CTD, that this enhances polyadenylation efficiency, and that the interaction can begin back at the promoter (Calvo and Manley, 2003). The initial indication of an early and direct linkage of transcription and polyadenylation factors came from the discovery that the general transcription factor TFIID, which has a central role in promoter recognition and assembly of preinitiation complexes during transcription initiation, could be copurified with CPSF. In detail, the interaction with TFIID recruits CPSF to the promoter and brings its transfer to Pol II concomitant with transcription initiation (Figure 1.14) (Dantonel et al., 1997). Moreover, the findings that transcripts generated by Pol II lacking a CTD are not processed efficiently (splicing, polyadenylation, and transcription termination are all inhibited), that *in vitro* CTD binds not only CPSF but also CstF, (McCracken et al., 1997) and it is required for the 3' cleavage reaction even in the absence of transcription (Hirose and Manley, 1998), confirmed the association between polyadenylation and transcription processes.

Moreover, it was observed that several transcriptional coactivators, such as the yeast Sub1 (PC4 is equivalent to Sub1 in humans) and Ssu72 factors, whose function is to assure proper assembly of the transcription preinitiation complex at the promoter and

to help the transcriptional machinery to identify the start site of transcription, are associated to components of the polyadenylation machinery. These interactions ensure proper loading of the polyadenylation factors onto the transcriptional apparatus and influence downstream events. For instance, Sub1 interacts with CstF to modulate its activity at the 3'-end, whereas Ssu72 works in the context of CPSF to facilitate cleavage (Calvo and Manley, 2003).

In addition, more recent studies in yeast point to the existence of gene loops, in which a transcriptionally active termination region can be physically linked to its promoter site, whose function is probably to promote transcriptional reinitiation by facilitating recycling Pol II from the termination site to the promoter. Interestingly, it was observed that the looping is dependent upon Ssu72 and Pta1 (an additional factor of the polyadenylation machinery) components of the transcription preinitiation-3'-end processing complex (Ansari and Hampsey, 2005; O'Sullivan et al., 2004).

All these evidences point to an intricate and complex network of interactions that link events occurring at the 5'-and 3'-ends of the gene. Although there is still much to learn about how all these dynamic interactions are orchestrated, a remarkable implication of these findings is that the efficiency of polyadenylation might vary depending on the early events that happened at the promoter, for instance, the efficiency of loading of the polyadenylation factors onto the CTD (Calvo and Manley, 2003).

1.12.2 - Transcription termination downstream of the poly(A) site -

This final stage in the transcription process is critical for successful gene expression. Transcription termination allows release of mRNAs from the site of transcription and of Pol II from the DNA template facilitating the recycling of the enzyme back to the promoter for further rounds of transcription. Moreover, it ensures that promoters are not perturbed by read-through polymerases that have failed to terminate at upstream genes. Finally, it can also affect the utilization of an upstream poly(A) site influencing the amount of transcript derived from that gene. Several evidences have elucidated that transcription termination and polyadenylation processes are coupled: in fact, mature mRNA 3′ ends are formed by cotranscriptional RNA processing at positions upstream of the termination site. Thus, transcript cleavage at the poly(A) site leaves two products which have quite different fates: the upstream product, destined to become mRNA, is stabilised by poly(A) addition, whereas the downstream product, uncapped at 5'-end, is highly unstable and is rapidly degraded (Rosonina et al., 2006).

Role of the poly(A) signal and polyadenylation factors in Pol II termination

The demonstration that transcription termination is dependent on the presence of a functional polyadenylation process provided the first indication that mRNA maturation events and transcription are coupled events (Logan et al., 1987; Proudfoot, 1989). For instance, 3′ end processing was shown to be dependent on the presence of Pol II CTD both *in vivo* (McCracken et al., 1997) and *in vitro* (Hirose and Manley, 1998), as described above. Moreover, it was evidenced that mutations of the signals that specify polyadenylation event can prevent subsequent termination (Proudfoot, 1989), that poly(A) signal strength is directly correlated to termination efficiency (Osheim et al., 1999) and that the dependence of Pol II termination on RNA processing extends to splicing of the terminal intron (Dye and Proudfoot, 1999). These observations can be explained by the involvement of the terminal 3′ splice and poly(A) sites to define the terminal exon as described above (Niwa et al., 1992). However, considering the absolute requirement of a poly(A) signal for transcription termination, it is most likely that the dependence of termination on splicing is an indirect effect. Moreover, transcriptional analyses in yeast provided evidence that at least several of the proteins involved in 3' processing, subunits of the yeast equivalents of both CstF and CPSF, are required for termination (Dichtl et al., 2002).

To address the mechanistic basis for the connection between termination and cleavage/polyadenylation, two models have emerged: the so-called “allosteric” and “torpedo” models. The allosteric model, also known as the “antiterminator” model, proposes that transcription of the poly(A) site triggers conformational changes of the Pol II elongation complex (EC); for example, by recruitment of a negative elongation factor or release of an antitermination factor. Such changes would destabilise the complex, resulting in termination (Logan et al., 1987; Proudfoot, 1989). The “torpedo” model proposes that upon endonucleolytic cleavage of the nascent pre-mRNA at the poly(A) site, a 5'→3' exonuclease degrades the downstream cleavage product while it is still tethered to Pol II. The exonuclease continues degrading the transcript until it reaches, and somehow destabilises the EC, causing termination (Connelly and Manley, 1988). Although both models rely on recognition of the poly(A) site, a fundamental difference is that only the “torpedo” model depends upon the successful endonucleolytic cleavage of the nascent RNA to create the entry site for the 5'→3' exonuclease. The results of studies on Pol II transcription termination carried out over the past decade have indicated that these two models are not mutually exclusive. Rather, a new version,

combining the antiterminator and torpedo models, is likely to prevail (Rosonina et al., 2006).

Role of Pausing of Pol II in transcription termination and polyadenylation

Since it is clear that RNA processing signals affect transcription, it follows that the reverse effect of transcriptional events influencing RNA processing occurs. Thus, transcriptional pause sites located downstream of the poly(A) site are thought to cause a transient pause to Pol II progression and so enhance poly(A) site recognition. Studies on a number of genes have identified such pause sites. The strongest evidence for an involvement of transcriptional pausing in 3′ end processing and termination comes from studies in yeast. In *S. pombe*, the poly(A) signals of the *ura4* and *nmt2* genes both possess downstream sequence elements (DSE) that are required for efficient 3′ end processing and induce transcription termination. Studies in mammalian cells also indicated the presence of transcription pause sites (where Pol II may pause as a result of protein roadblocks). One of these sites was discovered between the closely spaced α-globin genes and the C2 and factor B genes. Analysis of pause sites in a coupled *in vitro* transcription-polyadenylation system showed that in some situations they can increase the efficiency of cleavage and polyadenylation and thereby promote termination (Proudfoot et al., 2002).

More recently, it was described that poly(A) site alone can pause the polymerase as it moves down on the template and consequently it promotes transcription termination (Orozco et al., 2002). This poly(A)-dependent transcriptional pause is mediated by CPSF. It specifically recognises poly(A) signal hexamer and, acting as a negative transcription elongation factor, it transmits a signal from the hexanucleotide motif to the body of the polymerase inducing the pause (Nag et al., 2007).

1.13 Transcriptional and post-transcriptional regulation of gene expression

One of the lessons learned from the sequencing of the mammalians genome is that diversity of gene expression is largely due to post-transcriptional mechanisms. In fact, initial estimates of as many as 120000 expressed genes in humans (Liang et al., 2000) are greatly in excess of the number of 20000–25000 protein coding genes (Consortium, 2004). Alternative transcription initiation correlated to differential promoters, alternative splicing, and alternative polyadenylation are the three mechanisms through which a variety of transcripts can be synthesised from a single

eukaryotic gene (Black, 2003; Edwalds-Gilbert et al., 1997; Landry et al., 2003). Therefore, the combination of these processes largely contributes to transcript diversity in complex genomes such as those of mammalians.

1.13.1 - Alternative promoters -

Transcription initiation of eukaryotic protein-coding genes is regulated by multiple binding DNA sequences, generally referred as transcription-control regions. These include *promoters* localised in the proximity of the transcription start site (TSS) and other types of sequences, called *enhancers* and *silencers*, located commonly far from the genes that they regulate (up to 50 kb upstream or downstream from the TSS or within an intron). In the promoter region it is possible to distinguish more conserved *core promoters elements* and other *proximal promoter elements* (Lodish, 2003).

The core promoters generally extend from ~40 bp upstream (– 40) to ~40 bp downstream (+ 40) of the TSS (+ 1) and contain different combinations of various functional DNA motifs (Figure 1.15). In the eukaryotic genes, it is the minimal DNA region that recruits the basal transcription machinery to direct efficient and accurate transcription initiation. In fact, its elements direct the recruitment and assembly of the class II basal/general transcription factors (TFIIA, TFIIB, TFIID, TFIIE, TFIIF and TFIIH) and RNA Pol II into the functional pre-initiation complex (PIC) at the TSS and thus determine the intrinsic "basal" (i.e., unregulated) transcription activity of the core promoter. The specific core promoter sequence also influences the transcriptional response of a given gene to particular enhancers and gene-specific transcription regulators. Thus, the information contained within the DNA sequence of the core promoter is critical for the proper regulation of gene-selective transcription in eukaryotes (Smale and Kadonaga, 2003).

As mentioned above, different sequence elements can co-occur in the same promoter, although certain combinations are more likely than others. It was found that the pattern of regulatory elements of a promoter is commonly conserved across orthologous genes. The best studied core promoter consensus motifs are the following ones (Sandelin et al., 2007; Smale and Kadonaga, 2003) (Figure 1.15):

- *TATA box*: located 28–34 bp upstream of the TSS, is the best known transcription factor binding site. Its consensus sequence, TATAA, is recognised by the TATA-box binding protein (TBP), which is part of the PIC. Binding of TBP to the TATA box enforces the PIC to select a TSS in a limited genomic space.

- *Initiator element (Inr)*: defined by the YYANWYY consensus where the A is at position +1. It is independent of the TATA box, although the two can occur together and act synergistically. The TATA and Inr elements are the only known core promoter elements that, alone, can recruit the PIC and initiate transcription.
- *Downstream promoter element (DPE)*: lies 28–32 bp downstream of the TSS in TATA-less promoters and it has a RGWYV consensus. Generally, it occurs together with Inr elements. The DPE is thought to have a similar function to the TATA box in directing the PIC to a nearby TSS.
- *TFIIB recognition element (BRE)*: has an SSRCGCC consensus and is located upstream of the TATA box in some TATA-dependant promoters. It can either increase or decrease transcription rates, although the details of this mechanism are unknown.
- *CpG island*: CpG islands are genomic regions devoid of methylation in which CG dinucleotides are over-represented. Commonly, 20-50 CG stretches are located within 100 bp upstream of the TSS. Only a fraction of CpG-associated promoters have TATA-like elements.

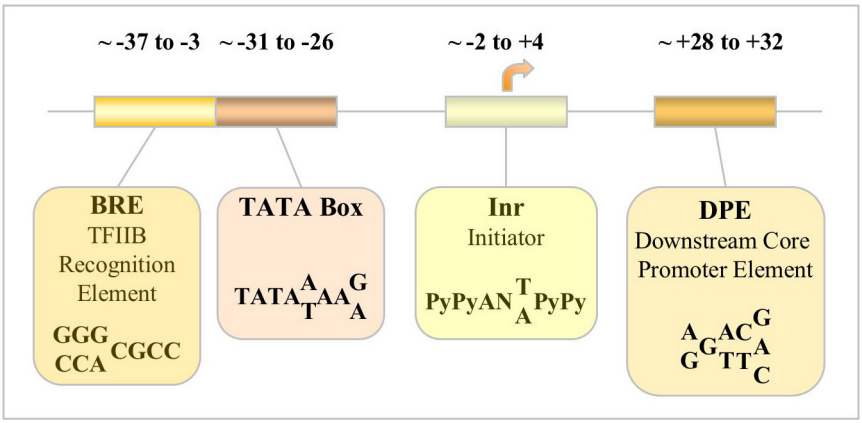

Figure 1.15: Core promoter consensus motifs. The diagram depicts some of the principal elements that can contribute to basal transcription from a core promoter. The numbers indicate the element positions in relation to the transcription starting site (TSS: +1). The consensus sequences that characterised each element are shown in the boxes (symbols: N, any nucleotide; A or G –Purine-; C or T -Pyrimidine-). The scheme is adapted from Smale and Kadonaga, 2003.

Proximal promoter elements are located in the sequence upstream of the core promoter, usually from -50 to -200 bp relative to TSS, and are frequently cell-type specific. There are multiple recognition sites for specific transcription factors and include (Lodish, 2003):

- *GC-boxes:* elements with a consensus GGGCGG that are often found within 100 bp of TSS and bound the Sp1 transcriptional factor (also called Sp1-boxes);

- *CCAAT-boxes:* elements typically located near position -75 whose consensus sequence GGCCAATCT. They are recognised by transcription factors CTF and CBF.

Both GC-and CCAAT-boxes modulate basal transcription of the core promoters operating as enhancer sequences.

Recently, the CAGE (Cap analysis of gene expression) tag analysis of the mammalian "promoterome" provided a truly global insight into the sequence structure of core promoters and the expression dynamics associated with core promoters. Strikingly, several classes of promoter types were identified on the basis of the differential usage of TSSs (Carninci, 2007). At the extreme ends of the spectrum, two significant classes of promoters can be defined: (*a*) "sharp" promoters, which have a relatively tightly defined TSS position within a few base pairs and (*b*) "broad" promoters, which show a random distribution of many TSSs in a 100-bp window. Remarkably, "sharp" promoters were found to be more likely associated with TATA boxes and to possess a higher frequency of transcription factor binding sites than broad peak promoters. The latter often carry CpG islands, are TATA-less, and are associated with less consensus binding sites. Moreover, it seems that TATA box-associated "sharp" promoters are involved in tight regulation of genes, which are often tissue-specific. In contrast, the "broad" promoters are often associated with ubiquitously expressed genes (housekeeping gene) (Carninci et al., 2006; Schug et al., 2005; Yang et al., 2007). In addition, from similar studies it became clear that the TATA box, which was once believed to be a general feature of core promoters, is only present in 10-20% of all human Pol II promoters, while 72-76% of human promoters are associated with CpG islands (Gershenzon and Ioshikhes, 2005; Saxonov et al., 2006; Yang et al., 2007). The existence of TATA-less promoters regulating tissue-specific genes (Gustincich et al., 2006; Nomoto et al., 1999) demonstrates that the regulatory logic suggested by the above genome-wide tendencies cannot be universally applied to gene activation.

A great number of rat, mouse and human genes are associated with more than one promoter region (Carninci et al., 2006; Cooper et al., 2006; Kimura et al., 2006; Landry et al., 2003). In detail, genome-wide analyses of mammalian genome evidenced that 52-58% of protein-coding genes are subjected to regulation by alternatives promoters (Carninci et al., 2006; Cooper et al., 2006; Kimura et al., 2006; Landry et al., 2003). The existence of alternative promoters for genes is an important source for generating protein and regulatory diversity. In fact, as Figure 1.16 shows, the presence

of differential promoters in one transcript and consequently their use can induce the formation of (Landry et al., 2003):

- *Transcript variants with diverse transcription pattern and translation efficiency.*

For many genes having multiple promoters no variation in the resulting proteins has been reported (60–80% of genes showing alternative promoters). In these genes, although the mRNAs have alternative initial exons, a common downstream exon contains the translation start site (AUG codon) and they therefore have the same open reading frame (ORF) (Figure 1.16 A). Although no protein isoforms are generated in these instances, the mRNA variants differ in their transcriptional patterns and translational efficiencies. These alternative promoters have different tissue specificity, developmental activity and/or expression level or the variant 5′ UTRs might differ in their secondary structure and/or presence of upstream ORFs, which can affect translation (Landry et al., 2003).

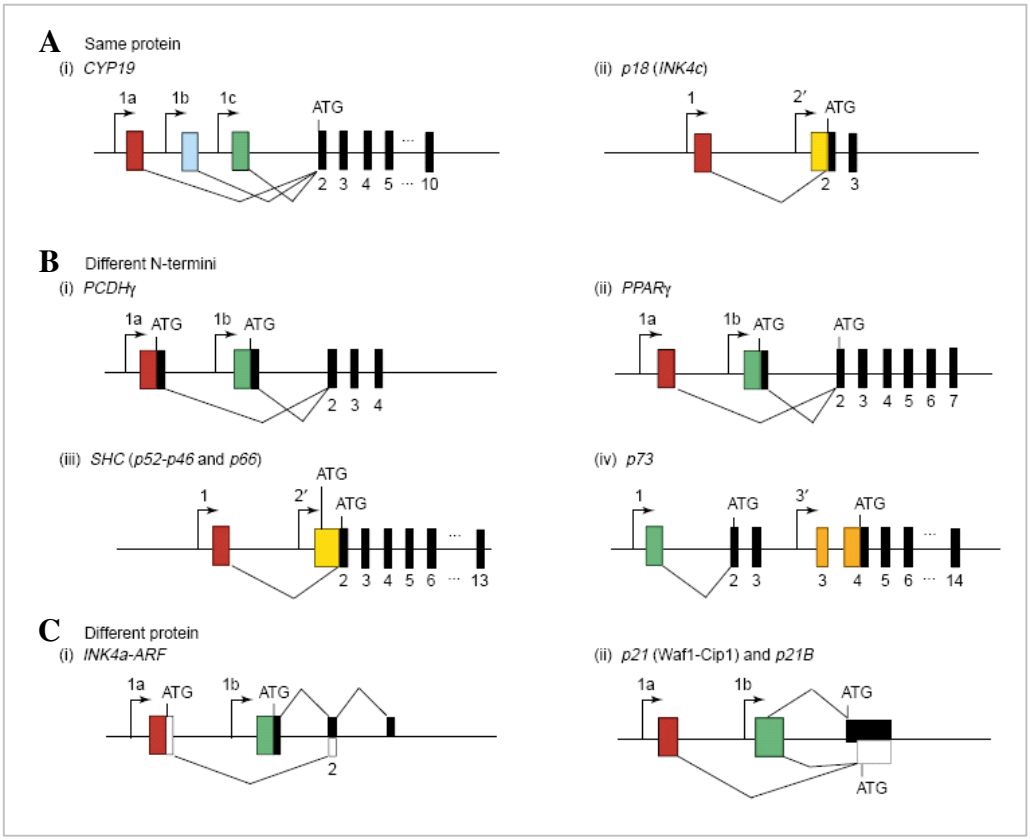

Figure 1.16: **The types and consequences of alternative promoters.** In Panels A and B are represented the use of multiple promoters producing mRNAs that does not result in protein isoforms. The use of the alternative promoters creating transcripts that code for different proteins, as they are translated in different reading frames (represented by the black and white boxes), is represented in Panel C. An example of genes representing each type of alternative promoter usage is given. In all the Panels, black and coloured boxes illustrate the variant 5′ initial exons and common coding exons, respectively, and splicing is represented by solid lines. 3′ UTRs are not shown. In some cases, not all promoters are shown. The figure is adapted from Landry et al., 2003.

- *Protein isoforms with different N-terminus*. In some cases, transcripts driven from different promoters are translated into distinct protein isoforms because their variant 5′ exons contain alternative ATGs. For some genes the use of alternative TSS results in proteins that differ in their N-terminus (Figure 1.16 B, i–iii) whereas for others, the use of an intronic promoter will result in a truncated or ΔN isoform (Figure 1.16 B, iv).
- *Different proteins encoded by alternative open reading frames.* The role of alternative promoters is not limited to simply generating mRNA that vary in their 5′ end: differential promoters can create different proteins through either alternative reading frames or splicing variation to create novel ORFs (Figure 1.16 C).

The function of alternative promoters might extend beyond the above-mentioned direct effects. In fact, they can play a role in regulating the splicing process indirectly altering the protein-coding potential of a transcript.

For several genes, including the human neuronal isoform of the nitric oxide synthase gene (*NOS1*)(Wang et al., 1999), the mouse *bcl-X* (Pecci et al., 2001) and human caspase-2 (*CASP2*) (Logette et al., 2003), the downstream alternative splicing that occurs in these transcripts correlates with the promoter used to generate the transcript. For example, usage of the second downstream noncoding first exon in the *CASP2* gene is associated with inclusion of the variable ninth exon, which produces the short isoform. Similarly the use of several of the *bcl-X* promoters is associated with an alternative splicing pattern that produces a specific ratio of long and short isoforms of the protein. Thus, for these genes, promoter choice appears to determine the inclusion or exclusion of an alternatively spliced exon.

Several mechanisms have been proposed to explain the observed connection between promoter usage and splicing events. Differential promoters can influence and regulate alternative splicing recruiting factors, such as SR proteins, and transcription factors with different types of activation domains and/or mechanistic properties, whose different actions on Pol II initiation and elongation affect alternative splicing differentially. Moreover, alternative promoters structure and occupation by different transcription factors can regulate Pol II elongation rates or processivity: low Pol II elongation rates or internal pauses for elongation would favour the inclusion of alternative exons governed by an exon skipping mechanism, whereas a highly elongating Pol II, or the absence of internal pauses, would favour exclusion of these kinds of exons. Probably, internal alternative splicing variants are the result of

important changes in pre-mRNA secondary structure resulting from different 5'-end sequences (Kornblihtt, 2005; Landry et al., 2003). However, neither of these mechanisms is necessarily exclusive and further studies will clarify the precise events involved in the coupling between transcription and splicing.

In addition, as we previously mentioned, the existence of gene loops, in which a transcriptionally active gene termination regions can be physically linked to its promoter site, suggests that the events that happen at the promoter can influence the efficiency of transcription termination and polyadenylation reactions (Ansari and Hampsey, 2005; O'Sullivan et al., 2004).

1.13.2 - Alternative splicing -

Alternative splicing is the most important posttranscriptional regulatory mechanism that causes genome diversity and functional complexity. It is a variant of the splicing process: during the pre-mRNA splicing event, exons can either be retained in the mature message or targeted for removal in different combinations to create a diverse array of mRNAs from a single transcript. Resulting mature mRNAs are either non-functional or might give rise to proteins with different activities and functions. This process is more a rule than an exception as it affects the expression of about 60% of human protein-coding genes and it explains how a vast mammalian proteomic complexity is achieved with a limited number of genes. There are several types of alternative splicing events leading to the generation of functionally distinct transcripts:

- *Use of cassette alternative exons*. The most common type of alternative splicing events (one third of all occurring) involves so called cassette type alternative exons. In this case an exon flanked by two introns can be spliced out of the transcript together with the introns. The event alters the sequence of amino acids in the expressed protein resulting in the loss of a protein region and, eventually, in the change of the ORF.
- *Use of alternative splice sites*. In this case alternative 5'- or 3'- splice sites in exon sequences are chosen. The use of an alternative site can lead to subtle variations in the final protein sequence inducing the presence or absence of specific aminoacidic portions and, the change of the ORF
- *Intron retention*. Instead of splicing out an intron, the intron is retained in the mRNA transcript. If a stop codon is not present in the intronic sequence, the intron can be traduced generating a shift in the ORF and consequently a different protein.

- *Mutually exclusion of exons*. In this splicing event, an exon can only be included into an mRNA when another exon is spliced out - or *vice versa*.
- *Use of alternative promoters and poly-A sites*. In this case, different sets of promoters and/or polyadenylation sites can be spliced with certain sets of other exons. Alternative splicing causing an alteration at any of the two RNA ends can thus lead to changes in protein production at the N and/or C terminus. On the other hand, as we previously pointed out (Section 1.11.1), changes in the 5'region of the new transcript influences subsequent alternative splicing events further downstream on the same RNA.

Therefore, during an alternative splicing event different exons of one transcript are combined in various ways. This process underlies a complex network of regulatory steps, influenced by a large number of factors and sequences. Splicing enhancers and silencers are sequences on the pre-mRNA, which can either lead to the use of a particular splice site or the skipping of this site. These sequences can be located in exons as well as in introns. Additionally external signals and factors influence the selection of splice sites. Proteins that bind to the pre-mRNA and/or the spliceosome can influence the splicing mechanism. Due to the presence of tissue-specific splicing factors that promote or inhibit splicing, the pre-mRNA is often spliced in a tissue-specific manner, depending on the pattern of regulatory proteins expressed in each cell type. The same principle is used in different developmental stages of organisms, also providing a diverse pattern of regulatory factors which control splicing (Black, 2003).

1.13.3 - Alternative polyadenylation -

A significant fraction of mRNA displays more than one polyadenylation site and is subjected to alternative processing at the 3'-end. Alternative polyadenylation is an additional widespread mechanism contributing to transcript diversity in eukaryotes: in fact, the use of one or the other poly(A) site produces mature transcripts with a different coding sequence or with 3' untranslated region (3'-UTR) of variable length. Distinct patterns of alternative polyadenylation have been evidenced (Edwalds-Gilbert et al., 1997) (Figure 1.17):

- *Alternative polyadenylation associated to tandem poly(A) sites*: in this case, multiple poly(A) sites are found within the same 3'-terminal exon and the alternative forms of mature mRNA generated by their use differ only in the length of 3'-UTR and not in the coding regions (Figure 1.17 A). Despite this alternative polyadenylation process induces the synthesis of mRNA having the same coding region it can likewise influence protein expression. As 3'-UTRs may contain regulatory elements affecting

mRNA stability, translation efficiency and localisation (Section 1.14.2), the choice of one of the tandem polyadenylation sites can strongly affect gene expression and transcript subcellular localisation, and consequently positively or negatively impact on the final amount and site of synthesis of protein product (Mignone et al., 2002). A great number of examples of transcription units with multiple, tandem poly(A) sites in a single 3'-terminal exon, have been described over the past years, indicating that this is the most diffuse mechanism of alternative polyadenylation.

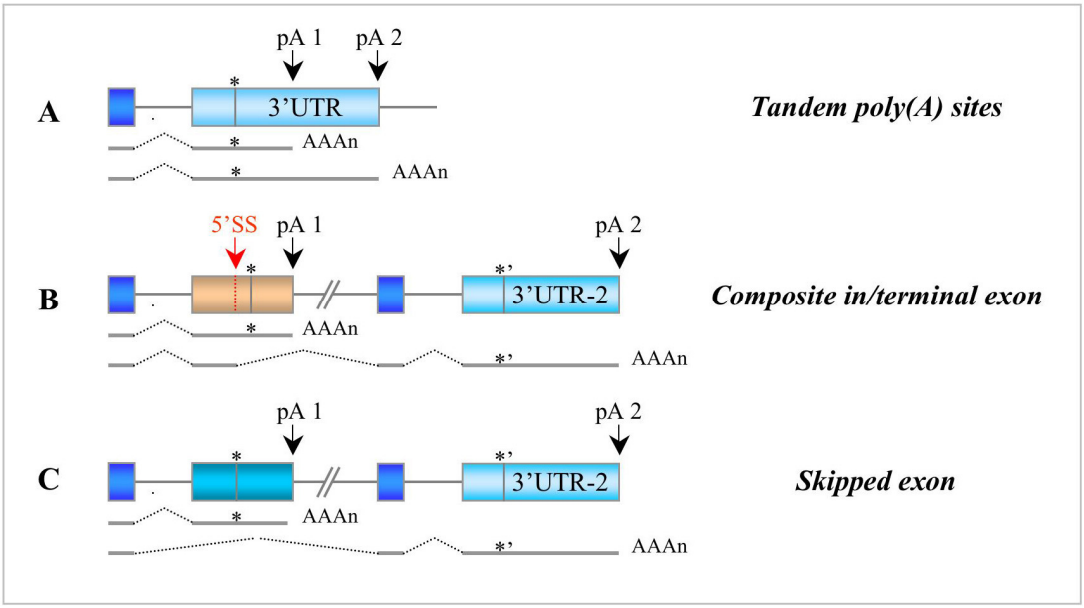

Figure 1.17: The 3' portions of genes leading to potential alternative poly(A) site selection. The figure shows the three type of exon arrangement that can produce alternative poly(A) site selection. Panel A represents genes having multiple poly(A) sites (pA1 and pA2) within the 3'-UTR (light blue box), arranged in tandem. Panel B shows genes having a composite exon (orange box) which can be used as internal or terminal exons (i.e. in/terminal) based on circumstances (the potential 5'-splice site in the composite 3'-terminal exon is indicated by the red arrow). Genes having different polyadenylation site (pA1 and pA2) located in two or more alternative spliced 3'-terminal exons (skipped exons) are represented in Panel C. All blue boxes are exons having typical 3' and 5'-splice sites. The site of the termination codon of the protein is indicated by the vertical bar and the asterisk (* and *' indicate the protein terminus in the 3'-UTR and 3'-UTR-2, respectively). The figure is adapted from Edwalds-Gilbert et al. 1997.

- *Alternative polyadenylation associated to composite exon* and *skipped exon*: in this case, poly(A) sites are located in different exons and the alternative polyadenylation process is related to splicing. In these cases alternative 3'-ends formation involves different 3'-terminal exons and consequently impacts the coding sequence: two or more final protein isoforms differing at their C-terminus and having often functional differences are generated.

1 Composite exon. Some genes have an exon which is a composite of 3' and 5'-splice sites followed closely by a poly(A) site (composite exon). These composite exons can serve as terminal or internal (i.e. in/terminal) based on circumstances: it is a 3'-

terminal exon when the 5'-splice site is not active and the downstream poly(A) site is recognised and used, while an internal exon when its 5'-splice site is used (Figure 1.17 B). For example, the immunoglobulin heavy chains gene has a composite exon. In immature B cells this exon is used as an internal one and the 3' processing machinery utilizes the polyadenylation site (pA2), located in a downstream terminal exon producing the membrane form of this protein, (which predominates in early developing B cells). Differently, in plasma cells the composite exon is recognised as the 3'terminal exon and so its downstream poly(A) (pA1) is used and the shorter, secreted form of the protein is synthesised (Zhao et al., 1999)

2 Skipped exon. Other genes have two or more alternative 3'-terminal exons encoding different C-terminus (skipped exons). They are processed into different mRNAs either by using the first 3'-terminal exon and its poly(A) site (pA1) or by skipping over that exon entirely and using the second 3'-terminal exon with its poly(A) site (pA2) in 3'-UTR-2 (Figure 1.17 C). Calcitonin/calcitonin gene-related peptide (CGRP) gene is classified in skipped exon category. It is processed into two mRNAs by using either the first alternative 3'-terminal exon with its poly(A) site (pA1) or skipping that exon entirely and including the second 3'-terminal exon into the transcript, using pA2 instead. In details, pA1 site is activated in thyroid while pA2 in neural tissue producing calcitonin and CGRP, respectively (Zhao et al., 1999).

- *Incidence of alternative polyadenylation* -

Several computational studies have been done on the incidence of alternative polyadenylation, mostly using an UTR-centred approach, where ESTs were mapped to UTR sequences. UTRs were used to represent transcripts in order to find the real 3′ end of an mRNA sequence. It was found alternative polyadenylation in 189 out of 1000 human EST clusters (Gautheret et al., 1998). Aligning ESTs to the 3'-UTRs from the UTRdb database (Pesole et al., 2000), Dr. Beaudoing identified that 29% of human genes were alternatively polyadenylated (Beaudoing et al., 2000). More recently, Dr. Iseli found that at least half of the human genes were alternatively processed at the 3'-end (Iseli et al., 2002). However, all of the above analyses have focused on the polyadenylation activities within or downstream of the normal 3'-terminal exon, since the majority of 3′-UTRs are located in the 3′-most distal exon. Therefore, they could only identify tandem poly(A) sites. More recently, using a gene-centred approach, where all the cDNA/ESTs mapping to the entire transcribed regions of mRNAs were considered, the incidence of both alternative polyadenylation coupled with splicing and

tandem polyadenylation was studied. This analysis estimated that a great proportion of human, mouse and rat genes have alternative polyadenylation: 49-54%, 31-32% and 28% in humans, mice and rats, respectively (Tian et al., 2005; Yan and Marr, 2005).

- *Distribution of alternative polyadenylation sites* -

By a bioinformatics approach it was evidenced the distance between adjacent poly(A) sites in the 3′-most exon, and that between the stop codon of a gene to its closest downstream poly(A) site. It was observed that they have a median value of approximately 300 nt for human and mouse genes. Diversely, the distance between alternative poly(A) sites localised in differential exons is often larger arriving to dozens of kb (Tian et al., 2005). Nevertheless, it is important to notice that, although typical tandem poly(A) sites within the 3'-most exon are located between 0 and 2 kb from the stop codon, EST sequence analyses have identified sites located at unexpectedly long ranges (5–10 kb) in a number of human and mouse genes generating extremely long 3'-UTR (Iseli et al., 2002; Lopez et al., 2006).

- *Molecular basis of alternative polyadenylation* -

Molecular mechanisms governing the choice of one of multiple poly(A) sites in a transcript that undergoes alternative polyadenylation are not completely elucidated. The efficiency of poly(A) sites commonly allows executing these decisions. Several studies have shown that the efficiency by which a poly(A) site is used correlates with the stability of the 3'-end-processing complex formed on that site. Considering that a stable polyadenylation complex is the consequence of multiple, cooperative interactions among the polyadenylation factors and the *cis*-regulatory sequences located in the polyadenylation region, it depends on the inherent strength of the polyadenylation signals located in the site and on the features of the *trans*-acting factors that catalyze or promote the polyadenylation reaction (Weiss et al., 1991).

The strength of a poly(A) signal seems to be in function of its sequence and its position in the UTR region (Beaudoing et al., 2000; Graber et al., 1999; Tian et al., 2005; Yan and Marr, 2005). *In silico* analyses of the distribution of signals in tandem alternatively polyadenylated mRNAs revealed that, as the number of poly(A) sites in an mRNA molecule increases, the proportion of canonical AAUAAA signals decreases. In other words, mRNAs with multiple poly(A) sites tend to use a higher proportion of less efficiently processed non-canonical hexanucleotide motifs (including the common AUUAAA) than mRNAs with a single poly(A) site. This differential rate is of

functional interest for transcripts with multiple poly(A) sites since it provides a means to control synthesis of specific mRNA forms, and thus to regulate gene expression: in fact, it is easier to modulate alternative processes when non-canonical, presumably weaker, signals are present. In addition, it was observed that the 3' distal site predominantly uses a canonical AAUAAA (generally processed more efficiently), while all other proximal sites tend to use non-canonical hexamers. More in general, there is a hierarchy: hexanucleotide motifs that are usually processed more efficiently ("strong" site) are more frequent at 3'-terminal sites. This observation is further supported by the evidence that the number of cDNA/EST sequences associated to the distal polyadenylation site is higher than that associated to proximal ones. Therefore, the distal site is generally the most efficient and the predominant form of alternatively polyadenylated mRNAs is usually the longest one. This high rate of long versus short 3'-UTRs might denote the tendency of the cell to privilege the formation of the more stable and actively transcribed form of mRNA: in fact, it was demonstrated that increasing the length of 3'-UTR, the stability and the translation efficiency of a poly(A) mRNA increases (Tanguay and Gallie, 1996). However, long 3'-UTRs are not necessarily more stable than shorter ones, especially since they often contain destabilisation signals (Mignone et al., 2002). In addition, as we mentioned above, the efficiency of a polyadenylation site does not strictly depend on the hexameric signal: "strong" sites may comprise variant AAUAAA signals while "weak" sites may contain canonical hexamers. In fact, it is known that sequence determinants affecting polyadenylation efficiency lie in the flanking USE and DSE. In detail, EST analyses evidenced that while USEs are indifferently associated with strong and "weak" poly(A) sites, DSEs are more conspicuous near "strong" poly(A) sites. DSE seems to act as an enhancer specifying or helping to distinguish the most efficient sites in case of alternative polyadenylation (Legendre and Gautheret, 2003; Prescott and Falck-Pedersen, 1994). Therefore, many regulated poly(A) sites are "strong" or "weak" because the signal sequences are high or poor matches to the consensus sequence or are in a favourable or unfavourable sequence context.

In addition, changing the activity or concentration of factors involved in mRNA 3'-end formation can influence the use of a 3'-end-processing sites. The efficiency of the process at the level of a poly(A) site is also determined by additional proteins that are able to positively or negatively influence the reactions (Edwalds-Gilbert et al., 1997). For instance, as discussed in Section 1.11.2, several splicing factors influence 3'-end

formation in specific contest, especially when poly(A) sites are located in different exons.

It was observed that often the choice of the polyadenylation site is related to tissue types, development stages and growth state (cell cycle state) of the cell or tissue (Beaudoing and Gautheret, 2001; Edwalds-Gilbert et al., 1997; Zhang et al., 2005). Recently, analysing cDNA/EST library information it was evidenced that ~10% of tandem poly (A) sites have a tissue specificity (Ara et al., 2006). A well-known example of alternative polyadenylation associated to different differentiation state of cells is the IgM heavy chain gene (Edwalds-Gilbert et al., 1997). During B lymphocyte activation, IgM heavy chain gene switches from using one poly(A) site to another, resulting in a shift in protein production from the membrane-bound form to the secreted form (Section 1.13.3). It was discovered that an increase in the CstF-64 levels during B cells maturation causes the preferential recognition of the poly(A) signal located downstream the composite exon (Takagaki et al., 1996). A tissue-specific regulation of alternative polyadenylation was detected in Calcitonin/calcitonin-related peptide (CGRP) gene. It was observed that pA1 site is activated in thyroid tissue by a downstream positive element that appears to involve recruitment of splicing factors, including U1snRNP, alternative splicing factor/splicing factor 2, (ASF/SF2), SR protein SRp20, and polypyrimidine tract-binding protein (PTB). In neural tissue this enhancer fails to act, and so the poly(A) site is spliced out and the resulting product CGRP is produced instead of calcitonin (Zhao et al., 1999).

These examples evidence that the choice of a particular poly(A) site in different cells or cell stages involves not only specific *cis*-acting elements but also specific *trans*-acting factors. Till now very little is known about the existence and activity of tissue- or stage-specific polyadenylation factors.

1.14 Untranslated regions of mRNAs

In eukaryotes, a mature mRNA has a tripartite structure consisting of a 5' untranslated region (5'-UTR), a coding region made up of triplet codons that each encode an amino acid and a 3'- untranslated region (3'-UTR) (Figure 1.18) (Mignone et al., 2002). Analyses of the human genome and the data available about other higher eukaryotic genomes have revealed that only a small fraction of the genetic material (~1.2% in humans) codes for protein. In humans, the UTRs of the transcripts are estimated to cover ~0.7% of the euchromatic genome (Consortium, 2004).

1.14.1 - <u>UTR features</u> -

5'-UTR are generally shorter than 3'-UTR in eukaryotes. The average length of 5'-UTRs is commonly conserved and ranges between 100 and 200 nt, whereas the average length of 3'-UTRs is much more variable among different eukaryotes, ranging from ~200 nt in plants and fungi to ~800 nt in humans and other vertebrates. It is striking that the length of both 5'-and 3'-UTRs varies considerably within a species, ranging from a dozen nt to a few thousand(Pesole et al., 2001). Even if the majority of the human and mouse transcript have a 3'-UTR between 0 and 2000 nt, several recent studies have evidenced the existence of long 3'-UTR (5-10 kb) for a number of gene (Iseli et al., 2002; Lopez et al., 2006; Tian et al., 2005).

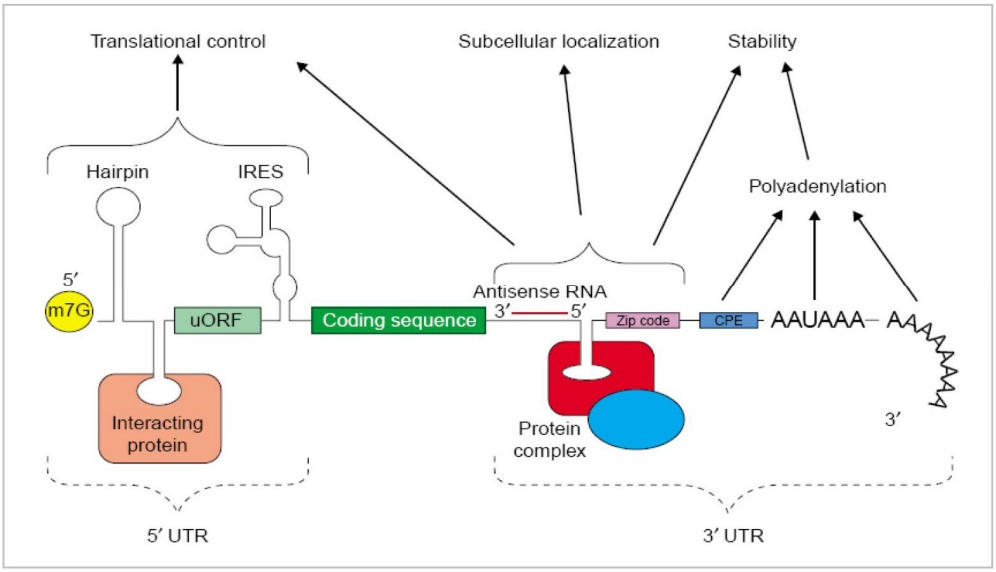

Figure 1.18: UTR-specific regulatory elements involved in post-transcriptional regulation of gene expression. The figure reports a schematic representation of the generic structure of an eukaryotic mRNA showing different types of UTR-specific regulatory elements involved in post-transcriptional regulation of gene expression. Abbreviations (from 5' to 3'): UTR, untranslated region; m7G, 7-methyl-guanosine cap; hairpin, hairpin-like secondary structures; uORF, upstream open reading frame; IRES, internal ribosome entry site; CPE, cytoplasmic polyadenylation element; AAUAAA, polyadenylation signal. The figure is adapted from Mignone et al., 2002.

The base composition of 5'-and 3'-UTR sequences also differs: the G+C content of 5'-UTR sequences is greater than that of 3'-UTR sequences (Pesole et al., 2001). There is also an interesting correlation between the G+C content of 5'-or 3'-UTRs and that of the third codon positions of the corresponding coding sequences, and a significant inverse correlation has been observed between the G+C content of 5'-and 3'-UTRs and their lengths. In particular, it has emerged that genes localised in large GC-rich regions of a chromosome (heavy isochores) have shorter 5'-UTRs and 3'-UTRs than genes located in GC-poor isochors. This suggests that genes requiring highly

efficient translation are located in GC-rich isochores and genes requiring fine modulation of expression are located in GC-poor isochores. This is in agreement with independent data from the literature concerning the location of housekeeping and tissue-specific genes, respectively (Pesole et al., 1999).

Finally, eukaryotic mRNAs are also known to comprise several types of repeats in the untranslated regions, including short interspersed elements (SINEs) such as Alu sequences, long interspersed elements (LINEs), minisatellites and microsatellites. In human mRNAs, repeats are found in about 12% of 5'-UTRs and 36% of 3'-UTRs. A lower repeat abundance is observed in other mammals (Pesole et al., 2001).Comprehensive analysis of the mammalian transcriptome shows that most genes express alternative UTRs. These result from multiple promoters and transcriptional start sites or a variation in the initiation site from one promoter, splicing and by using alternative polyadenylation sites (Carninci et al., 2005). As it was explained in Section 1.13, over half of mammalian genes have alternative promoters and are alternatively polyadenylated. In addition, alternative splicing within UTRs occurs in the transcripts of at least 13% of genes (Carninci et al., 2005). An independent study estimated that alternative splicing is present in 12% and 3% of the 5′ and 3′ UTR of genes, respectively (Nagasaki et al., 2005).

1.14.2 - <u>UTR function</u> -

UTRs are known to play crucial roles in the post-transcriptional regulation of gene expression, including modulation of mRNA nuclear export, cytoplasmic localisation, translational efficiency and stability (Mignone et al., 2002). The importance of UTRs in regulating gene expression is underlined by the finding that mutations that alter the UTR, especially within the 3'-UTR, can lead to serious pathologies (Chen et al., 2006; Chen et al., 2006; Conne et al., 2000). Regulatory motifs associated with these activities have been identified in both 5′ and 3′ UTR of the transcripts (Figure 1.18). Sections of UTRs, and the regulatory motifs therein, are highly conserved between orthologous humans and rodents genes and some of them are found in a substantial proportion of transcripts (Jareborg et al., 1999; Makalowski and Boguski, 1998; Pesole et al., 2001; Xie et al., 2005), underling the important post-transcriptional regulatory roles of UTRs. The main UTR motifs able to modulate gene expression are (Figure 1.18):

- *Binding sites for regulatory proteins*

Regulatory proteins bind to specific RNA sites, ranging from short, primary sequence elements to specific secondary structures, and can modulate many aspects of mRNA function (Derrigo et al., 2000). Examples include:

1. *AU-rich elements (AREs).* AREs are sequence elements of 50–150 NT that are rich in adenosine and uridine bases, located in the 3'-UTR of genes. They have been identified by their capacity to provoke degradation of the host mRNA by a mechanism dependent on deadenylation (shortening of the poly(A) tail). However, depending on the cellular context and the precise stimulus, the presence of an ARE can also lead to the stabilisation of an mRNA. Based on the number and the distribution of AUUUA pentamers, AREs have been grouped into three classes. Class I AREs contain several dispersed copies of the AUUUA motif within U-rich regions. Class II AREs possess at least 2 overlapping UUAUUUA (U/A)(U/A) monomers. Class III AREs are much less well defined, they are U-rich regions but contain no AUUUA motif. To date, at least a dozen of ARE-binding proteins (ARE-BPs) have been identified: AUF1 (also named hnRNPD), the Hu family (in particular HuR) and Tristetraprolin (TTP) are the most extensively studied. These proteins can either promote or inhibit the degradation of ARE-containing mRNAs. In fact, it was observed that the same ARE-BPs (AUF1, TTP, etc) are able to recruit to the mRNA the exosome (a complex of 3'-5' exoribonuclease) and/or associate with P-bodies (structures containing mRNA decapping and degradation factors), while other factors (HuR) or the previous one in different conditions (AUF1) are involved in increasing stability preventing exosome mediated degradation. I. Despite AREs are the best known determinants of mRNA stability/instability, these elements are also responsible of translational repression. The inhibitory effects of ARE-BPs on mRNA translation could be mediated by two mechanisms. ARE-dependent inhibition of translation could ensue from the deadenylation of the target mRNA leading to a loss of PABP bound to the mRNA poly (A) tail which, in turn, would destabilise the eIF4E-cap interaction. An alternative mechanism brings into play stress granules (granules that not contain decapping factors and whose function is to sequester untranslated mRNA): in fact, it was observed that they contain untranslated mRNAs and are associated with several ARE-BPs (Barreau et al., 2005).

2. *Iron-response elements (IREs).* They are hairpin structural (stem-loop) motifs within the 5′ or 3′ UTRs of genes involved with iron metabolism. These elements, that are targets of IRE-binding proteins (IRPs), can regulate the mRNA translation and

stability. At low iron concentration, active conformational IRPs are able to bind the loop of the IREs located at the 5'-UTR blocking the 40S ribosomal subunit from scanning for the AUG start codon, thereby inhibiting translational initiation, and/or can also interact with IREs located in the 3'-UTR protecting the transcript from an endonucleolytic cleavage (Haile, 1999).

- *Secondary structure*

In addition to acting as binding sites for some regulatory proteins, secondary structure within 5′ UTRs can strongly influence translational efficiency. Most stable structured 5′ UTRs repress cap-dependent translation by inhibiting binding or scanning of the translational machinery. Whereas, some structural motifs located just upstream the AUG initiation codon act as *internal ribosome entry sites* (IRES) inducing cap-independent translation (Pickering and Willis, 2005).

- *Upstream open reading frames (uORFs)*

uORFs are short open reading frames located within 5′ UTR. They are created when an in-frame stop codon is found following an upstream AUG and before the main start codon. uORFs inhibit mRNA translation by restricting the access of ribosomes to the correct start codon and moreover reduce its stability. They are believed to function via small *cis*-acting peptide products that reduce the initiation of translation of downstream ORFs (at the correct start codon) by stalling the ribosome at the end of the uORF, thereby exposing the mRNA to degradation (Oyama et al., 2004; Vilela and McCarthy, 2003). The specific mechanism that induced the degradation of uORF-containing transcript is not clear.

- *Binding sites for regulatory RNAs*

Regulatory RNAs, such as small interfering RNAs (siRNAs) and microRNAs (miRNAs), bind to target transcripts by base-pairing leading to changes in mRNA stability or translational efficiency (Storz et al., 2005). Numerous highly conserved motifs targets of miRNA have been identified in the 3'-UTR of several orthologous genes by a comparative analyses(Xie et al., 2005). Furthermore, 3'-UTR have also been found to constitute preferred targets of *cis*-encoded natural antisense transcripts (Sun et al., 2005). miRNAs and siRNAs are ~21-26 nt RNA molecules functionally equivalent, but distinguishable by their mode of biogenesis. miRNAs are produced from genome-encoded transcripts that form stem-loop structures. In contrast, siRNAs are produced from long double-stranded RNA (dsRNA) precursors, which can be either endogenously produced or exogenously provided. Final processing step of these regulatory RNAs

appears coupled to their assembly into the RNA-induced silencing complex (RISC), which is the effector of RNAi. In a variety of organisms, the key component of the RISC complex is a member of the Argonaute protein family. In general, the perfect or near perfect base pairing associated with siRNAs and some miRNAs can direct target mRNA endonuclease cleavage leading to RNA degradation, referred to as "slicer" activity (degradation by exosome 5'- to-3' exonucleases activity), whereas the imperfect base pairing associated with other miRNA leads to repression of translation. One additional requirement for the cleavage activity is the presence of a specific Argonaute protein within RISC (for example, Ago2 in *Drosophila* and mammalian cells). Several data suggest the hypothesis that miRNAs could in some cases increase decapping rates and the consequent 5'-3' degradation. Because decapping generally occurs following translation repression and mRNA exiting translation, miRNAs might induce decapping as a downstream consequence of repressing translation. In fact, miRNA can interfere with the translation of its target mRNA by imperfect base pairing. It has to be noted that efficient translation repression by miRNAs often utilizes multiple miRNA-binding sites for the same miRNA or a combination of several different miRNAs. Two possibly overlapping mechanisms by which miRNA and RISC might repress translation have been proposed. In one model, a component of RISC, directly or through additional factors, inhibits the function of some translation initiation factor, thus leading to the mRNA exiting translation and accumulating in P-bodies. Alternatively, or in addition, RISC might contain or recruit proteins that promote the assembly of an mRNP that can accumulate within P-bodies and be sequestered from the translation machinery (Valencia-Sanchez et al., 2006).

- *Cis-acting elements involved in mRNA localisation*

In eukaryotic cells, mRNA localisation is a common mechanism for targeting transcripts encoding specific proteins to regions of the cell where they are required. This process is required for creating and maintaining cell polarity especially during development, differentiation and in specialised cells. It can also repress translation until the messenger is localised. Moreover, it allows a cell to respond rapidly to a local requirement for the protein, and makes it possible to regulate gene expression independently in different parts of the cell. This is particularly important in large, highly polarized cells, such as neurons, where the translation of localised mRNAs in growth cones might be important for axon guidance, and the local control of protein synthesis in dendrites is thought to contribute to synaptic plasticity (Martin, 2004; Martin and

Zukin, 2006). Finally, transcript localisation is clearly more efficient than the mechanisms of protein localisation, because the same mRNA molecule can serve as a template for multiple rounds of translation. There are three main mechanisms for the asymmetric distribution of mRNAs (St Johnston, 2005):

1. *Local protection from degradation*: mRNAs can be localised by degrading all the transcripts that are not in the correct place (for example: hsp83 mRNA of the *D. melanogaster* oocytes);

2. *Diffusion and anchoring*: transcripts can also become localised by passively diffusing through the cytoplasm until they are trapped by a localised anchor which is commonly a cytoskeleton component (such as nanos, gcl, Cyclin B mRNAs, in the *D. melanogaster* oocytes);

3. *Active transport and anchoring*: in this case functional cytoskeleton and specific motor proteins interacting with the target transcript allows its subcellular localisation. Most of the best-characterised examples of mRNA localisation are thought to occur by this mechanism (for example: myelin basic protein –MBP- mRNA is transported down the long processes of oligodendrocytes of the central nervous system).

In all these cases, localisation of mRNA in the somatic and germinal cells is mediated by *cis*-acting elements located mainly in the 3'-UTR (there are also rare examples of elements in the 5'-UTR or even in the coding sequence). These elements are known as mRNA localisation signal (LS) or zipcodes. LSs are highly variable in length and structure. In fact, they can have a complex secondary or tertiary structure, or they can be short, defined nucleotide sequences, sometimes in repeated elements, or multicomponents units spanning over hundreds of nucleotides. In a number of localised mRNAs, the existence of multiple, partially redundant LS have been observed indicating that cooperative interaction between them are required to achieve optimal localisation efficiency. Localisation depends not only on the mRNA signals but also on the *trans*-acting factors that interact with these regions to form the critical localisation complex. In fact, the formation and the exact composition of these complexes determine the events involved in localisation: the transport (mediated by the interaction between complexes and microfilaments motor -myosin- and/or microtubule motors -dynein and kinesin-), and the local anchoring. In various experimental systems localisation complexes have been found in cytoplasmic granules. The *trans*-acting factors are either dsRNA or ssRNA-binding proteins able to shuttle between the nucleus and the cytoplasm. Among these, there are "destination specific" transport and anchoring

proteins as well as more general “adaptor” protein (such as staufen). In addition, proteins of hnRNP family, splicing factors, polyadenylation related factors and translational factors are implicated in mRNA localisation. All these observations lead to the concept that the mRNA becomes “tagged” for transport and localisation by the binding of specific proteins in the nucleus and during RNA processing and export, and so it is likely that nuclear events influences subsequent events in the cytoplasm (Chabanon et al., 2004).

In conclusion, UTRs containing several distinct *cis*-acting signals can be considered critical multifunctional regulatory region having a fundamental roles in modulation of gene expression

1.14.3 - Function of alternative UTRs -

The potential significance of mRNA variants having different UTR becomes clear considering the influence that UTRs can have on gene expression. The UTR variants may differ by their stability, translational efficiency or cellular localisation thus contributing to tissue-specific or developmental stage-specific regulation of gene function. In fact, the UTRs can determine tissue-specific or development stage-specific expression when regulatory motifs are included in certain mRNA variants but not in others. Recent reports have described genes that express multiple UTRs often showing them to have cell type-specific expression patterns or differential effects on protein expression However, there are still relatively few genes for which it has been established the roles of multiple UTRs in determination of the tissue-or stage specificity

AIMS of the THESIS

We are interested in the understanding of the function of the β-adducin gene, covering aspects related to the transcriptional and post-transcriptional regulation of its pre-mRNA, and the function of the protein in tissues.

One of the aims of the thesis is to identify the alterations in the composition of the cytoskeleton induced by the absence of β-adducin in mouse erythrocytes, lens fibre cells and other non-erythroid tissues, and the determination of potential compensatory mechanisms. We expect that the understanding of the molecular events associated to the lack of β-adducin in tissues may shed light in the comprehension of the following phenomena:

- the molecular causes that induce osmotic fragility and elliptocytosis in RBCs, and the consequent mild haemolytic anaemia in β-adducin KO animals;
- the molecular alterations in cardiac muscle cells, undetected in previous studies, that could justify the hypertension evidenced in mutant mice;
- the function of β-adducin in other cell-types rich in actin cytoskeleton such as eyes lens fibre.

The second goal of this work is to detect novel cytoskeletal alterations in the erythrocytes of β-adducin and dematin double KO mutant mice in order to elucidate the molecular basis underlying the severe haemolytic anaemia detected in those animals. We expect to more deeply understand the functions of these two actin-binding proteins in stabilising actin protofilaments and, consequently, the membrane skeleton of RBC.

The third aim of this thesis is to elucidate the mechanisms of regulation that are at the base of brain and haematopoietic tissue-specific expression of the β-adducin gene. In particular, we are interested in the characterisation the molecular bases of the long 8–9 kb β-adducin mRNA detected in brain of humans and rodents instead of the 3.5–4.5 kb spleen transcript and its potential function. The understanding of these mechanisms is particularly relevant because of the importance that the 3'-UTR function has gained during the last few years due to the appearance in the regulatory scenario of small RNAs, performing the fine-tuning regulation of gene expression, which is in many cases unexpectedly associated to human disorders.

2 MATERIAL and METHODS

2.1 Chemical reagents

General chemicals were purchased from Sigma Chemical, Merck, Gibco BRL, Life Technologies, AnalaR, BDH Laboratory Supplies, Fluka, Riedel-de-Hael, BD Bioscience, Amersham Biosciences, Pharmacia, Analyticals and Invitrogen

2.2 Standard solutions

All solutions are identified in the text where used except for the following:

- PBS: 137 mM NaCl, 2.7 mM KCl, 10 mM Na_2HPO_4, 1.8 mM KH_2PO4, (pH 7.4).
- 10X protein sample buffer: 20% w/v SDS, 1 M DTT, 0.63 M Tris-HCl (pH 7), 0.2% w/v bromophenol blue, 20% v/v glycerol, 10 mM EDTA (pH 7).
- 5X SDS-PAGE running buffer: 30 g/l Tris base, 147 g/l glycine, 5 gr/L SDS.
- 10X protein blotting buffer: 30 g/L Tris base, 147 g/L glycine.
- TE: 10 mM Tris-HCl (pH 7.4), 1 mM EDTA (pH 7.4)
- 10X TBE: 108 g/l Tris, 55 g/l boric acid, 9.5 g/l EDTA
- 5X DNA sample buffer: 50% w/v sucrose, 25% w/v urea, 0.025% w/v bromophenol blue, 5X TBE.
- 10X MOPS: 0.2 M MOPS (pH 7), 50 mM CH_3COONa (pH 8), 10 mM EDTA (pH 8).
- 1X RNA sample buffer: 50% v/v deionised formamide, 1X MOPS, 6% v/v formaldehyde, 1 µl (1 mg/ml) ethidium bromide (EtBr) per 20 µl sample buffer.
- 20X SSC: 3 M NaCl, 0.3 M sodium citrate, (pH 7).
- Sequencing gel loading buffer: 98 % v/v deionised formamide, 10 mM EDTA (pH 8), 0.025 % w/v xylene cyanol FF, 0.025 % w/v bromophenol blue.
- 50X Denhardts Solution: 5 g ficoll (Type 400, Pharmacia), 5 g polyvinylpyrrolidone, 5 g bovine serum albumin (BSA) and ddH_2O to 500 ml. Filtered and stored at −20°C.

2.3 Enzymes

- Restriction enzymes were purchased from Amersham Pharmacia Biotech or New England Biolabs.

- DNA modifying enzymes: *Taq Polymerase*, *T4 DNA ligase* and *T7 or T4 RNA polymerase* were obtained from Roche Diagnostics, *Klenow fragment* of *E.Coli*, *T4 Polynucleotide kinase* and *Calf Intestinal Alkaline Phosphatase* were obtained from New England Biolabs. *PfuTurbo DNA polymerase* was from Stratagene.
- Exonucleases: *RNase A* was purchased from Sigma Chemicals. The 10 mg/ml stock solution of RNase A was prepared in ddH_2O and boiled for 10-20 min to destroy trace amounts of DNase activity. *Proteinase K* was purchased from Sigma chemicals. and stocks prepared at concentrations of 10 mg/ml.

All enzymes were used following the manufacturers' instructions.

2.4 Synthetic oligonucleotides

Synthetic DNA oligonucleotides were purchased from Sigma-Genosys.

2.5 Radioactive isotopes

[α-^{32}P] dCTP was supplied by Amersham Bioscience.

2.6 Bacterial culture media and strain

The *E.Coli* K12 strain DH5α was transformed with the plasmids described in this study and used for their amplification. Plasmids were maintained in the short term as single colonies on agar plates at 4 °C but for long term storage they were kept on glycerol stocks made by adding sterile glycerol to a final 30% v/v concentration to liquid bacterial cultures. Glycerol stocks were stored at –80 °C. When necessary, from the glycerol stocks an overnight culture of bacteria was grown in Luria-Bertani medium [LB medium: per litre: 10 g Difco Bactotryptone, 5 g Oxoid yeast extract, 10 g NaCl, (pH 7.5)]. Bacterial growth media were sterilised before use by autoclaving. When appropriate, ampicillin was added to the media at a final concentration of 200 μg/ml.

2.7. Cell culture

HeLa cells were used for transfection experiments; this cell line was derived from cervical cancer cells taken from Henrietta Lacks, who died in 1951.

2.8 Mice

β-adducin deficient mice having C57Bl/6 genetic background were used for several experiments. The target disruption of the gene has been previously performed in

our lab(Muro et al., 2000). C57BL/6 control mice were either obtained from Harlan Italy or bred in the ICGEB facilities (Trieste, Italy). β-adducin mutant mice having C3H genetic background were also analysed. To transfer the β-adducin gene mutation to a C3H genetic background, the mutant mice were backcrossed with C3H mice (Harlan, Italy) for six additional generations. All murine strains were housed in rooms at 24 °C with 12 hour light dark cycles. Mice were fed with standard food and water *ad libitum*. In all experiments, +/+, and -/- (and also +/- when used) mice were age- and sex-matched.

Some experiments were performed analysing samples derived from β-adducin null mice (AKO) generated by Dr. Gilligan's laboratory in the Yale University School of Medicine, New Haven, (USA)(Gilligan et al., 1999). Samples obtained from headpiece domain of dematin deficient mice (DKO) (Khanna et al., 2002)and double knock-out mice lacking β-adducin and headpiece domain of dematin (DAKO) were created at Chishti's laboratory in the University of Illinois College of Medicine, Chicago, (USA)(Chen et al., 2007).

2.9 Preparation of DNA

2.9.1 - Preparation of genomic DNA -

Mouse tail biopsies (0.5-0.8 cm) were treated with 600 µl of lysis solution [50 mM Tris-HCl (pH 8), 100 mM EDTA (pH 8), 0.5% w/v SDS, and 200 µg/ml proteinase K] and incubated overnight at 57 ºC. The mix was centrifuged 15 min at 14000 rpm in a 5415-D rotor (Eppendorf). 500 µl of supernatant were recovered and added to 500 µl of isopropanol and mixed by inversion. The mix was centrifuged in identical conditions and the pellet was washed with 80% v/v ethanol. The final pellet (genomic DNA) was resuspended in 200 µl of TE prewarmed at 65 ºC, leaving overnight at 37 ºC to facilitate the dissolution. The DNA was then checked by electrophoresis on a 0.6% w/v agarose gel, quantified by spectrophotometic analyses and stored at 4 °C until use.

2.9.2 - Small-scale preparation of plasmid DNA from bacterial cultures -

Rapid purification of small amounts of recombinant plasmid DNA was basically performed with the method described in Sambrook et al. 1989 (Sambrook, 1989). Briefly, alkaline lysis of recombinant bacteria was performed by resuspending the bacterial pellet in 100 µl of solution I [50 mM glucose, 25 mM Tris-HCl (pH 8), 10 mM EDTA (pH 8)]. 200 µl of solution II (0.2 M NaOH, 1 % w/v SDS) were then added and

the contents mixed by inversion. 150 µl of solution III [3 M sodium acetate (pH 5.2)] were then added and the contents mixed by inversion. The bacterial lysate was then centrifuged in a 5415-D rotor (Eppendorf) at 14000 rpm and the supernatant transferred to a new tube. An equal volume of 1:1 v/v phenol:chloroform solution was added to the supernatant. The tube was then vortexed and centrifuged as above. An equal volume of chloroform was added to the supernatant. The tube was again vortexed and centrifuged as above. The aqueous phase containing the DNA was then recovered and the DNA pelleted by ethanol precipitation. The final pellet was resuspended in 50 µl of ddH_2O and the RNA was eliminated adding 3µl of RNAse A (10mg/ml) and incubating the final DNA sample at 37 °C 30 min. 5 µl of such preparation were routinely taken for analysis by restriction enzyme digests.

2.9.3 - Large-scale preparations of plasmid DNA from bacterial cultures -

Large scale preparations of plasmid DNA were carried out by JetStar columns (Genomed Gmbh, Germany) according to the manufacturers' instructions. In order to get a good amount of plasmid, we left a 50 ml of overnight bacterial culture using LB medium. This DNA purified procedure was used to obtain the plasmid DNA utilized for transfection experiments.

2.10 Preparation of total RNA

2.10.1 - Isolation of total RNA from organs/tissues -

Total RNA was prepared from tissues by the guanidinium thiocyanate procedure(Chomczynski and Sacchi, 1987). Organs were removed, quickly frozen in liquid nitrogen and stored at −80 °C until use. Then, they were transferred to 8 ml of ice-cold Solution D (4M guanidine thiocyanate, 25 mM sodium citrate, 100 mM β-mercaptoethanol, 0.5% w/v lauroylsarcosine) and completely homogenized in series of 20 sec by using the Ultra-Turrax T-25 Basic homogenizer (Ika-Werke).After adding 0.8 ml of 2M sodium acetate (pH 4), 8 ml of phenol (saturated with water) and 1.6 ml of chloroform to the homogenate, the whole mix was vortexed, kept on ice for 15 min and centrifuged in a 5810-R rotor (Eppendorf) at 3500 rpm for 20 min at 4°C. The aqueous phase was separated and subjected to a second phenol-chloroform extraction to improve the sample separation from proteins and fatty acids. The RNA was then precipitated by the addition of one volume of isopropanol, kept for one hour at −20°C and centrifuged in a 5415-D rotor (Eppendorf) at 14000 rpm for 15 min at 4°C. RNA pellets were

washed once in ice-cold 70% v/v ethanol, resuspended in a total volume of 200-400 µl of double distilled water (ddH_2O), separated in aliquots frozen immediately in dry-ice and kept at −80°C until use. RNA integrity was confirmed by running the samples on 1% native agarose gel and quantified by spectrophotometric analysis.

2.10.2 - Isolation of total RNA from cells in culture -

After removal of the culture medium and two washes in cold PBS 0.8 ml of Solution D (4M guanidine thiocyanate, 25 mM sodium citrate, 100 mM β-mercaptoethanol, 0.5% w/v lauroylsarcosine), 0.8 ml of phenol (saturated in H_2O) and 80 µl of 2M sodium acetate (pH 4) were added to a 35 mm Petri dish. Lysis was carried out by shaking for 15 min at 4 °C. To the lysate was added 160 µl of chloroform, and the mix was then vortexed, incubated for 15 min on ice, and centrifuged at 14000 rpm in a 5415-D rotor (Eppendorf) for 15 min at 4 °C. The aqueous phase was separated, added of one volume of phenol (saturated in H_2O) and ¼ volume of chloroform, reincubated on ice and recentrifuged. The supernatant was added of one volume of ice-cold isopropanol, left for one hour at −20°C and centrifuged at the previous conditions. The pellet was then washed with 70% v/v ethanol and resuspended in 50-100 µl of ddH_2O. After the determination of the RNA concentration and integrity, total RNA was aliquoted and conserved at -80 °C.

2.11 Estimation of nucleic acid concentration and quality

2.11.1 - Spectrophotometric analysis -

Nucleic acid concentration was determined by measuring the absorbance at 260 nm and 280 nm with a spectrophotometer (Jenway). An optical density of 1.0 at 260 nm is usually taken to be equivalent to a concentration of 50 µg/ml for double stranded DNA, 40 µg/ml for single stranded DNA and RNA, and approximately 20 µg/ml for single-stranded oligonucleotides samples. The ratio of values for optical densities measured at 260 nm and 280 nm is considered as 1.8 for pure sample of DNA and 2 for RNA and these are reduced by protein contaminants (Sambrook et al. 1989). Therefore, these values were used to determinate not only the concentration but also the purity of the samples.

2.11.2 - UV fluorescence of inter-calated ethidium bromide -

Double-stranded nucleic acids size-fractionated on agarose gels can be visualised after staining with ethidium bromide (0.5 μg/ml) since fluorescence of this compound is enhanced by intercalation between bases in a double stranded nucleic acid. Therefore, it has been possible to estimate or semiquantitate DNA or RNA on a gel by comparing the intensity of UV-induced fluorescence of the sample with that of a known standard sample. This procedure was mostly performed by eye.

2.12 Electrophoretic separation of nucleic acid

2.12.1 - Agarose gel for DNA separation -

Double-stranded DNAs (restriction fragments of plasmid or genomic DNA and PCR products) were size fractionated by electrophoresis in agarose gels ranging in concentrations from 0.6% w/v (large fragments) to 2% w/v (small fragments). The gels were prepared melting the right weight of agarose (EuroClone) in 1X TBE containing ethidium bromide (0.5 μg/ml) in the microwave oven. When the agarose gel was solidified, DNA samples, diluted in 1X DNA loading buffer, were loaded into submerged wells of the gels and separated by electrophoresis in 1X TBE buffer at 80-100V for a time depending on the fragment length expected and gel concentration. DNA was visualised by UV transillumination and the result recorded by digital photography. The DNA bands were sized by confront to the molecular weight standards (1 kb DNA ladder, Invitrogen). Horizontal gels were routinely used for visualization of PCR product, fast analysis of DNA restriction enzyme digests, estimation of DNA concentration, or DNA fragment separation prior to elution from the gel.

2.12.2 - Denaturing polyacrilamide gels for DNA separation -

DNA fragments obtained from the primer extension and RNase protection assays were fractionated according to size on gels containing 6 to 8% acrylamide, 0.32-0.42% bis-acrylamide (19:1 acrylamide:bis-acrylamide, AccuGel, National Diagnostics), 7M urea, 1X TBE. To promote and catalyse the polymerisation of this mixture 400 μl of a 10% w/v ammonium persulphate solution and 40 μl TEMED were added per 50 ml of gel mix. The gel was formed between two 38 x 20-40 cm glass plates separated by 0.4 mm teflon spacers. Radiolabelled samples were mixed with denaturing loading buffer and loaded in sequencing gel These were subsequently separated by vertical electrophoresis in 1X TBE running buffer at 45 W. DNA fragments were detected by

autoradiography using X-OMAT AR film (Kodak, USA) at room temperature (RT) by overnight exposure.

2.12.3 - Agarose gel for RNA separation -

Total RNA was separated by electrophoresis in 1% w/v horizontal native agarose gels containing ethidium bromide (0.5 μg/ml) and 1X TBE similar to that used for DNA. Samples containing 1X DNA sample buffer (RNase free) were loaded into submerged wells. The gels were run at 80-100V in 1X TBE running buffer for 20 min. RNA was visualised by UV transillumination and the result recorded by digital photography. Native agarose gel electrophoresis of RNA was used to value the integrity of the total RNA preparation: in fact, the total RNA quality and also its quantity were deduced from the ribosomal 28 S, 18 S and 5S RNA bands that are usually visible.

2.12.4 - Denaturing agarose gels for RNA separation-

Total RNA was separated in 1-1.5% agarose-formaldehyde denaturing gel. The proper weight of agarose (Seakem LE agarose, BioWhittaker Molecular Application) was dissolved in 72 ml of ddH_2O in the microwave oven. 18 ml of 37% formaldehyde (12.3 M final concentration) and 10 ml 10X MOPS (1X final concentration) were added to the hot agarose solution and the mix was dripped in the electrophoretic hold. When the agarose gel was solidified, the samples, resuspended in 1X RNA sample buffer containing ethidium bromide, were denatured at 65 ˚C for 5 min, immediately chilled, loaded and then run at 5 V/cm in 1X RNA running buffer (12.3 M formaldehyde, 1X MOPS, in ddH_2O). Often a RNA size marker (Gibco BRL) was loaded to allow the identification of the bands size and to ensure the gel was run properly. RNA was visualised by UV transillumination and the recorded by digital photography. Agarose-formaldehyde gels were used to obtain a optimized total RNA separation before blotting in the Northern Blot experiments.

2.13 Elution and purification of DNA fragments from gels

This protocol was used to purify small amounts (less than 1 μg) of DNA for sub-cloning. The DNA samples were separated by electrophoresis onto an agarose gel as described previously. The DNA was visualized with UV light and the required DNA fragment band was excised from the gel. This slab was cut into pieces, and the QIAquick Gel Extraction Kit (Qiagen) was used according to the manufacturer's instructions. Briefly, 300 μl of gel solubilisation Buffer QG were added for each 100

mg of the gel slice pieces and incubated at 55 ˚C for 15 min vortexing every 5 min. The mixture was loaded into a prepared QIAquick column and it was centrifuged at maximum speed for 1 min. The flowthrough was discarded. 750 µl of Buffer PE were added into the spin column and after 2 min, the column was centrifuged in the same conditions twice. The flowthrough was again discarded both times. To elute the bound DNA, 30-50 µl of pre-warmed ddH_2O were added onto the centre of the silica matrix of the spin column and the system was centrifuged for 2 min. The amount of DNA recovered was approximately calculated by UV fluorescence of intercalated ethidium bromide in an agarose gel electrophoresis.

2.14 Enzymatic modification of DNA

2.14.1 - Restriction enzymes -

Restriction endonucleases were used in the construction and analysis of recombinant plasmids. Each restriction enzyme cuts optimally in a buffer of specific ionic strength. All buffers were supplied by the same company that supplied the enzymes and were used according to the manufacturer's instructions.

For analytical digests 100-500 ng of DNA were digested in a volume of 20 µl containing 1 U of the appropriate restriction enzyme. The reaction was incubated for 2-3 hours generally at 37 °C. Preparative digestion was made of 2-10 µg DNA using the above conditions and 5 U of restriction enzyme for µg of DNA in 200 µl reaction volume.

2.14.2 - Large fragment of E.Coli Polymerase I and T4 Polynucleotide Kinase-

These enzymes were used to treat PCR products for blunt-end ligation during construction of recombinant plasmids. The large fragment of DNA Polymerase I (Klenow) is a proteolytic product of *E.Coli* DNA Polymerase I. It retains polymerisation and 3'->5' exonuclease activity, but has lost 5'->3' exonuclease activity. This was useful for digesting specific residues added by Taq DNA polymerase at the 3' terminus to create compatible ends for ligation. T4 Polynucleotide Kinase catalyses the transfer of phosphate from ATP to the 5'-hydroxyl terminus of DNA. It is useful for the addition of 5'-phosphate to PCR products to allow subsequent ligation.

Briefly, PCR product was incubated at 90°C to inactivate Taq Polymerase. Klenow fragment (5 U) and $MgCl_2$ to a final concentration to 5 mM were added to 40 µl of PCR product. The mixture was incubated at R.T. for 15 minutes and then the enzyme

inactivated at 80 °C for 20 min. EDTA to a final concentration of 0.2 mM, ATP to a final concentration of 1 mM, (10 U) of T4 Polynucleotide Kinase and the proper quantity of 10X Kinase buffer were added to the above mixture and incubated at 37 °C for 30 min. The enzymes were inactivated by incubation at 80 °C for 20 min.

2.14.3 - T4 DNA ligase -

T4 DNA ligase catalyses the formation of a phosphodiester bond between adjacent 3'- hydroxyl and 5'-phosphoryl termini in DNA, requiring ATP as a cofactor in this reaction. This enzyme was used to join double stranded DNA fragments with compatible sticky or blunt ends, during generation of recombinant plasmid DNAs.

Generally, 20 ng of linearized vector were ligated with a 5-10 fold molar excess of insert in a total volume of 20 µl containing 1X ligase buffer and 1U of T4 DNA ligase. Reaction was carried out for 2-4 hours at R.T. for sticky end ligations and O.N. at 16 °C for blunt end ligations. In some reactions synthetic oligonucleotides were included in the reaction. In these cases, the amounts added to each reaction to obtain inclusion of oligonucleotides in the resulting plasmid were about 100 fold molar excess over the DNA vector.

2.15 Synthesis of cDNA

To synthesise cDNA, 1-2 µg of total RNA was used. The proper volume of RNA was combined with ddH_2O to10 µl final volume, denatured at 90 °C for 5 min and then placed in ice. 10 µl of the reaction solution [1µl of ologo(dT) (200 ng/µl) or random primers (hexanucleotides, 200 ng/µl), 1.5 µl of 5 mM dNTP mix, 4 µl of RT buffer (5X, Invitrogen), 2 µl of 0.1 M DTT (10X), 1µl of RNaseIn (40 U/µl) (Invitrogen) and 50U of M-MLV reverse transcriptase (RT) (Invitrogen)] were added to the RNA volume. The reaction mix was incubated for one hour at 37°C. Following RT reaction, the cDNA was used for PCR or conserved at -20 °C.

2.16 Amplification of selected DNA or cDNA fragments

The polymerase chain reaction was performed on cDNA or genomic DNA or plasmid DNA following the basic protocol accompanying the Taq DNA Polymerase enzyme. The volume of the reaction was usually 50 µl with 1X Taq buffer, dNTP mix (200 µM final concentration), appropriate sense and antisense oligonucleotide primers (15 µM final concentration), and 2.5-5 U of Taq DNA Polymerase.

Primers	Sequence 5'- 3'	PCR reaction
m β-Add 12 ex dir 1	TGGATGAAGGCTGATGAA	Fig. 3.14 -3.15, pair "a"
m β-Add 11 bis ex rev	GTCCTCCCTGGACCTCACAGC	Fig. 3.15, pair "a"
m β-Add 16 ex rev 1	AGGAGGAGGAGCCGAGCGTA	Fig. 3.14, pair "a"
h β-Add 11 ex dir 1	ATCGCCACCCCTTTGTTCA	Fig. 3.16 B,
h β-Add 16 ex rev 1	TGTCTCTGCCTCCTTCGCTG	h βAdd Total Probe
m β-Add brain dir 2	CTCTGGACTTGACTCTGACTGC	Fig. 3.18 B-C,
m β-Add brain rev 1	CTCGCATCCATCCCCAAAT	m βAdd Brain Probe
5'βNC (rat)	GGAACCCAGTAGGATGAACC	Fig. 3.18 A, primer extension
m β-Add brain dir 1	AGCGGAAGAGCTGTGAGTCCA	Fig. 3.20 C, pair "a"
m β-Add 94 dir 1	CAAAGGCAGGATGAGAGCGAGT	Fig. 3.20 C, pair "b"
m β-Add spleen dir 1	AGTCTTCAAGGATGGAGGATAG	Fig. 3.20 C, pair "c"
m β-Add common rev1	GCAAGTACTCAGGATCATCT	Fig. 3.20 C, pair "a", "b" and "c"
m β-Add 94 dir 33	GGACAGGGGAGGGCGTGGTT	Fig. 3.20 E, pair "d"
m β-Add 94 dir 49	GGTTCAGCAGGAGACAAAGG	Fig. 3.20 E, pair "e"
m β-Add common rev 368	CCCTCTTCTTCTGCTCCATC	Fig. 3.20 E, pair "d" and "e"
h β–Add ex 1 dir 2	CCCCAAACCCATAAAATAAC	Fig. 3.21 C,
h β–Add 548 rev 1	TCGTCCTCTGAGAAGCGGTC	pair "a"
h β–Add ex 66 dir 2	TGCAAAAGTAGCAGCAGCTCA	Fig. 3.21 C,
h β–Add ex 3 rev 1	CTCTGCAGGATCATGGTGACG	pair "g"
m β-Add 16 ex dir 2	TGAGTGATGGATGGAAGAAC	Fig. 3.22 B,
3' m β-Add rev 4	CCTTCATCTCCAGTGCTAAT	pair "a"
3' m β-Add dir 1	TTCCCTTCTGCCTTCTCAAC	Fig. 3.22 B-C
3' m β-Add rev 1	CCAACTTTATCTCTCAGCAC	pair "b"/Probe 1
3' m β-Add dir 2	GCATTCATTAGGCATCCATT	Fig. 3.22 B,
3' m β-Add rev 5	CACATCACAGGAGCAAATA	pair "c"
3' m β-Add dir 4	TGGGAGTGGTTGTGGTCTGC	Fig. 3.22 B,
3' m β-Add rev 2	GGGCTCTGGGAAGTAATCAC	pair "d"
3' m β-Add dir 5	CACTAAGCCCAACCGAACTC	Fig. 3.22 B, pair "e"
3' m β-Add rev 3	ACCCACAGCATTACTTACGA	Fig. 3.22 B-C, pair "e"/Probe 2
3' m β-Add dir 3	GAGCCACCCAATCATAAGAC	Fig. 3.22 C, Probe 2
h β-Add 17 ex dir 1	CTTGTCCCTATCTGTCCATC	Fig. 3.24 B,
3' h β-Add rev 1	ACATCGTTTGCCACTTATTA	pair "a"
3' h β-Add dir 1	TCCCTTGATGCCTTCTTTTA	Fig. 3.24 B,
3' h β-Add rev 2	ACACCAAGACAAAATAAAACT	pair "b"
3' h β-Add dir 2	GGTGGCTGAATGGAGACTGT	Fig. 3.24 B,
3' h β-Add rev 3	GTTTACCCTCCACATACCTT	pair "c"
3' h β-Add dir 3	AGTGTGGGGGAAAATGCTAT	Fig. 3.24 B,
3' h β-Add rev 4	ACCTAAGTATGAACCAATGCG	pair "d"
3' h β-Add dir 4	GCTGGGAGTGTTCTTATGT	Fig. 3.24 B,
3' h β-Add rev 5	GCAAAATAAAAGCCCAAGAAAA	pair "e"
r β-Add 16 ex dir 1	TCTAAGTCACCCTCCAAAAA	Fig. 3.23 B,
3' r β-Add rev1	GTGATGGGGTTGGGAATGTC	pair "a"
3' r β-Add dir 1	GCCCACAGACCAGAAGATGC	Fig. 3.23 B,
3' r β-Add rev 2	CTCAGCACCGACTCACACAA	pair "b"
3' r β-Add dir 2	TAATGACAGACAACCCAATG	Fig. 3.23 B,
3' r β-Add rev 3	GCTTTCACAATCCCTCCTCA	pair "c"
3' r β-Add dir 3	TCACAGCCTCAGACCCTATTC	Fig. 3.23 B,
3' r β-Add rev 4	ATTTGGGTGCCTTGGGAACA	pair "d"
3' r β-Add dir 4	CTGAGGTGGGTGGTCTAATA	Fig. 3.23 B,
3' r β-Add rev 5	CACAGAGAAACCCACAAGC	pair "e"
m β-Add 14 ex dir 1	AAGAAGGAGGTGGAAAGGAA	Fig. 25 A,
m β-Add 16 ex rev 1	TCCTCCTTCCCATTCACCAC	m β–Add97 Probe
m β-Add ex 11 bis dir	GTCCGGTACAGCAGAGACTG	Fig. 25 B,
m β-Add ex 11 bis rev	GTCCTCCCTGGACCTCACAGC	m β–Add63 Probe
dT-anchor 1	TAGGAATTCTCGAGCGGCCGCT(17)A/C/G	Fig 3.32 A and B, pair "a"
mXhoI dir1	CCGCTCGAGTCTGCCTTTCTCTATGCTA	Fig 3.32 A and B
anchor 1	TAGGAATTCTCGAGCGGCCGC	pair "b"

Table 2.1: List of oligonucleotides used for mRNA analysis (performed by RT-PCR, 3'RACE-PCR and Primer Extension) and for the synthesis of dsDNA Northern blot probes (obtained by PCR).

In general, 2 µl of the RT reaction (cDNA), 0.1 ng for plasmid and 100-500 ng of genomic DNA were used for amplification. The amplification was performed on a Cetus DNA Thermal Cycler (Perkin Elmer) or on a Gene Amp PCR System (Applied Biosystems) and the cycles were determined for each reaction in relation to the length of the DNA fragment to amplify and to the chemical features of the oligo primers involved in the reaction. Generally, conditions for PCR were: 1 cycle (initial denaturation step at 95 °C for 2 min), 25-35 cycles (denaturation step at 95 °C for 30 sec; annealing step at 56-58 °C for 30 sec; extension step at 72 °C for 1-1.5 min), 1 cycle (final extension step at 72 °C for 10 min). To verify the correct size of the PCR products and to optically quantify, ~1/5 of the PCR volume were separated in agarose gel for DNA.

RT-PCR reactions were performed to identify specific fragments of the β-adducin transcript. Moreover, several PCR-products obtained from genomic DNA were gel purified and cloned into plasmids or labelled and used as probes. Table 2.1 shows the oligonucleotide primers used to performe β-adducin expression analyses and to synthesise the numerous Northern blot analyses probes.

2.17 Preparation of bacterial competent cells

Bacterial competent cells were prepared following the method described by Chung(Chung et al., 1989). *E.Coli* strains were grown overnight in 5 ml of LB at 37°C. The following day, 100 ml of fresh LB were added and the cells were grown at room temperature for 4-5 h until the OD_{600} was 0.3-0.4. The cells were then put in ice and centrifuged at 4 °C and 1000g (Eppendorf, 5810-R rotor) for 15 min. The pellet was resuspended in 10 ml of cold TSS solution [10% w/v PEG molecular weight 4000, 5% v/v DMSO, 35mM $MgCl_2$, (pH 6.5) in LB medium]. The cells were aliquoted, rapidly freeze in liquid nitrogen and stored at –80°C. Competence was determined by transformation with 0.1 ng of pUC19 and was deemed satisfactory if this procedure resulted in more than 100 colonies (transformation efficiency $\geq 10^5$ cfu/ug).

2.18 Transformation of bacteria

Transformation of ligation reactions were performed using 1/2 of the reaction volume. Transformation of clones was carried out using 1ng of the plasmid DNA. The DNA was incubated with 60 µl of competent cells for 30 min on ice. The cells were shock 2 min at 42 °C. After the step of heat shock, 100 µl of LB were added and the

bacteria allowed recover for 10-15 min at 37 °C. The cells were then spread on agarose plates containing the appropriate antibiotic. The plates were then incubated for 12-15 hours at 37 °C.

When DNA inserts were cloned into β-galactosidase-based virgin plasmids, 70 µl of IPTG 100 mM and 36 µl of X-Gal (4 % w/v in dimethylformamide) were spread onto the surface of the agarose prior to the plating to facilitate screening of positive clones (white colonies) through identification of galactosidase activity (blue colonies) which indicates the negative clones.

2.19 Sequence analysis for cloning purpose

Sequence analysis of plasmid DNA was performed using the CEQ 2000 sequencer (Beckman Coulter). The plasmid DNA of interest (approximately 100 ng) was purified through a MicroSpin S-400 HR Column (Amersham). The DNA was then amplified using fluorescent labeled dideoxy nucleotide terminators according to the manufacturer's instructions. The samples were analysed by loading them into the automatic sequencer.

2.20 Construction of the β-adducin chimeric minigene constructs

The minigenes used for the transfection experiments were created modifying a construct previously generated in our laboratory: pBS SV40 αGlobin. In this construct SV40 promoter sequence (352 bp) and the genomic sequence of human αGlobin (1071 bp) were cloned in the pBS II KS plasmid (Stratagene). The last part of the 3rd exon of αGlobin (344 bp) containing the polyadenylation sites was removed by digesting the construct with BstEII (located in the 3rd exon) and SalI (located in the pBS II KS polylinker) and replaced with a linker (linker 2) containing several unique restriction sites. The linker was generated using the primers indicated in Table 2.2. The different fragment containing the tissue-specific polyadenylation sites of β-adducin and their flanking sequences [insert $mSPA_1$ (1401 pb spanning from bases 16 to 1417 relative to the last 16 exon of mouse β-adducin), insert $mSPA_{2\text{-}3}$ (576 pb spanning from 1418 to 1994 relative to the last exon of mouse β-adducin) and $mBRA_4$ (1166 pb spanning from bases 5404 to 6570 relative to the 16 exon of mouse β-adducin), Table 2.2] were obtained by PCR from mouse genomic DNA, while PCR from human genomic DNA was used for generating the insert containing the polyadenylation site of β-globin [insert

hβGlo pA (345 bp) from bases 135 to 480 relative to the 3 exon of human β-globin]. In these reactions the primers showed in Table 2.2 were used. Each pair of oligonucleotides have a specific tails containing restriction enzyme sites required for the cloning strategy: 5'-end sites necessary for subcloning the inserts in pUC19 vector and internal sites essential for the step of cloning in the final minigenes. The PCR products were separated in agarose gels, cut from the gel and the DNA, purified as explained previously and subcloned in pUC19 (New England Biolabs). The intermediate pUC19 construct was then sequenced by CEQ 2000 sequencer (Beckman) as described above. Sequencing excluded the presence of mutations within the insert. To prepare the final chimeric minigene constructs the $mSPA_{1,}$ $mSPA_{2\text{-}3}$ $mBRA_4$ inserts, obtained degesting the intermedie pUC19 construct with the enzymes specific for the internal restriction enzyme site, were cloned in the correct sites of the linker 2 of the the pBS SV40-αGlo-linker2 construct. The final chimeric minigenes were used to transfect HeLa cells as described above.

Primers	**Sequence 5'- 3'**	**Inserts**	**Intermediate minigenes**
linker 2 dir 1	gtgacctacgtagcggccgcgacgtcccgcggactagtct	Linker2	pBS SV40-αGlo-linker2
linker 2 dir 2	taagtctagaatcgatgatatcagatctcatatgctgcaggaattcg		
linker 2 rev 1	tcgacgaattcctgcagcatatgagatctgatatcat		
linker 2 rev 2	cgattctagacttaagactagtccgcgggacgtcgcggccgctacgtag		
BamHI-SpeI SP A1 dir 1	cgggatccactagtaagtcagcgaagccaacaca	-$mSPA_1$-	pUC19-$mSPA_1$-
PstI-XhaI SP A1 rev 1	aactgcagtctagagtgatgggcttgggaatgc		
SP A2A3 dir 3 *KpnI-ClaI* tail	ggggtaccatcgattcttgcatcctgaagcttg	-$mSPA_{2\text{-}3}$-	pUC19-$mSPA_{2\text{-}3}$-
SP A2A3 rev 1 BamHI-BglII tail	cgggatccagatctcgactgtggtgggatttc		
BR A4 dir 1 *KpnI-NotI-NdeI* tail	ggggtaccgcggccgccatatgagtgtctcgtaagtaatgct	-$mBRA_4$-	pUC19-$mBRA_4$-
EcorI BR A4 dir 1 *BamHI-SacII-EcoRI* tail	cgggatccccgcgggaattcaccacttttcaccttattct		
hβGlo ex 3 *SalI* dir 1	tttctcgacgtccaatttctattaaaggttcc	-hβGlo pA-	pUC19-hβGlo pA-
3' hβGlo *SalI* rev 1	acttgaatccttttctgagggtcgactaagg		

Table 2.2: List of oligonucleotides used for the construction of the β-adducin chimeric minigenes.

2.21 *In vitro* site directed mutagenesis

In vitro site directed mutagenesis is a rapid and high efficient procedure that allows site-specific mutagenesis in double-stranded plasmids. The method is performed using the high fidelity *PfuTurbo* DNA polymerase and a temperature cycler.

The double-stranded DNA vector of interest (50 ng) and the two synthetic oligonucleotides primers, each complementary to opposite strands of the vector,

containing the desiderate mutations (125 ng of each) were diluted into the Puff DNA Pol reaction mix (2.5 U/µl *PfuTurbo* DNA polymerase, 1X reaction buffer, 200 µM dNTP mix). The complete mix was introduced in the temperature cycler [Gene Amp PCR System (Applied Biosystems)] and the primers were extended during temperature cycling by the *PfuTurbo* DNA polymerase [cycling parameters: 1 cycle (initial denaturation step at 95°C for 30 sec) and 18 cycles (denaturation step at 95°C for 30 sec; annealing step at 55 °C for 1 min; extension step at 68 °C for 1 min/kb of plasmid length)]. At the end of the reactions the incorporation of oligo primers generates a mutated plasmid containing nicks. After the temperature cycling, 10 U/µl of Dpn I restriction enzyme were added to the amplification reaction and an incubation of 1h at 37 °C followed. After the temperature cycling, the amplification product was treated with Dpn I restriction enzyme (10 U/µl of the enzyme, incubation of 1h at 37 °C). Considering that the DpnI endonuclease is specific for methylated DNA and that DNA isolated from almost all *E.Coli* strains is dam methylated (therefore susceptible to DpnI digestion), this specific restriction enzyme was used to digest the parental DNA template and to select for mutation-containing synthesised DNA. The mutated and nicked vector DNA containing the mutation is then transformed into *E.Coli* K12 strain DH5α cells having a higher grade of competence (transformation efficiency $\geq 10^6$ cfu/ug). A more efficient transformation procedure was used. The DpnI –treated DNA was incubated with 50 µl of competent cells for 30 min on ice. The cells were shock 45 sec at 42°C and then placed for 2 min in ice. After these steps, 500 µl of NZY^+broth [1% NZ amine (casein hydrolysate), 0.5% yeast extract, 0.5% NaCl, 12.5 mM $MgCl_2$, 12.5 mM $MgSO_4$, 20 mM glucose, (pH 7.5)] preheated to 42 °C were added and the bacteria allowed recover for 1 h min at 37 °C with shaking. The cells were then spread on agarose plates containing the appropriate antibiotic. The plates were then incubated for 12-15 hours at 37 °C.

This method was used to create the deletions constructs of β–adducin chimeric minigines. Intermediate pUC19 construct containing the single inserts (pUC19-$mSPA_1$-, pUC19-$mSPA_{2\text{-}3}$- and pUC19-$mBRA_4$-) were used as the double-stranded DNA template. The two synthetic oligonucleotides primers containing the mutations specific for each template were show in the Table 2.3. In each pair of primers we introduced a unique restriction site to allow a rapid screening of the positive clones. The polyadenylation regulatory element was deleted in each case as indicated in the Table

2.3. The mutated inserts were then excised from pUC19 construct and cloned in the correct site in the final chimerical minigenes.

Template constructs	Primers	Sequence 5'- 3'	Deleted regulatory element
pUC19-mSPA$_1$-	mSPA1 hexa.motif *Xho I* dir 1	tctcacaggctgaaaacccagctcgagcttaa	ATTAAA motif of mA$_1$ site
	mSPA1 hexa.motif *Xho I* rev 1	ttaagctcgagctgggttttcagcctgtgaga	
	mSPA1 U-motif *Eag I* dir 1	ctatgagcccaggagcccaccggccgaaaa	U-rich element of mA$_1$ site
	mSPA1 U-motif *Eag I* rev 1	ttttcggccggtgggctcctgggctcatag	
pUC19-mBRA$_4$-	mBRA4 hexa.motif *Eco RV I* dir 1	ctgcagatcttaccctccagatatccttggcttc	AGTAAA motif of mA$_4$ site
	mBRA4 hexa.motif *Eco RV I* rev 1	gaagccaaggatatctggagggtaagatctgcag	
	mBRA4 U-motif *Bcl I* dir 1	gtggactctgatcatgggcagatcttaccct	U-rich element of mA$_4$ site
	mBRA4 U-motof *Bcl I* rev 1	agggtaagatctgcccatgatcagagtccac	

Table 2.3: List of oligonucleotides used for creating deletion constructs of the β-adducin chimeric minigenes.

2.22 Cell culture maintenance

HeLa cell line was cultured in Dulbecco's modified Eagle's medium with glutamax (Gibco) supplemented with 10% fetal bovine serum and 1X antibiotic-antimitotic solution [100X of solution contains in 1 ml: 10000U penicillin, 10 mg streptomycin, 25 μg amphotericin B, (Sigma)]. 100 mm Petri dishes containing a confluent monolayer of cells were treated with 0.1% w/v trypsin as follows. Cells washed twice with PBS solution, were incubated at 37 °C with 1 ml of PBS/EDTA/trypsin solution (PBS containing 0.04% w/v EDTA and 0.1% w/v trypsin) for 2 minutes or until cells were dislodged. After adding 4-5 ml of media, cells were pelleted by centrifugation and resuspended in 5 ml pre-warmed medium. 1-2 ml of this cell suspension was added to 10 ml medium in a fresh plate and was gently mixed before incubation.

2.23 Cell culture transient transfections

Liposome-mediated transfections of HeLa cells were performed using Lipofectamine 2000 transfection reagent (Invitrogen) and the plasmid DNA used for transfections was purified with JetStar columns (Genomed). One day before transfection, 3 x 10^5 cells were plated in 35 mm Petri dish with 2 ml of growth medium without antibiotics for allowing cells to be 90-95% confluent at the time of transfection.

For each transfection reaction, 3 µg of construct DNA were diluted in 250 µl of Opti-MEM I medium (Gibco) without serum and mixed with 10 µl of transfection reagent also diluted in 250 µl of the previous medium. The mixture was incubated at room temperature for 20 minutes to allow the formation of DNA-liposome complexes, then added to the cells in 1.5 ml of serum free Opti-MEM I medium and finally incubated at 37 °C in a CO_2 incubator. After 18 h the cells were harvested. RNA isolation was performed using RNA as above described.

2.24 Northern Blot analysis

Different amounts of total RNA were loaded and run on an agarose-formaldehyde gel (1.2-1.5% w/v agarose, 12.3 M formaldehyde, 1X MOPS) at 65 V for approximately 4 h in 1X RNA running buffer. The gel was photographed under UV light and washed three times (15 min each) with large volumes of ddH_20. Then, the gel and the nylon membrane [Hybond-N^+ (Amersham Pharmacia biotech)] used for the successive blotting were incubated with 20X SSC for 15 min. The RNA was transferred to the nylon membrane by capillary blotting in 20X SSC during 16-20 h. The membrane was dried on a Whatman 3 MM filter paper for al least 15 min and the RNA was bound to the membrane by UV cross-linking (2X, 0.25J). To check blotting efficiency and also to normalise the Northern Blot the membrane was visualized and photographed under UV light. Then, the membrane was prehybridised for at least 1h and hybridised to the radiolabelled probe in 5ml of a commercial hybridisation solution [Ultrasensitive Hybridisation Solution (Ambion)], at 42 or 65 °C (in accordance to the features of the DNA probe) for 24 h. Three different washing solutions were used to clean the hybridised membrane. Firstly, three washes of solution I (2X SSC, 0.1% w/v SDS) were performed to remove the excess of the hybridisation probe. Secondly, the membrane was washed with more stringent solutions to eliminate non specific hybridisation: solution II (0.2X SSC, 0.1% w/v SDS) and III (0.1X SSC, 0.1% w/v SDS). After each wash the membrane was checked for radioactive signal using a geiger (Canberra Packard SRL) to evaluate if continue or suspend the washing. All washes were carried out using 100 ml of solution, at 42-65 ˚C, and with agitation for 15 min. Finally, the membrane was immediately covered with plastic wrap mounted on Whitman 3 MM filter paper and exposed overnight using Cyclone screen (Cyclone, Storage Phosphor System, Canberra Packard SAL) or BIOME MS film (Kodak) at -80 °C with BIOME

intensifying screen Quantification of the radioactive signal was obtained as explained later on.

2.24.1 - Hybridisation probes preparation -

The different DNA fragment that are used as Northern Blot hybridisation probes were obtained by RAT- PCR from total RNA of the right specie (m β-Add brain probe; β-Add total probes of mouse, rat and human; m β-Add63 probe; m β-Add97 probe) or PCR from genomic DNA (m β-Add 3'-UTR probes 1 and 2; m β-Add 16 ex probe; m-BR-A4 probe; h β-Glo pA probe). The specific oligonucleotide primers used for the reactions were indicated in Table 2.1. In all cases, the PCR product were separated in agarose gels and the band corresponding to the desired fragment in each case was cut from the gel and the DNA was purified as explained previously.

Radioactive probes were generated from 50 ng of DNA by the Rediprime II Random Prime Labelling System (Amersham Bioscience) using [α-^{32}P] dCTP (Amersham Bioscience) and were then purified from unincorporated nucleotides by Nick columns (Amersham bioscience). Both the labelling and the probe purification were carried out according to the manufacturers' instructions.

2.24.2 - Reutilisation of Northern blot membranes -

Removal of radioactive probes from membranes for subsequent rehybridisation was performed by incubation of the blot in sterile boiling ddH_2O containing 0.5% w/v SDS solution at 65 °C for approximately 30 min (twice), shaking frequently. The blot was removed from the stripping solution, allowed to cool on a Whatman 3 MM filter paper, and sealed in a plastic bag and stored at 4 °C or R.T. until use. The membranes were subjected to autoradiography or analysed by Cyclone screen (Storage Phosphor System, Canberra Packard SRL) to check successful stripping.

2.25 RNase protection assay and Primer extension assay

These experiments were performed essentially as described in Sambrook et al. 1989 (Sambrook, 1989) by Giulia Devescovi.

Briefly, for the RNase protection assay, overlapping fragments covering the entire rat β-adducin cDNA sequence were subcloned from a full-length rat cDNA clone into the pBS-II-KS plasmid (Stratagene). Each of the DNA subclones was linearized, the antisense strand synthesised radioactively (in the presence of [α-^{32}P] UTP) with either T7 or T4 RNA polymerase and purified through denaturing acrylamide gels. Each

[^{32}P]-labelled antisense RNA probe was incubated with rat brain or spleen total RNA in solution to allow the hybridisation of the probe with its specific target RNA and then each mix was treated with RNase A. Free probe and others single-stranded RNA are digested with RNase. The remaining "RNase-protected" β-adducin RNA hybrids of each reaction were resolved on denaturing polyacrylamide gels and visualized by autoradiography.

For primer extension, the oligonucleotide 5'βNC (Table 2.1), complementary to the end of the 99 bases rat exon 2 was annealed to rat spleen and brain RNA and the RT reaction was performed in the presence of radioactive [α-^{32}P] dCTP to produce single-stranded cDNA using the RNA as the template. The resulting primer extension products were run in denaturing acrylamide gels and exposed for autoradiography. A manual sequencing reaction was also run along with the primer extension and RNase digested products to precisely determine the size of the extended products.

2.26 3'-Rapid Amplification of cDNA Ends (3'-RACE-PCR)

3'-RACE-PCR is a technique used to obtain the 3'-end of an mRNA. After the cDNA synthesis, a first PCR was performed using as forward primer an internal oligonucleotide (complementary to the cDNA) and as a reverse primer an oligo(dT) that terminates in A, C or G linked to a specific 5′ extension sequence (anchor). In a second PCR the first PCR product was amplified with a reverse primer which anneals in the anchor and a forward primer located downstream of that used in the first reaction to give further specificity to the reaction (seminested PCR). This technique was used to determine the polyadenylation site of the endogenous β–adducin mRNAs, and to compare the 3'-end of the transcript generated after transfection with control chimeric minigenes and deletion mutant constructs of β-adducin. *BR A4 dir 1 KpnI-NotI-NdeI tail* (Table 2.2) and *dT-anchor 1* (Table 2.1) were used in the first PCR reaction, while *mXhoI dir 1* and *anchor 1* in the second (Table 2.1). The PCR product of the second reaction was separated by agarose gel for DNA, visualized by UV transillumination and finally the result recorded by digital photography.

2.27 *In situ* hybridisation assay

In situ hybridisation was performed in collaboration with Dr. Tongiorgi's laboratory at the BRAIN Centre for Neuroscience, Department of Biology, University of Trieste, Trieste (Italy).

2.27.1 - Tissue preparation -

Adult mice were anaesthetized and perfused through the left ventricle with cold PBS, followed by cold 4% paraformaldehyde in PBS. Brains were extracted and postfixed in the same fixative for 2 h at 4 °C and then stored in 20% sucrose and 4% paraformaldehyde in PBS at 4 °C until cutting. Brain sections were cut at 40 μm using a microtome, collected in 4% paraformaldehyde in PBS and stored at 4 °C until the hybridisation phase.

2.27.2 - Probe preparation -

Antisense and sense cRNA probes were obtained by *in vitro* transcription of a 312 bp cDNA fragment encoding for the exons 11-13 of mouse β-adducin, cloned in the pBS-II-SK vector (Stratagene). The 312 bp dsDNA fragment was obtained by RT-PCR from mouse spleen total RNA using the sense primer named m β-Add 11 ex dir 1 (5'-aagcagcagaaggaaaagac-3') and antisense primer PIN A (5'-ctcttctctgcgatgaca-3'). The biotin-labelled cRNA probes were synthesised in presence of biotin–UTP according the manufacturer's instructions of a commercial biotin-RNA labelling kit (Boehringer Mannheim).

2.27.3 - Hybridisation -

Briefly, brain sections were washed in PBS plus 0.1% Tween 20 (PBST), permeabilized by treatments with 2.3% sodium-m-periodate in ddH_2O for 5 min, 1% sodium borohydrate in 0.1 M Tris-HCl (pH 7.5) for 10 min and proteinase K (8 μg/ml) in PBST. The proteinase K reaction was blocked by washing sections in PBST and fixing in 4% paraformaldehyde in PBS for 5 min. After prehybridisation for 1 h in hybridisation mix at 55 °C [50% deionized formamide, 20 mM Tris-HCl (pH 7.5), 1 mM EDTA (pH 8), 1X Denhardt's solution, 330 mM NaCl, 100 mM dithiothreitol, 0.5 mg/ml salmon sperm DNA and 0.5 mg/ml polyadenylic acid], free-floating sections were transferred into hybridisation mix containing 100 ng/ml of the antisense or sense probe and incubated overnight at 55 °C. Sections were washed for 30 min twice in 2X standard saline citrate containing 0.1% Tween 20 (SSCT) and 50% formamide followed by a 20 min wash in 2X SSCT at 55 °C. Then two washes were performed for 30 min in 0.05X SSCT at 60 °C. Sections hybridised with biotin-labelled probes were incubated for 30 min at R.T. with avidin-biotin-horseradish peroxidase complex diluted 1:100 in PBS. After washing in PBS, specific signal was revealed by developing sections in 3-3′-diaminobenzidine tetrahydrochloride [10 mg of 3-3′-diaminobenzidine in 15 ml of

50mM Tris-HCl (pH7.5)] for 7 min at R.T. and counterstained with 0.5% cresyl violet. After washing, sections were collected on gelatin-coated slides, dried in an oven at 55 °C for 30 min, further dehydrated in 100% methanol for 2 min, cleared in xylene and mounted in DPX resin.

2.28 Database and bioinformatics analyses

The search for alternative exons in the β-adducin gene required analysis of both cDNA and expressed sequence tag (EST) sequences in the Genbank. To identify candidate first exons or alternative internal exons, we used each of the β-adducin exon sequences as probes for BLAST species-specific searches of Genbank. The candidate sequences that were found contiguous to β-adducin exons were checked for proper splicing and their chromosomal location was determined by BLAST analysis against the complete genome using the NCBI browser (http://www.ncbi.nlm.nih.gov/BLAST/). The alignment of the ESTs with the β-adducin genomic sequence and the detection of the ESTs containing poly(A) tails were analysed manually with the help of the UCSC Genome Browser (http://genome.ucsc.edu/). The coordinates of the chromosomal position of the exons and introns listed in Table 6 refer to that used in the ENSEMBL browser developed by the EMBL, EBI and Sanger Institute (http://www.ensembl.org/index.html). In order to confirm experimentally that these sequences were bona fide exons in the β-adducin gene, RT–PCRs were performed from brain and spleen total RNA.

Promoter analysis was performed with both the DNAstar Lasergene program and the TESS browser from the University of Pennsylvania (http://www.cbil.upenn.edu/cgi-bin/tess/tess?RQ=WELCOME). A selection of the predicted transcription factor binding sites that displayed a high score and were present in both analyses is shown in Figure 19 A and B.

Predictions of regulatory sequences in the β-adducin 3'-UTR were performed with several softweres:

1. UTRScan (http://www.ba.itb.cnr.it/BIG/UTRScan/),
2. MiRanda (http://www.microrna.org/),
3. TargetScan (http://www.targetscan.org/),
4. RegRNA (http://regrna.mbc.nctu.edu.tw/html/prediction.html).

Regulatory sequences detected in all the different prediction analyses were considered in the Discussion (Section 4B.10.2).

2.29 Preparation of RBCs protein extracts: ghosts, cytoskeletons, and cytoplasms

2.29.1 - Ghost and cytoplasm-

Erythrocyte ghosts were prepared from freshly drawn blood anticoagulated in 2 mM EDTA. RBCs were isolated from the other components of blood by mixing 1 volume of blood with 4 volume of sedimentation buffer [150 mM NaCl, 5mM sodium phosphate (pH 7.5), 0.75 % w/v Dextrane 500] at 4 ˚C. After incubating 1 hour at 4 ˚C, the supernatant was removed, and the settled erythrocytes were washed two times with 4 volumes of PBS and centrifuged at 6000 rpm 10 min 4 ˚C in HS-4 rotor (Sorvall Instruments). Any remaining buffy coat (neutrophils, platelets, lymphocytes, monocytes) was carefully removed because it is an important source of protease activity. The washed erythrocytes were lysed by rapid addition of 10 volumes of ice-cold lysis buffer [7.5 mM sodium phosphate, 1 mM EDTA (pH 7.5), and 2X protease inhibitors cocktail (Roche), containing or not 2mM $MgCl_2$]. The lysed cells were frozen/thawed twice in dry-ice to facilitate the lysis and immediately centrifuged at 40000 rpm 40 min 4 ˚C in Ti60 rotor (Beckman). The supernatant was considered as the cytoplasm fraction of red blood cells diluted in the lysis buffer. The pelleted ghosts were washed twice with lysis buffer (with or without 2mM $MgCl_2$) and centrifuged 30 min in the same conditions. The final ghost pellets were resuspended in the same buffer at 1/15 of starting volume by using a Dounce homogeniser 15 min at 4 ˚C. Ghost protein extracts were sonicated (3x10 sec on ice), and their protein determination was carried out and conserved at –80 ˚C.

2.29.2 - Cytoskeleton -

To prepare RBCs membrane cytoskeleton, the final ghost pellets were resuspended with 10 volumes of a Triton X-100 containing solution [10 mM Tris-HCl (pH 8.2), 100 mM NaCl, 1 mM EDTA, 2 mM DTT, 0.5 % v/v Triton X-100 and protease inhibitors containing or not 2mM $MgCl_2$] by using a Dounce homogeniser. The mix was incubated 15 min 4 ˚C to facilitate the extraction and centrifuged at 16000 rpm 40 min 4 ˚C in Ti60 rotor (Beckman). The pellet was resuspended and reextracted in the same Triton X-100 containing solution. The final pellet (cytoskeleton) was resuspended by using the Dounce homogeniser at 4 ˚C in the previous buffer without Triton (when the extract was analysed by SDS-PAGE) or in the 2D buffer [7 M urea, 2 M thiourea, 3% CHAPS, 400 mM DTT, 2% IPG-buffer and 2X protease inhibitor cocktail (Roche)]

(when the cytoskeleton was separated by 2D electrophoresis). Finally, the resuspended pellets were sonicated (3x10 sec on ice), the determination of protein concentration was carried out and the cytoskeletal sample was aliquoted at –80 ˚C.

2.30 Preparation of tissue protein extracts: total homogenates and cytoskeleton

2.30.1 - Total organ homogenates -

Adult mice were killed by cervical dislocation. Blood contamination was eliminated by extensive PBS perfusion of the mouse tissues. Organs were removed from the animals and frozen in liquid nitrogen until use. 2 ml of tissue lysis buffer [150 mM NaCl, 50 mM Tris-HCl (pH 8), 1 % w/v NP40, 2X protease inhibitor cocktail (Roche)] were added to the frozen tissue and homogenised on ice with a polytron [Ultra-Turrax T25 Basic homogenizer (Ika-Werkwe)] at maximal speed. Nuclei and debris were removed from the homogenate by centrifugation at 15000 rpm (5415-D rotor, Eppendorf) for 10 min at 4 ºC. The supernatant was decanted and recentrifuged in the same conditions for 5 min. The protein determination of the final supernatant (tissue total homogenate) was performed and the sample was conserved at -80 ºC until it will be used.

2.30.2 - Cytoskeleton -

To prepare cytoskeleton from organs, the final total tissue extracts were homogenised on ice for 1 min by using a Dounce homogeniser ice to facilitate the lysis of cells not lysed in the previous steps and immediately centrifuged at 40000 rpm 40 min 4 ˚C in Ti60 rotor (Beckman). The pellets were resuspended in 1 ml of a Triton X-100 containing solution [10 mM Tris-HCl, (pH 8.2), 100 mM NaCl, 1 mM EDTA, 2 mM DTT, 0.5 % v/v Triton X-100 and 2X protease inhibitor cocktail (Roche)]. The mix was incubated 15 min 4 ˚C to facilitate the extraction and centrifuged at 40000 rpm 40 min 4 ˚C in Ti60 rotor (Beckman). The resulting pellet (cytoskeleton) was resuspended by using the Dounce homogeniser at 4 ˚C in the previous buffer without Triton and sonicated (3x10 sec on ice). The protein concentration was determined and the cytoskeletal preparations were frozen and conserved at –80 ˚C.

2.31 Isolation and extraction of lens plasma membranes

Lens plasma membranes proteins were prepared as described by Dr. Fowler(Woo and Fowler, 1994). Adult animals (mice and rabbit) were sacrificed and lenses were dissected from their eyes. The lens nucleus was removed immediately and discarded, while the remaining capsule, ephotelial and cortical fiber cells were kept on ice or quick frozen in liquid nitrogen before use. Lens were washed in PBS and then homogenized on ice using the Dounce homogeniser in the lens buffer [100 mM NaCl, 20 mM Hepes (pH 4.5), 2 mM $MgCl_2$, 1 mM EGTA, 1mM DTT and 2X protease inhibitor cocktail (Roche)] at 16 mouse lens/ml (~30mg/ml). The resulting homogenate was centrifugated at 20000 rpm 20 min 4 ˚C in Ti60 rotor (Beckman). The supernatant was removed and the pellet was resuspended to the initial volume in lens buffer using the Dounce homogeniser followed by vortexing. The centrifugation step was then repeated, followed by two more round of resuspension and centrifugation. The resulting pellet (plasma membranes) was resuspended in the lens buffer at 1/15 of the initial volume and sonicated (3x10 sec on ice). Finally, the determination of protein concentration was carried out and the lens plasma membranes extract was aliquoted and stored at –80 ˚C.

2.32 Protein quantification

The protein concentrations were measured by triplicate by using the Bradford method [Protein Assay Kit (Bio-Rad)] as recommended by the manufacturers.

2.33 Electrophoretic separation of proteins

2.33.1 - Denaturing polyacrylamide gel electrophoresis (SDS-PAGE) -

Different amounts of proteins extracts were mixed with protein sample buffer (2X final), denatured for 5 min at 95 °C, ice-cooled and then loaded into the gels. Conventional slab gel SDS-PAGE was performed in 10 x 12 cm or 16 x 18 cm vertical gels (Hoefer Pharmacia Biotech, Inc), with the required percentage (mostly 8 or 10 %) of polyacrylamide (37.5:1 acrylamide:bis-acrylamide, Ultra pure ProtoGel, National Diagnostics), depending on each case. Solutions used for preparing the *5% stacking gels* were: polyacrylamide diluted 1:6, 1/2 volume of 0.5M Tris pH 6.8, 0.1% SDS, 0.1% Ammonium persulfate, and 1µl/ml TEMED. Solutions used for preparing the *running gels* were: the right volume of polyacrylamide mix, 1/2 volume of 1.5 M Tris (pH 8.8), 0.1% SDS, 0.1% Ammonium persulfate, and 1µl/ml TEMED. The electrophoretic run

was performed at 25-30 mA for 4-5 h or overnight at 5-7 mA using 1X running buffer for SDS-PAGE. After running, gels were either stained with coomassie Blue R250 in methanol-water-acetic acid or transferred to nitrocellulose membrane for western blot analysis.

2.33.2 - Bi-dimensional electrophoresis (2D-Gels) -

a) First dimension: isoelectrofocusing (or IEF)

This dimension separates proteins by their charge (isoelectric point -pI-). 100-300 µg of the protein extract resuspended in 2D buffer [7 M urea, 2 M thiourea, 3% CHAPS, 400 mM DTT, 2% IPG-buffer and 2X protease inhibitor cocktail (Roche)] were loaded into commercial dehydrated IPG strips [Immobilized pH Gradients stipt (Bio-Rad)]. Different pH ranges strips were used (3–10 linear or non linear, 4–7 and 5–8 linear; 13 or 17 cm long). After the loading of the sample the Protean IEF (Bio-Rad) cell was set to a first rehydration phase and a second separation phase following the protocol described by the manufacturer.

b) Second dimension: SDS-PAGE

The second dimension separates proteins by their size (molecular weight). At the end of IEF the IPG strips were equilibrated to give proteins a negative charge and reduce their reformed disulphide bridges. The equilibration phase was carried out in two steps, both of 10 min incubation using 2 similar buffers: DTT-equilibration buffer (50 mM Tris-HCl (pH 8.8), 6 M urea, 30% v/v glycerol, 2% w/v SDS, 2% w/v DTT and 0.025% w/v bromophenol blue) and iodoacetamide-equilibration buffer (the previous one containing 2.5% iodoacetamide instead of 2% w/v DTT). The proteins on the equilibrated IPG strips were separated by the conventional SDS-PAGE. The preparation and running of the SDS-PAGE was performed as described above, with the only exception that the stacking gel was eliminated and the IPG strip was loaded directly on the vertical running gel. After running, gels were silver stained. The spots were visually analysed and will be further examined by proteomics.

2.34 Polyacrylamide gel staining

2.34.1 - Coomassie blue staining -

Following SDS-PAGE, gels were soaked O.N. in Coomassie staining solution (0.2% w/v Coomassie brilliant blue R 250, 10% v/v acetic acid, 40% v/v methanol, 50% v/v H_2O) and destained in the destain solution (10% v/v acetic acid, 25% v/v methanol,

65% v/v H_2O) until appearance of the bands. The stained gels were conserved in 1% acetic acid for some days and dried by gel-dryer usage (Bio-Rad, Hercules).

2.34.2 - Silver staining -

After the second dimension of the bidimensional electrophoresis the proteins were simultaneously fixed and stained using Vorum silver stain protocol(Mortz et al., 2001). The 2D gel was fixed for 2 h or O.N. in the fixing solution (50% v/v methanol, 12% v/v acetic acid, 0.05% w/v formalin) and washed in 35% v/v ethanol (3X for 20 min). A brief incubation (2 min) with 0.02% of $Na_2S_2O_3$ was performed for sensibilizing the subsequent steps. The gel was again rapidly washed in ddH_2O (3X for 5 min) and incubated in the cold staining solution (0.2% w/v $AgNO_3$ and 0.076% w/v formalin) for 20 min. After two washes of 1 min in ddH_2O, the gel was soaked in the developer solution (6% w/v Na_2CO_2, 0.05% w/v formalin and 0.0004% w/v $Na_2S_2O_3$) for the time sufficient to stain the proteins. When the protein-spots were visible the staining reaction was blocked with the stop solution (50% v/v methanol and 12% v/v acetic acid). 1% acetic acid was used to conserve the stained gels for some days.

2.34.3 - Stained gel analysis -

The gel images obtained by both the staining techniques were acquired with the VersaDoc Imaging System (Bio-Rad) and bands or spots quantified with the help of the Quantity One software (Bio-Rad).

2.35 Proteomic analysis

2.35.1 - Protein digestion and extraction from SDS-PAGE -

The selected bands and spots (from the SDS–PAGE and 2D gels, respectively) were excised from the coomassie blue or silver stained gel and cut in to little pieces. Coomassie blue stained gel fragments were incubated in 1ml of equilibration buffer [100 mM ammonium bicarbonate (pH 8)] two or more times (1 h on electric shaker, for each wash) till the pH of the surnatant was 8. Differently, Silver stained gel fragments were washed with 300 µl of ddH_2O (15 min) to eliminate the acetic acid residues, incubated in 50 µl of a destain solution (15 mM potassium ferrocianate and 50 mM sodium triphosphate) the time sufficient to discolour the pieces and then washed again with ddH_2O in the previous condition. Then the fragments were washed in sequence with the following buffers (300 µl of each, for 15 min): 100% w/v acetonitrile, 100 mM ammonium bicarbonate (pH 8), 100 mM ammonium bicarbonate (pH 8) in 50% w/v

acetonitrile and 100% w/v acetonitrile. In each step the supernatant was discarded and finally the gel pieces were dried via SpeedVac (SC100, Savant). Reduction and alkylation of the protein were performed incubating the gel dried fragments in different solutions [A: 50 µl of 10mM DTT in100 mM ammonium bicarbonate (pH 8) -1h, 56 °C-; B: 50 µl of 50 mM iodoacetamide in 100 mM ammonium bicarbonate (pH 8) -30 min, R.T.-; C: 300 µl of 100 mM ammonium bicarbonate (pH 8)-15 min, R.T.-; D: 20 mM ammonium bicarbonate (pH 8) in 50% w/v acetonitrile -15 min, R.T.-; E: in acetonitrile -5 min, R.T.-]. After the last wash the gel pieces were again dried via SpeedVac (SC100, Savant. To digest the proteins contained in the gel 10 µl of trypsin solution [100 mM ammonium bicarbonate (pH 8) containing 0.1 µg/µl trypsin (Promega)] were added to the fragments. After 2 min, 100 µl of the equilibration buffer were added and the enzymatic reaction was carried out for 12 h at 37 °C. The supernatant containing the digestion products was collected. Gel pieces were incubated with 100 µl of ddH_2O (5 min) and then with 100 µl of 60% v/v acetonitril and 1% v/v trifluoreacetate to extract the hydrophilic and hydrophobic peptides, respectively, remained in the gel matrix. The supernatants collected from the last two steps were added to the previous one and dried via SpeedVac. The dried peptides were conserved at -80 °C till mass spectrometry analysis.

2.35.2 - Mass spectrometry analysis -

The digestion products extracted from the acrylamide gel bands or spots were separated by micro-high pressure liquid chromatography and analysed by electrospray ionization mass spectrometry (Finnigan LCQ DECA, Thermo-Finningan Corp., San Jose, CA). The tandem mass spectrometry data were analysed with MASCOT (Matrix Science) and SEQUEST (ThermoFinnigam) software. These analyses were performed with the help of Yuna Ayala in collaboration with the Proteomic Laboratory of ICGEB.

2.36 Western blot analysis

Protein extracts separated by SDS-PAGE were transferred to nitrocellulose membranes (Hybond-C Extra, Amersham) either for 2.5 h at 200 mA or O.N. at 50 mA in the presence of 1X protein blotting buffer supplemented with methanol at 5, 10 or 20%. Following a blocking step of 1h at R.T. or O.N. at 4 °C in the appropriate buffer (5-10 % w/v non fat dry milk in PBS) the membranes were incubated for one hour with the primary antibody and then washed 3 times in PBS with or without 0.2-0.5% Tween-

20 (Sigma). Next, the appropriate secondary antibody (directed against mouse, rabbit or goat Immunoglobulins) conjugated with horseradish peroxidise (HRP) (Dako Cytomation, 1:2000) was used for incubating the membrane, for one hour and others washes were performed. Antibodies were diluted in washing solution and all washes were carried out during 15 min (2-3 solution changes) in volumes of 15-20 ml. A chemiluminescent reaction, generated by adding the chemiluminescent ECL- substrate (Enhanced Chemi-Luminiscent, Amersham Biosciences) to the membrane, was used to impress films (Hyperfilm-ECL, Amersham Biosciences) and obtain the signal. Serial ECL expositions of the membranes (sec to a few min) were performed to determine the optimum linear range to quantify the signals. Film images were then acquired with the Versadoc scanner (Bio-Rad) and quantification of the signals was performed with the help of the Quantity One software (Bio-Rad). Slight modifications of this basic protocol were introduced according to the antibodies utilised in each case.

2.36.1 - Antibodies -

Several primary antibodies were used for the western blot experiments. Anti-α- and β-adducin polyclonal antibodies were generated by immunizing rabbits with recombinant full-length rat α- and β-Add97 adducin subunits, respectively. Anti-γ-adducin antibodies were obtained by immunizing rabbits with the recombinant C-terminal region of the mouse γ-subunit (GeneBank Accession Number: AF189 772). The antibodies against adducin showed no cross-reactivity in the conditions used in the experiments. Monoclonal antibodies anti-CapZ-α and -β (5B12.3 and 3F2.3, respectively) and anti-α-tropomyosin (CH1) were from Developmental Studies Hybridoma Bank at the University of Iowa. The CH1 monoclonal antibody was generated using adult heart tropomyosin (mainly α-TM isoform) as antigen(Lin et al., 1985). Anti-protein 4.1 was a gift from Dirk Hofer, Anatom. Institut, Wurzburg, Germany, anti-p55 (sc-13603) and anti-tropomodulin (sc-19206) were from Santa Cruz Biotechnology, anti-dematin (D77620) was from BD Transduction Laboratories, and anti-actin (A2066) was from Sigma.

2.36.2 - Reutilisation of Western blot membranes -

Removal of primary and secondary antibodies from membranes for subsequent reprobing with other antibodies was possible following the protocol recommended by the booklet of ECL system, (Amersham Bioscience). Thus, the membrane was submerged in 200 ml of stripping buffer [2 % w/v SDS, 62.5 mM Tris-HCl (pH 6.8),

100 mM 2-mercaptoethanol] and incubated at 65 ˚C for 30-45 min with agitation. Then the membrane was washed twice (10 min each) in PBS at R.T. incubated with secondary antibodies and immunodetection was performed, as previously described, to check the removal of the primary antibodies. After 1 h blocking in milk, membranes were incubated with a different primary antibody.

2.37 ECapZ binding assay to erythrocytes mutant and control ghosts

HPLC-purified human erythrocyte adducin was prepared by M. Marro at ICGEB. Briefly, ghosts from β-adducin deficient erythrocytes (20 μg) were incubated with increasing amounts of HPLC-purified human adducin (0.7, 1.4 and 2.8 μg) in 200 μl of binding buffer [20 mM Hepes (pH 7.3), 100 mM KCl, 2 mM $MgCl_2$, 1 mM EGTA, 0.1% Triton X-100, and 1 mM DTT] for 30 min at 0 °C. Control reactions were performed in the same conditions but omitting ghosts and adding 20 μg of BSA or by omitting purified adducin. After the incubation, 200 μl of the same buffer containing 10% sucrose were added to the samples and centrifuged for 10 min at top speed in a 5415-D rotor (Eppendorf) (4 °C) to separate membrane-associated adducin from unbound adducin in the supernatant. The pellets were resuspended in the 2X protein sample buffer, separated by electrophoresis on 10% SDS–PAGE and blotted onto a PVDF membrane. Membrane was analysed with antibodies against ECapZβ and β–adducin as previously described.

3 RESULTS

Chapter A

Characterisation of erythroid and non-erythroid cytoskeleton in β-adducin deficient mouse

Although the membrane skeleton has been previously analysed in RBCs lacking β-adducin, the alterations in its composition and structure have been only partially elucidated (Gilligan et al., 1999; Muro et al., 2000). Chapter A reports the consequences of the absence of β-adducin in the architecture of the cytoskeleton of erythroid and non-erythroid cells of mutant mice.

3A.1 Analysis of the protein component of RBC skeletons by SDS-PAGE and mass spectrometry

During the last years the human erythrocyte membrane has been deeply characterised and the components of RBC ghosts and skeletons are very well known.

We have shown that one of the consequences of β-adducin deficiency was the alteration in the relative amounts of α- and γ-adducin, and several unknown skeletal proteins (Muro et al., 2000). To determine the identity of these proteins we prepared skeletal extracts from normal and mutant β-adducin erythrocytes, separated them by SDS-PAGE and the bands showing different levels were analysed by mass spectrometry. As can be observed in Figure 3.1, normal levels of α– and β–spectrin, Band 3, Protein 4.2 and Protein 4.1 were detected in β–adducin deficient RBCs skeletons. However, we observed a minor reduction in actin levels in the extracts of mutant red cells (Figure 3.1), confirming previous results (Muro et al., 2000). Differences in at least other eight bands (numbered 1 to 8 in Figure 3.1) were also observed. The bands of apparent MW of 100, 85, 65 and 32 kDa (Figure 3.1, *Bands 1, 2, 3* and *8,* respectively) were observed only in preparations of control mice, while those having an apparent MW of 60, 55, 38 and 35 kDa (Figure 3.1, *Bands 4, 5, 6* and *7,* respectively) were exclusive of mutant mice. These bands were cut from the gel, digested with trypsin and the resulting peptide fragments were analysed by mass

spectrometry. The mass spectrometry data was analysed using two different algorithms (SEQUEST and MASCOT). Both software packages identify the potential candidate proteins through a statistical evaluation of cross correlations or matches between the observed data and that already present in protein databases. These results are summarized in Table 3.1.

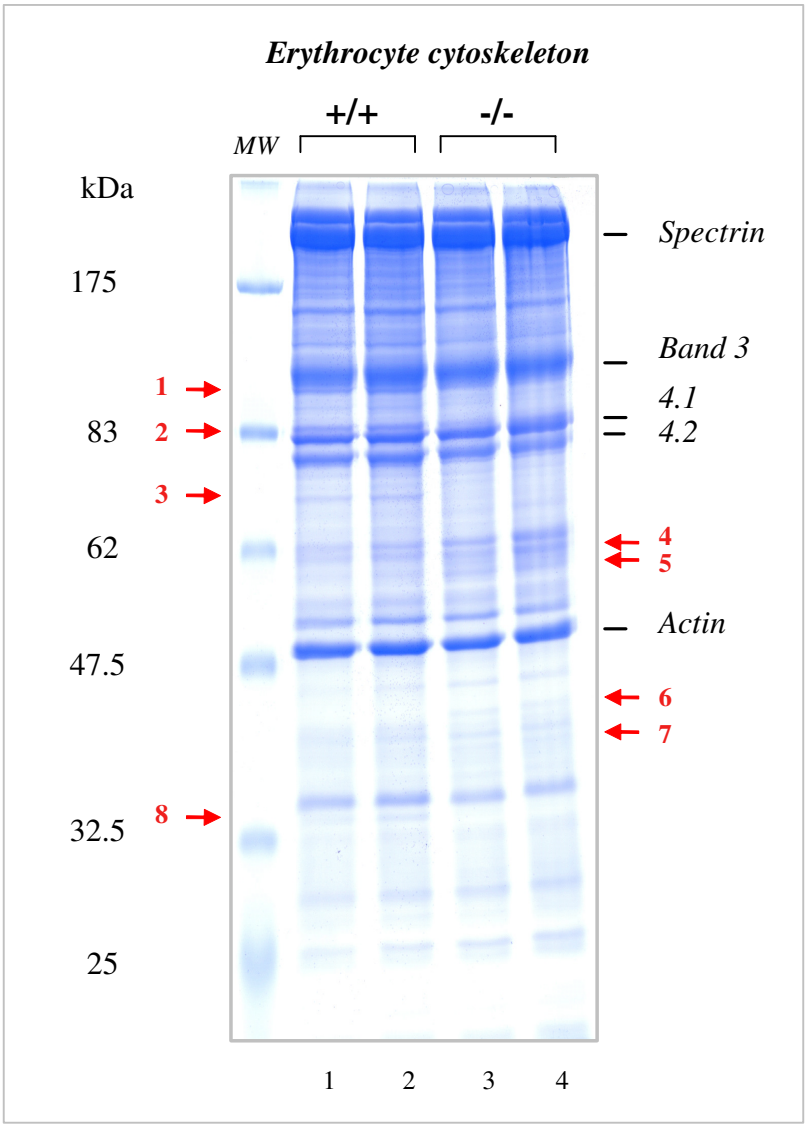

Figure 3.1: SDS-PAGE analysis of RBCs skeletal proteins. Different preparation of control and mutant (Lanes 1-2, and 3-4, respectively) erythrocyte membrane cytoskeleton (80 µg) were separated by SDS–PAGE (10%) and Coomassie blue stained. The major RBC skeletal proteins are indicated in the right with their names, while molecular weight markers on the left. The bands corresponding to unknown proteins that show different levels between control and mutant preparations are indicated with red arrows and numbers from 1 to 8.

Bands	*Cytoskeleton*	*Observed MW (kDa)*	*PROTEINS*	*Expected MW (kDa)*	*Peptide matched*	*Sequence coverage*
1	**+/+**	**100**	• TER ATPase	90	22	24 %
			• β-spectrin	245	22	11 %
			• α-spectrin	280	17	7 %
			• Band 3	100	13	10 %
			• MEB 3	102	13	10 %
2	**+/+**	**85**	• Protein 4.1	80	30	29 %
			• β-spectrin	245	16	8 %
			• α-spectrin	280	9	4 %
			• Ankyrin	121	2	1 %
3	**+/+**	**65**	• α–spectrin	280	19	9 %
			• β–adducin	81?	14	16 %
			• β-spectrin	245	9	5 %
			• Protein 4.1	80	6	10 %
			• α-adducin	81?	2	3 %
4	**-/-**	**60**	• γ–fibrinogen	50	8	13 %
			• β–fibrinogen	55	5	10 %
			• α-tubulin	50	4	13 %
			• α-spectrin	280	3	1 %
			• Dematin	48-52	2	6 %
5	**-/-**	**55**	• γ-fibrinogen	50	11	19 %
			• β-fibrinogen	55	7	3 %
			• α-spectrin	280	7	12 %
			• β-spectrin	245	3	2 %
			• Dematin	48-52	2	5 %
6	**-/-**	**38**	• **ECapZ-α**	32	17	69 %
			• ribosomal protein L6	33	16	42 %
			• β-spectrin	245	7	4 %
			• ubiquitin	34	2	32%
			• aquaporin 1	29	4	15 %
7	**-/-**	**35**	• **ECapZ-β**	30	15	50 %
			• ribosomal protein L7	29	8	28 %
			• ribosomal protein S6	28	6	20 %
			• ribosomal protein S2	31	7	25 %
8	**+/+**	**32**	• **α-tropomyosin**	29	28	68 %
			• β-tropomyosin	32	9	20 %
			• ribosomal protein L7	29	9	21 %
			• ribosomal protein S3	26	6	30 %
			• histon H1	21	3	10 %

Table 3.1: Results of mass spectrometry analyses of skeletal proteins separated by SDS-PAGE. The table summarizes the results obtained from the mass spectrometry analyses of the bands (numbered from 1 to 8) corresponding to unknown proteins showing different levels between control and mutant skeletal preparations in SDS-PAGE of Figure 3A.1.

The output of the mass spectrometry analysis evidenced more than one protein species present in each one of the analysed bands (Table 3.1). To distinguish the specific results from noise, we re-examined the obtained mass spectrometry data considering the following parameters:

- *Molecular size:* the expected molecular weight of the identified proteins was compared to that observed in the original gels;
- *Peptide match:* is the number and length of experimental peptides that match with the fragments of the theoretical proteins identified by the software. The probability that a peptide obtained by mass spectrometry belongs to a specific protein is directly proportional to the length of the experimentally identified fragment;
- *Sequence coverage:* it is the percentage between the number of aminoacids in the experimental peptides matching the protein and those of the full length protein itself. A value of 100% indicates that peptides covering the complete primary sequence of the protein were obtained;
- *Function of the identified protein and its subcellular or tissue localisation.*

We observed that peptides of proteins having a higher expected molecular weight than the observed ones were present in the majority of the analysed bands, suggesting that they were probably degradation products of higher molecular weight proteins. In the case of the bands having 85, 60 and 55 kDa of observed MW (Figure 3.1, *Bands 2, 4* and *5*) the mass spectrometry analysis revealed the presence of α- and β-spectrin peptides, proteins having a higher expected MW than the observed one. The 65 kDa band (Figure 3.1, *Band 3*) found in +/+ skeleton extracts was probably a degradation product of β-adducin as numerous peptides of the β subunit were detected by the analysis (Table 3.1).

After an accurate analysis of the mass spectrometry data we focused our attention to the following three proteins:

1) **ECapZ-α**: corresponds to the 38 kDa band detected only in the mutant erythrocyte skeleton extracts (*Band 6,* Figure 3.1 and Table 3.1);

2) **ECapZ-β**: corresponds to the 35 kDa band observed in the -/- RBC skeleton samples exclusively (*Band 7,* Figure 3.1 and Table 3.1);

3) **α-tropomyosin**: corresponds to the 32 kDa band detected only in the control skeleton erythrocyte preparations (*Band 8,* Figure 3.1 and Table 3.1).

A

>gi|1345694|sp|P47753|CAPZA_MOUSE **F-ACTIN CAPPING PROTEIN ALPHA-1 SUBUNIT (CAPZ)**gi|595917|gb|AAC00566.1| (U16740) capping protein alpha 1 subunit (Mus musculus) (MASS=32752)

DFEDR**VSDEE KVR**IAAK**FIT HAPPGEFNEV FNDVRLLLNN DNLLREGAAH AFAQYNMDQF TPVKIEGYDD QVLITEHGDL GNSR**FLDPR**N QISFKFDHLR** KEASDPQPED VDGGLK**SWRE SCDSALRAYV KDHYSNGFCT VYAKTIDGQQ TIIACIESHQ FQPK**NFWNGR** WRSEWK**FTIT PPSAQVVGVL KIQVHYYEDG NVQLVSHK**DV QDSVTVSNEI QTTK**EFIKII ESAENEYQTA ISENYQTMSD TTFK**ALR**RQL PVTRTKIDWN KILSYKIGKE MQNA**

>average mass = **32733**

position	sequence (**NCBI BLAST** link)
6- 13	VSDEEKVR
277- 284	IGKEMQNA
258- 264	RQLPVTR
96- 100	FDHLR
225- 228	EFIK
272- 276	ILSYK
265- 271	TKIDWNK
102- 116	EASDPQPEDVDGGLK
90- 95	NQISFK
192- 208	IQVHYYEDGNVQLVSHK
165- 170	NFWNGR
65- 84	IEGYDDQVLITEHGDLGNSR
46- 64	EGAAHAFAQYNMDQFTPVK
18- 35	FITHAPPGEFNEVFNDVR
229- 254	IIESAENEYQTAISENYQTMSDTTFK
36- 45	LLLNNDNLLR
177- 191	FTITPPSAQVVGVLK

Protein Coverage: 196/284 = **69.0%** by amino acid count, 22492/32733 = **68.7%** by mass

B

>gi|1345668|sp|P47757|CAPZB_MOUSE **F-ACTIN CAPPING PROTEIN BETA SUBUNIT ISOFORMS 1 AND 2 (CAPZ)**gi|1083244|pir||B54819 actin-capping protein beta chain, splice form 1 - mouse•gi|500747|gb|AAA52226.1| (U10406) capping protein beta-subunit, isoform 1 (Mus musculus) (MASS=31345)

MSDQQLDCAL DLMR**RLPPQQ IEK**NLSDLID LVPSLCEDLL SSVDQPLKIA RDKVVGKDYL LCDYNRDGDS YR**SPWSNKYD PPLEDGAMPS AR**LR**KLEVEA NNAFDQYRDL YFEGGVSSVY LWDLDHGFAG VILIK**KAGDG SKKIKGCWDS IHVVEVQEKS SGRTAHYKLT STVMLWLQTN K**SGSGTMNLG GSLTR**QMEKD ETVSDCSPHI ANIGR**LVEDM ENK**IR**STLNE IYFGKTKDIV NGLR**SLDAIP DNHKFKQLQR ELSQVLTQRQ VYIQPDN

>average mass = **31327**

position	sequence (**NCBI BLAST** link)
15- 23	RLPPQQIEK
16- 23	LPPQQIEK
216- 223	LVEDMENK
236- 244	TKDIVNGLR
238- 244	DIVNGLR
182- 195	SGSGTMNLGGSLTR
95- 108	KLEVEANNAFDQYR
96- 108	LEVEANNAFDQYR
226- 235	STLNEIYFGK
73- 92	SPWSNKYDPPLEDGAMPSAR
109- 135	DLYFEGGVSSVYLWDLDHGFAGVILIK

Protein Coverage: 111/277 = **40.1%** by amino acid count, 12394/31327 = **39.6%** by mass

C

>gi|136097|sp|P21107|TPMI_**MOUSE TROPOMYOSIN 5**, CYTOSKELETAL TYPE□gi|111212|pir||S11390 tropomyosin 5 - mouse□gi|54912|emb|CAA37782.1| (X53753) tropomyosin 5 (Mus musculus) (MASS=29021)

MAGTTTIEAV KR**KIQVLQQQ ADDAEERAER** LQREVEGERR AR**EQAEAEVA SLNRRIQLVE EELDRAQERL ATALQKLEEA EKAADESER**G MKVIENR**ALK DEEKMELQEI QLK**EAK**HIAE EADRKYEEVA RKLVIIEGDL ERTEERAELA ESR**CR**EMDEQ IRLMDQNLK**C LSAAEEK**YSQ KEDKYEEEIK ILTDKLK**EAE TR**AEFAER**SV AKLEK**TIDDL EDKLK**CTKEE HLCTQRMLDQ TLLDLNEM

>average mass = **29002**

position	sequence (**NCBI BLAST** link)
117- 124	HIAEEADR
147- 153	AELAESR
191- 195	ILTDK
125- 131	KYEEVAR
203- 208	AEFAER
77- 89	LEEAEKAADESER
156- 162	EMDEQIR
70- 76	LATALQK
163- 169	LMDQNLK
178- 190	YSQKEDKYEEEIK
191- 197	ILTDKLK
117- 131	HIAEEADRKYEEVAR
43- 55	EQAEAEVASLNRR
43- 54	EQAEAEVASLNR
13- 27	KIQVLQQQADDAEER
14- 27	IQVLQQQADDAEER
13- 30	KIQVLQQQADDAEERAER
14- 30	IQVLQQQADDAEERAER
216- 225	TIDDLEDKLK
132- 142	KLVIIEGDLER
55- 65	RIQLVEEELDR
132- 146	KLVIIEGDLERTEER
55- 69	RIQLVEEELDRAQER
56- 65	IQLVEEELDR
56- 69	IQLVEEELDRAQER
98- 113	ALKDEEKMELQEIQLK
105- 113	MELQEIQLK
133- 142	LVIIEGDLER

Protein Coverage: 168/248 = **67.7%** by amino acid count, 19825/29002 = **68.4%** by mass

Figure 3.2: Mass spectrometry results of ECapZ-α (A), ECapZ-β (B) and α-tropomyosin (C) obtained by SEQUEST analysis. In the three Panels the peptides product of the trypsin digestion experimentally identified by mass spectrometry are evidenced in red at the level of the total protein sequence. The same single peptides with their relative position in the protein sequence are listed in blue. The protein coverage (percentage) is also indicated for each result at the bottom of each panel.

A high score of peptide mach and sequence coverage were obtained only for these three proteins (Table 3.1 and Figure 3.2 A, B, and C). Moreover, the experimentally identified peptides that match with the three molecules have a remarkable length. Additionally, these proteins were not only components of the RBC skeletal network whose physical localisation and role were close to that of adducin (Bennett and Gilligan, 1993), but also there was a precise agreement between the observed and expected molecular weight of those proteins (Figure 3.2, A, B, and C).

In addition, even if protein 4.1 was identified in *Band 2* and dematin in *Bands 4* and *5* and their expected MW were similar to the observed ones (Figure 3.1 and Table 3.1), the low score of peptide matching and sequence coverage, in particular for

dematin, suggested that the mentioned bands were not that identified by mass spectrometry (Table 3.1).

3A.2 2-D gels and mass spectrometry analysis of the protein component of RBC skeleton

To confirm the differences detected by SDS-PAGE (Figure 3.1 and Table 3.1) and to detect other alterations in the β-adducin -/- RBC skeletal composition, we performed the high-resolution two-dimensional (2D) electrophoresis technique. It is based in the sequential separation of the proteins using two different principles: isoelectric focusing (IEF) for the first dimension and SDS-PAGE for the second one.

Equal amounts of skeletal protein extracts from RBCs of mutant and control mice were initially separated using IPG strips having a broad pH range (pH 3-10 linear) (Figure 3.3 A and B). As most skeletal proteins showed an isoelectric point between pH 4 and 8, we then used a more restricted pH range to improve the resolution in the 2D-gel (pH 5-8 linear IPG strip) (Figure 3.3 C and D). Several differences in the number and intensity of spots between β-adducin deficient and normal erythrocyte skeletons were detected in the silver stained 2D gels (Figure 3.3), suggesting that both protein composition and the levels of some polypeptides were altered in the RBC skeletal network of β-adducin deficient mice.

The identity of the spots showing major differences (Figure 3.3) was determined by mass spectrometry. On the contrary to that obtained from the previous SDS-PAGE analyses, single proteins with an elevated score of peptide matching and sequence coverage were identified from the 2D analysis (Table 3.2). These observations indicated that the proteomic analysis performed after the 2D gel separation produced more reliable results than those previously obtained (Figure 3.1 and Table 3.1).

As Table 3.2 shows, the data obtained by this second proteomic analysis were in agreement with those previously obtained (Table 3.1). In fact, the second mass spectrometry analysis indicated that the spots of 38 and 35 kDa were the ECapZ-α and ECapZ-β subunits, respectively (Figure 3.3 B and D, *Spots 4* and *5* and Table 3.2). They showed an approximated pI of 5.4 and 5.7, respectively, and were visible only in the preparation from mutant mice. The *Spot 6*, identified as α-tropomyosin, was detected only in wild type samples (Figure 3.3 A). It had an approximate pI of 4.6 and a relative

MW of 30 kDa. Moreover, *Spot 1* (Figure 3.3 A) was associated to β-adducin and, as expected, was absent in the extracts of KO animals.

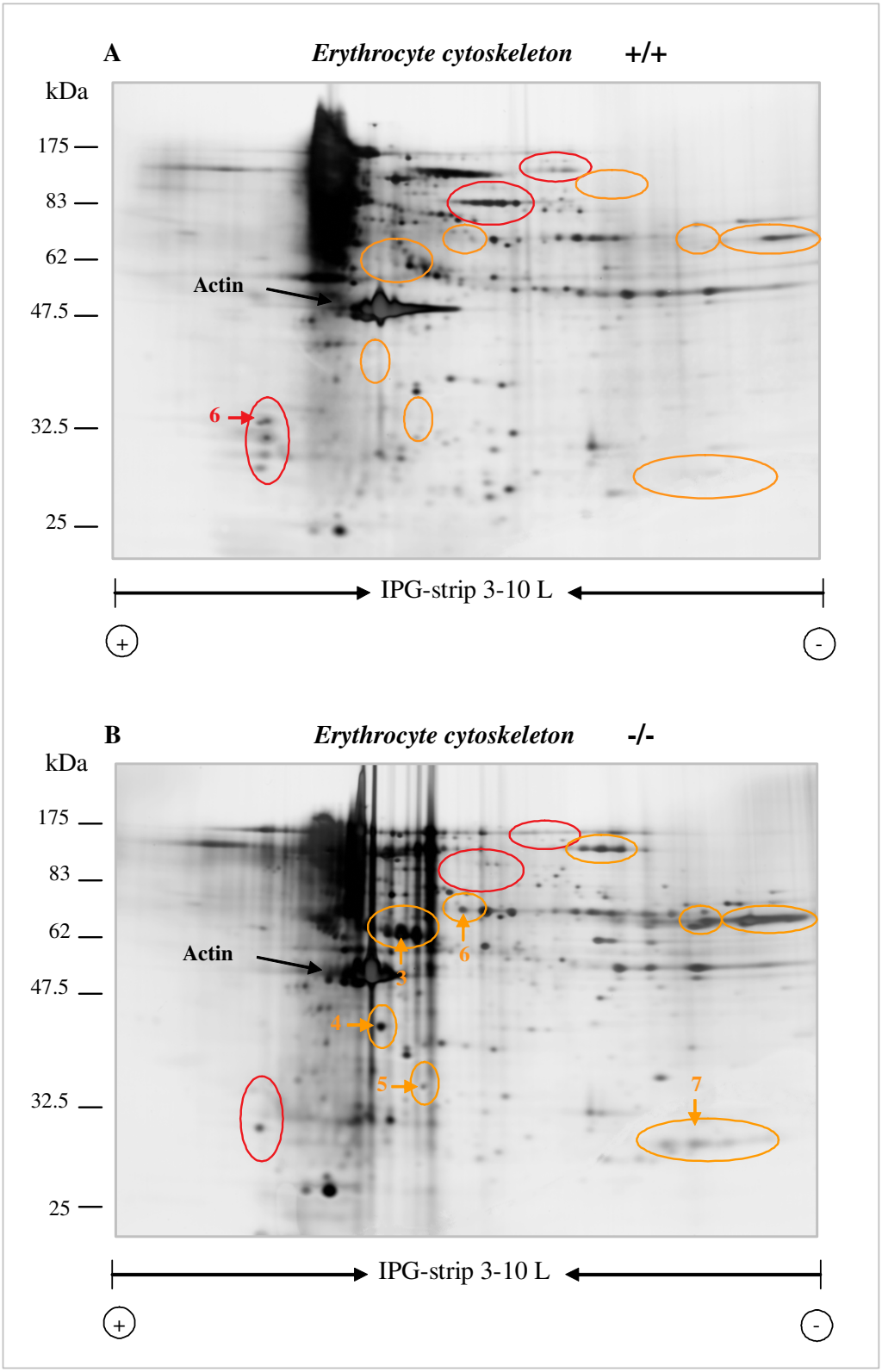

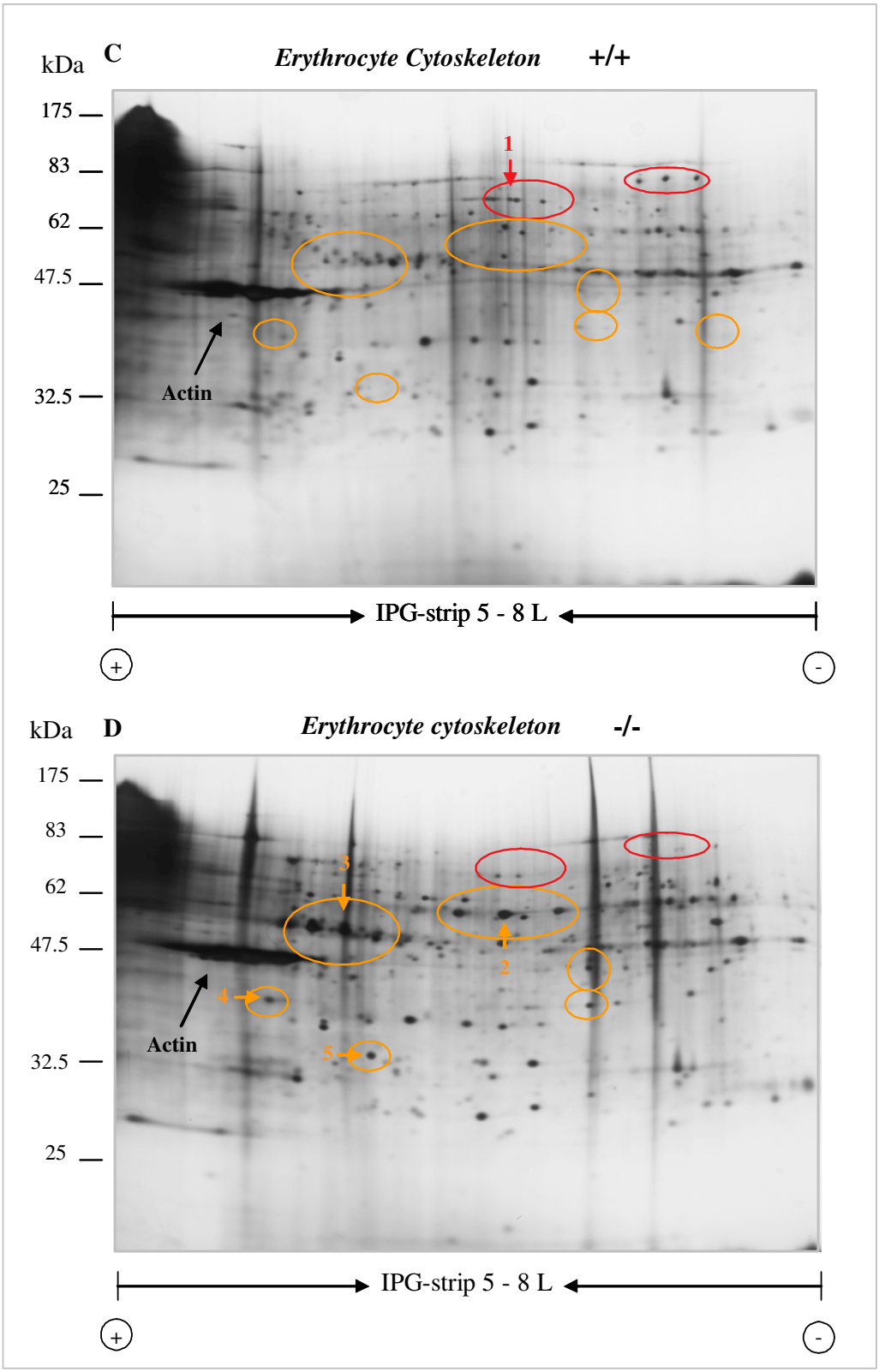

Figure 3.3: 2-D electrophoresis analyses of erythrocytes skeletal proteins. Control (A and C Panels) and mutant (B and D Panels) RBC cytoskeleton samples (100 µg) were separated by 2D electrophoresis and silver stained. Proteins were resolved in the first dimension using IPG strips with 3-10 linear pH range in Panels A and B, while with a 5-8 linear pH range in Panels B and C. The second dimension was run on a 10% SDS-PAGE. Molecular weight markers are indicated on the left, while acid and basic sides by the symbols "+" and "-", respectively. The red and orange circles indicate stronger and weaker spots, respectively, as visualized in the +/+ gels and compared with those of the -/-. The spots analysed by mass spectrometry are indicated with arrows and numbers from 1 to 7.

The identification of proteins not associated to the erythrocyte skeletons such as β- and γ–fibrinogen (*Spots 2* and *3* of figure 3.3 D and *Bands 4* and *5* of SDS-PAGE analyses of figure 3.1) could be due to the abnormal uptake of plasma proteins by a rupture-resealing mechanism in the more fragile membrane of the mutant erythrocytes. A second and less probable hypothesis could be that plasma fibrinogen interacts and co-purifies with some elements of the membrane protein network of β–adducin mutant RBC during the cytoskeleton purification.

Spot	*Cytoskeleton*	*PROTEIN*
1	**+/+**	- β-adducin
2	**-/-**	- β-fibrinogen
3	**-/-**	- γ-fibrinogen
4	**-/-**	- **ECapZ-α**
5	**-/-**	- **ECapZ-β**
6	**+/+**	- **α-tropomyosin**
7	**-/-**	- β-globin

Table 3.2: Results of mass spectrometry analyses of skeletal proteins separated by 2D gels. The table summarizes the results obtained from the mass spectrometry analyses of the spots (numbered from 1 to 7) corresponding to proteins showing different levels between control and mutant skeletal preparations in 2D gels of Figure 3.3.

3A.3 ECapZ-α, -β and α-tropomyosin: Western blot quantification in erythrocytes

We next performed Western blot analysis using antibodies directed against ECapZ-α, -β, and α-tropomyosin to confirm the mass spectrometry results and the differences in gel-staining patterns showed above (Figures 3.1 and 3.3, Table 3.1 and 3.2). As previous studies highlighted that the α- and β- subunits of ECapZ were abundant in RBC cytoplasm (Kuhlman and Fowler, 1997), we decided to test the levels of the two proteins not only in the erythrocyte cytoskeletons but also in the RBC cytoplasmatic fractions of KO and control animals.

3A.3.1- ECapZ-α and -β-

Western blot analysis with monoclonal antibodies directed against both subunits of ECapZ showed a remarkable ~9-fold increase of both proteins in the skeletal fractions of mutant animals (Figure 3.4 A, C and D, Table 3.3) confirming the data

obtained in the SDS-PAGE, 2D gels and mass spectrometry analyses (Figure 3.1 and 3.3, Table 3.1 and 3.2).

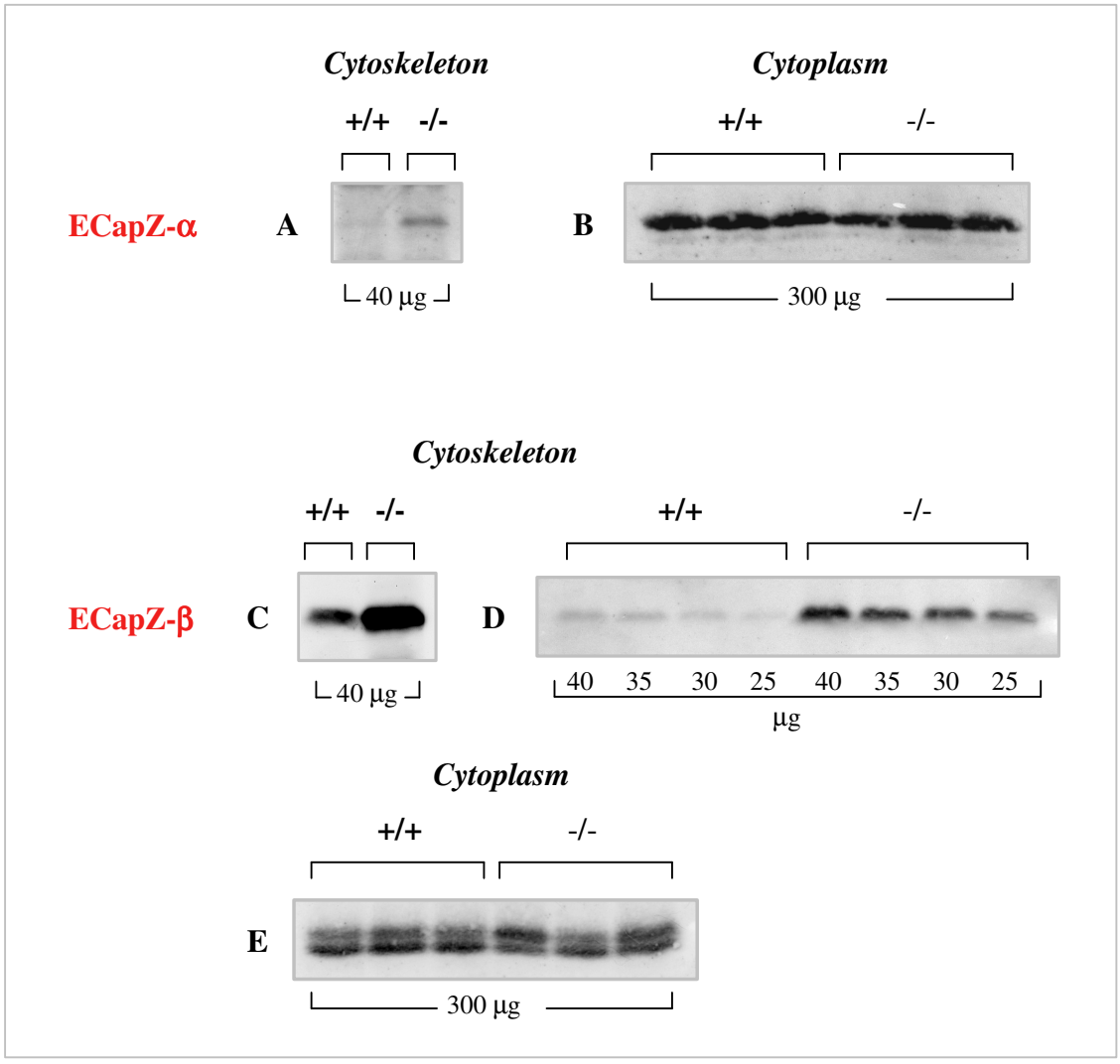

Figure 3.4: ECapZ-α and –β levels in erythrocyte skeletal and cytoplasmic preparations of mutant and control mice. Western blot analyses were performed using antibodies against the α (A and B Panels) and β subunits of ECapZ (C, D and E Panels). Control and mutant RBC skeletal samples were analysed in A (40 µg), C (40 µg), and D (25-30-35-40 µg), while in B and E erythrocyte cytoplasm (300 µg) of three groups of +/+ and -/- animals were tested.

On the contrary, both the RBC cytoplasmic fractions purified from +/+ and -/- animals contained similar amounts of the two ECapZ subunits (Figure 3.4 B and E). As can be seen in Figure 3.4 E, a doublet was detected in the cytoplasmatic fractions in which the lower mobility band co-migrates with the skeletal band detected with the antibody against ECapZ-α while the higher mobility one was β subunit-specific. This double signal could be caused by a cross reaction of the antibody against ECapZ–α or by a partial degradation of the larger ECapZ-β subunit.

RBC skeletal PROTEINS	*Confirmed by MS/WB*	*LEVELS in +/+ mice*	*LEVELS in -/- mice*	*P value*
α-adducin	No/Yes	100±6	26±6	≤ 0.01
γ-adducin	No/Yes	100±15	365±18	≤ 0.01
ECapZ-α	Yes/Yes	ND	100*	NA
ECapZ-β	Yes/Yes	100±20	880±153	≤ 0.01
α-tropomyosin	Yes/Yes	100±12	35±9	≤ 0.01
actin	No/Yes	100±2	83±8	≤ 0.01
tropomodulin	No/Yes	100±13	165±5	≤ 0.05
dematin 52 kDa	No/Yes	100±8	179±20	≤ 0.05
dematin 48 kDa	No/Yes	100±3	94±4	NS
p55	No/Yes	100±2	105±7	NS
protein 4.1	No/Yes	100±9	91±11	NS

Table 3.3: Analysis of cytoskeletal proteins in RBCs from mutant and control mice. The levels of the various erythrocytes cytoskeletal proteins shown in Western blot analyses of Figures 3.4, 3.5, 3.6, 3.7 and 3.8 were quantified as described in the Materials and Methods Section. The numbers indicate the relative amounts of each protein in cytoskeleton extracts relative to that found in the control extracts (Mean ± St Dev, n=3). "MS" and "WB" stands for Mass Spectrometry and Western Blot, respectively; "ND": not detected; "NA": not applicable; "NS": non significant. * An arbitrary value of 100 was given as no signal was detected in control mice, in the case of ECapZ-α. P-value was calculated using the Student T-Test.

3A.3.2- α-tropomyosin -

The same skeletal preparations from KO and control mice were analysed by Western blot using a monoclonal antibody against α-tropomyosin. We observed a ~65% reduction of this protein in the erythrocyte cytoskeletons of mutant mice (Figure 3.5 A and Table 3.3) confirming the previous results (Table 3.1 and 3.2). We were not able to detect any smaller extra bands in the extracts from mutant animals suggesting the absence of important proteolytic degradation during protein preparation.

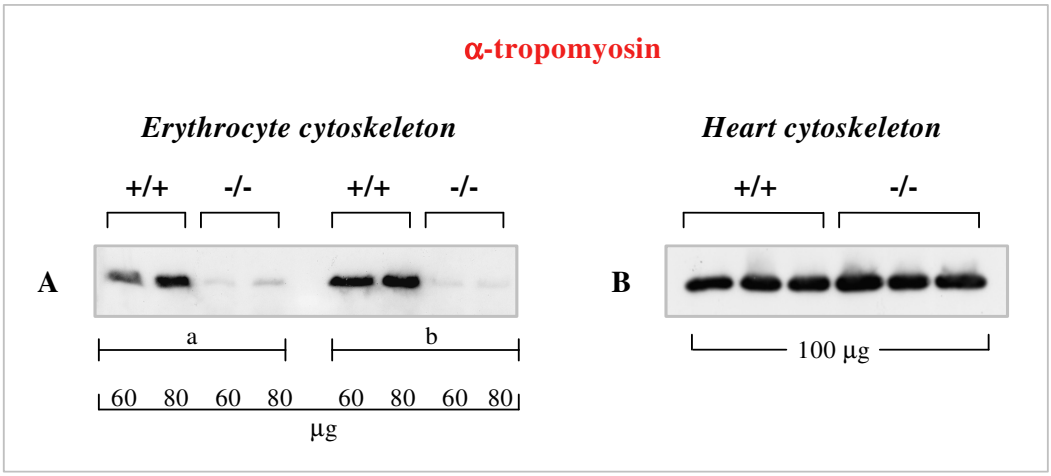

Figure 3.5: α-tropomyosin levels in RBC and heart cytoskeletal preparation of mutant and control mice. Different amounts of +/+ and -/- erythrocyte skeleton (60 and 80 µg) of two preparations [Panel A: skeletal pellets were resuspended in the IPG buffer (a) or in the commonly used resuspension solution (b)] and heart skeleton extracts (100 µg) prepared from three different animals for genotype (Panel B) were analysed by Western blot using the antibody against α-tropomyosin.

In addition, the cytoplasmic fractions from both control and β-adducin deficient RBCs did not show any signal, confirming previous reports (Kuhlman and Fowler, 1997). These results confirm a decrease in the α-tropomyosin levels in the skeletons of mutant mice and suggest that it is not localised in RBC cytoplasm of mutant mice.

3A.4 Analysis of the other major protein components of the RBC membrane cytoskeleton

The levels of many skeletal proteins, such as tropomodulin, are too low to be detected by Coomassie blue or silver staining of SDS-PAGE or 2D gels (Bennett and Gilligan, 1993). Therefore, the main actin-associated proteins were detected by the more sensitive Western blot technique to determine whether their expression levels could be modulated by the absence of β-adducin.

3A.4.1- α and γ-adducin -

Western blot analysis confirmed the previously reported differences in α- and γ-adducin levels in the cytoskeletal preparations of mutant erythrocytes (Muro et al., 2000). The α-subunit levels in mutant animals were reduced to about 75% of those of control mice (Figure 3.6 A and Table 3.3). Instead, we observed the expected 4-fold upregulation of the γ subunit level in -/- animals RBC skeleton (Figure 3.6 B and Table 3.3).

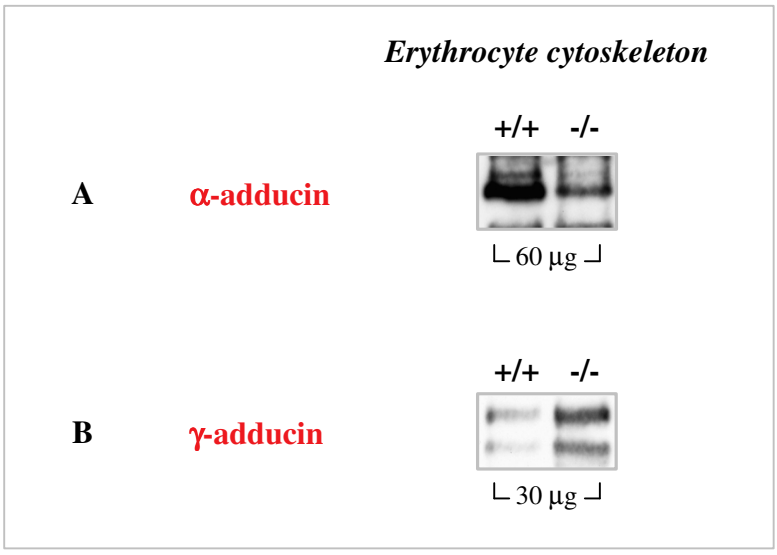

Figure 3.6: α- and β-adducin levels in erythrocyte cytoskeleton of mutant and control mice. Western blot analyses were performed on of +/+ and -/- RBC skeletal samples (30 and 60 µg, in Panel B and A, respectively) using antibodies against the α (Panel A) and γ subunits of adducin (Panel B).

3A.4.2 - Actin, tropomodulin and dematin -

Actin. We observed a ~15% decrease in the actin levels of cytoskeletal preparations of mutant erythrocytes (Figure 3.7 A and Table 3.3) confirming previous results of our laboratory (Muro et al., 2000). No smaller extra bands in the mutant extracts were detected, suggesting that the decrease in actin was not the consequence of increased proteolytic degradation during the protein extraction procedure.

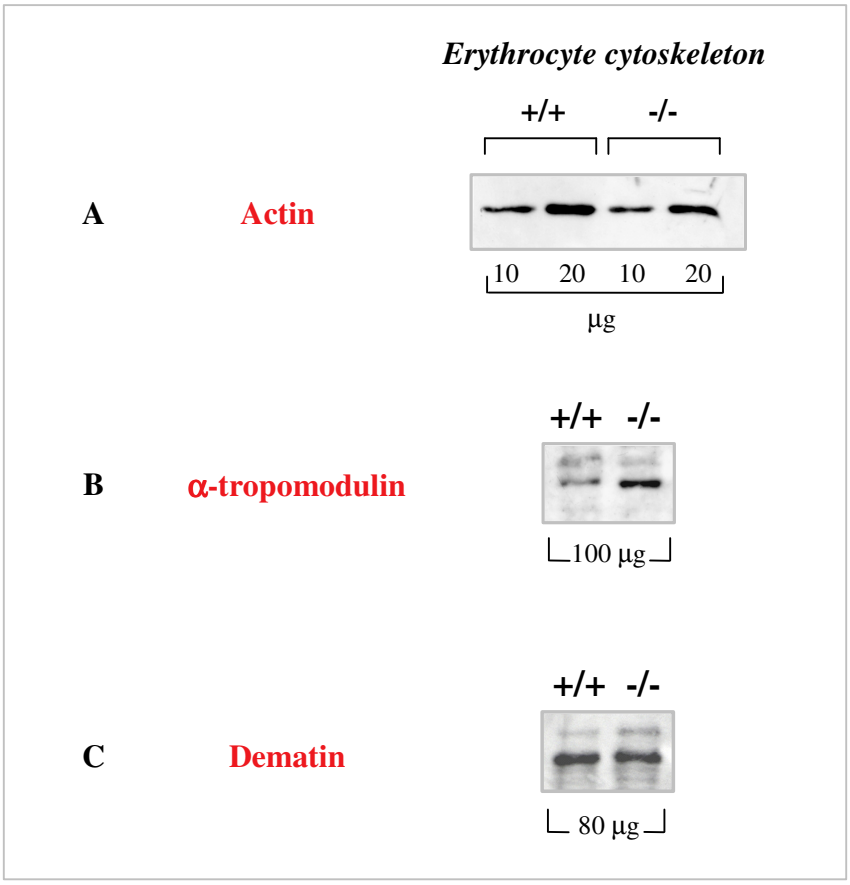

Figure 3.7: Actin, tropomodulin and dematin levels in RBC cytoskeleton of β-adducin deficient and control mice. Different amounts of +/+ and -/- erythrocyte skeletal samples (10-20 µg in A, 100 µg in Panel B and 80 µg in Panel C) were analysed by Western blot analyses using antibodies against actin, tropomodulin and dematin in Panel A, B and C respectively.

Tropomodulin. Considering the close physical and functional link between tropomyosin and tropomodulin (Weber et al., 1994) we investigated whether the observed α-tropomyosin reduction could influence tropomodulin levels in the RBC skeleton of the mutant mice. When skeletal protein preparations were analysed by Western blot we observed an upregulation (~65% increase) of tropomodulin levels in the mutant erythrocyte samples (Figure 3.7 B and Table 3.3). In addition, we were neither able to detect tropomodulin in cytoplasmic preparations from control animals, as reported previously by another group (Kuhlman and Fowler, 1997), nor from mutant preparations (data not shown).

Dematin. Since adducin and dematin are two proteins of the skeleton junctional complexes showing similar functions binding and bundling F-actin (Azim et al., 1995; Kuhlman et al., 1996; Mische et al., 1987), we investigated whether dematin levels were altered in the β-adducin mutant RBC cytoskeletons. Western blot analysis showed a minor decrease of the main band of 48 kDa and a ~79% increase of the 52 kDa band in the mutant protein extracts (Figure 3.7 C and Table 3.3). A similar minor reduction in the amounts of the 48 kDa dematin band was observed in the RBC skeletons and ghosts of the β-adducin KO animal generated by Dr. Gilligan's group (Chen et al., 2007).

The data presented above indicate that the presence of β-subunit in RBC skeleton is critical to maintain normal levels of several cytoskeletal proteins such as actin, tropomyosin, tropomodulin α– and γ–adducin, and dematin.

3A.4.3- Protein 4.1 and p55 -

We also analysed by Western blot the levels of two other protein components of erythrocyte cytoskeleton: Protein 4.1 and p55.

Protein 4.1. The mass spectrometry analysis (Table 3.1) detected the presence of numerous Protein 4.1 peptides covering 29% of the protein when the 85 kDa band was analysed. Therefore, to validate the proteomic data we determined its levels by Western blot analysis. Antibodies against Protein 4.1 revealed similar levels of the factor in both +/+ and -/- extracts (Figure 3.8 A and Table 3.3).

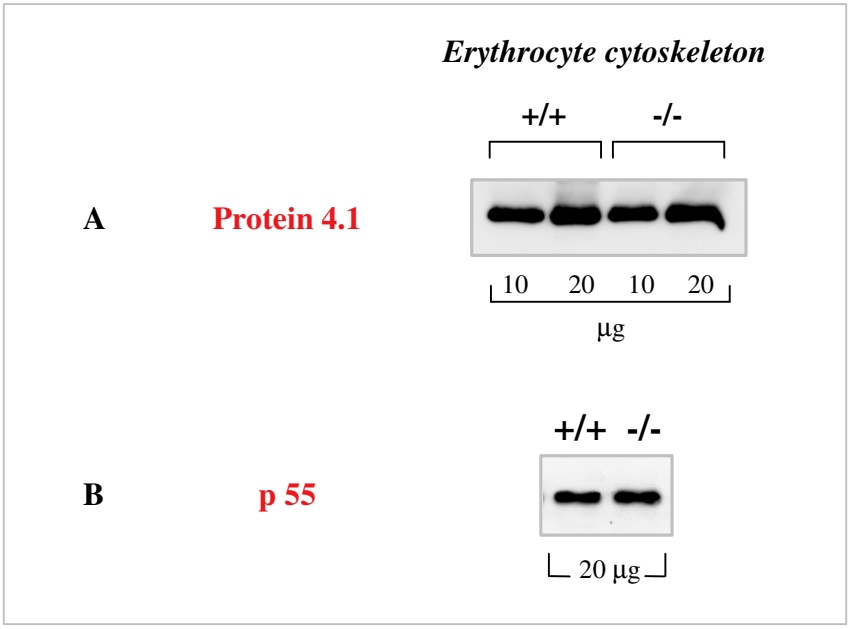

Figure 3.8: Levels of Protein 4.1 and p55 in erythrocyte skeletal preparations from mutant and control mice. Western blot analyses performed on different amounts of control and mutant RBC skeletal samples (10-20 µg in A and 20 µg in B) using antibodies against the Protein 4.1 and p55 are shown in Panels A and B, respectively.

p55. Previous evidences suggested that erythroid p55 may function as an adaptor protein stabilising membrane-cytoskeletal interactions and cell shape via Protein 4.1 and Glycophorin C (Marfatia et al., 1995; Marfatia et al., 1994). The altered morphology of β−adducin deficient RBC (Muro et al., 2000) suggested that the levels of p55 could be altered in the erythrocyte skeleton. However, we observed no significant differences between protein extracts of wild type and KO erythrocytes when we analysed the p55 expression levels by Western blot (Figure 3.8 B and Table 3.3).

To obtain increased stability in the actin filaments during the erythrocyte cytoskeletal extraction procedure, the protein extracts were also prepared using a protocol that contained 2 mM Mg^{2+} in the extract buffer (Kuhlman and Fowler, 1997) instead of the one used in the experiments reported above (without Mg^{2+}). Similar skeletal proteins differences between mutant and controls samples were observed when we repeated the experiments using the Mg^{2+} extracts (data not show and Table 3.3). As expected, the levels of some of the actin-associated proteins were reduced in skeletons prepared in the absence of Mg^{2+} in comparison to the preparations including the ion, confirming previous data suggesting its skeleton-stabilising role during protein preparation (Kuhlman and Fowler, 1997).

To verify whether the observed differences were dependent on the genetic background of the mice we performed protein preparations from erythrocytes of control and β-adducin deficient mice having a C3H genetic background. We observed similar results to the ones obtained previously using RBC skeletons prepared from mice having a C57Bl/6 genetic background (data not shown).

3A.5 Determination of the levels of ECapZ-α, -β and α-tropomyosin in other mouse tissues

Since combinations of α/γ as well as α/β oligomers of adducin are found in numerous non-erythroid cells (Section 1.7.3) (Dong et al., 1995; Gardner and Bennett, 1986) and previous studies performed in our laboratory had shown that β subunit expression levels depended on the tissue analysed (unpublished data), we performed Western blot analysis to determine the expression levels of CapZ-α and -β, and α-tropomyosin in non-erythroid tissues. Lung, liver, heart, brain, spleen and kidney total and cytoskeletal protein preparations of control and mutant mice were analysed by Western blot.

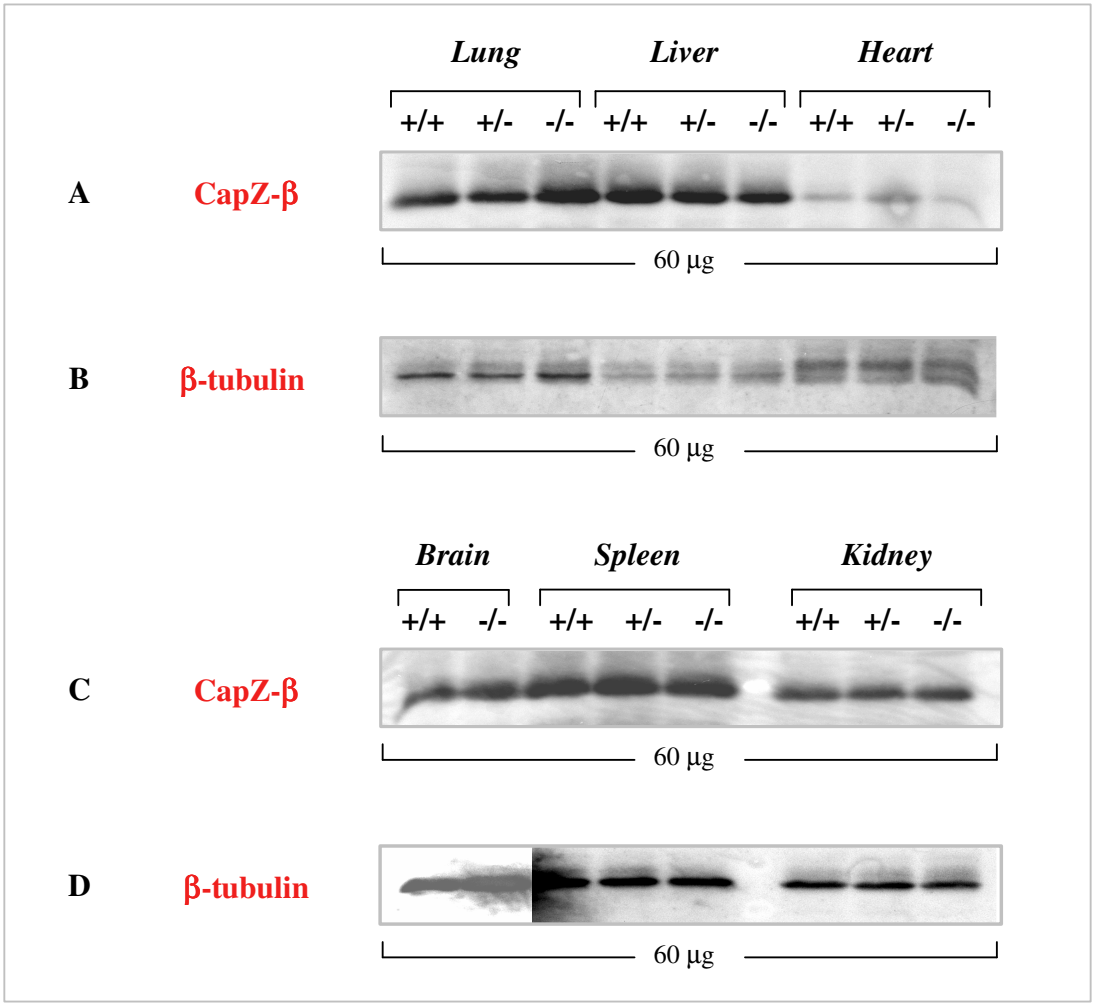

Figure 3.9: ECapZ-β levels in different mouse tissues. Western blot analyses of lung, liver, heart, brain, spleen, and kidney total extract (60 µg) from adult wt (+/+), heterozygous (+/-) and homozygous mutant (-/-) performed with antibodies against the β subunit of ECapZ are shown in Panels A and C, respectively. The same membranes previously analysed with ECapZ-β immunoglobulines were tested with antibodies against β-tubulin in B and D Panels. Since the signal generated by β tubulin in brain was very high the portion relative to brain samples in Panel D derived from brief time of exposition of the membrane.

3A.5.1- CapZ-α and -β-

Western blot analysis of the total protein extracts from control, heterozygotes and KO mice using antibodies against CapZ-β showed that the levels of the β subunit remained unchanged (Figure 3.9 A and C). Normalization of the same membrane with anti β-tubulin antibody showed that the slightly observed differences among the extracts were due to minor imbalances in the loaded samples (Figure 3.9 B and D). When we tested the CapZ-α protein expression in the same tissue preparations, a very weak signal was obtain (data not show), probably as a consequence of a low antibody affinity.

As no differences in CapZ level were observed in total cell extracts, we prepared cytoskeletal fractions of some of previously selected tissues to enrich in skeletal proteins. Since hypertension, neurophysiological and behavioural alterations were

observed in mutant mice suggesting the presence of molecular damage in the cells of heart and brain (Muro et al., 2000; Rabenstein et al., 2005), we prepared skeletons from these organs. However, as Figure 3.9 A and C shows, no significant differences were observed in the β–adducin KO preparations.

3A.5.2- α-tropomyosin -

α-tropomyosin is the predominant isoform expressed in the mature heart as α/α homodimer. It is one of the main contractile proteins of the cardiac sarcomere that, together with actin and troponin, creates the complex serving to modulate sarcomere function (Wolska and Wieczorek, 2003). Total α-tropomyosin deficiency is incompatible with life in mice (Blanchard et al., 1997; Rethinasamy et al., 1998) while mutations within this protein impair severely its function within the sarcomere (Wolska and Wieczorek, 2003).

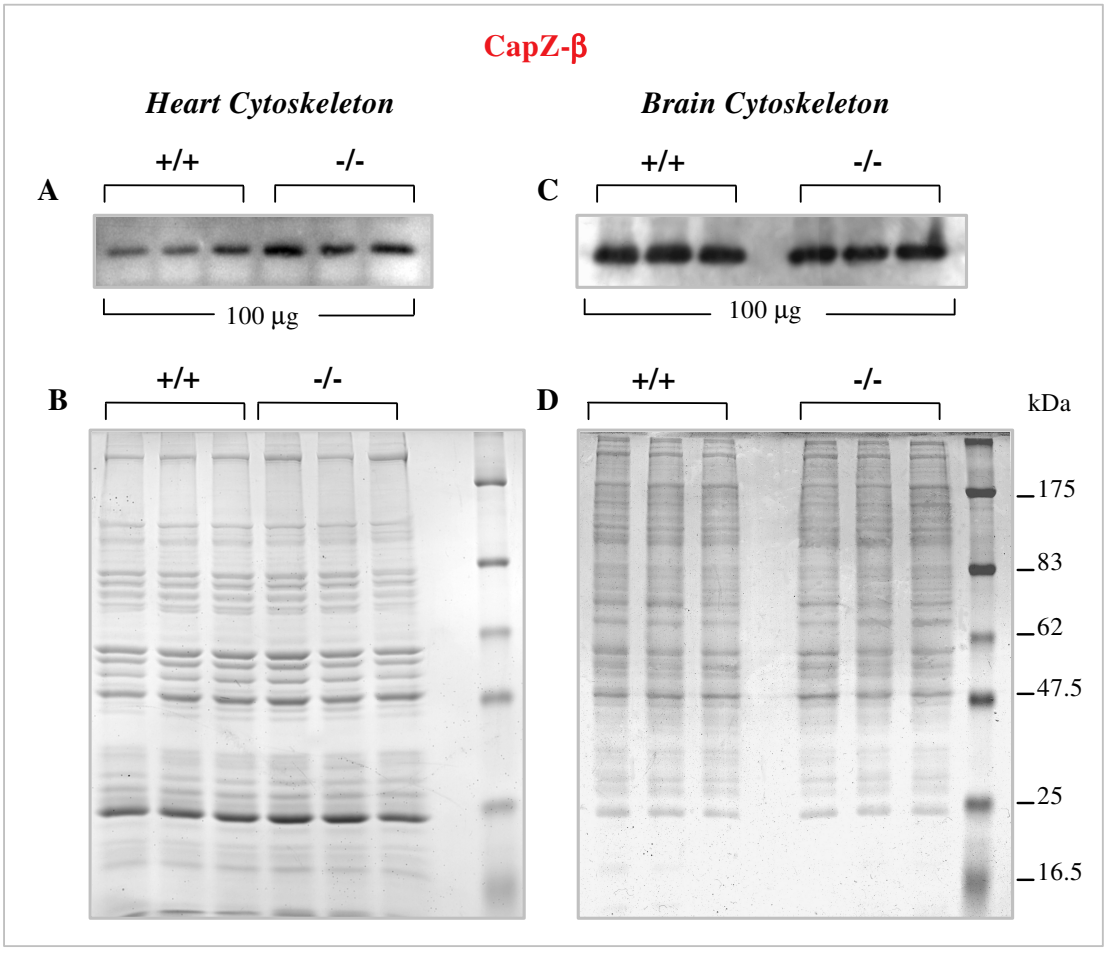

Figure 3.10: Level of ECapZ-β in heart and brain cytoskeletal preparations of β-adducin deficient and control mice. The same amount (100 µg) of different skeletal preparations derived from three different hearts (Panel A) and brains (Panel C) of +/+ and -/- adult mice were analysed by Western blot using antibodies against ECapZ-β. The samples analysed in Panels A and C, separated by 10% SDS–PAGE and Coomassie blue stained, are shows in Panels B and D, respectively. Molecular weight markers are indicated on the right of Coomassie gel in B and D Panels.

Taking into account above mentioned evidences and that heart functional alterations have often structural-molecular basis (Wolska and Wieczorek, 2003), we hypothesised that a variation in the amount of α-tropomyosin in the cardiomyocytes could be associates to the increased heart rate and hypertension observed in the KO mice (Muro et al., 2000). However, the Western blot revealed that no significant differences were detectable between heart skeleton samples of mutant and control mice generated by the unequal amount of loaded samples (Figure 3.5 A and B).

3A.6 Cytoskeleton characterisation of β-adducin and dematin double KO mice

Recently, a double knock-out mouse strain lacking both β-adducin and the headpiece domain of dematin (DAKO) was generated and characterised by Chishti's group and his collaborators revealing several alterations in RBC skeletal components such as spectrin, actin and Protein 4.1 (Chen et al., 2007) (Section 1.8).

In collaboration with Chishti's group we further analysed the levels of expression of other actin-binding proteins that might compensate for the absence of β-adducin and dematin in the single and double mutant mice. Control, DKO, AKO and DAKO erythrocyte skeleton protein samples were run on SDS-PAGE and blotted onto nitrocellulose membranes by Chishti's collaborators. We tested them with antibodies against α- and β-adducin, the two subunits of ECapZ, α-tropomyosin and tropomodulin.

3A.6.1- Adducin subunits -

Chishti's group was unable to detect any α-adducin in the AKO or DAKO erythrocyte ghosts presumably because of the low reactivity of the their polyclonal antibody (Chen et al., 2007). However, when we analysed the membranes using our polyclonal anti-α-adducin antibody a clear signal was detected, confirming the low reactivity of Chishti's antibodies. As expected, the levels α-adducin was also decreased (~30%) in AKO mutant preparations from Chishti's laboratory (Figure 3.11 A and Table 3.4), similarly to that observed with our β-adducin KO skeletal extracts (Figure 3.8 A and Table 3.3) (Gilligan et al., 1999; Muro et al., 2000). We also detected a minor downregulation of the α–subunit (~10%) in the single dematin mutant (Figure 3.11 A and Table 3.4). Interestingly, in the DAKO sample the α-adducin band was virtually not detected: a very weak signal was only seen when longer exposition time of the

membrane was used (data not show). These results indicated that that α–adducin was almost absent in DAKO erythrocytes.

As expected, when we used the antibody against β-adducin, no bands were obtained neither in AKO nor in DAKO skeleton samples (Figure 3.11 B), as was clearly showed in previous works (Chen et al., 2007; Gilligan et al., 1999).

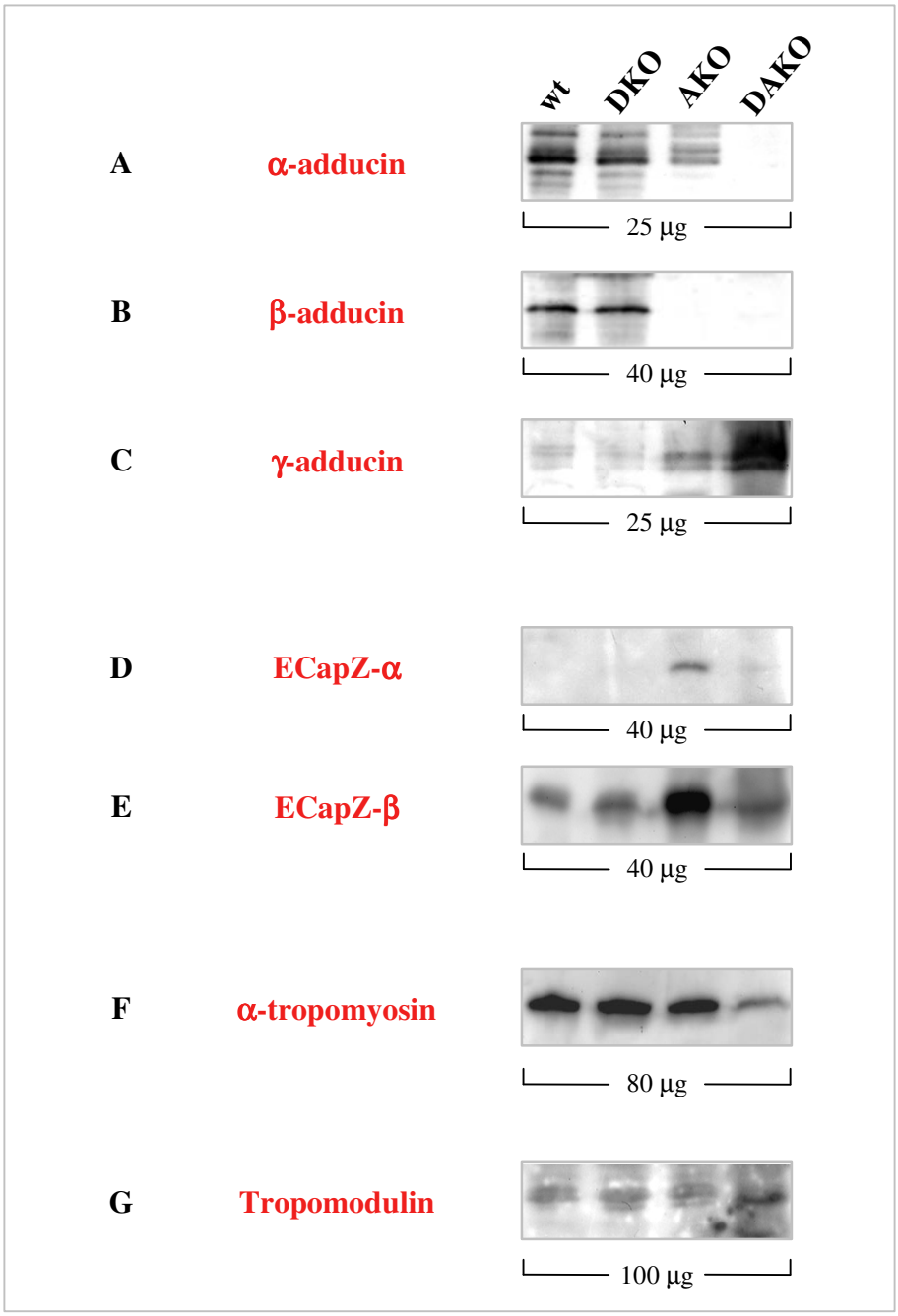

Figure 3.11: Levels of the major RBC cytoskeletal proteins of dematin KO (DKO), adducin KO (AKO), double dematin-adducin deficient (DAKO) mice and control animals (wt). Different amounts of DKO, AKO, DAKO and wt skeletal preparations (25 µg in A and C; 40 µg in B, D and E; 80 µg in F; 100 µg in G) were analysed by Western blot using antibodies anti α- and β- and γ-adducin, ECapZ-α and β, tropomyosin and tropomodulin in Panels A, B, C, D, E, F and G, respectively.

We observed a ~1.5-ford increase in the γ-adducin levels in the AKO sample, similar to that previously observed (Gilligan et al., 1999; Muro et al., 2000). The DAKO extracts showed an even higher upregulation of the γ-subunit (~ a 3-fold increase) (Figure 3.11 C and Table 3.4). Differently, no significant alterations of γ adducin levels are detected in the DKO extracts. γ-adducin is normally seen as a clear and sharp doublet of slightly lower molecular than that observed for α- and β-adducins (Figure 3.6 B). While testing the RBC skeleton samples prepared by our collaborators we were able to detect two more diffuse bands. We have no precise explanation about this but we suppose that these differences in the γ-subunit antibody signal could be due to lower resolution of the region of the gel corresponding to the high molecular weight proteins.

The observed differences in the levels of α- and γ-adducin between the Gilligan's and ours mutant animals (Gilligan et al., 1999; Muro et al., 2000) were probably caused by variations in the preparation of the RBCs skeletal samples. In fact, Chishti's group preparations were performed in less stringent conditions producing the less evident changes in levels of the two subunits in the mutant RBCs skeleton.

RBC skeletal PROTEINS	*LEVELS in wt mice*	*LEVELS in DKO mice*	*LEVELS in AKO mice*	*LEVELS in DAKO mice*
α-adducin	100±5	90±6	67±1	27±40
β-adducin	100	100	ND	ND
γ-adducin	100±16	98±17	155±10	321±13
ECapZ-α	ND	ND	100*	ND
ECapZ-β	100±15	117±2	205±18	118±1
α-tropomyosin	100±5	102±6	95±3	67±21
tropomodulin	100±6	94±7	107±3	166±8

Table 3.4: Levels of cytoskeletal proteins in RBCs from wt, DKO, AKO and DAKO mice. The levels of the various erythrocytes cytoskeletal proteins shown in Figure 3.11 were quantified as described in Materials and Methods Section. The numbers indicate the relative amounts of each protein in cytoskeleton extracts relative to that found in control extract (Mean ± St Dev, n=3 different exposition time of one or two Western blot experiments). "ND": not detected; "NA": not applicable; "NS": non significant. * An arbitrary value of 100 was given as no signal was detected in control mice, in the case of ECapZ-α.

3A.6.2- ECapZ-α and -β-

The Western blot analyses of the membranes with antibodies against ECapZ-α and -β showed a remarked increase (more than 2-fold increase) of both subunits in the erythrocyte skeleton of AKO mutants (Figure 3.11 D and E, and Table 3.4), similarly to what we had previously reported for our β-adducin mutant extracts (Figure 3.4 A and C,

and Table 3.3). However, no differences were observed in the DKO skeleton samples. As Figure 3.11 D shows, the signal of the ECapZα subunit was very weak, similar to the one normally observed in our cytoskeletal preparations. In the DAKO samples the high background observed did not allow a precise quantification, but it appears that the β-subunit levels were apparently similar (or just a minor increase was detected) to those of the wt extract (Figure 3.11 E and Table 3.4).

3A.6.3- α-tropomyosin -

When we tested Chishti's membranes with antibodies against α-tropomyosin we observed only a very slight reduction on the AKO ghost extracts (Figure 3.11 F and Table 3.4). This was different to previous results of our β-adducin -/- RBC skeletal samples, where the decrease was of about 65% (Figure 3.5 A and Table 3.3). No significant alteration in the level of the protein was detected in DKO. Interestingly, we observed a downregulation of α-tropomyosin levels in the DAKO samples (~35% reduction) (Figure 3.11 F and Table 3.4).

The different results obtained from the two single β-adducin mutants (compare Figure 3.5 A and Table 3.3 with Figure 3.11 F and Table 3.4) could be explained by the variations between the skeleton preparation protocols used in each laboratory. The protocol used by our collaborators contained KCl in the solutions, while ours protein extracts have been prepared in the absence of the salt. As mentioned above (Section 3A.4), the presence of salts in the protein extraction solutions enhances the stability of the actin filaments. Dr. Fowler's and Mohandas' groups showed, using human red cells, that the absence of Mg^{2+} during the RBC skeleton preparation produced a major decrease of tropomyosin (An et al., 2007; Kuhlman and Fowler, 1997). Therefore, the differences in α-tropomyosin levels between ours and Chishti's laboratories could be explained by an enhanced skeleton-stabilisation of the AKO skeletons when prepared in the presence of KCl.

3A.6.4- Tropomodulin -

Western Blot analysis revealed a very weak and spread band in both the three mutants and the control extracts (Figure 3.11 G). Unfortunately, the antibody against tropomodulin we posses in the laboratory have very low reactivity and it was difficult to state whether the protein levels varied among the different samples. It appeared that tropomodulin levels in the DKO were slightly reduced in comparison to AKO and wt skeleton extracts. We speculate that the protein was up-regulated in the DAKO

preparation, even if it was difficult to precisely quantify this band (Figure 3.11 G and Table 3.4).

3A.7 Purified adducin is incorporated into adducin deficient ghosts

To determine whether purified adducin (as α/β heterodimer) is incorporated into cytoskeletons from β-adducin deficient mice to eventually replace ECapZ, we performed a binding assay utilizing ghosts from KO mice and purified human erythrocyte adducin.

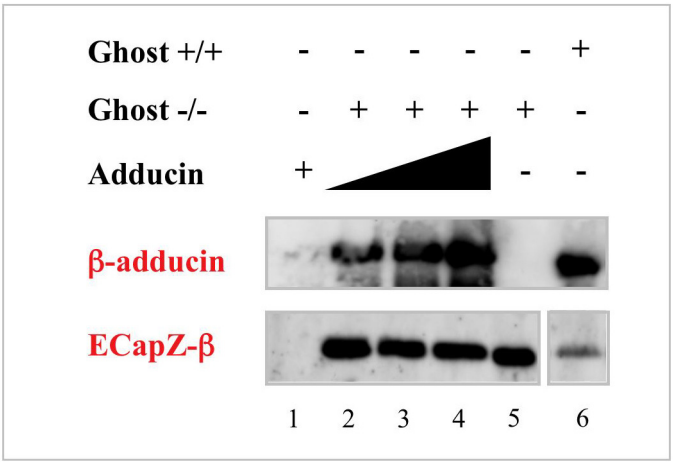

Figure 3.12: *In vitro* purified adducin incorporation assay. Ghosts from mutant mice were incubated with increasing amounts of purified human adducin (0.7, 1.4 and 2.8 µg in Lanes 2, 3 and 4, respectively) and the membrane-skeleton (pellet) was separated from the soluble fraction through a sucrose cushion. β-adducin and ECapZ-β protein levels were detected by Western blot analysis. Lane 1 contains 2.8 µg of adducin plus 20 µg of BSA. Lanes 5 and 6 contain 20 µg of mutant and control ghost protein preparations, respectively, that underwent the same experimental procedure as the other Lanes. Quantification of the bands showed an increase of β-adducin and a decrease of ECapZ-β (relative values of β-adducin: 8, 91, 111, 131, 0 and 100 for Lanes 1–6, respectively; relative values of ECapZ-β: 0, 1280, 1069, 985, 1210 and 100 for Lanes 1 to 6, respectively; ratio β-adducin/ECapZ-β: 7.1, 10.5 and 13.5 for Lanes 2–4, respectively).

Figure 3.12 shows the Western blot analysis of both β-adducin and ECapZ-β after incubation of a fixed amount of mutant ghosts with increasing amounts of purified human adducin. We observed that β-adducin was incorporated into adducin deficient ghosts in a dose-dependent manner (Figure 3.12, Lanes 2-4). The α-adducin subunit was incorporated in a similar manner to the β subunit (not shown). ECapZ-β levels decreased after the incubation of mutant ghosts with increasing amounts of adducin (Figure 3.12, Lanes 2-4). The control lane confirmed that the purified adducin did not auto-precipitate (Figure 3.12, Lane 1) as it included the maximum amount of adducin used in lane 4 (2.8 µg) plus an amount of BSA similar to that of ghosts used in the other Lanes (20 µg). Quantification of the bands indicated that the ratio between adducin and

ECapZ increases with the addition of higher amounts of adducin supporting the idea that the incorporation of ECapZ in RBC skeleton is a compensatory mechanism triggered by the absence of β-adducin.

3A.8 Eye lens fibre cell skeleton characterisation of β-adducin KO mice

As previously mentioned in the Introduction (Section 1.6), several studies have evidenced that vertebrate eye lens contains many, if not all, of the components of the spectrin-based membrane skeleton detected in erythrocyte. Considering this evidence, to investigate whether the absence of the β-adducin may alter the protein composition and the skeletal network of eye lens, as observed in erythrocytes, we quantified the levels of the main skeletal components in lens of mutant and control mice by Western blot analysis.

We collected eyes from β-adducin -/- and control animals, lenses were dissected from eyes and pooled, and plasma membranes were purified. As an extra control, lens plasma membranes extract was prepared from a rabbit. We utilized the lens plasma membranes isolation and extraction protocol described in previous studies (Woo and Fowler, 1994). The purification was done in presence of $MgCl_2$. As Figure 3.13 shows, we compared the mouse eye lens plasma membranes with the corresponding ghosts erythrocyte protein preparations, which had been prepared with solutions containing $MgCl_2$.

3A.8.1 - Adducins -

We observed that α- and γ-adducin levels in mutant were different to those of the control extracts, and the variation in lens plasma membranes had a similar trend to that previously observed in the cytoskeletal preparations of erythrocyte. In fact, the levels of the α-subunit were reduced to about 60-70% of that of the wt mice in both RBC ghosts and lens fibre membranes of mutant animals (Figure 3.13 A and Table 3.5). We also observed the upregulation of γ-adducin levels (~35% increase) in lens membranes from mutant animals (Figure 3.13 C and Table 3.5), similar to that observed in RBC ghosts.

As expected, when we used the antibody against β-adducin, no signal was detected in lens membrane and erythrocyte ghost samples of mutant animals (Figure 3.13 B).

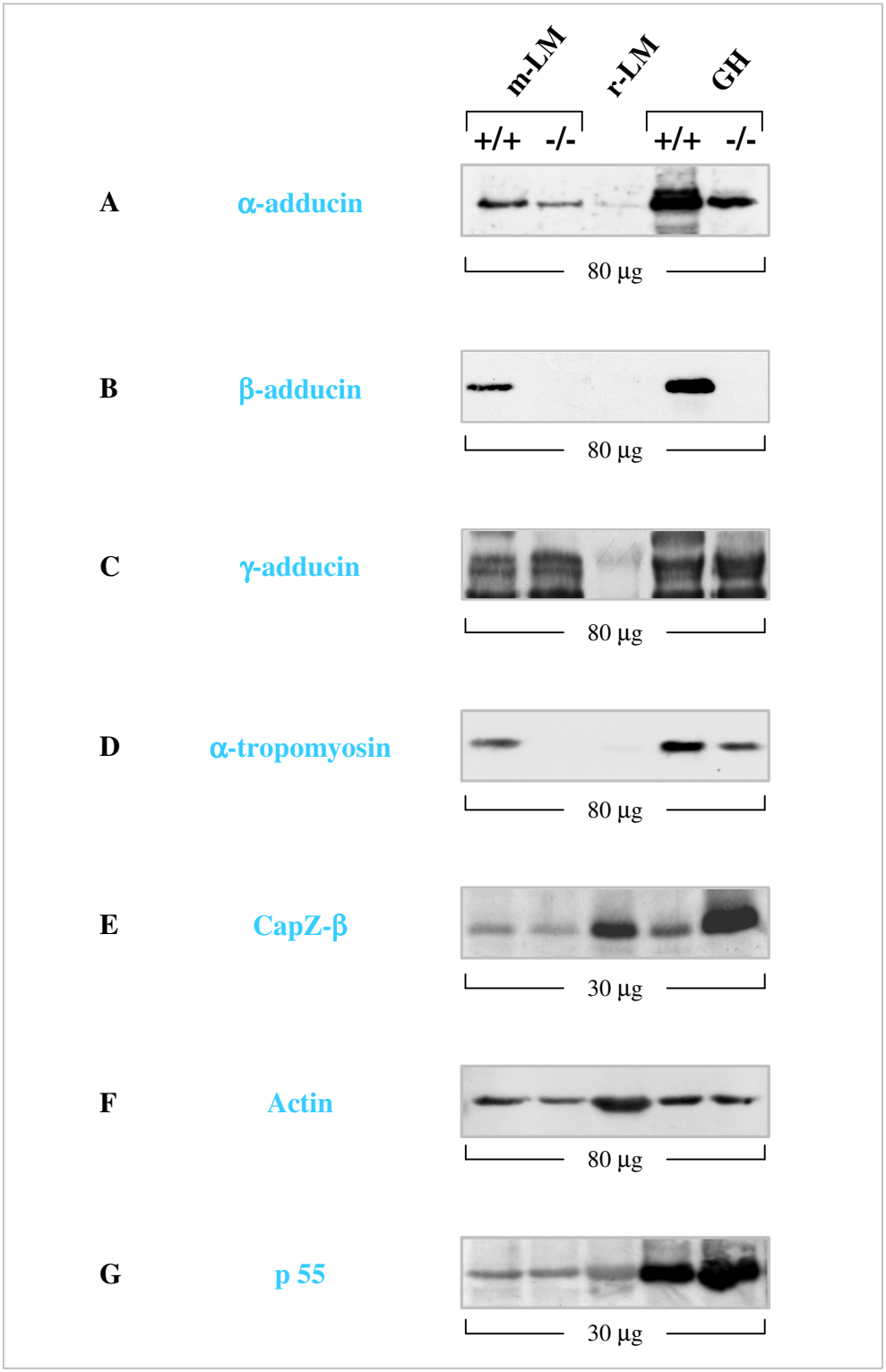

Figure 3.13: Levels of the major cytoskeletal proteins of lens fibres of β-adducin mutant and control mice. Different amounts of mouse lens membranes (m-LM; -/- and +/+), mouse RBC ghost (GH; -/- and +/+) and rabbit lens membranes (r-LM) preparations (80 µg in Panels A, B, C, D and F; 30 µg in Panels E and G) were analysed by Western blot using antibodies anti α- and β- and γ-adducin, tropomyosin, CapZ-β, actin and p55 in Panels A, B, C, D, E, F and G, respectively.

LENS membrane PROTEINS	*LEVELS in +/+ mice*	*LEVELS in -/- mice*
α-adducin	100±11	42±16
β-adducin	100	ND
γ-adducin	100±3	137±2
α-tropomyosin	100	ND
CapZ-β	100±11	82±14
actin	100±7	79±9
p55	100±2	98±2

Table 3.5: Levels of lens membrane proteins in lens fibres from mutant mice. The levels of the various mouse lens membranes proteins shown in Western blot analyses of Figures 3.13 were quantified as described in Materials and Methods Section. The relative amounts of each protein in lens membrane extracts relative to that found in the control extract is indicated by numbers (Mean± St Dev, n=3 different exposition time of one or two Western blot experiments). "ND": not detected; "NA": not applicable; "NS": non significant.

3A.8.2- Tropomyosin -

Interestingly, we observed a drastic downregulation of α-tropomyosin in mutant lens membranes (Figure 3.13 D and Table 3.5), even higher to that observed in RBC skeleton extracts (Figure 3.5 A and Table 3.3). However, comparing the signal intensity between lens and ghost wt samples we were able to state that the relative levels of α-tropomyosin in lens membranes seemed to be lower to those present in erythrocyte ghosts. This observation could justify the absence of signal in mutant lens membranes.

3A.8.3- CapZ-α and -β -

The Western blot analysis of lens membranes indicated that the variation of CapZ-β levels in the mutant lens showed an opposite trend to that observed in ghosts and skeletons of erythrocytes (Figure 3.13 E and Table 3.5 versus Figure 3.4 C and D and Table 3.3). In fact, the amount of the β subunits was slightly decreased (~20%) in mutant lens samples (Figure 3.13 E and Table 3.5), while it was strongly increased in the RBC ghosts and skeleton preparations from mutant mice (Figure 3.13 E and Figure 3.4 C and D). Unfortunatly, when we used the CapZ-α monoclonal antibody we were not able to detect any signal, even after loading a very high amount of protein extract (data not show). This negative result was probably caused by the low antibody reactivity.

3A.8.4- Actin -

A ~20% decrease was observed in the levels of actin in lens membranes of mutant mice (Figure 3.13 F and Table 3.5). A similar downregulation of actin was

previously detected in ghost extracts and evidenced in the cytoskeletal preparations of KO erythrocytes (Muro et al., 2000) (Figure 3.7 A and Table 3.3).

3A.8.5 - p55 and Tropomodulin -

We observed no significant differences in p55 expression levels in lens membranes between wt and KO samples (Figure 3.13 G and Table 3.5). No differences in the p55 levels were detected between control and mutant ghosts (Figure 3.13 G) skeleton extracts (Figure 3.8, B and Table 3.3).

Using antibodies anti tropomodulin we were not able to detect that protein in the lens plasma membrane neither in mutant nor in control animals (data not show).

In conclusion, the absence of β-adducin from the skeleton of both erythrocytes and lens fibre cells induces significant alterations in the protein composition of their skeletal network.

Chapter B

Characterisation of the β-adducin gene structure and its tissue-specific expression

Although the existence of tissue-specific transcript and protein isoforms of β-adducin has been known for more than twenty years (Section 1.7), both determination of the gene structure and the molecular characterisation of the mRNA isoforms are still incomplete. This chapter reports all evidences that allowed us to describe the complete architecture of the *Add2* gene and the primary structure of β-adducin mRNA in humans, rats and mice, and a series of preliminary experiments aimed to characterise the molecular mechanisms regulating tissue-specific alternative polyadenylation of the β-adducin pre-mRNA transcript.

3B.1 Analysis of the tissue-specific expression of β-adducin 63 and 97 mRNA families during mouse development

To investigate whether the expression of the Add63 and Add97 β-adducin families of transcripts was correlated to specific tissues during mouse maturation we analysed their pattern of expression in different tissues of embryos, newborns and adult mice.

Total RNA was prepared from different organs of 13.5 days embryos, newborn, 14 days-old and adult mice and was analysed by semiquantitative RT-PCR (Figures 3.14 and 3.15).

To analyse the expression levels of Add97 family of transcripts, we used primers that amplified from mouse 12th exon to the 16th exon (exons 14 to 16 are not present in Add63 mRNAs) (Figure 3.14 A, primers "a" and Table 2.1). A PCR product was observed for brain, liver, lung and heart in embryos, although the amount of product in the lung was low (Figure 3.14 B). In newborn mice Add97 appeared to be present in all the analysed tissues, with reduced levels in heart (Figure 3.14 C). When we analysed 14 days-old animals, we observed high levels of the Add97 mRNA family only in brain and spleen, while the apparent levels of this mRNA family in the other tissues was reduced (Figure 3.14 D). This trend was increased in adults, as Add97 expression was visible only in brain and spleen, while no signal was obtained in other tissues (Figure 3.14 E).

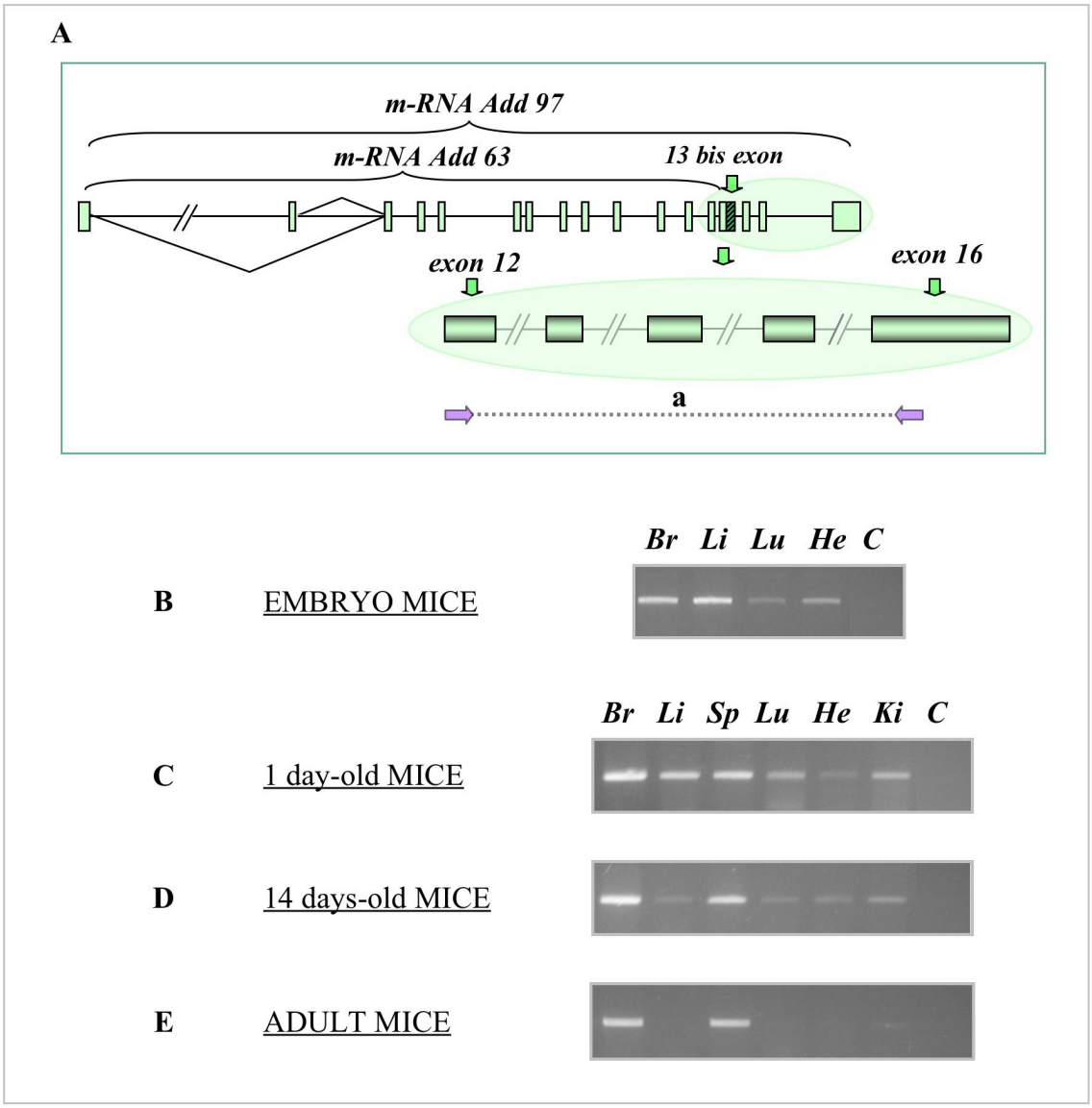

Figure 3.14: β-Add97 adducin mRNAs family expression in different tissues during mouse maturation. Panel A shows a schematic representation of the β-adducin gene. The exons included in the Add97 and Add63 mRNAs families of β-adducin are indicated. In the scheme are also shown the positions of the oligonucleotides used in the semiquantitative RT-PCR reaction for amplifying the cDNA region from mouse 12th exon to the 16th exon (primer pair "a"). Panels from B to E show the pattern of expression of β-Add97 adducin mRNAs in brain, liver, spleen, lung, heart, and kidney of newborn (C), 14 days-old (D) and adult mice (E) and also in brain, liver, lung and heart of 13.5 days embryo (B). These results were obtained using primer pair "a".

To determine the expression pattern of Add63 in mice we used the same RNA samples with a pair of primers that amplify a fragment specific of Add63 family of transcripts (from exon 12th to exon 13th) (Figure 3.15 A, primers "a" and Table 2.1). We observed that Add63 expression at high levels mainly in brain and haematopoietic tissues (liver and spleen, from embryos and adults, respectively) at all ages analysed. Bone marrow was not analysed. In embryos and young animals there was a minor and non-consistent expression in the other organs (Figure 3.15 B, C, D and E). Add63 expression in adult tissues was restricted exclusively to spleen, while weak band was

detected only in brain suggesting that very low levels of this mRNA family are also present in neuronal tissues (Figure 3.15 E).

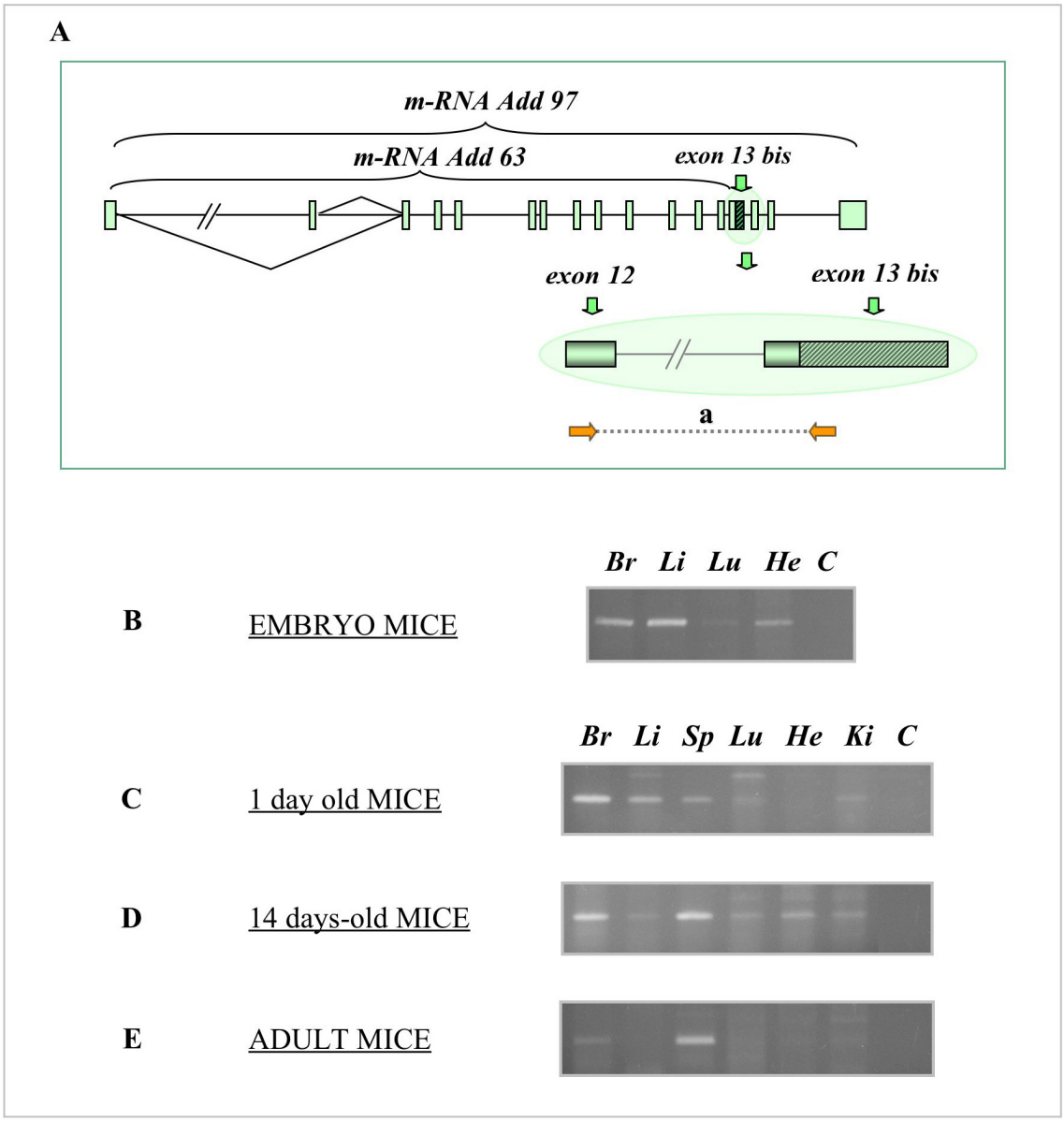

Figure 3.15: Expression pattern of β-Add63 adducin mRNAs in several tissues during different mouse maturation stages. A scheme of β-adducin gene indicating the positions of the oligonucleotides used in the RT-PCR reaction for amplifying the cDNA region from mouse 12th exon to the 13th bis exon (primer pair "a") was showed in Panel A. Panels from B to E show the semiquantitative RT-PCR results obtained amplifying with primer pair "a" the total RNA prepared from brain, liver, spleen, lung, heart, and kidney of newborn (C), 14 days-old (D) and adult mice (E) and also from brain, liver, lung and heart of 13.5 days embryos (B).

These results revealed that both β-adducin mRNAs families are expressed in most analysed tissues of embryos and newborn animals, with higher levels in brain and spleen. In adult animals, expression on both Add97 and Add63 mRNAs seem to be restricted to neuronal and erythroid tissues, although Add63 expression in brain was at low levels.

3B.2 Analysis of β-adducin transcripts in the brain and spleen from rodents and humans

To further investigate on the tissue-specific expression of the β-adducin gene, brain and spleen total RNA of mice and rats, and commercial human preparations were analysed by Northern blot. Species-specific β-adducin cDNA probes (*β-Add Total Probes*, Figure 3.16 A) directed against a constitutive region revealed the expected β-adducin bands in the range of 3.5–4.5 kb in spleen of all three analysed species (Figure 3.16 B, Lanes 2, 4 and 7). It has been suggested that the multiple bands are generated by alternative splicing of β-adducin pre-mRNA (Gilligan et al., 1997; Tisminetzky et al., 1995). Northern blot analyses showed that the brain β-adducin mRNA of rats and mice had 8–9 kb (Figure13.6 B, Lanes 1, and 3), a length that was not consistent with the expected one of the mRNA considering the size of the β-adducin subunit in the same tissue:in fact, it has an apparent molecular weight of 110 kDa, only slightly higher than that of 97 kDa observed in spleen (Bennett et al., 1988; Joshi et al., 1991; Tripodi et al., 1991). This minor size difference between brain and erythrocyte β-adducins has been proposed to be due to post-translational modifications (Bennett et al., 1988; Muro et al., 2000), but, to our knowledge, there is no report showing neither the reasons for substantial differences between the mRNA and protein size nor the complete identity of the brain mRNA or protein isoforms.

In addition, Figure 3.16 showed that a similar size differences between brain and bone marrow mRNA were also observed in humans. A band of 8–9 kb was detected by Northern blot analysis of human brain RNA (Figure 3.16 B, Lane 5). It is interesting to note that the bands observed in humans were slightly bigger than those of mice and rats (Figure 3.16 B, Lines 5 and 7 vs. 1-4). This could be related to the differences in the β-adducin length of the cDNAs reported in mice, rats and humans (the reported erythroid β-adducin full-length cDNAs in mouse, rat and humans have 3119, 3115 and 3938 bp, respectively) [(Joshi et al., 1991; Muro et al., 2000; Tripodi et al., 1991), ENSEMBL and Table 3.7]. Regrettably, we were not able to detect a clear signal of human spleen RNA sample (Figure 3.16 B, Lane 6) even when we tested a spleen mRNA from a different commercial supplier. This might be due to the fast degradation of the RNA in this tissue before sample preparation. Significant RNA degradation was also observed in human brain and bone marrow samples (Figure 3.16 B, Lanes 5–7) and some of the

observed bands might be the result of alternative splicing and/or degradation products (indicated by an asterisks in Figure 3.16 B).

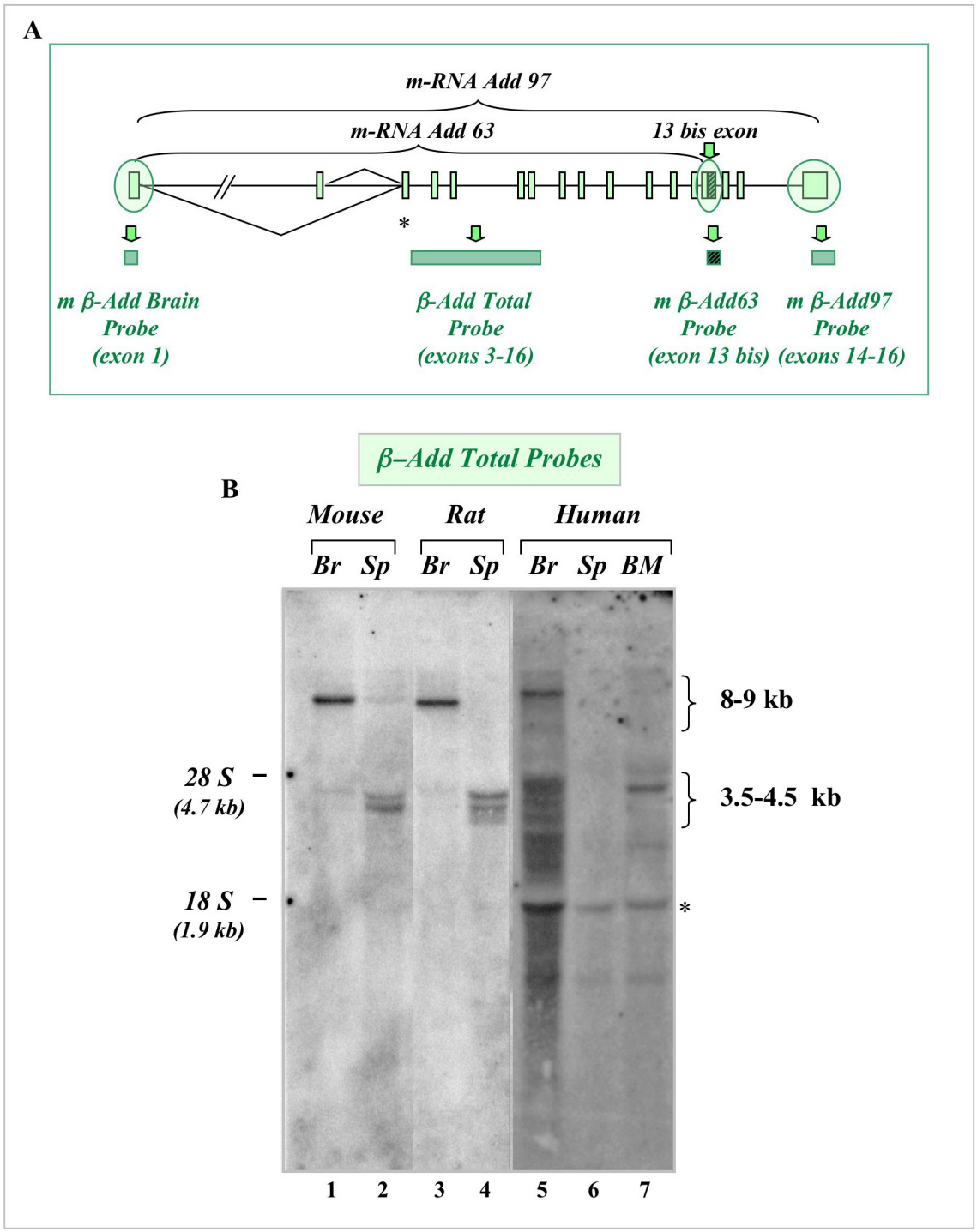

Figure 3.16: Northern blot analysis of brain and spleen β-adducin transcripts. A scheme of the β-adducin gene showing the probes used in the Northern blot experiments is shown in Panel A. The asterisk in the first common exon indicates the position of the oligonucleotide used in the Primer Extension Experiment shown in Figure 3.18 A. Northern blot analysis of mouse, rat and human brain and spleen RNAs (25 µg per lane) using the Add97-specific *β-Add Total Probe* (exons 3-16) is shown in Panel B. In Lane 7, human bone marrow RNAs was loaded (25 µg). All RNAs were run in the same agarose formaldehyde gel (1.2%), transferred to Hybond-N^+ membrane and hybridised with rodents (mouse-rat) and human β-adducin probes (Lanes 1–4 and 5–7, respectively). The bands observed in human brain and bone marrow samples (Panel B, Lanes 5–7) generated by RNA degradation and/or alternative splicing are indicated by an asterisk. The 28S and 18S rRNAs are indicated on the left.

These results allowed us to conclude that the brain β-adducin mRNA contains about 5–6 kb of extra sequences in all three analysed species. Therefore, we focused our analysis on the understanding of the molecular basis that might generate the 8-9 kb brain-specific β-adducin transcript. We hypothesised that the long mRNA could be the result of one of the following molecular processes:

- Tissue-specific use of alternative promoters;
- Tissue-specific alternative splicing associated to the presence of new previously undetected exons;
- Tissue-specific use of alternative polyadenylation signals.

In the following sections of the Thesis we aimed to validate or exclude each of these potential mechanisms.

3B.3 Characterisation of the β-adducin 5'-UTR in rats and mice

To identify the molecular basis of the size differences between brain and spleen β-adducin mRNAs we performed RT–PCR analysis of brain and spleen total RNA from mice, rats and humans covering the complete 5'-UTR, coding regions and 3'-UTR of the reported β-adducin sequences in all three species. It produced in all cases the expected products and no extra bands of previously undetected alternatively spliced exons appeared, that might explain the size differences between brain and spleen β-adducin mRNAs (data not show).

To rule out that the amplification of a putative longer PCR product could be competed-out by the smaller expected product, we performed RNase protection analysis of rat brain and spleen total RNA utilizing overlapping antisense riboprobes encompassing the entire reported cDNA sequence of the β subunit. Again, no extra bands were observed when probes corresponding to the coding exons were used, indicating the absence of previously undetected exons inserted within the reported β-adducin open reading frame (ORF) (data not shown, Giulia Devescovi). In addition, this experiment demonstrated that the ORFs of erythrocyte and brain β-adducin subunits were identical, providing supporting evidence that the size differences between brain and erythrocyte β-adducin observed in the Western blot analysis are probably due to post-translational modifications (Bennett et al., 1988; Joshi et al., 1991; Muro et al., 2000; Tripodi et al., 1991).

								Genomic Localization 6qC3			Genomic Localization 4q22-44			Genomic Localization 2p13.3		
Exon number	Exon name	MOUSE size	RAT size	HUMAN size	homology mouse-rat	homology mouse-human	homology rat-human	Chr 6 Mouse From	Chr 6 Mouse to	Chr 6 Mouse size	Chr 4 Rat From	Chr 4 Rat to	Chr 4 Rat size	Chr 2 Human From	Chr 2 Human to	Chr 2 Human size
5' UTR brain *		355	352	465												
5' UTR spleen*		167	187	465*												
5' UTR bone marrow	E1 human			229**												
exon 1	brain exon (mice and rats)	219	219	312	0.9406	0.5297	0.5297	86,458,032	86,458,250	219	120,168,650	120,168,868	219	70,906,984	70,906,673	312
intron 1-2								86,458,251	86,512,277	54,027	120,168,869	120,238,552	69,684	70,906,672	70,851,972	54,701
94 bp exon mouse		94		94	NA	NA	NA	86,481,684	86,481,774	91						
intron 94 pb exon-exon2								86,481,775	86,512,277	30,503						
111 bp intron human				111	NA	NA	NA							70906501	70906390	112
intron 112 pb exon-exon 2														70906389	70,851,972	54,418
142 bp exon human				142	NA	NA	NA							70906257	70906116	142
intron 142 pb exon-exon 2														70906114	70,851,972	54,143
exon 1E (human)	E1 human			76										70856544	70856468	77
exon 1E	spleen exon	31	54					86,507,735	86,507,765	31	120,221,140	120,221,193	54			
intron 1-2		4512	17,359	4,496				86,507,766	86,512,277	4,512	120,221,194	120,238,552	17,359	70856467	70,851,972	4,496
exon 2	common exon	102	99	119	0.8824	0.5300	0.7100	86,512,278	86,512,379	102	120,238,553	120,238,651	99	70,851,971	70,851,853	119
intron 2-3		3015	3410	6623				86,512,380	86,515,394	3,015	120,238,652	120,242,061	3,410	70,851,852	70,845,230	6,623
exon 3	ATG exon	217	217	217	0.9355	0.8203	0.8157	86,515,395	86,515,611	217	120,242,062	120,242,278	217	70,845,229	70,845,013	217
intron 3-4		859	1945	1766				86,515,612	86,516,470	859	120,242,279	120,244,223	1,945	70,845,012	70,843,247	1,766
exon 4		139	139	139	0.9712	0.9568	0.9496	86,516,471	86,516,609	139	120,244,224	120,244,362	139	70,843,246	70,843,108	139
intron 4-5		5781	5169	7924				86,516,610	86,522,390	5,781	120,244,363	120,249,531	5,169	70,843,107	70,835,184	7,924
exon 5		152	152	152	0.9605	0.8947	0.9079	86,522,391	86,522,542	152	120,249,532	120,249,683	152	70,835,183	70,835,032	152
intron 5-6		426	402	443				86,522,543	86,522,968	426	120,249,684	120,250,085	402	70,835,031	70,834,589	443
exon 6		81	81	81	0.9506	0.9012	0.8889	86,522,969	86,523,049	81	120,250,086	120,250,166	81	70,834,588	70,834,508	81
intron 6-7		3203	2713	3168				86,523,050	86,526,252	3,203	120,250,167	120,252,879	2,713	70,834,507	70,831,340	3,168
exon 7		150	150	150	0.9467	0.8933	0.8933	86,526,253	86,526,402	150	120,252,880	120,253,029	150	70,831,339	70,831,190	150
intron 7-8		1740	1744	1473				86,526,403	86,528,142	1,740	120,253,030	120,254,773	1,744	70,831,189	70,829,717	1,473
exon 8		144	144	144	0.9792	0.9306	0.9444	86,528,143	86,528,286	144	120,254,774	120,254,917	144	70,829,716	70,829,573	144
intron 8-9		2435	2494	2663				86,528,287	86,530,721	2,435	120,254,918	120,257,411	2,494	70,829,572	70,826,910	2,663
exon 9		99	99	99	0.9798	0.8586	0.8687	86,530,722	86,530,820	99	120,257,412	120,257,510	99	70,826,909	70,826,811	99
intron 9-10		3228	3724	4256				86,530,821	86,534,048	3,228	120,257,511	120,261,234	3,724	70,826,810	70,822,555	4,256
exon 10		177	177	177	0.9492	0.8814	0.8870	86,534,049	86,534,225	177	120,261,235	120,261,411	177	70,822,554	70,822,378	177
intron 10-11		1388	1901	4629				86,534,226	86,535,613	1,388	120,261,412	120,263,312	1,901	70,822,377	70,817,749	4,629
exon 11		258	258	258	0.9574	0.8876	0.8798	86,535,614	86,535,871	258	120,263,313	120,263,570	258	70,817,748	70,817,491	258
intron 11-12		1050	776	826				86,535,872	86,536,921	1,050	120,263,571	120,264,346	776	70,817,490	70,816,665	826
exon 12		120	120	120	0.9833	0.9000	0.8917	86,536,922	86,537,041	120	120,264,347	120,264,466	120	70,816,664	70,816,545	120
intron 12-13		422	423	872				86,537,042	86,537,463	422	120,264,467	120,264,889	423	70,816,544	70,815,673	872
exon 13		90	90	90	0.9556	0.8556	0.9000	86,537,464	86,537,553	90	120,264,890	120,264,979	90	70,815,672	70,815,583	90
intron 13-14		1722	1721	1970				86,537,554	86,539,275	1,722	120,264,980	120,266,700	1,721	70,815,582	70,813,613	1,970
exon 13bis (Add63)		1571	1466	1795	0.8087	0.6197	0.5748	86,537,464	86539034	1,571	120,264,890	120266355	1,466	70,815,672	70813878	1,795
Add63 poly A signal								86,539,010	86539015	6	120266331	120266336	6	70813900	70813895	6
exon 13bis poly A site								86,539,034				120,266,355			70,813,878	
exon 14		154	154	148	0.9740	0.8701	0.8506	86,539,276	86,539,429	154	120,266,701	120,266,854	154	70,813,612	70,813,465	148
intron 14-15				1351										70,813,464	70,812,114	1,351
exon 15***				86	NA	NA	NA	Not Present			Not Present			70,812,113	70,812,028	86
intron 15-16***		957	982	234				86,539,430	86,540,386	957	120,266,855	120,267,836	982	70,812,027	70,811,794	234
exon 16***		126	126	129	0.8968	0.7829	0.7829	86,540,387	86,540,512	126	120,267,837	120,267,962	126	70,811,793	70,811,665	129
intron 16-17***		7630	6926	9142				86,540,513	86,548,142	7,630	120,267,963	120,274,888	6,926	70,811,664	70,802,523	9,142
exon 17 A1***	A1	1079	1055	1095	0.8972	0.7188	0.7166	86,548,143	86,549,221	1,079	120,274,889	120,275,943	1,055	70,801,450	70,801,445	6
spleen Poly A signal								86,549,197	86,549,202	6	120,275,922	120,275,927	6	70,801,426		
spleen poly A site		1079	1055	1095				86,550,221			120,275,944			70,802,522	70,801,426	1,097
exon 17 A2***	A2-3	1551-1624	1507-1514	1603-1644	0.8900	0.6832	0.6803	86,548,143	86,549,767	1,625	120,274,889	120,276,414	1,526	70,800,920		
spleen Poly A signal								86,549,196	86,549,201	6	120,275,921	120,275,926	6	70,802,522	70,800,920	1,603
spleen poly A site		1551-1624	1507-1514	1603-1644				86,549,220			120,276,414			70,800,940	70,800,935	6
exon 17 A3***	A3	NA	NA	2532	NA	NA	NA	Not present			Not present			70,802,522	70,799,990	2,533
spleen Poly A signal														70,800,037	70,800,032	6
spleen poly A site				2532											70,799,990	
exon 17 brain A4***, ****	A4	6,034	5592	6951	0.8129	0.5746	0.5842	86,548,143	86,554,176	6,034	120,274,889	120,280,485	5,597	70,802,522	70,795,572	6,951
brain Poly A signal								86,554,151	86,554,156	6	120,280,460	120,280,465	6	70,795,597	70,795,592	6
brain poly A site		6034	5592	6951				86,554,176			120,280,485			70,795,572		

	Mouse	*Rat*	*Human*
ADD 97 family:			
cDNA bone barrow	3.119	3115	3.702
cDNA spleen A1	3.119	3115	3.430
cDNA spleen A2	3.591	3.567	3.743
cDNA spleen A3	3.664	3.574	4.631
cDNA brain A4	8.262	7817	9.286
ADD 63 family:			
cDNA bone marrow	3.331	3.246	3.617
cDNA spleen	3.331	3.246	3.853
Full length ORF (Add97)	2178	2178	2181
Add63 ORF	1689	1689	1618
Add97 Full length Protein (kDa)	80639	80573	80851
Pre-mRNA length	96.144	111.835	111.412

Table 3.7: Different β-adducin full-length transcript sizes in mouse, rat and humans. In the table are indicated the length (bp) of the β-adducin transcript forms (βAdd63 and βAdd93 mRNAs families) considering the information reported in Table 3.6.

When we performed the RNase protection analysis using a probe covering the 5'-UTR of the reported rat β-adducin sequence (315 bp sequence indicated in Figure 3.17 A and B as *Spleen Probe*) we detected the expected 168 bases protected fragment for the spleen RNA (Figure 3.17 B, Lanes 2–3), but a smaller protected fragment of ~100 bases was present in the brain RNA samples (Figure 3.17 B, Lanes 4–5). These results suggested the presence of different 5'-UTR in β-adducin mRNAs from brain and spleen.

Table 3.6: Exon and intron sizes and chromosomal location of exons in the β-adducin genes of mice, rats and humans. The chromosomal location of exon and introns is referred to ENSEMBL (http://www.ensembl.org/index.html). The position of the putative poly(A) signals and sites are indicated. The homology between species of exonic sequences is indicated. The human 5'-UTR spleen corresponds to that transcribed from the exon 1 (marked by an asterisk) while that of bone marrow corresponds to the mRNA transcribed from the exon E1 (marked by two asterisks). The numbers of the exons make reference to the human ones. The exon 15 has been described humans but not for mice and rats and the rodent exons 15 and 16 correspond to the human ones 16 and 17, respectively (indicated by three asterisks). In the annotated mouse genomic sequence a 100 bp undetermined region close to the 3'-end was present. "NA", Not Applicable. The annotated mouse genomic sequence contains a 100 bp undetermined region located 308 bp upstream of the A_4 poly(A) site (indicated by four asterisks). This region was sequenced after PCR cloning and we found that the boundaries of the annotated sequence were contiguous without a gap.

To identify the brain-specific sequence revealed in the RNase protection experiment shown in Figure 3.17 B, we performed 5'-RACE analysis of rat brain total RNA.The 5'-RACE experiments led to the cloning and sequencing of a novel brain-specific exon (Figure 3.19 A). The longest clone contained a novel sequence of 258 bases (GenBank accession no. DQ231568). To verify the RACE results we performed RNase protection experiments using the novel brain exon as the probe (295 bp sequence indicated as *Brain Probe* in Figure 3.17 A and B). The analysis produced the expected protected fragment of 198 bases in brain RNA samples (Figure 3.17 C, Lanes 11–12) while a protected fragment of 104 bases was observed in spleen RNA samples (Figure 3.17 C, Lanes 9–10). These results confirmed the presence of two tissue-specific exons in the β-adducin mRNA: the novel exon in brain (containing 258 bp) and the previously reported 54 bp exon in spleen (Yenerel et al., 2005).

To determine the transcription initiation site of the β-adducin mRNAs in rat brain and spleen we performed a primer extension experiment utilizing an oligonucleotide (Figure 3.16) complementary to the 3'-end of the first reported exon common to brain and spleen mRNAs, containing 99 bases (Figure 3.18 A). Primer extension analysis of rat brain RNA showed two main bands of about 300 and 320 bases, ending very close to the 5'-end of the longest cDNA clone obtained by RACE–PCR of brain RNA (Figure 3.18 A, Lanes 5–6 and Figure 3.19 A). Two main bands of 163 and 168 bases were observed by primer extension of spleen RNA, the bigger one coinciding with the reported transcription initiation site of the rat β-adducin gene and the smaller one starting only 5 bases downstream of that site (Figure 18 A, Lanes 3–4, and Figure 3.19 B). The putative transcription initiation sites (indicated with +1 and boldface as determined by primer extension) and the specific brain and spleen exons (underlined) of the β-adducin gene are shown in Figure 3.19 A and B. The transcription site determined by the primer extension experiment exactly coincided with that reported for the mouse β-adducin mRNA (ENSEMBL, transcript ENSMUST00000077101, Figure 3.19 A and B). The RNase protection assays, 5'RACE PCR and primer extension experiments had been previously performed in our laboratory by Giulia Devescovi.

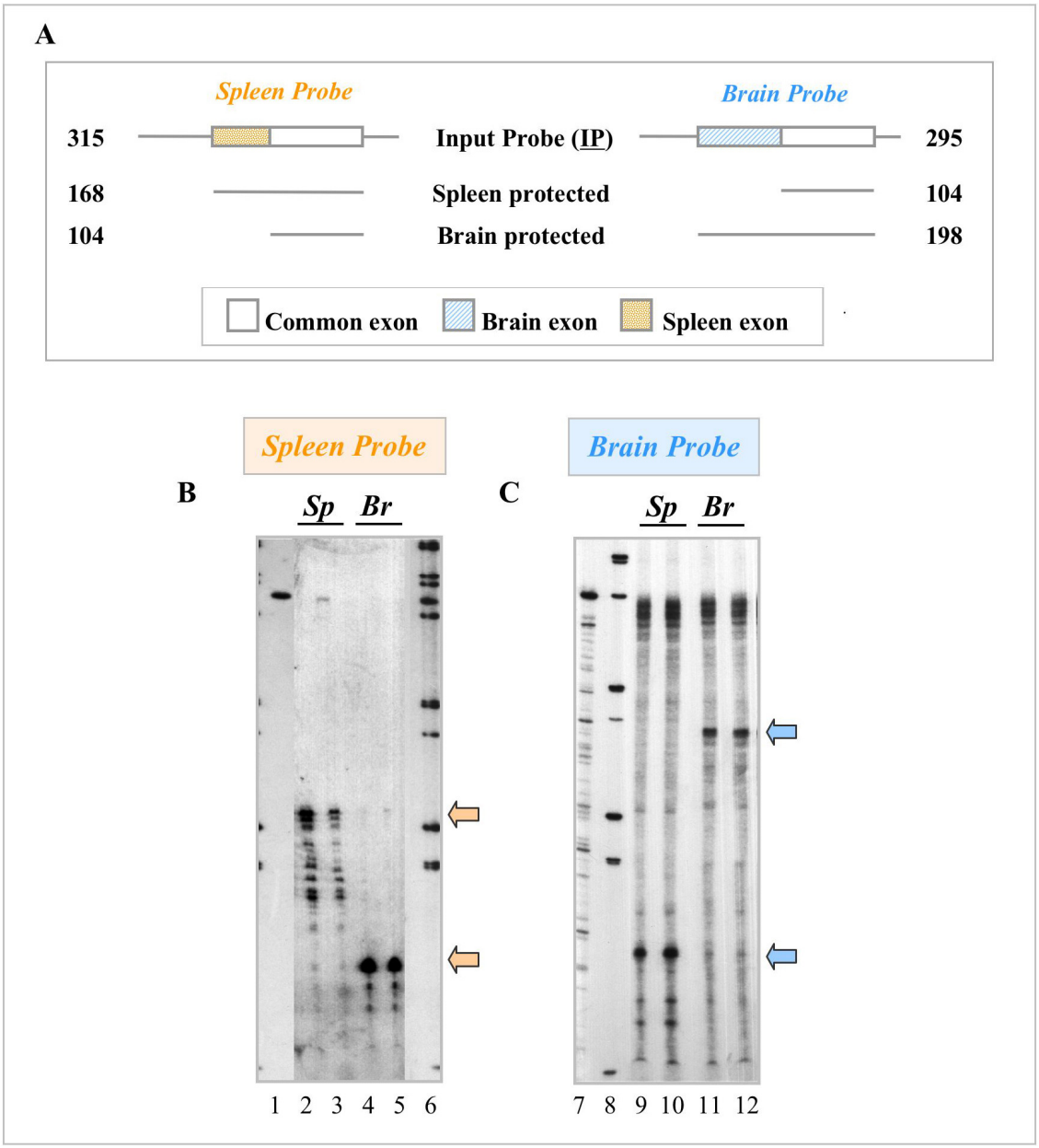

Figure 3.17: Detection of brain- and spleen-specific β-adducin exons in rats. In panel A is illustrated a schematic representation of the riboprobes, used in the RNase protection experiment shown in B and C (*Spleen* and *Brain Probes*, respectively). The input probe and the size of the protected fragments for each probe and each tissue are indicated. Lanes 1 and 7 correspond to the undigested probe (input probe), Lanes 6 and 7 are radioactive molecular weight markers, Lanes 2–3 and 9–10 spleen RNA, and Lanes 4–5 and 11–12 brain RNA. The arrows indicate the protected fragments.

To confirm the tissue-specific expression of each exon, we performed Northern blot analysis of mouse cerebellum, brain and spleen RNA samples with a probe specific for the brain first exon (*m β-Add Brain Probe,* Figure 3.16 A). As it is shown in Figure 3.18 B, a band of about 8–9 kb was observed in cerebellum and brain RNA samples (Lanes 1–2), while no band was observed for spleen RNA (Lane 3). In addition, taking advantage of the availability of the β-adducin KO mice previously generated in our laboratory (Muro et al., 2000), we also analysed RNA samples prepared from the brain

of KO mice using the same β-adducin brain-specific probe. The band observed in the Northern blot analysis of mutant brain RNA had a small reduction in size in comparison to that of the control (Figure 3.18 C). This indicated, unambiguously, that it was not the result of unspecific hybridisation: the shift of the band in -/- brain RNA sample was due to the targeted deletion in the β-adducin locus that corresponds to a reduction of 744 bases in the β-Add97 mRNA (exons 9 to 13) (Muro et al., 2000).

In conclusion, these Northern blot results confirmed the existence of tissue-specific exons in rodents, as seen by the RNase protection and primer extension experiments, and suggested a link between the use of the brain-specific promoter and the presence of the 8–9 kb long brain-specific mRNA.

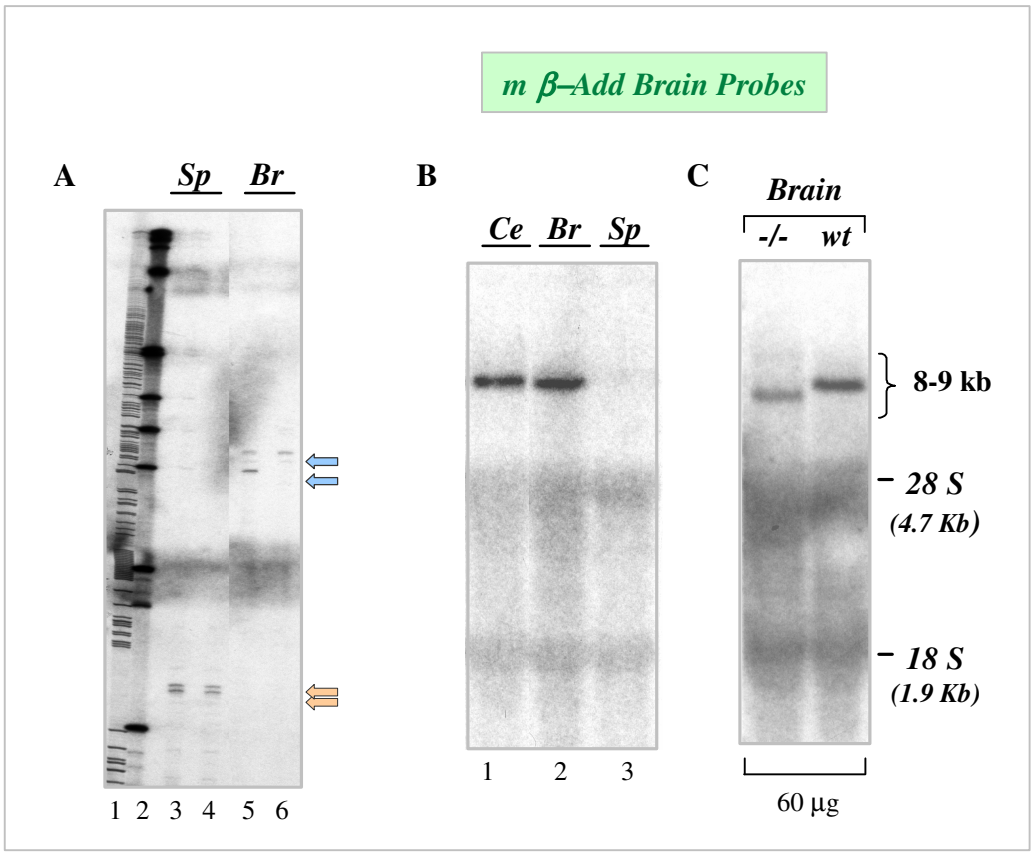

Figure 3.18: Brain- and spleen-specific β-adducin exons are identified in both rats and mice. The primer extension experiment is shown in panel A. A primer annealing in the boundary between the constitutive 99 bp and the 217 bp exons (exons 2 and 3, respectively, present in both the brain and spleen forms of the β-adducin mRNA) was used. The arrows indicate the primer extension products observed in brain and spleen RNAs. Lanes 3–4 and 5–6 correspond to spleen and brain RNAs, respectively. Lane 2 is a radioactive molecular weight marker, and Lane 1 is a one-lane Sanger sequencing reaction using the same primer. Panel B and C show Northern blot experiments of cerebellum, brain and spleen mouse RNA (Lanes 1–3 in Panel B, respectively) and brain RNA from mutant and control mice (Lanes 1 and 2 in Panel C (60 µg, for each sample) respectively, with a probe corresponding to the mouse brain-specific exon (the position of the *m β–Add Brain Probes* is indicated in Figure 3.16 A). The position of the 28S and 18S rRNA is indicated on the left.

3B.4 Structure of the brain and spleen-specific promoter

The 5'-end of the human β-adducin mRNA has been determined by RACE analysis of RNA from a neuronal cell line and, using the amplified product as probe, the genomic region comprising the putative promoter of the human β subunit was cloned (Gilligan et al., 1997). We compared the sequence of the mouse and rat 5'-end data with that reported by Gilligan et al. of the human 5'-end of β-adducin mRNA. The alignment of the genomic sequences of the brain and spleen-specific first exons of the three species and their upstream 300 bp putative promoters (Figure 3.19 A and B) suggested a different genomic structure for the 5'-ends for the rodent β-adducin gene.

While there was an almost perfect matching in the length and a high degree of homology of the protein coding exons among the three species (Muro et al., 2000), the conservation and length of the first exon highly differed (Figure 3.19 A, B and Table 3.6). In fact, the human first exon was 312 bp long, while that of mice and rats had 219 bp. In addition, cloning and sequencing of the genomic regions showed 90.8 and 94.1% of homology between the putative brain promoter regions (up to position –300 bp) and the brain-specific exons, respectively, between rats and mice (Figure 3.19 A and Table 3.6). On the contrary, the conservation between the human and rodent promoter regions and first exons was only 47 and 53%, respectively (Figure 3.19 A and Table 3.6). Sequence comparison of the spleen-specific promoter region and first spleen-transcribed exon of rat and mouse β-adducin (mE1 and rE1, respectively) with the recently reported human erythroid-specific exon (hE1) (Yenerel et al., 2005) showed 84% homology between rat and mouse, while the homology between mE1 and rE1 sequences and the hE1 exon were only of 43% and 47%, respectively (Figure 3.19 B and Table 3.6).

We performed a promoter prediction analysis *in silico* using two different programs (DNAstar Lasergene program and TESS browser from the University of Pennsylvania) to determine putative transcription factors binding sites in the brain and spleen promoters of mice, rats and humans. The predicted transcription factor binding sites that displayed a high score and were present in both analyses were selected and are displayed in Figure 3.19. This *in silico* prediction showed that the putative promoter sequences 5'-to the mouse and rat brain-specific exons (mN1 and rN1 exons, respectively, where N indicates neuronal) contained a consensus Inr sequence and several potential transcription binding sites (Figure 3.19 A). Moreover, the analysis evidenced that just a few transcription factor sites were common to the brain promoter of all three species.

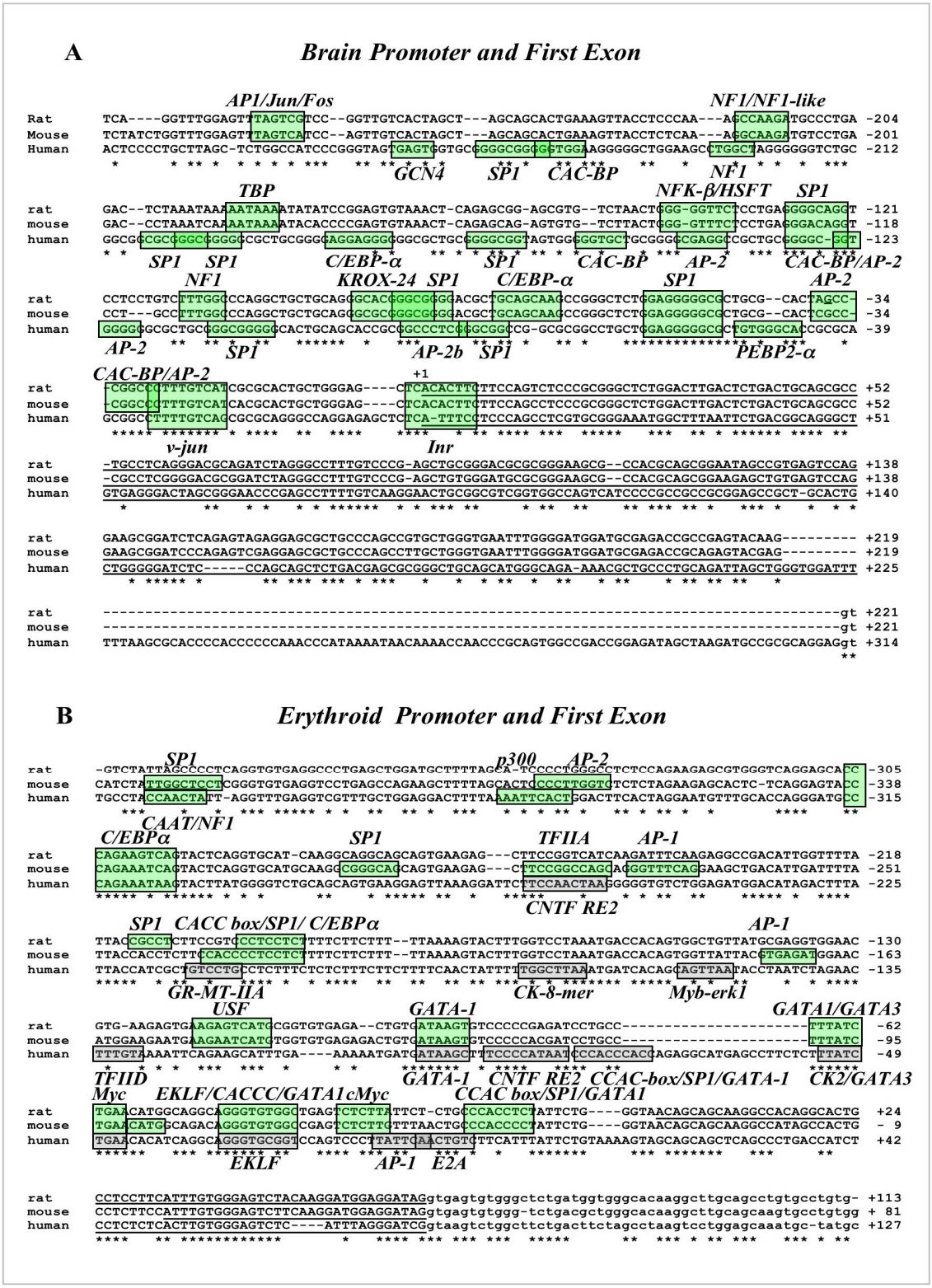

Figure 3.19: Comparison of the brain- and erythroid-specific promoters and first exons of mouse, rat and human β-adducins. In both Panels the exonic sequences (mN1 and rN1 exons for mice and rats, respectively in Panel A and mE1, rE1 and hE1 exons for mice, rats and humans, respectively in Panel B) are underlined. The putative promoter sequences (approximately 300 bp) are shown upstream the exonic sequences. Numbers are relative to the transcription initiation site (indicated by "+1"). The predicted transcription factor binding-sites are indicated. The transcription sites determined by the primer extension experiment are in boldface, and correspond to the first base of the brain exon in Panel A and the first and fifth base of the rat spleen exon in Panel B. In addition, in Panel A the first base (guanine) of the longest RACE clone is underlined.

Numerous SP1 binding sites were predicted in the human promoter and were not so profuse in the rodent promoter. SP1 is a transcription factor found in many housekeeping genes that binds to GC rich regions and, in accordance with this observation, the GC value of the human promoter was 79% while in the rat and mouse brain rodent promoters it was of 55–60% supporting the observed differences in structure and suggesting a diverse transcriptional regulation of this β-adducin gene promoter in the different species.

Similarly to that observed for the human erythroid promoter (Yenerel et al., 2005), both the rat and mouse spleen promoters contained a conserved Inr sequence (Weis and Reinberg, 1992). In addition, other potential transcription sites were found within these rat and mouse promoters and are shown in Figure 3.19 B. We observed that between rodents and humans most binding sites were not conserved. However, those of the haematopoietic GATA transcription factor family (Orkin, 1992), predicted for the human erythroid E1 promoter (Yenerel et al., 2005), were present in conserved regions of the rodent promoters.

3B.5 Analysis of the tissue-specific expression of β-adducin mRNA

In order to investigate whether the indicated above structural differences between human and rodent promoters might be correlated to functional differences we studied the activity of the tissue-specific promoters in mouse and human.

The pattern of expression of the brain and spleen-specific β-adducin exons in different tissues of embryos, newborns and mice of different ages were analysed. Using primers that amplify from the first brain-specific exon (mN1) to the constitutive 217 bp 3^{nt} exon (Figure 3.20 B, primers "a" and Table 2.1), we observed that the mouse brain-specific promoter was active in the brain of embryos, postnatal 1- and 14-day-old animals, and adult mice (Figure 3.20 C, primers "a"). On the contrary, no expression was observed in other tissues (Figure 3.20 C, primers "a"). Oligonucleotides that amplify from the first spleen exon (mE1) to the 3^{nt} exon (Figure 3.20 B, primers "c" and Table 2.1) evidenced that the spleen promoter was active in liver embryo and placenta [haematopoietic organs in embryo life (McGrath and Palis, 2005)], and had a low level of expression in other embryonic tissues (Figure 3.20 C, primers "c"). In 14-day-old mice, the expression in the liver and other tissues seemed to be completely shutdown and was active only in the spleen and bone marrow (Figure 3.20 C, primers "c").

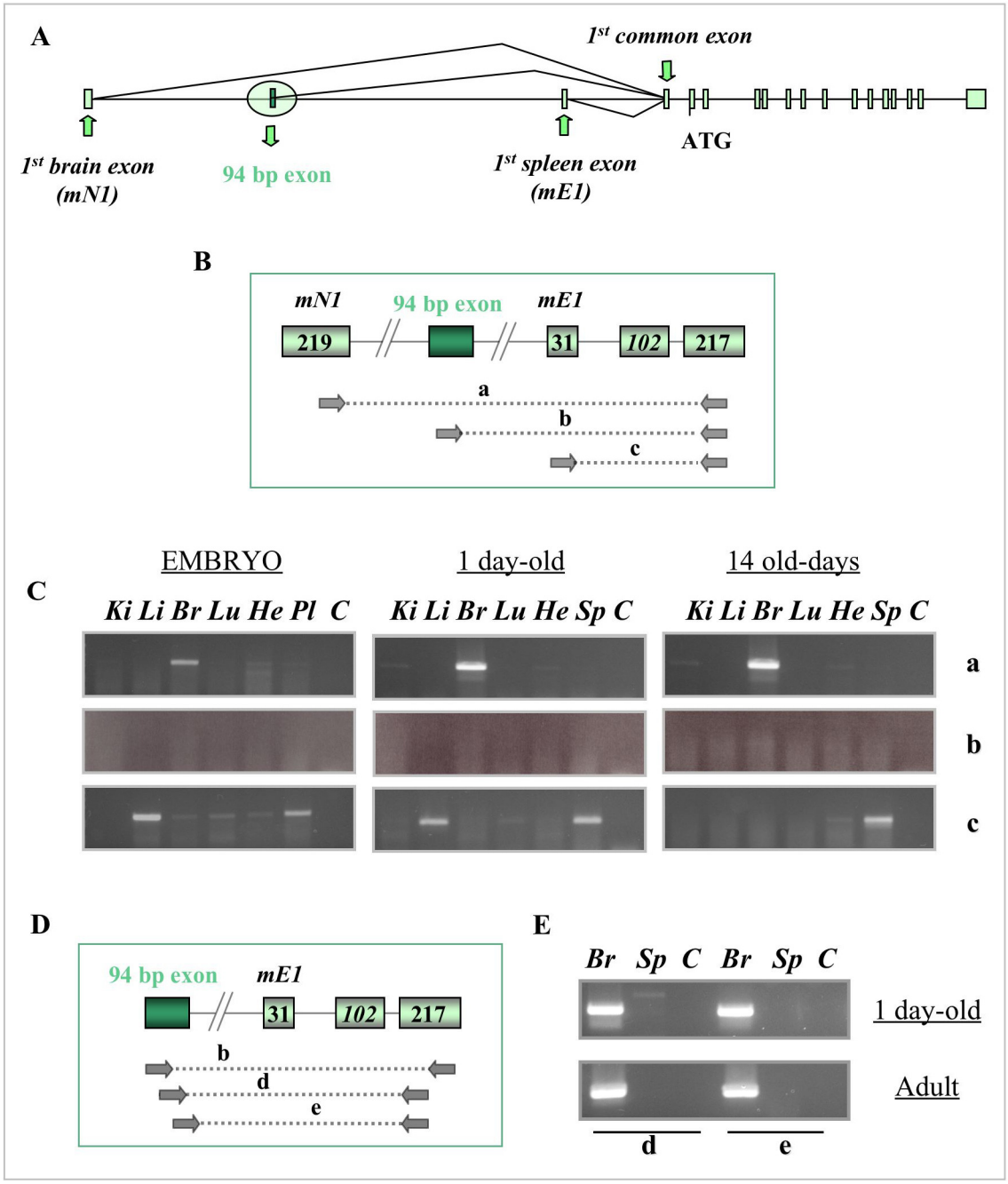

Figure 3.20: Analysis of tissue-specific promoter activity and the identification of a new potential β–adducin exon in mice. Panel A contains a scheme of the mouse β-adducin gene showing the position of the known exons and of the 94 bp potential exon (boxes). Schemes of Panels B and D indicate the positions of the oligonucleotides utilized in the RT-PCR reaction of Panels C and E, respectively. In Panel C, brain (Br), spleen (Sp), kidney (Ki), liver (Li), lung (Lu), heart (He) and placenta (Pl) RNA samples were analysed with primer-pairs "a" and "c", which amplified from the first brain and spleen exons, respectively, to the constitutive 217 bp 3rd exon, and with primer pair "b", which amplified the new 94 bp exon. Semi-nested PCRs with two different sets of oligonucleotides, (primer pairs "d" and "e") used on brain (Br) and spleen (Sp) RNA from 1 day old and adult mice are shown in Panel E.

To determine the expression pattern of the human exon 1 we used the same RNA samples with the pair of primers that amplify the fragment from human exon 1 to exon 3 (Figure 3.21 B, primers "a" and Table 2.1). A strong PCR product was observed for

brain and spleen (Figure 3.21 C, primers "a"), while the amount of RT–PCR product observed in lung and bone marrow was lower.

This experiment strongly suggests differences in activity and tissue-specificity between the rodent and human brain-specific promoter. In fact, while those of mice and rats were active only in brain, the human one was active not only in brain but also in spleen, and to a much lesser extent in lung and bone marrow. Those detected variations might be related to the structural and base composition differences among the promoters, as described above and shown in Figure 3.19 A and B.

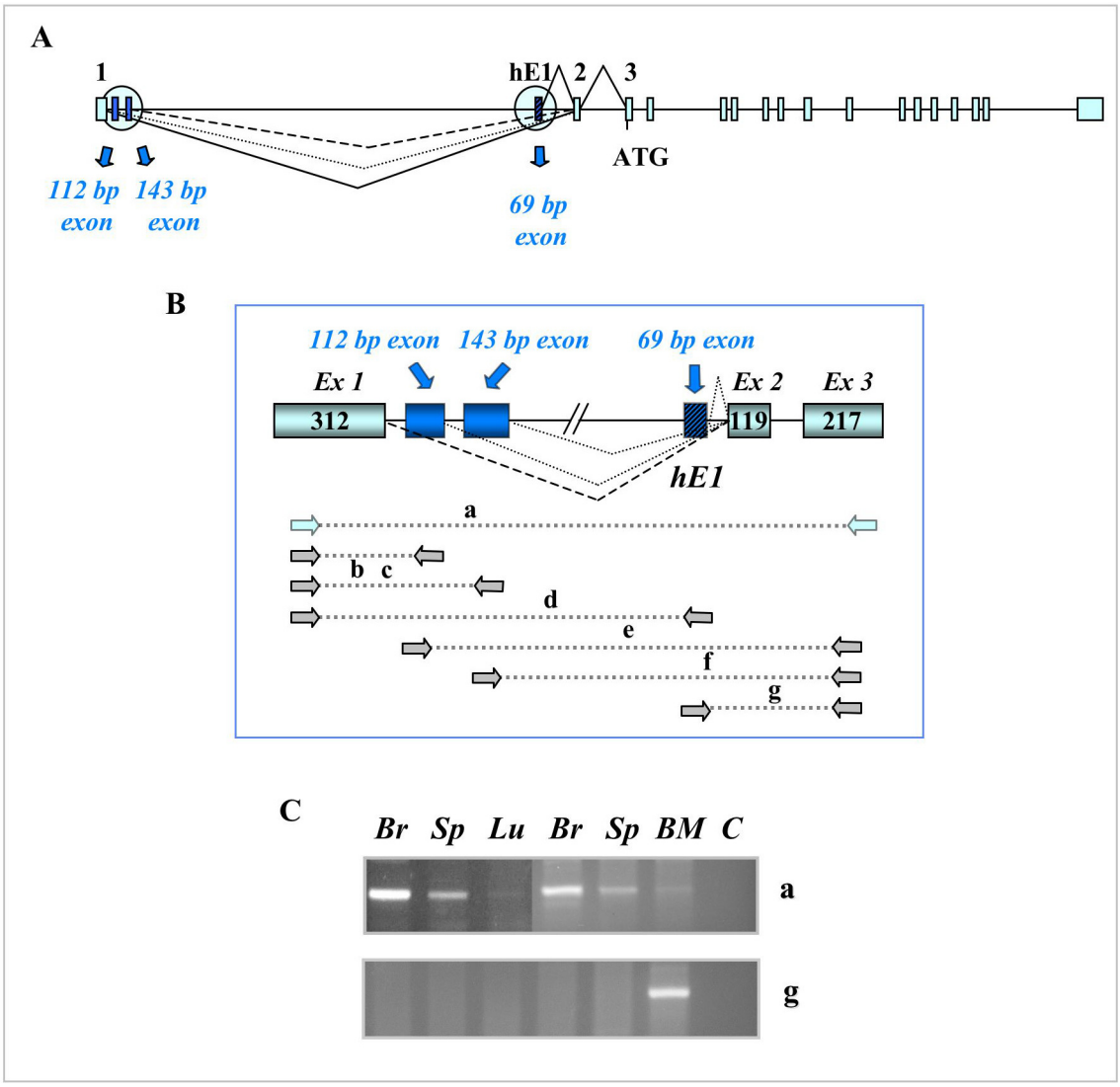

Figure 3.21: Analysis of tissue-specific promoter activity and of the new potential β-adducin exons in humans. Panel A shows a schematic representation of the human β-adducin gene structure indicating the position of the new potential exon. The open boxes indicate exons 1–17; the 112 bp, the 143 bp and the 69 bp erythroid-specific E1 exons are indicated. A scheme indicating the positions of the oligonucleotides utilized in the RT-PCR reaction of Panel C are shown in Panel B. RNA samples from two different preparations of brain (Br) and spleen (Sp), lung (Lu) and bone marrow (BM) were analysed with the different primer-pairs described in Panel B. No product was obtained after the first round of amplification using primer pairs "b", "c", "d", "e" and "f" (data not shown). Panel C shows the PCR results obtained using the primer pairs "a" and "g" that amplified a product from exon 1 to exon 3, and from exon E1 to exon 3, respectively.

3B.6 Analysis of new putative exons and tissue-specific expression of β-adducin mRNA

With the aim to characterise the brain-specific 8-9 kb β-adducin mRNA, we searched for new previously undetected exons that could justify the presence of the long brain transcript.

We looked for ESTs containing β-adducin exonic sequences contiguous to novel sequences: we performed a BLAST alignment between each of the β-adducin exons sequences and the EST database, and the ESTs containing β-adducin exon sequences flanked by novel sequences were selected. Finally, to locate their chromosomal positioning we run a BLAST alignment between the novel sequences and the genome database. If the novel sequences were located in the same chromosomal region of the analysed exon sequence, it could suggest that these sequences might be new exons. We performed this database search for mice and humans β-adducin known exons and identified a set of ESTs that contained contiguous novel sequences only within the 5'-region of the transcript, suggesting the presence of other alternative promoters (Figure 3.20 A and 3.21 A, and Table 3.6).

Among the detected sequences, we identified the mouse EST CA317234, which is consisted of a 94 bases novel sequence located upstream of the 102 bp exon 2 of the mouse β-adducin gene (Figure 3.20 A and Table 3.6). RT-PCR analysis using primers that annealed to the novel exon and to exon 3 (Figure 3.20 D, primers pair "b", "d" and "e") amplified a PCR product only after nested PCR of 1 day-old and adult mouse brain RNAs suggesting a low level of expression of the 94 bp novel exon (Figure 3.20 E, primers "d" and "e"). No product was obtained from mouse spleen RNA samples (Figure 3.20 E, primers "d" and "e").

Three putative novel exons were detected among the human ESTs (ESTs BU159646, AU142416 and BI914212). Their length was 112 bp, 143 bp and 69 bp, respectively, and were located upstream of the 119 bases exon 2 of the human β-adducin mRNA (Figure 3.21 A and Table 3.6). RT-PCR analysis of the 112 bp and 143 bp novel exons failed in all cases to detect a PCR product from brain and spleen RNAs, even after performing nested PCRs utilizing different sets of primers (data not shown and Figure 3.21 B primers "b", "c", "d", "e", and "f"). A prominent product was only detected in the bone marrow RNA sample and corresponded to the 69 bp exon (Figure

3. 21 C, primers "g"), which was recently reported as an erythroid exon (hE1) of 76 bases (Yenerel et al., 2005).

In conclusion, these analyses revealed the existence of new tissue-specific β-adducin first exons transcribed from alternative promoters: the brain 94 bp exon of mouse and the 79 bp erythroid-specific human one. However, the levels of the β-adducin mRNAs transcribed from those new promoters were, apparently, very low.

3B.7 Mouse, rat and human brain 3'-UTR characterisation

We showed above the existence of a brain-specific first exon, its putative promoter for rats and mice and a novel 94 bp brain-specific exon in mice. However, despite the presence of the 94 bp exon and the fact that the first exon was longer than that used in spleen (219 bp vs. 31 bp, respectively), the observed size differences between brain and spleen mRNAs (Figure 3.16 and Table 3.6) were not accounted.

Therefore, to determine the molecular basis of the brain 8–9 kb β-adducin mRNA we focused the search in the 3'-UTR region. Database search (UCSC Genome Browser http://genome.ucsc.edu/) showed the presence of EST transcripts in mice, rats and humans in the regions downstream of the reported 3'-UTR of the β subunit, which in all three cases had not been annotated as part of the β-adducin mRNA. A scheme showing the alignment of this genomic region with the available mouse ESTs is shown in Figure 3.22 A. Rat and human ESTs distribution covered a similar region to that of mice (Figure 3.23 A and 3.24 A).

To determine whether those ESTs could belong to the β-adducin brain mRNA, a series of overlapping RT–PCR analyses were performed using RNA from brain and spleen, prepared from mouse, rat and human tissues. As schematically shown in Figure 3.22 A, 3.23 A and 3.24 A, the first pair of primers (called "a" in Figure 3.22 A, 3.23 A, 3.24 A and Table 2.1) should amplify a portion of the known β-adducin 3'-UTR and up to 800–1100 bases, depending on the species, of the sequences downstream of the reported 3'-UTR of β subunit. The other pairs of primers ("b", "c", "d" and "e" in Figure 3.22 A, 3.23 A, 3.24 A and Table 2.1) were complementary to sequences downstream to the annotated β-adducin 3'-UTR, and were designed in order that each PCR product overlapped the flanking ones covering the entire region up to the most downstream EST shown in Figures 3.22 A, 3.23 A and 3.24 A.

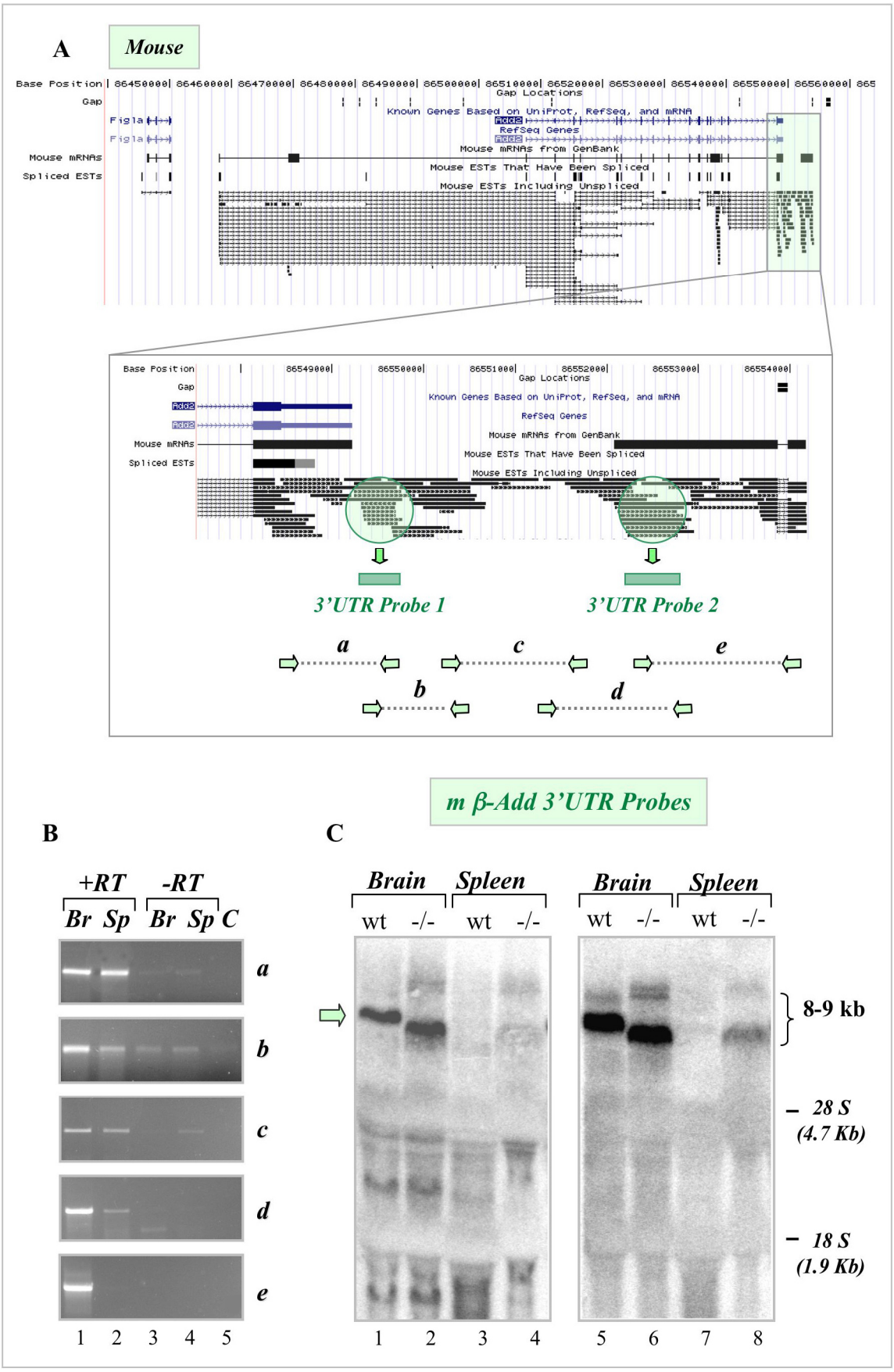
A
Mouse
Base Position
Gap
Gap Locations
Known Genes Based on UniProt, RefSeq, and mRNA
RefSeq Genes
Mouse mRNAs from GenBank
Mouse ESTs That Have Been Spliced
Mouse ESTs Including Unspliced
Mouse mRNAs
Spliced ESTs
3'UTR Probe 1
3'UTR Probe 2
a
b
c
d
e
m β-Add 3'UTR Probes
B
+RT
-RT
Br Sp Br Sp C
1 2 3 4 5
C
Brain Spleen Brain Spleen
wt -/- wt -/- wt -/- wt -/-
8-9 kb
28 S
(4.7 Kb)
18 S
(1.9 Kb)
1 2 3 4 5 6 7 8

Figure 3.22: The identification of an unusually long 3'-UTR in brain β-adducin mRNA of mouse. Panel A shows a scheme of the mouse genomic region downstream of the reported poly(A) site [it was downloaded from the UCSC browser before the publication of the results (Costessi et al., 2006)]. The ESTs mapping in the region are indicated. The position of the primers used the RT–PCRs shown in Panel B and the probes used in the Northern blot experiment of Panel C are schematically indicated. RT–PCR products obtained after amplification of mouse brain and spleen RNAs with the overlapping set of primers from "a" to "e" are shown in Panel B. Lanes 3–4 were performed with the same RNAs used for Lanes 1–2 but without the reverse transcriptase reaction. Lane 5 corresponds to the PCR without the addition of cDNA. Panel C shows the Northern blot experiments of brain (Lanes 1, 2, 5 and 6) and spleen (Lanes 3, 4, 7 and 8) total RNA (30 µg for each Lane) from control (Lanes 1, 3, 5 and 7) and β-adducin KO mice (Lanes 2, 4, 6 and 8). Two identical membranes were hybridised with the *3'-UTR Probes 1* and *2* (Lanes 1–4 and 5–6, respectively). An arrow indicates the detected bands. The position of the 28S and 18S rRNA is indicated.

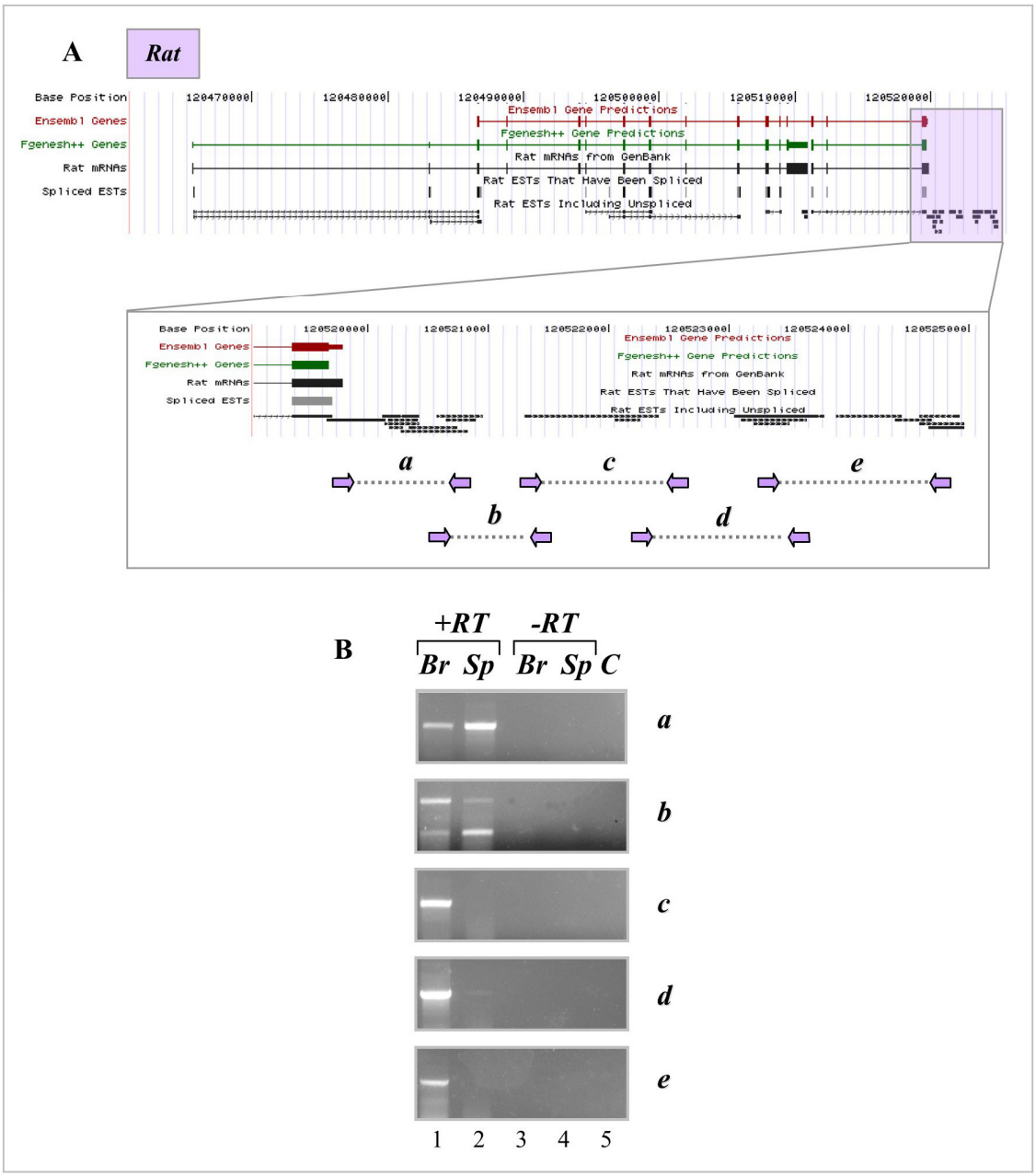

Figure 3.23: The discovery of a 5-6 kb 3'-UTR in brain β-adducin mRNA of rats. Panel A shows a scheme of the rat genomic region downstream of the reported polyadenylation site (UCSC browser). The ESTs corresponding to that region and the position of the PCR primers used the RT–PCRs experiments shown in Panel B are indicated in the scheme. PCRs were performed as described in the Legend of Figure 3.22.

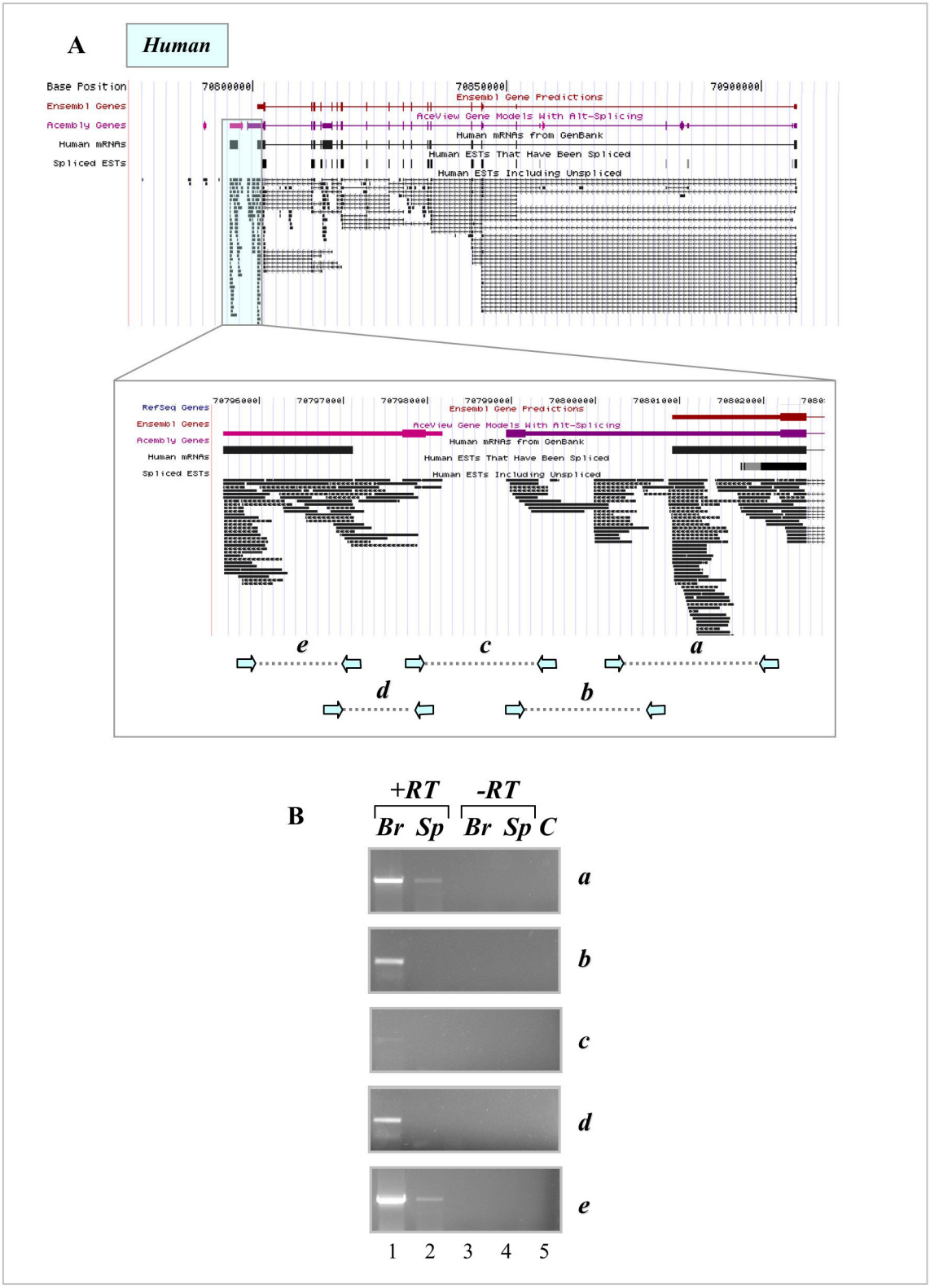

Figure 3.24: An unusually long 3'-UTR is detectable in brain β-adducin mRNA of humans. A scheme of the human genomic region downstream of the reported polyadenylation site, downloaded from the UCSC browser before the data publication (Costessi et al., 2006), is shown in Panel A. The ESTs corresponding to that region and the position of the PCR primers used the RT–PCRs shown in Panel B are indicated. PCRs are performed as indicated in the Legend of Figure 3.22.

The RT–PCR analysis showed specific PCR products in brain samples for all primer pairs used (Figure 3.22 B, 3.23 B and 3.24 B, Lanes 1). In addition, no RT-PCR product was generated using a reverse primer located 80 bases after the end of the last reported EST (containing the putative polyadenylation site) with the forward one used in pair "e", suggesting that all the β-adducin brain mRNA ends at the same site (Figure 3.22 A, 3.23 A and 3.24 A and data not shown). These results strongly suggested that the 8–9 kb mRNA transcript observed in brain comprises a 5-6 kb 3'-UTR and could be generated by alternative usage of tandem polyadenylation sites.

To confirm this hypothesis we performed Northern blot analysis of mouse brain and spleen RNAs using two different probes of 600 and 800 bp that mapped downstream of the stop codon of the β subunit transcript located in exon 16, in the novel 3'-UTR of brain β-adducin mRNA (*3'-UTR Probe 1* and *3'-UTR 2* starting ~1400 and 3500 bases downstream of the stop codon, respectively; Figure 3.22 A). Both probes showed the presence of a band of similar size to that detected for the mouse brain β-adducin mRNA using a probe containing the ORF (Figure 3.22 C, Lanes 1 and 5 versus Figure 3.16 B, Lane 1), confirming that the difference in size of the brain transcript was due to the presence of an extremely long 3'-UTR. In addition, taking advantage of the β-adducin KO mice previously generated in our laboratory (Muro et al., 2000), we run in the same gel RNA samples prepared from the brain of KO mice and we also observed a high molecular weight band having a small reduction in size. This indicated, unambiguously, that the detected band was indeed the product of the β-adducin gene and not the result of unspecific hybridisation (Figure 3.22 C, Lanes 2 and 6). A faint band of similar size to that observed in brain RNA samples of KO mice was also observed for spleen RNA samples of KO mice (Figure 3.22 C, Lanes 4 and 8). These bands could be the result of altered polyadenylation regulation in the spleen of the β-adducin deficient mice due to the loss of important regulatory sequences by the targeted genomic deletion. In fact, no band was observed in the spleen RNA samples of control mice (Figure 3.22 C, Lanes 3 and 7).

These Northern blot results strongly indicated that the long β-adducin mRNA observed in brain could be generated by alternative usage of polyadenylation sites.

3B.8 Analysis of the Add63 family of transcripts in brain and its relative expression with respect to Add97 transcripts

To extend our analysis to the Add63 family of transcripts, generated by the retention of the intron that follows exon 13 and the use of a downstream alternative polyadenylation signal (Tisminetzky et al., 1995; Tripodi et al., 1991), we performed a Northern blot analysis of cerebellum, brain and spleen mouse RNAs using specific probes to detect the Add97 and Add63 families of mRNAs (Figure 3.25).

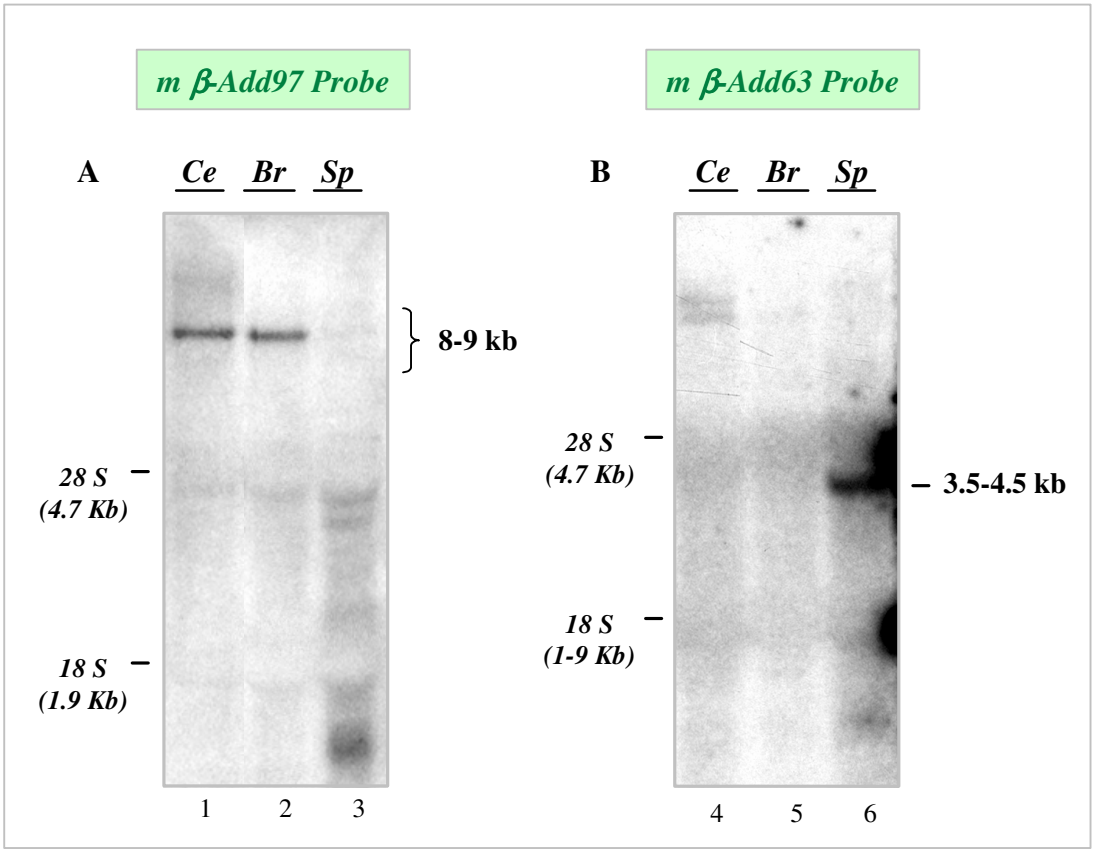

Figure 3.25: Northern blot analysis of the Add97 and Add63 β-adducin mRNA. Cerebellum (Ce), brain (Br) and spleen (Sp) total mouse RNA (30 µg in Lanes 1 and 4, 2 and 5, and 3 and 6 in Panels A and B, respectively) were loaded in identical agarose formaldehyde gels (1.2%), blotted onto Hybond-N^+ and hybridised with the *m β-Add97* and *m β-Add63 Probes* (described in Figure 3.16 A) in Panels A and B, respectively. The 28S and 18S rRNAs are indicated.

Using the *m β-Add97 Probe*, which contained only exons 14 to 16, not present in Add63 mRNAs (Figure 3.16 A), we were able to detect a strong band of 8-9 kb and a fainter doublet of 3.5-4.5 kb in cerebellum and brain samples, while in spleen RNA a doublet in the 3.5-4.5 kb region was clearly evident and the 8-9 kb band was hardly visible as expected (Figure 3.25 A).

The probe specific for the Add63 family of transcripts, containing only sequences from the exon 13bis (not present in Add97 mRNAs) (Figure 3.16 A, *m β-*

Add63 Probe), detected a weak doublet of 8-9 kb in cerebellum and brain but the bands in the 3.5-4.5 bases region were not visible, while in spleen a strong signal of a single band was observed, that was similar in size to that of higher molecular weight-band of the doublet observed with the *m β-Add97 Probe* in spleen (Figures 3.25 B versus A).

The presence in cerebellum of the high molecular weight band in the Add63 family of transcripts suggests that neither the polyadenylation site present in the exon 13bis was not efficiently used nor intron 13 was spliced out. The absence of any band (high or low molecular weight) in brain suggest that the efficiency of exon 13-exon 14 splicing was higher reducing the amount of the Add63 family of mRNA. The observed doublet with the *m β-Add63 Probe* in cerebellum could be due to alternative splicing variants that retain the exon 13bis, as determined by RT-PCR analysis (data not shown). Northern blot analysis using the *m β-Add97 Probe* showed that the Add97 family of transcripts has a long 3'-UTR in brain.

In addition, these experiments also showed the relative abundance of the Add97 and Add63 family of mRNAs in brain and spleen. In fact, despite the same amounts of total RNA were loaded in the Northern blot experiment shown in Figure 3.25, the stronger signal using the *m β-Add97 Probe* is seen in cerebellum and brain (Figure 3.25 A, Lanes 1-2), while it is observed in spleen with the *m β-Add63 Probe* (Figure 3.25 B, Lane 6). These results confirmed the data obtained by RT-PCR in the previous tissue-specific expression analysis of β-adducin (Figures 3.14 and 3.15). In addition, the exposition time of the Add63-blot was five times longer than that of the Add97-membrane, suggesting that the Add63 family of transcripts is considerably less abundant than the Add97 forms. Alternatively, the differences in the intensity of the Add 97 and Add63 specific bands could be due to the different efficiency of each probe.

3B.9 Identification of a highly conserved brain-specific polyadenylation site used in mice, rats and humans

To confirm the existence of a brain-specific β-adducin alternative polyadenylation site, we run a BLAST search using the genomic sequences of the region downstream of the known β-adducin poly(A) site reported in the last exon looking for EST sequences of mouse, rat and human (Figures 3.22 A, 3.23 A and 3.24 A). The detected sequences were examined for the presence of poly(A) tails after the alignment.

N	Species	EST	Poly(A) site	Poly(A) tail	Position *	Tissue	Age
1	Human	H63708	hA1	no	1070	liver spleen	20 weeks fetus
2	Human	CN428094	hA1	no	1094	embryonic stem cells, DMSO-treated H9 cell line	NA
3	Human	BQ716022	hA1	no	1118	Lupski_sympathetic_trunk	adult 16 yr
4	Human	H63978	hA2	no	1602	liver spleen	20 weeks fetus
5	Human	AF090096	hA2	no	1603	lung	fetal
6	Human	BC008709	hA2	yes	1603	eye retinoblastoma	NA
7	Human	BC065525	hA2	yes	1603	eye retinoblastoma	NA
8	Human	CN480603	hA2	yes	1603	condrosarcoma Cell Line CS8	NA
9	Human	AA448280	hA2	yes	1603	testis	NA
10	Human	AA703034	hA2	yes	1603	liver spleen	20 weeks fetus
11	Human	AI133421	hA2	yes	1603	liver	fetal
12	Human	BM671370	hA2	yes	1603	Foveal and Macular Retina	NA
13	Human	BU733807	hA2	yes	1603	Foveal and Macular Retina	NA
14	Human	BU178973	hA2	yes	1603	eye retinoblastoma	NA
15	Human	BU620744	hA2	yes	1603	condrosarcoma Cell Line	NA
16	Human	T96149	hA2	yes	1603	liver spleen	20 weeks fetus
17	Human	AA478560	hA2	no	1603	melanocyte 2NbHM, pregnant uterus NbHPU, and fetal heart NbHH19W	NA
18	Human	AA055514	hA2	no	1603	heart	19 weeks fetus
19	Human	N74221	hA2	no	1603	liver spleen	20 weeks fetus
20	Human	W86292	hA2	no	1603	liver spleen	20 weeks fetus
21	Human	AI248103	hA2	no	1608	Soares_fetal_liver_spleen_1NFLS_S1	20 week fetus
22	Human	T03505	hA2	no	1610	total brain	72 day
23	Human	AW444494	hA2	yes	1639	kidney	NA
24	Human	BF507552	hA2	yes	1639	lung	NA
25	Human	BF111420	hA2	yes	1639	NA	NA
26	Human	AI743720	hA2	yes	1639	NA	NA
27	Human	AI469906	hA2	yes	1644	NA	NA
28	Human	AA629795	hA2	yes	1644	cell line NCI-H69	NA
29	Human	T91890	hA3	no	2525	liver spleen	20 weeks fetus
30	Human	T91153	hA3	no	2525	liver spleen	20 weeks fetus
31	Human	R02130	hA3	no	2531	liver spleen	20 weeks fetus
32	Human	T90561	hA3	yes	2532	liver spleen	20 weeks fetus
33	Human	AA608592	hA3	yes	2533	lung carcinoma cell line NCI-H69	NA
34	Human	AI566854	hA3	yes	2533	brain anaplastic oligodendroglioma	NA
35	Human	AW874561	hA3	yes	2533	uterus tumor	NA
36	Human	AW445023	hA3	yes	2533	brain	NA
37	Human	AW451990	hA3	yes	2533	breast	NA
38	Human	AI559357	hA3	yes	2533	brain	NA
39	Human	AI362970	hA3	no	2533	brain anaplastic oligodendroglioma	NA
40	Human	AI369409	hA3	no	2533	brain anaplastic oligodendroglioma	NA
41	Human	AI870632	hA3	no	2533	brain anaplastic oligodendroglioma	NA
42	Human	CD247459	hA3	yes	2533	embryonic stem cells, WA01, passage 38	NA
43	Human	AU149490	hA3	no	2536	brain NTS cell line	NA
44	Human	BU633436	hA3	yes	2536	Human Chondrosarcoma Grade 3 cell line mix	NA
45	Human	BX107761	hA3	yes	2536	liver-spleen	fetal 22 weeks
46	Human	BX431608	hA4	no	6938	brain	fetal
47	Human	BX454686	hA4	no	6943	brain	fetal
48	Human	AA351748	hA4	no	6946	brain	infant
49	Human	AA350937	hA4	no	6946	brain	infant
50	Human	AA349557	hA4	no	6946	brain	infant
51	Human	AI419136	hA4	no	6946	brain-glioblastoma	NA
52	Human	AI372610	hA4	no	6946	brain	72 days
53	Human	AI681065	hA4	no	6946	lung-carcinoid	NA
54	Human	AI097640	hA4	no	6946	brain-glioblastoma	NA
55	Human	AW150845	hA4	yes	6946	uterus-endometrial adenocarcinoma	NA
56	Human	AW152196	hA4	yes	6946	brain tumors pool	NA
57	Human	AW152202	hA4	yes	6946	brain tumors pool	NA
58	Human	AW589730	hA4	yes	6946	pooled germ cell tumors	NA
59	Human	AW136843	hA4	yes	6946	brain	NA
60	Human	AW026658	hA4	no	6946	brain-glioblastoma	NA
61	Human	BE042928	hA4	no	6946	lung-carcinoid	NA
62	Human	BF439845	hA4	no	6946	brain-glioblastoma	NA
63	Human	D59839	hA4	no	6946	brain polyA+	fetal
64	Human	Z41378	hA4	no	6946	total brain	3 months
65	Human	CR741427	hA4	yes	6946	brain glioblastoma	NA
66	Human	AI290859	hA4	no	6946	lung-carcinoid	NA
67	Human	BM702947	hA4	yes	6946	Retina Foveal and Macular	adult
68	Human	AA351433	hA4	no	6947	brain	infant
69	Human	AW204454	hA4	yes	6947	NA	NA
70	Human	AW294960	hA4	yes	6947	lung	NA
71	Human	BF444931	hA4	yes	6947	lung-carcinoid	NA
72	Human	AA350706	hA4	no	6948	brain	infant
73	Human	BX097901	hA4	yes	6951	brain	93 days
1	Mouse	AK014496	mA1	no	1076	liver	14.0 embryo
	Mouse	BY564735	mA1	no	1068	spleen	
2	Mouse	NM-013458,2	mA1		1076		NA
3	Mouse	BU850901	mA2-3	yes	1549	brain	NA
4	Mouse	AI414956	mA2-3	yes	1551	total embryo	13.5-14.5
5	Mouse	BY607573	mA2-3	yes	1551	visual cortex	NA
6	Mouse	AW048717	mA2-3	yes	1556	brain	1 month
7	Mouse	BY760493	mA2-3	no	1567	liver	13.5 embryo
8	Mouse	AI596349	mA2-3	yes	1622	total embryo	13.5-14.5
9	Mouse	BX637441	mA2-3	yes	1622	testis, bones, brain, thymus, kidney, embryo, , osteoclasts, spleen	NA
10	Mouse	BQ176418	mA2-3	yes	1624	brain-subfornical organ and postrema	adult
11	Mouse	AI835996	mA4	yes	5932	olfatory bulbs	1 month
12	Mouse	BE651947	mA4	yes	5932	olfatory bulbs	1 month
13	Mouse	BF460712	mA4	yes	5934	embryonic retina	embryo
14	Mouse	BU700211	mA4	yes	5934	brain-subfornical organ and postrema	adult
15	Mouse	CF744570	mA4	no	5934	whole brain	newborn
16	Mouse	BY630902	mA4	no	5934	visual cortex	NA
17	Mouse	BY640439	mA4	yes	5934	visual cortex	NA
18	Mouse	AI835294	mA4	yes	5934	hippocampus	1 month
19	Mouse	BE996420	mA4	yes	5934	retina	NA
20	Mouse	BG976853	mA4	yes	5934	mammary-infiltrating ductal carcinoma	5 months
1	Rat	BF420440	rA1	yes	1052	heart	16,5 embryo
2	Rat	CR467480	rA1	yes	1052	NA	NA
3	Rat	BI281934	rA1	yes	1055	kidney	NA
4	Rat	AI044553	rA2-3	yes	1589	rat placenta, adult lung,brain, liver, kidney, heart, spleen, ovary, and muscle	embryo
5	Rat	CR469107	rA2-3	yes	1589	NA	NA
6	Rat	AW532712	rA4	no	5558	brain	adult
7	Rat	AW528715	rA4	yes	5592	brain	adult
8	Rat	AI575812	rA4	yes	5592	eye	adult

*** the end of the EST clone relative to start of last exon is indicated**

We found several ESTs containing a poly(A) tail such as AW152196, AW136843, BX097901 and CR741427 for human, ESTs AI575812, AW528715 for rat and, ESTs BY640439, BF460712 and BU700211 for mouse (Table 3.8). Interestingly, numerous ESTs containing a poly(A) tail have been identified in neuronal tissues (Table 3.8). A complete list of the ESTs that mapped in the polyadenylation regions is shown in Table 3.8. More in detail, the detected EST-containing poly(A) tails were found at chromosomal positions 86554176, 120280485 and 70795572 for mouse chromosome 6q, rat chromosome 4q and human chromosome 2p, respectively (Tables 3.6 and 3.8), thus generating extremely long brain-specific last exons of 6034, 5592 and 6951 bases and a 3'-UTR of 5831, 5289 and 6642 bases for mouse, rat and human, respectively (Figure 3.26 A, Table 3.6 and 3.7). This *in silico* strategy confirmed the use of a brain-specific polyadenylation site in all three analysed species. We called these distal brain-specific polyadenylation sites mA_4, rA_4 and hA_4 for mice, rats and humans, respectively (Figure 3.26 A and C). The following observations support the hypothesis that the brain β-adducin pre-mRNA is completely polyadenylated at the proposed A_4 site in all the three species: a) the observation that other ESTs that mapped nearby upstream to those mentioned above did not contain the characteristic poly(A) tail; b) no ESTs mapping downstream of the detected brain polyadenylation site were present, as can be seen in Figures 3.22 A, 3.23 A and 3.24 A, and c) the absence of an RT–PCR product with primers at either side of the mA_4 poly(A) site (data not show).

In order to identify sequence similarities among the brain 5-6 kb 3'-UTRs of mouse, rat and human, that may suggest a common brain-specific polyadenylation mechanism in the three species, we retrieved the DNA sequences of all three species of the last exon up to the brain poly(A) sites, including the downstream regions adjacent to the cleavage site. Sequence comparison showed a very high degree of conservation of the 3'-UTR of the brain β–adducin transcript, especially in the region close to the polyadenylation site used in brain. In fact, we observed a 99.1% homology between mouse and rat sequences, and a 75% homology among all three species when the regions flanking the distal brain polyadenylation signal (~200 bp) were compared (Figure 3.26 C).

Table 3.8: List of the human, mouse and rat ESTs mapping in the genomic regions upstream of the different β-adducin polyadenylation sites A_1, A_{2-3}, and A_4. The polyadenylation region and position of the 3'-end of the sequences (the last non-adenosine base when there was a poly (A) tail) are indicated, according to the scheme shown in Figure 3.26 A. The tissue of origin and age are specified when available.

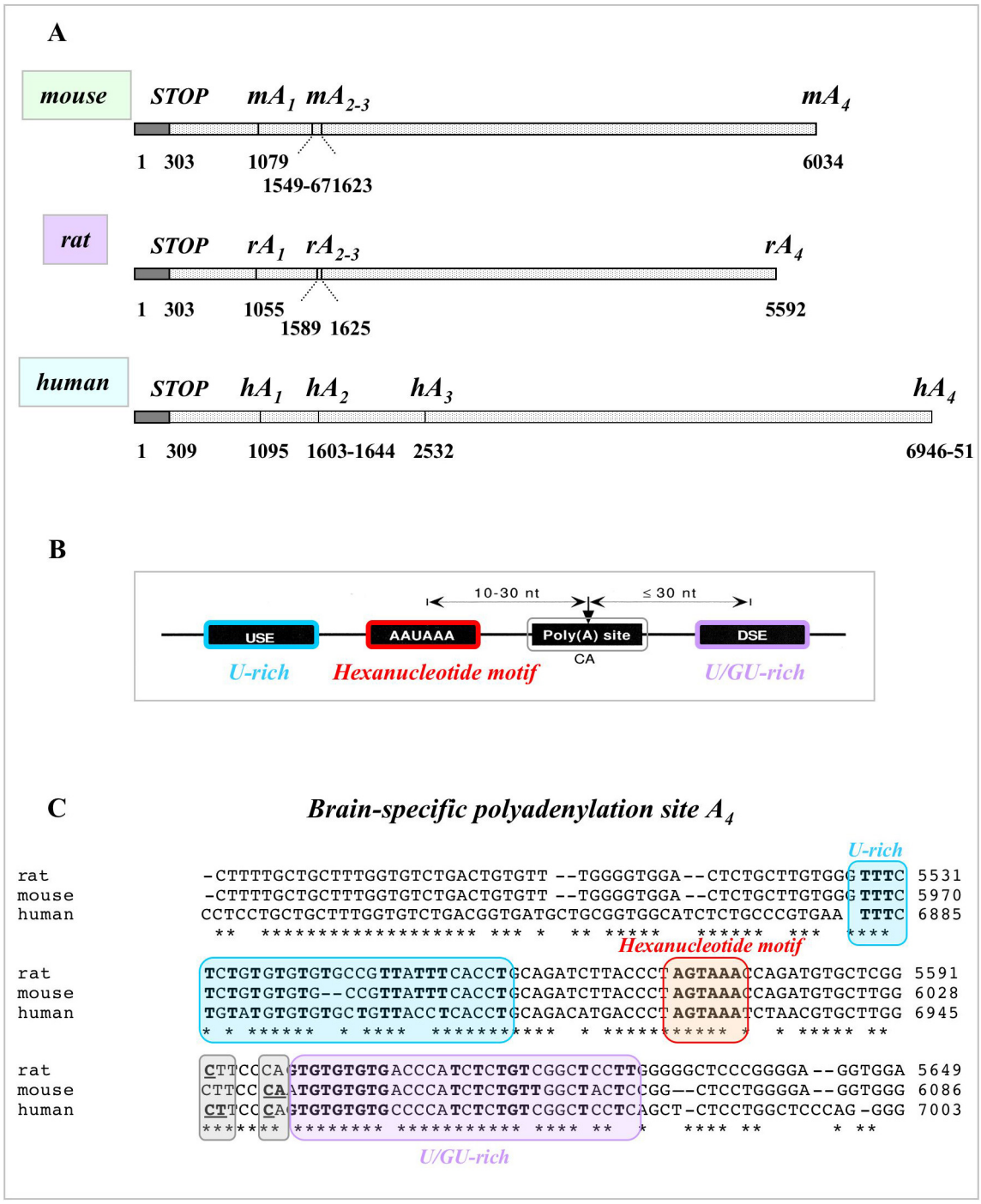

Figure 3.26: β-adducin brain-specific alternative polyadenylation sites. A schematic representation of the last exon of the β-adducin gene is shown in Panel A. The ORF (gray box), the stop codon and the positions of the different polyadenylation sites (A_1, $A_{2\text{-}3}$, and A_4), relative to the start of the last exon, are indicated. The 3'-UTR (5731, 5289 and 6642 bases for mice, rats and humans, respectively) are indicated as a light gray box. Panel B shows a scheme of the elements found in the polyadenylation region of genes: USE [upstream element (light blue)]; poly(A) site (gray), hexanucleotide motif (red) DSE [downstream element (violet)]. Panel C shows the sequence comparison among rats, mice and humans of the brain-specific polyadenylation regions. The AGTAAA motifs, the poly(A) sites, the U-rich and U/UG-rich elements are indicated. Numbers are relative to the first base of the last exon of each species.

A further analysis of the sequences lead to the identification of all elements required for polyadenylation in mammals in all three species (Zhao et al., 1999): the hexanucleotide motif, a putative poorly conserved U/GU-rich downstream elements

(DSE) downstream of the poly(A) site and a putative U-rich region (upstream element, USE) located upstream of the hexameric motif (Figure 26 B and C). The hexamer variant AGTAAA was found in the brain polyadenylation region in all three species instead of the more common and highly conserved AATAAA hexanucleotide motif. The detection in the sequences of the mentioned polyadenylation elements strongly confirmed the results showed above indicating that the brain β-adducin transcript is polyadenylated at the proposed site indicated as A_4.

3B.10 Identification of several proximal spleen polyadenylation sites in mice, rats and humans

Using the same bioinformatic approach described above for the identification of the A_4 brain-specific polyadenylation site, we were able to identify two proximal polyadenylation regions in rodents and three in humans that might generate the spleen β-adducin mRNA. A scheme of the last β-adducin exon showing the relative position of all the polyadenylation sites found in all three species is shown in Figure 3.26 A.

The first one was located between bases 1000 and 1150 relative to the start of the last exon (named mA_1, rA_1 and hA_1, for mice, rats and humans, respectively; Figure 3.26 A), generating a 3'-UTR of about 750–800 bases and showed a high conservation among the three species (Figures 3.26 A and 3.27 A).

The second region was between bases 1480–1640 and had more than one cleavage site (named $mA_{2\text{-}3}$, $rA_{2\text{-}3}$, and hA_2 for mice, rats and humans, respectively). The third polyadenylation site (hA_3) mapped at position 2532 of the last human exon and its functionality was supported by the presence of several ESTs containing a poly(A) tails (Figure 3.26 A and Table 3.8).

The human polyadenylation hA_2 region had two polyadenylation sites, one located at position 1603, and the other at position 1639-1644 of the start of the last exon (Figure 3.26 A and 3.27 B). The presence of both sites was supported also by the presence of numerous ESTs having poly(A) tails (Figure 3.24 A and Table 3.8). Although the putative human polyadenylation signal of hA_2 region was not conserved in rodents as they bear a deletion of that element, some ESTs with a variable position of the poly(A) tails were found in the $mA_{2\text{-}3}$ and $rA_{2\text{-}3}$ regions (Table 3.8) although no obvious consensus polyadenylation signals were identified in this rodent region (Figure 3.27 B, underlined region). The deposited cDNAs of human β-adducin, ending at the hA_2 region and the available ESTs data support these observations as only two ESTs

corresponding to the hA_1 region were detected that did not contain a poly(A) tails (Figure 3.27 B and Table 3.8, EST CN428094 and BQ716022). The presence of the proximal poly(A) site hA_3 mapping at position 2532 of the last exon is supported by the presence of numerous EST containing poly(A) tails (EST AI566854, AW451990, AW445023 and AA608592) (Table 3.8).

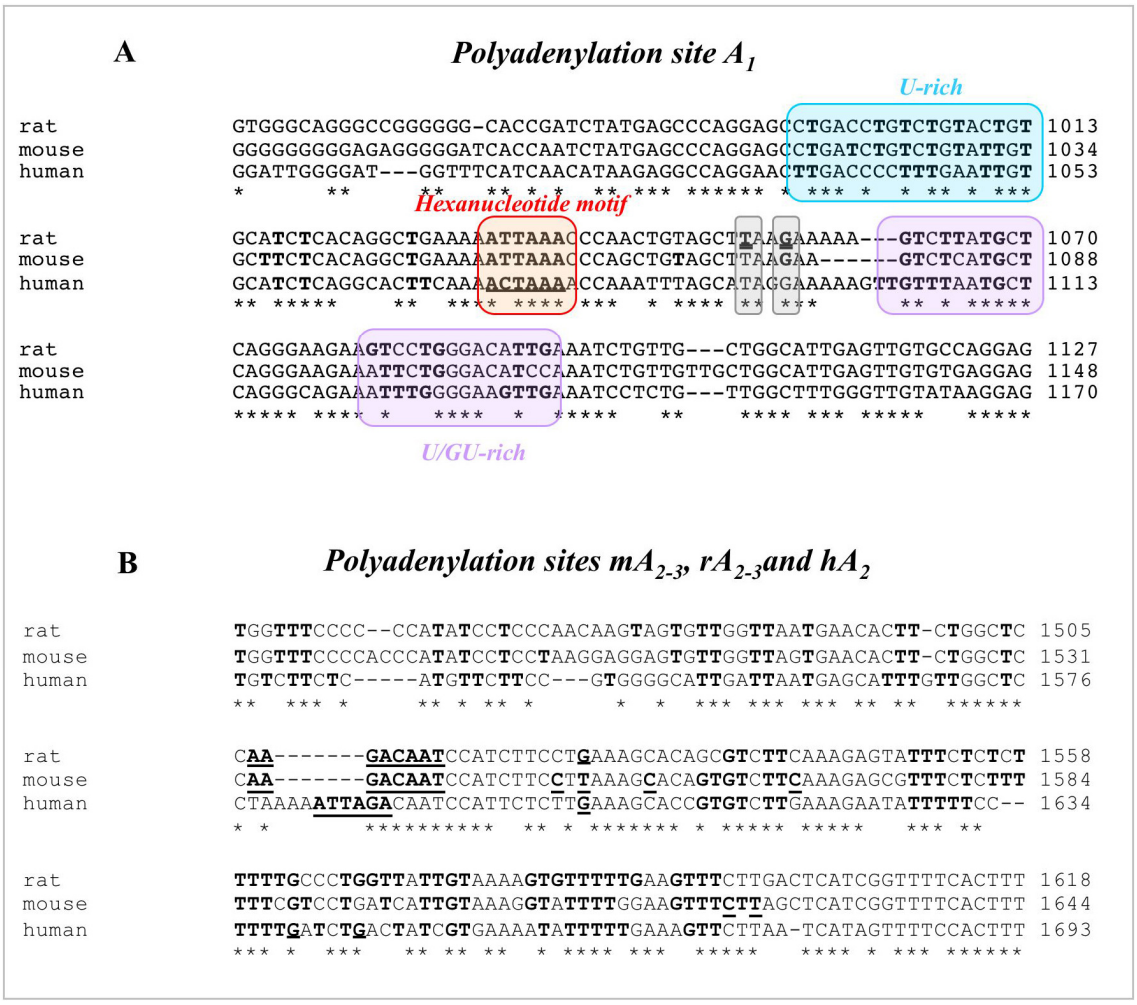

3.27: Sequence comparison of the spleen polyadenylation regions in rats, mice and humans. The A_1 polyadenylation region is shown in Panel A, while $mA_{1\text{-}3}$, $rA_{1\text{-}3}$ and hA_2 polyadenylation regions, are depicted in Panel B. The β-adducin genomic sequence corresponding to the polyadenylation region of the reported human exon 17 was compared to the homologous sequences in rats and mice. The rodent sequences have a deletion corresponding to the hexameric motif present in the human sequence (Panel B, underlined). The polyadenylation site is located approximately 15 bases downstream of the hexanucleotide element (boldface and double underlined). The hexanucleotide motif, U-rich and U/GU rich elements are shown in boldface and, in Panel A, they are also evidenced in red, blue and violet boxes, respectively.

In addition, we found full-length cDNAs and ESTs containing poly(A) tails at the polyadenylation regions $mA_{2\text{-}3}$, and rA_1 and $rA_{2\text{-}3}$ for mice and rats, respectively, located at 1000-1150 bp and 1480-1640 bp relative to the start of the last exon, but not for the mA_1 region. For example, the mRNA sequences BY564735 and AK014496 (both from a RIKEN full length cDNA library from spleen and liver embryo RNA) that

corresponded to the mA_1 region from mouse did not contain a poly(A) tail, while it was found in the rat sequences BI281934, CR467480 and BF420440 that corresponded to the rA_1 polyadenylation region (located at about 1055 bases downstream of the start of the last exon), in the mouse sequences BX637441, BQ176418, BU850901, AI414956, AW048717 and AI596349, and in the rat sequences AI044553 and CR469107 that corresponding to the second $mA_{2\text{-}3}$ and $rA_{2\text{-}3}$ polyadenylation regions (that are located at about 1600 bp of the start of the last exon).

Moreover, the sequences corresponding to the polyadenylation region of the human exon 17 and the homologues regions of rats and mice were compared. We observed a sequence homology of 88%, 63% and 62% for rat-mouse, rat-human and mouse-human, respectively (Figure 3.27 A).

The analysis of the sequences highlighted the presence in all three species of all expected polyadenylation elements in the site A_1 (Zhao et al., 1999) (Figure 3.27 A, hexanucleotide polyadenylation element, U-rich and U/GU-rich elements). The highly conserved hexanucleotide motif of A_1 was ATTAAA in rodents, while ACTAAA in human. On the contrary, a low homology with the canonical polyadenylation elements was observed aligning the $mA_{2\text{-}3}$, $rA_{2\text{-}3}$ and hA_2 containing regions. The highly variable position of the poly(A) tails in rodents for the second $mA_{2\text{-}3}$ and $rA_{2\text{-}3}$ polyadenylation regions could be related to these observed low grade of homology (Figure 3.27 B).

Additional supporting evidence of the presence of numerous proximal spleen-specific polyadenylation signals in the three species derived from the observation that more than one band was present in the 3.5–4.5 kb region in the Northern blot shown in Figure 3.16 B. In fact, we observed two bands in rat and mouse spleen samples that might correspond to the mRNA forms utilizing the A_1 and $A_{2\text{-}3}$ polyadenylation sites. In the human brain, we saw three bands that might be the results of the use of the hA_1, hA_2 and hA_3 poly(A) sites (Figures 3.16 B and 3.26 A). In the bone marrow sample we mainly detected the higher molecular weight band, which might correspond to the use of the hA_3 polyadenylation site. Moreover, the human bands were of higher molecular weight than the rodent ones, which is on line with the expected position of the different polyadenylation sites and, in consequence, the length of the human transcripts (Figures 3.16 B and 3.26 A). Alternatively, these bands might be the consequence of alternative splicing events of the β-Add97 and β-Add63 families of transcripts. However, this possibility is less probable as the Add63 levels were much lower than those detected for the Add97 family of transcripts (Figure 3.25 A and B) and we have observed no other

major bands in the RNase protection experiment of the complete β-adducin ORF that might have been produced by alternative splicing. Northern blot experiments using specific probes able to recognise the β-adducin mRNA forms generated by the use of the different proximal polyadenylation sites will allow us to confirm the hypothesised association between the band present in the 3.5–4.5 kb region of previous analyses (Figure 3.16 B) and the use of the proximal spleen-specific polyadenylation signals.

To conclude, all these experimental and *in silico* data confirmed the presence of several spleen-specific polyadenylation signals in mice, rats and humans.

3B.11 *In vivo* alternative polyadenylation analysis of β-adducin pre-mRNA

The described bioinformatic approaches, RT-PCR and Northern blot analyses revealed that the architecture of the β-adducin gene is extremely complex with alternative use of tissue-specific promoters and polyadenylation sites. We clearly evidenced that the pre-mRNA of the β subunit is processed at many alternative polyadenylation sites: the proximal ones are mainly used in erythroid tissues, while the distal site is used exclusively in brain.

The presence of alternative polyadenylation has been identified in several genes (Edwalds-Gilbert et al., 1997; Tian et al., 2005; Yan and Marr, 2005), however the molecular mechanisms that determine the use of a particular polyadenylation site among several ones are not well understood.

In order to understand the regulatory mechanisms involved in the brain- and spleen-specific polyadenylation of the β-adducin mRNAs, we set up an *in vivo* polyadenylation assay. We created two chimeric minigene constructs containing the complete human α-globin gene with its last part of the 3rd and last exon replaced by the mouse β-adducin 3'-UTR sequences containing the spleen and brain polyadenylation signals sequences, with their respective flanking regions. The chimeric constructs were under the control of the SV40 promoter (Figure 3.28).

As Figure 3.28 B shows, the pBS SP-BR pA construct comprises a part of the mouse β-adducin 16th exon including both the spleen-specific mA_1 and the brain-specific mA_4 polyadenylation signals. The mA_1 polyadenylation site is followed by about 350 bp of the downstream flanking region (Figure 3.28 A and B). A 1200 bp fragment of the distal 3'-UTR regions containing the mA_4 polyadenylation site was inserted downstream (Figure 3.28 A and B).

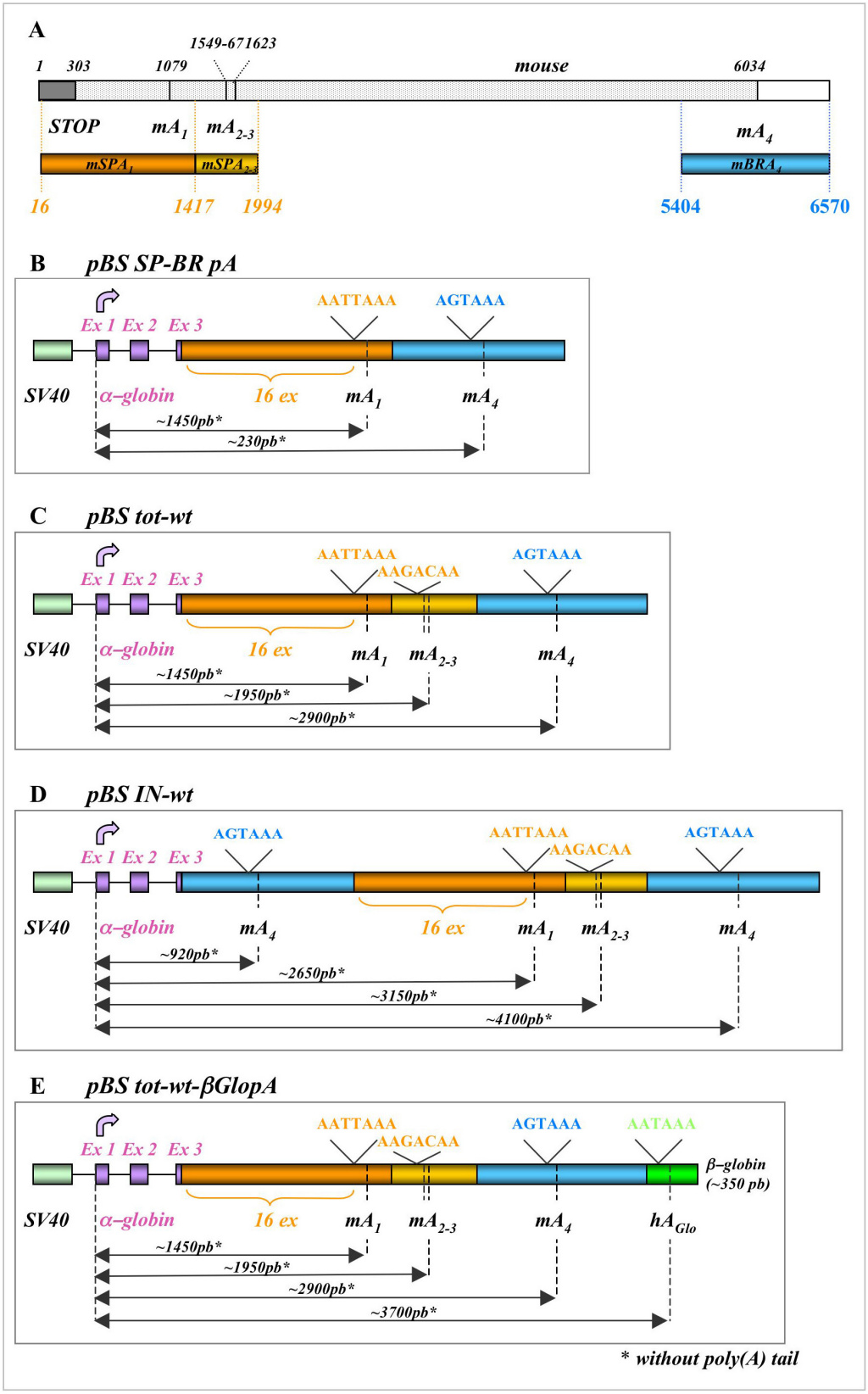

Figure 3.28: Schematic representation of the chimeric minigene constructs. In Panel A the different 3'-UTR fragments containing the tissue-specific polyadenylation sites of mouse β-adducin ($mSPA_1$, $mSPA_{2-3}$ and $mSBR_4$) used for creating the β-adducin chimeric minigenes are indicated as orange, yellow and blue boxes, respectively. Fragments $mSPA_1$, $mSPA_{2-3}$ and $mSBR_4$ span from bases 16 to 1417, from 1417 to 1994 and from 5404 to 6570, respectively, relative to the first base of the mouse β-adducin exon 16th. Schemes of the *pBS SP-BR pA*, *pBS tot-wt*, *pBS IN-wt* and *pBS tot-wt-βGlopA* constructs are shown in Panels B, C, D and E, respectively. The length of the expected transcripts is indicated.

The pBS tot-wt minigene, which mimics the structure and the arrangement of the polyadenylation sites in the β-adducin transcript, comprises the proximal spleen polyadenylation sites (mA_1 and mA_{2-3} plus 450 bp of the downstream sequence) followed by the distal 3'-UTR region containing the mA_4 signal (Figure 3.28 A and C). The SV40 promoter drives transcription of the minigenes, which should initiate at the 1st α-globin exon. Polyadenylation and transcription termination of the transcript should occur at one of the polyadenylation signals inserted, generating transcripts of different lengths depending on the site selected.

These constructs were first tested by Northern blot analysis of total RNA prepared from transiently transfected HeLa cells. A probe complementary to the common region of the mouse 16th exon (*mβ-Add 16 ex Probe*, Figure 3.29 A) detected a clear signal in each analysed RNA preparation (Figure 3.29 B, Lanes 2 and 3, *Band A* and *B*). This probe was able to identify all the mRNA forms generated by the use of the different polyadenylation sites located in the minigenes. The size of the observed bands (about 3.2 kb for *Band A* and 2.6 kb for *Band B*, Figure 3.29 B Lanes 2 and 3) matched with the expected dimension of that generated by the use of mA_4 brain-specific polyadenylation site (Figures 3.29 D, 3.28 B and C). To confirm the use of the brain-specific site we hybridised a similar membrane with a probe that can recognise only the transcripts using the mA_4 site (*mBR-A_4 Probe*, Figure 3.29 A). As can be seen in Figure 3.29 C (Lanes 6 and 7), signals of the same size of *Bands A* and *B* were obtained using the *mBR-A_4 Probe* suggesting that the main products used the mA_4 site. As a positive control we used total mRNA of mouse brain and we detected the expected 8-9 kb band (Figure 3.29 C, Lanes 8), confirming the specificity of the hybridisation.

To investigate whether the use of the brain distal polyadenylation signal in the 3'-UTR sequence could be influenced by its position, in a "first come, first served" basis, we decided to modify the natural order of the tissue-specific β-adducin polyadenylation sites in the constructs. So, we created a construct where the distal mA_4 region was placed before the proximal mA_{1-3} region used in erythroid tissues. This construct, called pBS IN-wt (Figure 3.28 D), was transfected into HeLa cells and the transcribed RNA was analysed by Northern blot. However, we were not able to detect any signal with either the *mβ-add 16 ex Probe* or the *mBR-A_4 Probe* (Figure 3.30 A and B, Lane 6 and Figure 3.31 A, Lanes 6 and 8). To discard eventual problems in the DNA preparation and on transcription, we repeated the experiment with a new pBS IN-wt DNA preparation, and we increased 10 time the amount of loaded sample, but no bands

were detected in the subsequent Northern blot experiments. These negative data suggest that the context in which the polyadenylation signal is introduced might strongly influence its strength and use.

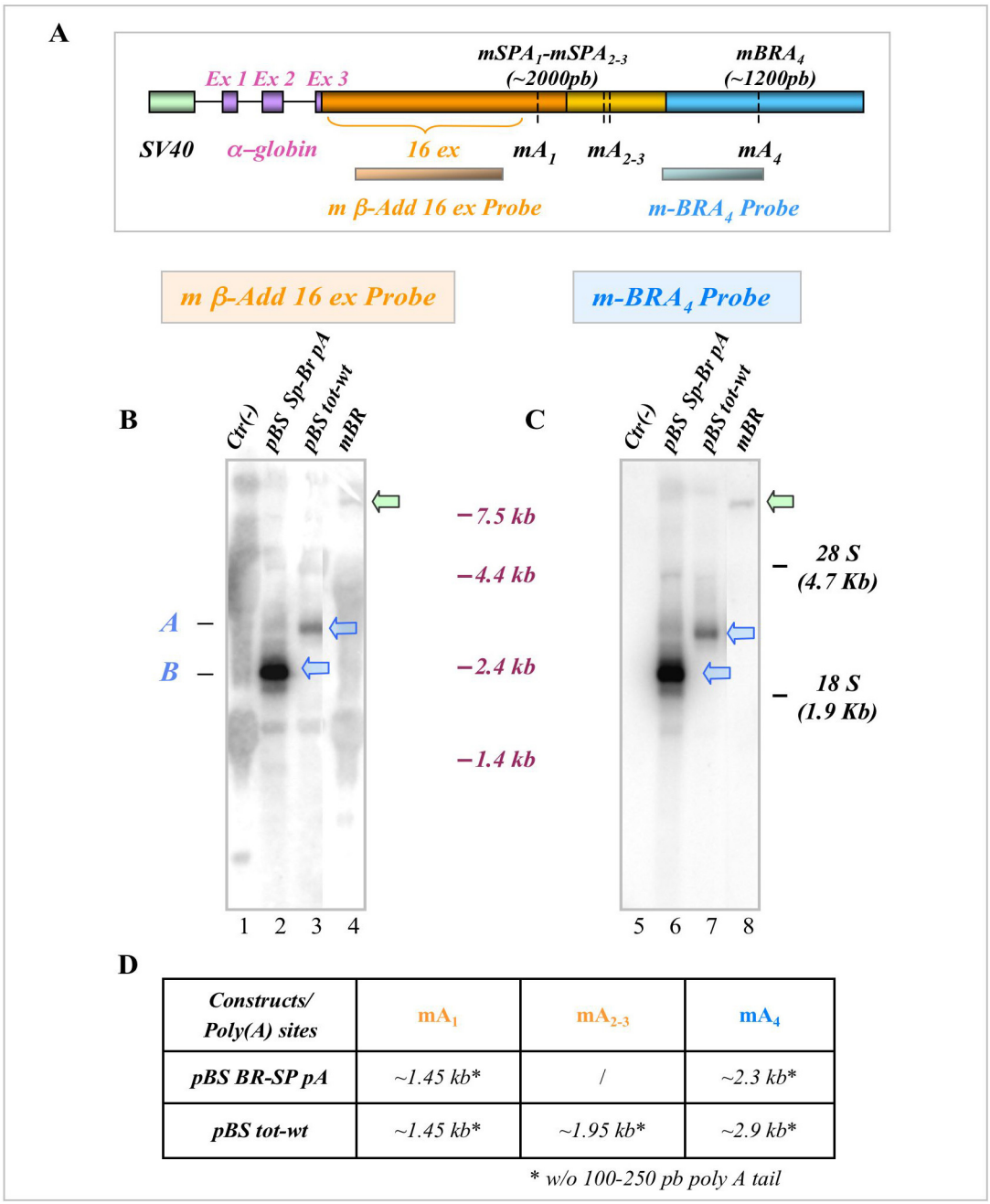

Figure 3.29: Alternative polyadenylation analysis of chimeric β-adducin mRNA in transfected HeLa cells. Panel A shows a scheme of the *pBS tot-wt* construct indicating the *m β-Add 16 ex* and the *m BRA$_4$ Probes* used in the experiments of Panels B and C, respectively. Northern blot analysis of total RNA from HeLa cells and brain of mouse are showed in Panels B and C. Total RNA (1.5 µg) prepared from HeLa cells previously transfected with *pBS SP-BR pA* (Lanes 2 and 6) and *pBS tot-w* (Lanes 3 and 7) were run in a agarose formaldehyde gel (1.5%), transferred to membrane and hybridised with the *m β-Add 16 ex Probe* and the *m BRA$_4$ Probe* (Lines 1–4 and 5–8, respectively). Lanes 1 and 5 (1.5 µg), and 4 and 8 (15 µg) contained untreated HeLa cells and mouse brain RNAs, respectively. Blue arrows and letters "A" and "B" indicate the detected bands in Lanes 3 and 2 of Panels B and C, respectively. Green arrows indicate the brain 8-9 kb β-adducin transcript in both Panels A and B. The 28S and 18S rRNAs and RNA markers are indicated in each Panel. The expected length of the transcripts is indicated in the table of Panel D.

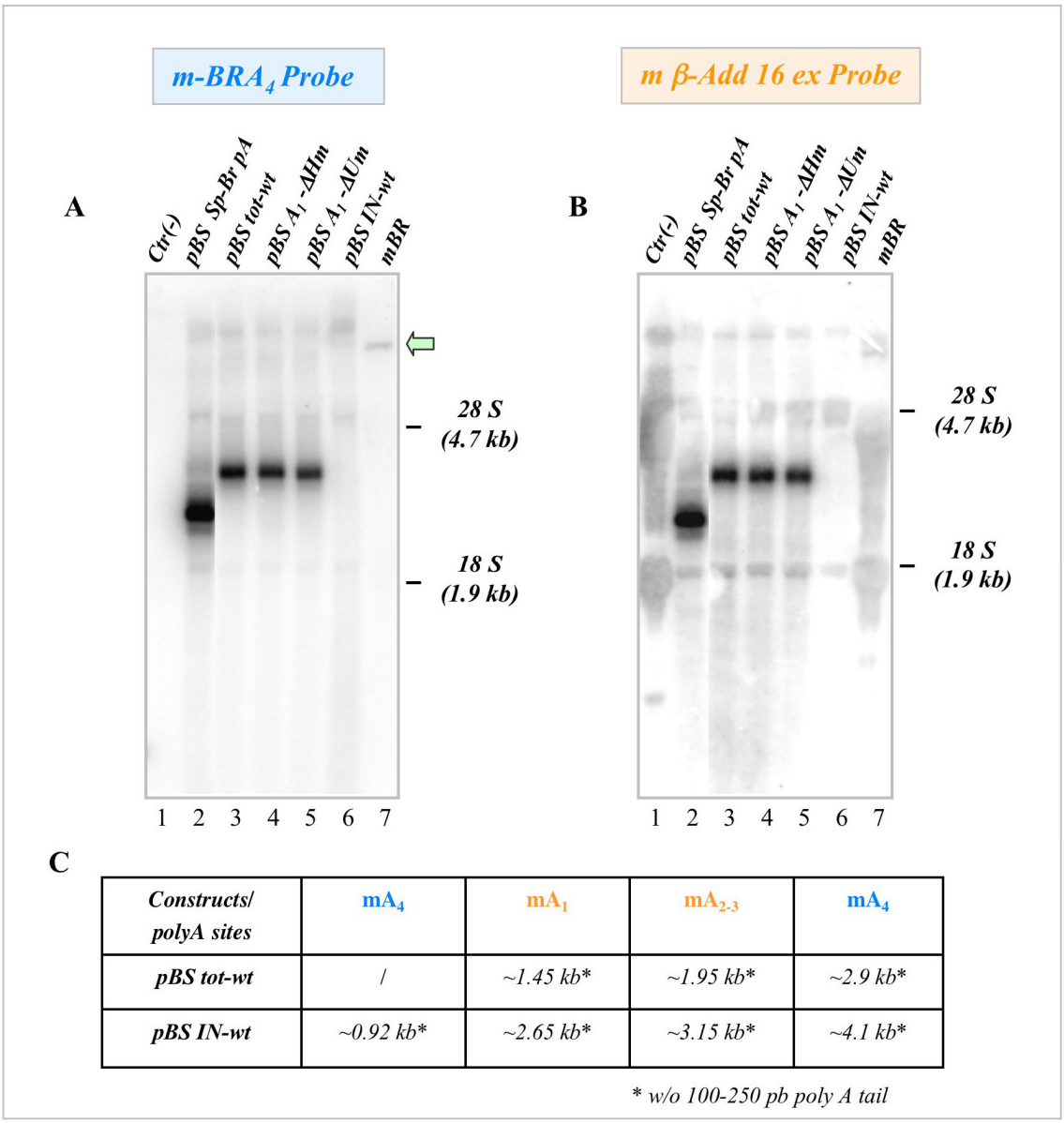

C

Constructs/ polyA sites	mA_4	mA_1	mA_{2-3}	mA_4
pBS tot-wt	/	*~1.45 kb**	*~1.95 kb**	*~2.9 kb**
pBS IN-wt	*~0.92 kb**	*~2.65 kb**	*~3.15 kb**	*~4.1 kb**

** w/o 100-250 pb poly A tail*

Figure 3.30: Deletion of the mA_1 hexanucleotide motif does not affect the polyadenylation efficiency at the brain-specific mA_4 poly(A) site. Northern blot analysis of total RNA from HeLa cells and brain of mouse are showed in Panels A and B, respectively. RNA prepared from HeLa cells previously transfected with *pBS SP-BR pA, pBS tot-wt, pBS A1-ΔHm, pBS A1-ΔUm, pBS IN-wt* and were loaded in Lanes 2-6 (1.5 µg) of Panels B and C, respectively. In Lanes 1 (1.5 µg) and 7 (15 µg) untreated HeLa cells and mouse brain RNAs were loaded. All RNAs were run in an agarose formaldehyde gel (1.5%), transferred to Hybond-N^+ membrane and hybridised with the *m β-Add 16 ex Probe* and the *m BRA_4 Probe* (Panels A and B, respectively). A green arrow indicates the brain 8-9 kb β-adducin transcript. The 28S and 18S rRNAs are indicated on the right of each panel. The expected length of the transcripts is indicated in the table of Panel C.

To investigate whether the use of the brain distal polyadenylation signal in the 3'-UTR sequence could be influenced by its position, in a "first come, first served" basis, we decided to modify the natural order of the tissue-specific β-adducin polyadenylation sites in the constructs. So, we created a construct where the distal mA_4 region was placed before the proximal mA_{1-3} regions used in erythroid tissues. This construct, called pBS IN-wt (Figure 3.28 D), was transfected into HeLa cells and the

transcribed RNA was analysed by Northern blot. However, we were not able to detect any signal with either the *mβ-add 16 ex Probe* or the *mBR-A$_4$ Probe* (Figure 3.30 A and B, Lane 6). To discard eventual problems in the DNA preparation and on transcription, we repeated the experiment with a new pBS IN-wt DNA preparation, and we increased 10 time the amount of loaded sample, but no bands were detected in the subsequent Northern blot experiments (data not shown).

These negative data suggest that the context in which the polyadenylation signal is introduced might strongly influence its strength and use.

3B.12 A cryptic polyadenylation site is activated by the deletion of the β-adducin hexanucleotide motif of the distal mA$_4$ site

Several *in vivo* and *in vitro* studies evidenced that mutation or deletion of the elements that define the polyadenylation signal reduced the efficiency or abolished the polyadenylation event (Hall-Pogar et al., 2005; Sadofsky and Alwine, 1984; Sheets et al., 1990; Wilusz et al., 1989).

To identify the contribution of the core elements that define the different β-adducin-specific polyadenylation sites to the 3'-end processing events, we created minigene constructs having single deletions in these putative elements (Figure 3.26 B).

Mutants of pBS tot-wt were prepared by PCR-based site-directed mutagenesis. These constructs were then transfected into HeLa cells and analysed as described above. Initially, we tested the effects on polyadenylation of the deletion of the hexanucleotide motif ATTAAA (pBS A$_1$-ΔHm) and the U-Rich motif (pBS A$_1$-ΔUm) of the mA$_1$ site (Figure 3.27 A). Both probes, *mβ-Add 16 ex Probe* and *mBR-A$_4$ Probe* (Figure 3.30 A and B, respectively), detected in both mutants a transcript having a similar size of that of the control (pBS tot-wt) (Figure 3.30 A and B, Lanes 4and 5 versus 3). This result was in line with previous data obtained transfecting constructs without deletions. In fact, when the polyadenylation machinery selected the brain-specific mA$_4$ polyadenylation site, deletions of the elements of the proximal mA$_1$ signal did not affect the processing at the mA$_4$ site and the same mRNA products were detected in the cells transfected with both wt and mutant constructs by Northern blot analysis.

We also prepared deletion mutants of the polyadenylation elements of the brain-specific mA$_4$ site: the hexanucleotide motif AGTAAA mutant (pBS A$_4$-ΔHm) and the U-Rich motif deletion one (pBS A$_4$-ΔUm) (Figure 3.26 C). Considering that the removal of the mentioned mA$_4$ sequences may produce the skipping of polyadenylation

at the mA_4 site, causing the degradation of the unprocessed mRNA, we introduced an extra polyadenylation signal downstream the mA_4 site to allow the formation of the mature transcript.

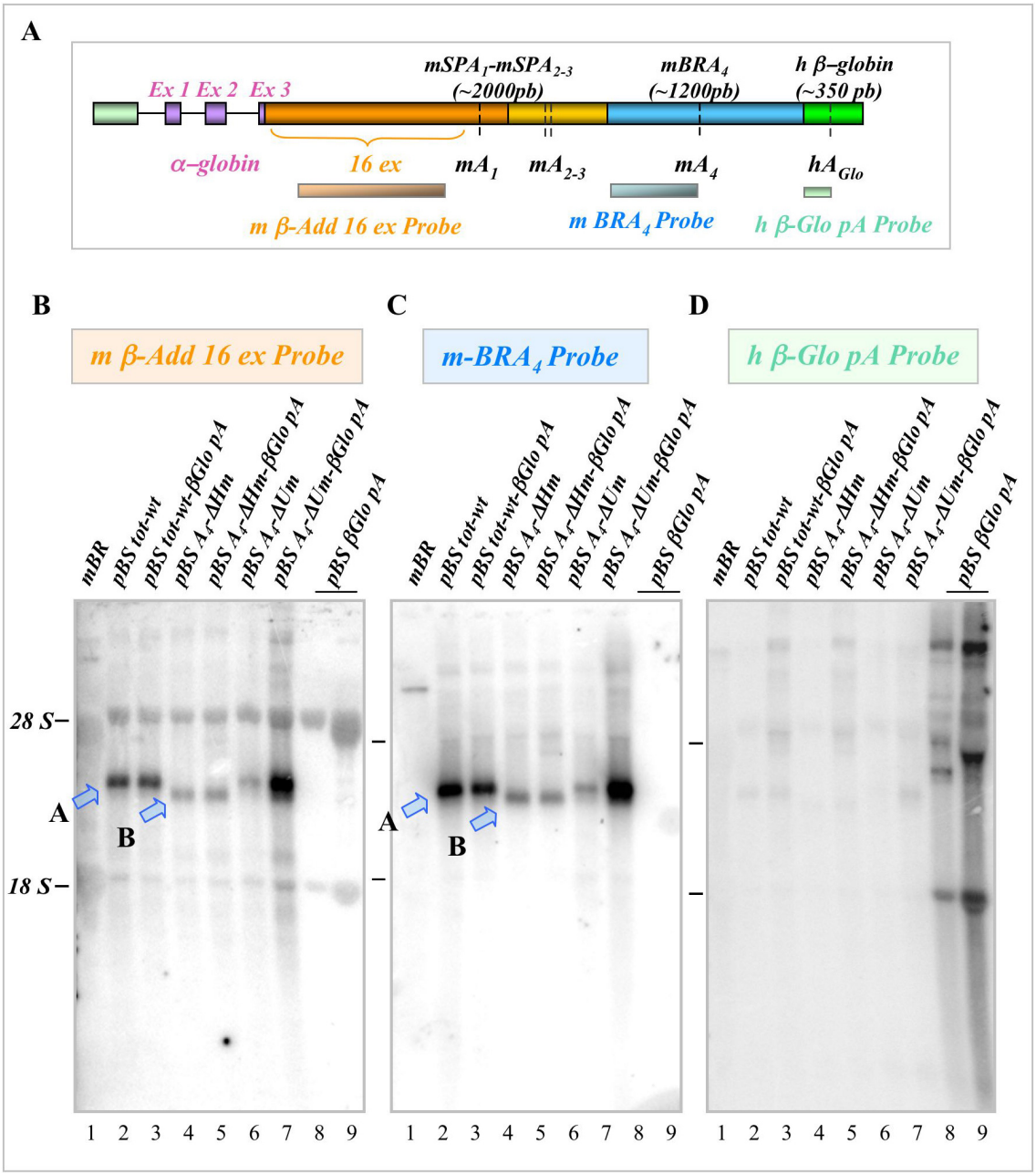

Figure 3.31: Effect of the deletion of the polyadenylation mA_4 elements on the 3'-end processing of chimeric β-adducin transcripts in HeLa cells. Panel A shows a scheme of the *pBS tot-wt-βGlo pA* construct indicating the *m β-Add 16 ex Probe*, *m BRA4 Probe* and *h βGlo pA Probe* used in the Northern blot experiments of Panels B, C and D, respectively. RNA prepared from HeLa cells previously transfected with *pBS tot-wt, pBS tot-wt-βGlo pA, pBS A4-ΔHm, BS A4-ΔHm-βGlo pA, pBS A4-ΔUm, pBS A4-ΔUm-βGlo pA* and *pBS βGlo pA* were loaded in Lines 2-9 (1.5 µg in all lines except for Lanes 9 of Panels B and D where 5 µg of samples were loaded) of Panels B, C and D, respectively. In Lanes 1 (15 µg) mouse brain RNAs were loaded. All RNAs were run in an agarose formaldehyde gel (1.5%), transferred to Hybond-N^+ membrane and hybridised with the *m β-Add 16 ex Probe*, *m BRA4 Probe* and *h βGlo pA Probe* (Panels A, B and C, respectively). On the left of each panel the 28S and 18S rRNAs are indicated. Blue arrows and letters "A" and "B" indicate the bands detected in Lines 2, 3 and 3, 5 of Panels B and C, respectively.

The extra polyadenylation site introduced was the strong and widely used in *in vitro* analyses one of the human β-globin poly(A) (Castelo-Branco et al., 2004). This site was cloned downstream the brain-specific 3'-UTR region of β-adducin in all the constructs mentioned above (Figure 3.28 E) (pBS tot-wt-βGlopA, pBS A_4-ΔHm-βGlopA and pBS A_4-ΔUm-βGlopA-).

When we analysed the effects of the U-Rich motif deletion in the mA_4 site we observed that the absence of this regulatory region seemed not to affect the use of mA_4 polyadenylation signal but alter the efficiency of polyadenylation. In fact, cells transfected with both mutant and control constructs produced different amounts of transcripts having the same size (Figure 3.31 B and C, Lanes 6 and 7 versus 2 and 3). Using a β-Globin-specific probe (*h β-GlopA Probe*, Figure 3.31 A) we were not able to detect any band (Figure 3.31 D, Lanes 3, 5, 7-9) suggesting that all the pre-mRNAs were processed at the mA_4 site. Unfortunately, the chimeric minigene containing the β-globin poly(A) region (pBS βGlopA) that was used as positive control did not produce any clear signal (Figure 3.31 D, Lines 8 and 9). These experiments will be repeated using the complete β-globin gene followed by its own poly(A) site in the pBS vector as positive control. However, these preliminary data indicate that the major effect of the presence of the extra β-globin site was to increase the efficiency of the polyadenylation event at the brain-specific mA_4 in the absence of the U-rich sequence.

When the cells were transfected with a minigene lacking the mA_4 hexanucleotide motif, we detected with the *mBR-A_4 Probe* (Figure 3.31 A) a weak band of slightly lower molecular weight than that observed in the pBS tot-wt control transfection, independently of the presence of the extra β-globin polyadenylation signal (Figure 3.31 B and C, *Band B* in Lanes 4 and 5 versus *Band A* in Lanes 2 and 3). To verify whether other polyadenylation signals were used (mA_1 or mA_{2-3} and hβ-GlopA), the same samples were tested with *mβ-add 16 ex Probe* and *mβ-GlopA Probe*. When the hybridisation was performed, no additional bands of lower size were evidenced with the *mβ-add 16 ex Probe* (Figure 3.31 A) indicating that the transcripts generated from these mutants were not polyadenylated at any of the spleen-specific sites (Figure 3.31 B Lanes 4 and 5). When *mβ-GlopA Probe* was used (Figure 3.31 A), no signal was detected (Figure 3.31 D, Lanes 4 and 5) suggesting that the β-globin polyadenylation site was not used. As we mentioned above, considering that the positive control construct for the β-globin-specific probe did not produce any signal (Figure 3.31 D,

Lanes 8 and 9), these experiments will be repeated using a new minigene as the positive control.

In conclusion, all these data suggest that the absence of the highly conserved brain hexanucleotide motifs did not induce the switch to any of the proximal polyadenylation sites located upstream but provoked a less efficient formation of a polyadenylated mRNA slightly shorter than that obtained by the use of the unaltered mA_4 site (Figure 3.31 B and C, Line 4 and 5), probably by the activation of a cryptic nearby polyadenylation site.

A detailed bioinformatic analysis showed no obvious alternative polyadenylation sites close to the mA_4 one that might explain the presence of a shorter mRNA product generated from the pBS A4-ΔHm construct.

Therefore, to define the cleavage site of the mRNA of *Band B* (Figure 3.31 B and C Lines 4 and 5) and, consequently, to identify the new cryptic alternative polyadenylation site we performed 3'-RACE-PCR. HeLa cells were transfected with the pBS A_4-ΔHm and the pBS tot-wt constructs, comprising or not the β-globin polyadenyaltion site, and total RNA was purified. Mouse brain total RNA was used as positive control. After the cDNA synthesis, a first PCR was performed using as forward primer an oligonucleotide that anneals at about 600 bases upstream the mA_4 site and as a reverse primer an oligo(dT) that 3' terminates in A, C or G linked to a specific 5′-extension sequence of ~20 bases (anchor) (Figure 3.32 A, primers "a"). In a second PCR the first PCR product was amplified with a reverse primer which anneals in the anchor and a forward primer located downstream of that used in the first reaction to give further specificity to the reaction (semi-nested PCR) (Figure 3.32 A, primers "b").

As Figure 3.32 B shows, bands of similar size to the expected length were obtained from both wt minigenes (Lanes 1 and 2; *Band A*) and mouse brain (Lane 5; *Band D*). On the contrary, two smaller bands were observed using mA_4 hexanucleotide mutant samples (Figure 3.32 B, Lanes 3 and 4, *Bands B* and *C*, respectively). It was interesting to notice that these PCR reactions produced a pattern similar to that observed in the Northern blot analysis for the same samples (Figure 3.32, Lanes 1, 2, 3 and 4 vs. Figure 3.31 B and C, Lane 2, 3, 4 and 5).

All 3'-RACE-PCR bands (*Bands A*, *B*, *C*, and *D* of Figure 3.32 B) were purified and sequenced. By this analysis, we demonstrated that the brain β-adducin is polyadenylated at the canonical poly(A) site confirming the previous results derived from analysis of ESTs (Table 3.8 and Figure 3.22 B).

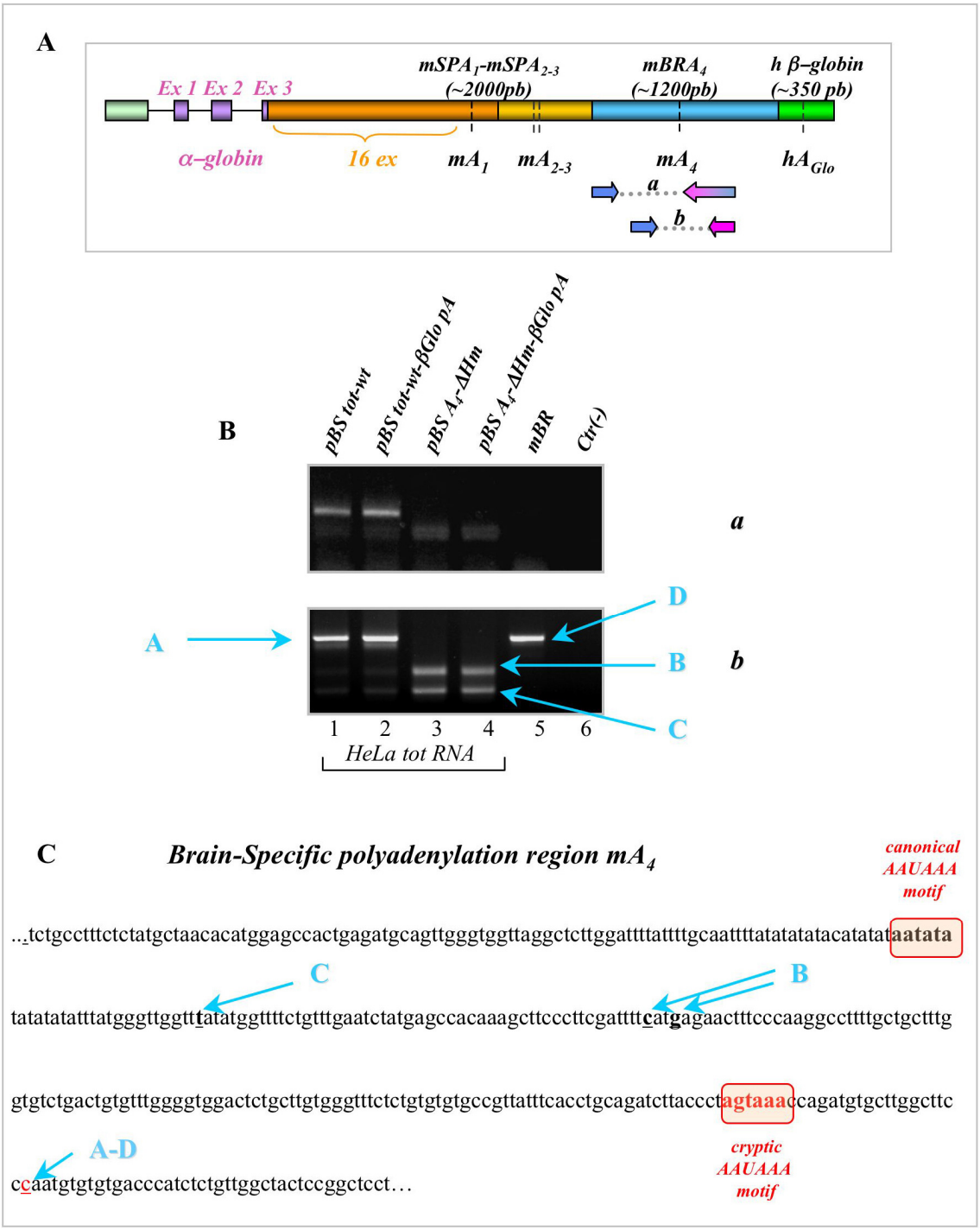

Figure 3.32: Deletion of the hexanucleotide motif of the canonical mA$_4$ site in chimeric β-adducin minigenes induces the use of a cryptic polyadenylation site in HeLa cells. Panel A shows a schematic representation of the *pBS tot-wt-βGlo pA* construct indicating the positions of the oligonucleotides used in the 3'-RACE-PCR reactions of Panel B. Panel B shows the semiquantitative RT-PCR and semi-nested-PCR results obtained amplifying with primer pairs "a" and "b", respectively, the total RNA prepared from mouse brain (Lane 5) and from HeLa cells previously transfected with *pBS tot-wt, pBS tot-wt-βGlo pA, pBS A$_4$-ΔHm* and *pBS A$_4$-ΔHm-βGlo pA* (Lanes 1-4). In Lane 6 the total RNA was omitted (-Ctr-). Blue arrows and letters from "A" to "C" indicate the bands detected from the semi-nested-PCR (primer pair "b") of Panel B. The sequences corresponding to the brain-specific polyadenylation region of β-adducin is reported in Panel C. The canonical and the cryptic polyadenylation sites detected by the sequencing of the Bands "A", "B", "C" and "D" of the 3'-RACE-PCR (Panel B, primer pair "b") are indicated by blue arrows. Red boxes show the hexameric motifs of the canonical and cryptic mA$_4$ sites.

In addition, the transcripts from the wt minigenes were also polyadenylated at the natural mA_4, demonstrating that the minigene constructs precisely reproduce the endogenous β–adducin gene. As expected, the mRNA generated by the constructs having a deletion in the mA_4 hexanucleotide motif was polyadenylated in different sites localised upstream to the canonical brain-specific site (Figures 3.32 C and 3.33). The two cleavage sites of *Band B* and the unique one of the *Band C* are indicated in Figure 3.32 C and 3.33.

Sequence analysis of the mouse region upstream of the mA_4 hexanucleotide element showed a putative alternative AATATA motif, localised ~20 nucleotides upstream the cleavage site of *Band C*. Moreover, U-rich and U/GU-rich sequences flanked the cryptic polyadenylation site.

Sequence comparison of the 3'-UTR regions located upstream the canonical brain polyadenylation signal among several vertebrates (humans, mice, rats, chimps, dogs and cows) showed that the homology between the species was very high not only in the motifs defining the canonical brain polyadenylation site but also in the upstream region where it is located the cryptic one (Figure 3.33). The observed alternative AATATA motif was highly conserved with the exception of humans and dogs. Similarly, the bases that defined the cleavage sites detected for the *Band B* and *C*, respectively, and the putative USE and DSE were highly conserved among all the selected species.

Figure 3.34 shows the grade of conservation of the 5-6 kb β-adducin 3'-UTR among numerous vertebrates obtained at the UCSC Genome Browser (http://genome.ucsc.edu/). Interestingly, the genomic regions containing the different polyadenylation sites were highly conserved. The high degree of conservation strongly suggests that these regions of the 3'-UTR might comprise important *cis*-acting elements that could be recognised by tissue-specific binding proteins.

In conclusion, the data obtained by Northern blot and 3'-RACE PCR products sequencing indicated that a cryptic polyadenylation site, localised upstream of the mA_4, were used in the absence of the natural mA_4 hexanucleotide motif. The observed reduction in the levels of transcript processed at the cryptic site could be related to a lower efficiency of polyadenylation at the site due to its lower strength, and/or to the probable degradation of the unprocessed pre-mRNA. However, the cause of the decreased processing of the pre-mRNA and the absence of the use of the downstream β–globin polyadenylation site remain to be determined.

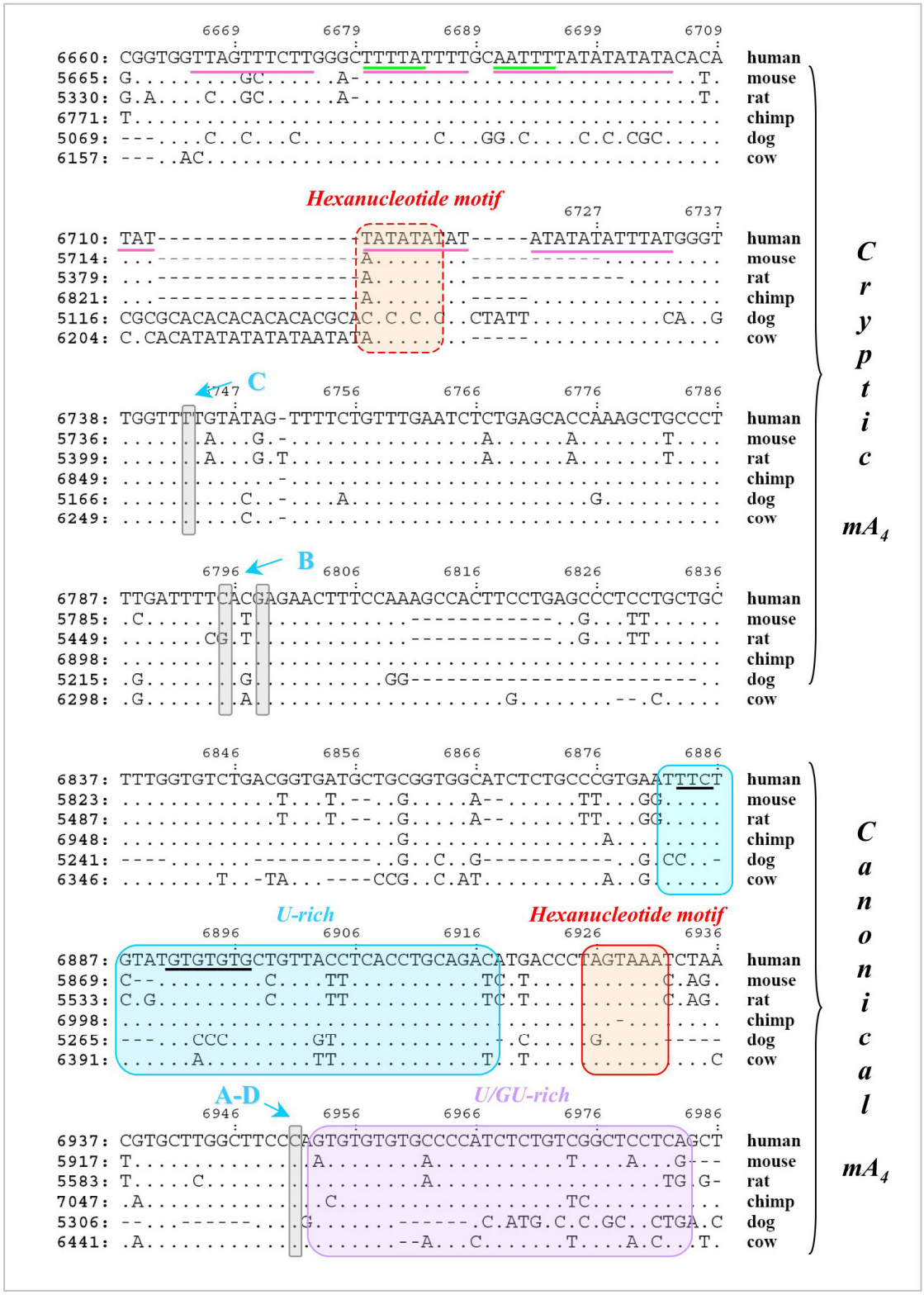

Figure 3.33: Canonical and cryptic β-adducin brain-specific polyadenylation sites. The figure shows the comparison among the genomic sequences of humans, mice, rats, chimps, dogs and cows in the brain-specific polyadenylation region. The hexanucleotide motifs of the canonical and cryptic A_4 polyadenylation sites are indicated in red boxes. Grey boxes show the cleavage sites: the cryptic A_4 identified by 3'-RACE (Figure 3.32 B) is indicated with letters "A" and "B", while the canonical one with "A"-"D". The U-rich and U/UG-rich elements are indicated by blue and violet boxes, respectively. AU-rich element, PTB binding sites and putative consensus sequences for CPEB are underlined in pink, black and green, respectively. Numbers are relative to the first base of the last exon of each species.

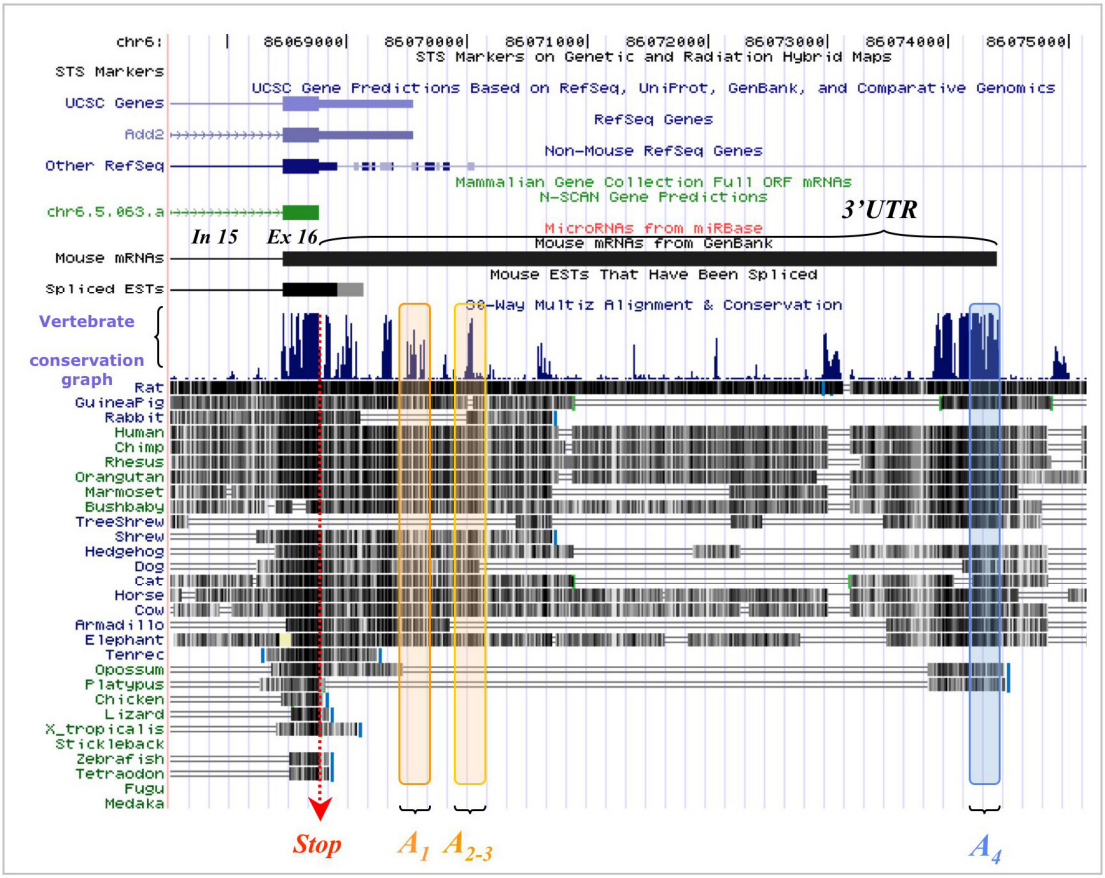

Figure 3.34: Conservation of the β-adducin 3'-UTR in vertebrates. The figure shows a schematic representation of the β-adducin genomic region corresponding to the last exon and the 5-6 kb 3'-UTR. The vertebrate species considered in the analysis are indicated. The height of the dark bleu bar in the centre of the figure indicates the grade of sequence conservation among the analysed vertebrates. All the data were obtained from the UCSC browser. The boxes indicate the genomic regions containing the spleen- and brain-specific polyadenylation signals.

The last two Sections (3B.11 and 3B.12) described a set of preliminary experiments to determine the mechanisms regulating tissue-specific polyadenylation of the β-adducin gene. Further experiments will be performed to explore more in detail the *cis*-acting sequences, protein factors and the molecular mechanisms involved in the tissue-specific regulation of β-adducin pre-mRNA 3'-end formation.

3B.13 β-adducin mRNA localisation in the brain of wt mice

As we mentioned in the Introduction (Section 1.14.2), several studies have shown that the 3'-UTR is involved in the subcellular localisation of the transcripts. The mRNA localisation has been studied exhaustively in neurons and many transcripts are localised in the axons and dendrites of these polarized cells (Gilligan et al., 1999; Rabenstein et al., 2005).

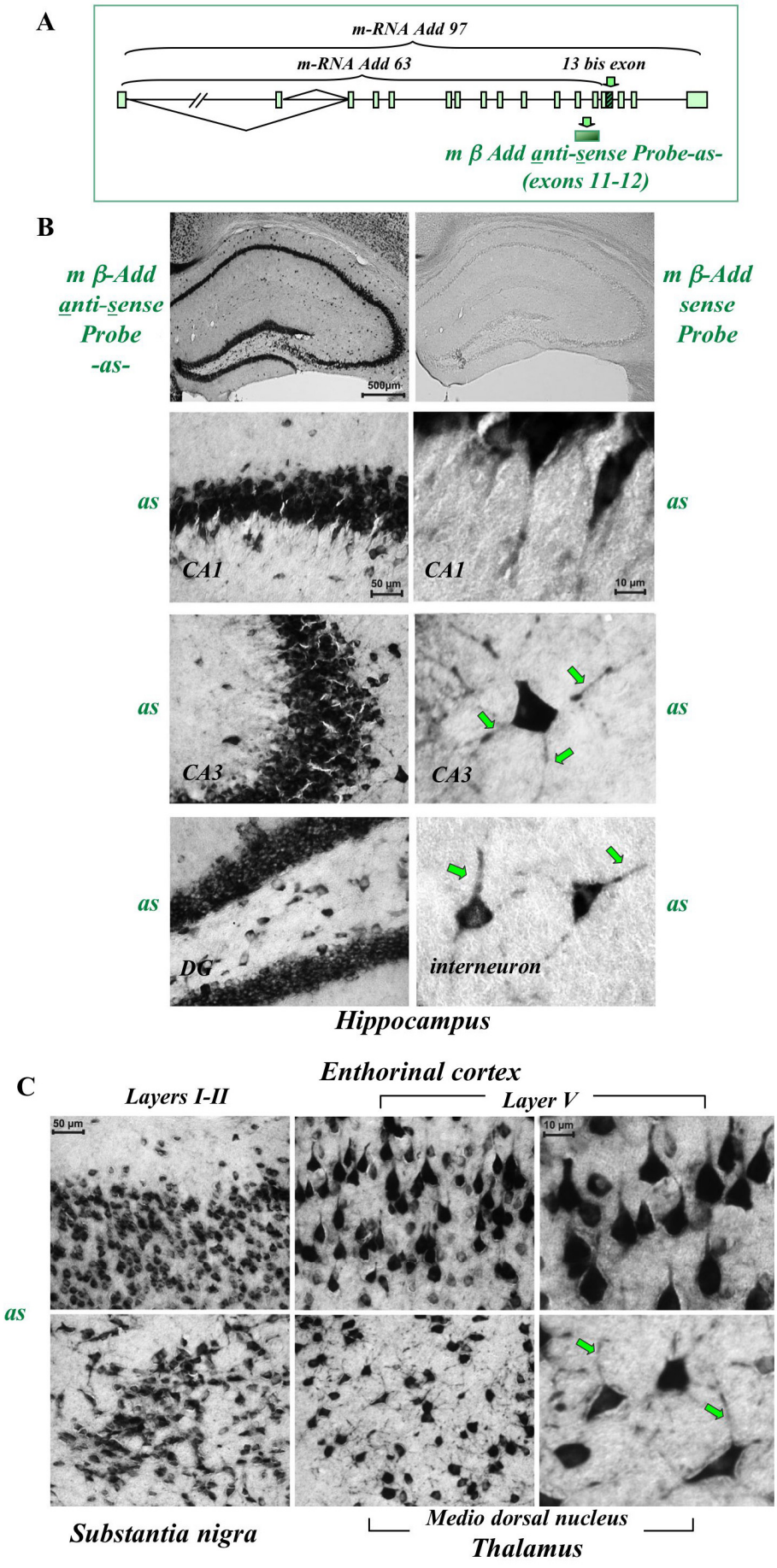
A
m-RNA Add 97
m-RNA Add 63
13 bis exon
m β Add anti-sense Probe-as-
(exons 11-12)
B
m β-Add anti-sense Probe -as-
m β-Add sense Probe
500µm
as
CA1
50 µm
CA1
10 µm
as
CA3
CA3
as
DG
interneuron
Hippocampus
C
Enthorinal cortex
Layers I-II
Layer V
50 µm
10 µm
as
Substantia nigra
Medio dorsal nucleus
Thalamus

In human brain, β-adducin expression is found to be highly enriched in hippocampus, corpus striatum, cerebral cortex and cerebellum and its expression levels correlate with cellular density (Gilligan et al., 1999; Rabenstein et al., 2005) (Section 1.7.6).

Taking into account that the brain β-adducin mRNA contains an extremely long 3'-UTR and the above mentioned evidences, we performed a more accurate analysis to determine its subcellular localisation in different structures of the brain. In collaboration with Dr. Tongiorgi's group (University of Trieste), we performed *in situ* hybridisation analysis of mouse brain tissue sections using an anti-sense probe for β-adducin (*β-Add anti-sense Probe -as-*, Figure 34 A). This probe was complementary to the mouse exons 11 and 12 and was able to hybridise with the two splicing families of β-adducin mRNA (Figure 3.35 A). As the main species detected in brain was the long form (8-9 kb mRNA), the β-adducin anti-sense probe detected the subcellular localisation of that peculiar 8-9 kb mRNA. As can be seen in Figure 3.35 B, the β-adducin transcript was found in the hippocampus, with high expression in *Cornu Ammonis* fields CA1-CA3 regions and dentate gyrus. The analyses also revealed a high expression of the transcript the in layer I-II and V of the entorhinal cortex, substantia nigra and medio dorsal nucleus of thalamus (Figure 3.35 C).

Interestingly, when we analysed higher magnifications of the images, we were able to observe that the β-adducin mRNA had a remarkable dendritic localisation. The arrows in Figure 3.35 B and C indicate the clear dendritic signal detected in all the neurons of the analysed brain portions.

Figure 3.35: β-adducin transcript subcellular localisation in neuronal tissues of mice. Panel A shows a scheme of the β-adducin gene indicating the positions of the probes used in the *in situ* hybridisation experiments of Panels B and C: the *m β-Add anti sense Probe* (*as*) and *m β-Add sense Probe* (exons 11-12). *In situ* hybridisation results obtained analysing regions of hippocampus (*Cornu Ammonis* fields CA1-CA3 regions and dentate gyrus) are shown in Panel B. *In situ* hybridisation analyses of layer I-II and V of the entorhinal cortex, substantia nigra and medio dorsal nucleus of thalamus sections are shown in Panel C. Dendritic localisation of β-adducin mRNA is indicated by green arrows in higher magnifications of Panels B and C.

4 DISCUSSION

Chapter A

The membrane skeleton organisation in cells of β-dducin deficient and β-adducin-dematin double mutant mice

4A.1 Cytoskeletal composition and structure in erythroid and non-erythroid cells of β-dducin KO mice

4A.1.1- The incorporation of ECapZ in RBC skeletons of mutant mice is a compensatory mechanism triggered by the absence of β-adducin -

SDS-PAGE and 2D gels, mass spectrometry and Western blot analyses revealed that the levels of several of the skeletal proteins in erythrocytes from β-adducin deficient mice were different from those found in control animals suggesting that both the actin filament-complex and actin polymerisation activity might be altered. One of the major changes was a ~9-fold upregulation of both subunits of the heterodimeric actin-capping protein ECapZ in cytoskeletal fractions of mutant RBCs (Figure 3.4 A and C). Moreover, the binding assay showed that purified α/β erythrocyte adducin was partially incorporated in adducin deficient ghosts in a dose-dependent manner, accompanied by a decrease in ECapZ-β levels (Figure 3.12).

As previously mentioned, CapZ is the main capping protein of the actin-filament darbed-ends in muscle, while ECapZ remains cytoplasmic in RBC and the capping function is performed by adducin (Fowler, 1996; Kuhlman and Fowler, 1997; Kuhlman et al., 1996). The fact that adducin is the erythrocyte actin capping protein despite its lower K_{cap} (20-100 fold) with respect to that of ECapZ is probably due to the fact that other proteins cooperate in the stabilisation of the binding of adducin to the actin-filaments darbed-ends *in vivo* (Kuhlman and Fowler, 1997), as already observed in the case of spectrin–actin complexes (Gardner and Bennett, 1987; Mische et al., 1987). In spite of this, we did not observe a complete displacement of ECapZ in mutant ghosts by exogenously added adducin, instead, increasing amounts of adducin produced a reproducible minor decrease in ECapZ levels in the ghost fraction (23% decrease in lane

4 of Figure 3.12). Obviously, these are *in vitro* experiments and may be far from what actually takes place during erythropoiesis, when the cytoskeleton takes its final structure and proteins are synthesised simultaneously and have to compete for a place in the skeleton structure.

However, the increased levels of both subunits of ECapZ in the cytoskeleton of mutant erythrocytes and the evidence that in an *in vitro* condition the ratio between adducin and ECapZ increases with the addition of higher amounts of adducin support the idea that the partial incorporation of ECapZ in RBC skeleton is a compensatory mechanism triggered by the absence of β-adducin.

Taking into account that under physiological conditions ECapZ is localised mainly in RBC cytoplasm while adducin stabilises the darbed end of the actin filament, we hypothesised that ECapZ is recruited from the cytoplasm to skeletal protofilaments in erythrocytes lacking β-adducin. The observation that similar levels of ECapZ α and β were present in the cytoplasmatic fractions of erythrocytes from β-adducin KO and normal mice suggested the absence of the hypothesised recruitment mechanism. However, considering that ECapZ is abundant in the cytoplasm which led us to load quantities of cytoplasm extracts approximately 25-fold lower than that used for the cytoskeleton, it is possible that a minimal decrease of ECapZ levels in the cytoplasm of mutant RBC might not be evident.

The mild haemolytic anaemia observed in KO animals (Gilligan et al., 1999; Muro et al., 2000), supports the assumption that the recruitment of ECapZ together with the increase of the γ-adducin subunit minimize the alterations of the RBC actin-spectrin based network preventing the development of more severe pathological states in the β-adducin deficient mice.

Adducin not only stabilises actin filaments by capping their fast-growing ends (Kuhlman et al., 1996), but also recruits spectrin to F-actin (Bennett et al., 1988; Gardner and Bennett, 1987; Hughes and Bennett, 1995) and bundles actin filaments (Mische et al., 1987; Taylor and Taylor, 1994). Probably even if ECapZ is partially incorporated into the skeletal network of mutant RBCs, it is not able to completely perform the wide variety of adducin activities. Therefore, the partial mechanism of compensation mediated by ECapZ, and the additional variations in the levels of α-tropomyosin, tropomodulin, actin, and α- and γ-adducin subunits (discussed in Section 4A.1.3) detected in membrane skeletons of mutant erythrocytes can generate junctional

complex alterations that compromise membrane stability, cell shape and consequently induce RBC fragility which finally causes mild haemolytic anaemia in the KO mice (Gilligan et al., 1999; Muro et al., 2000).

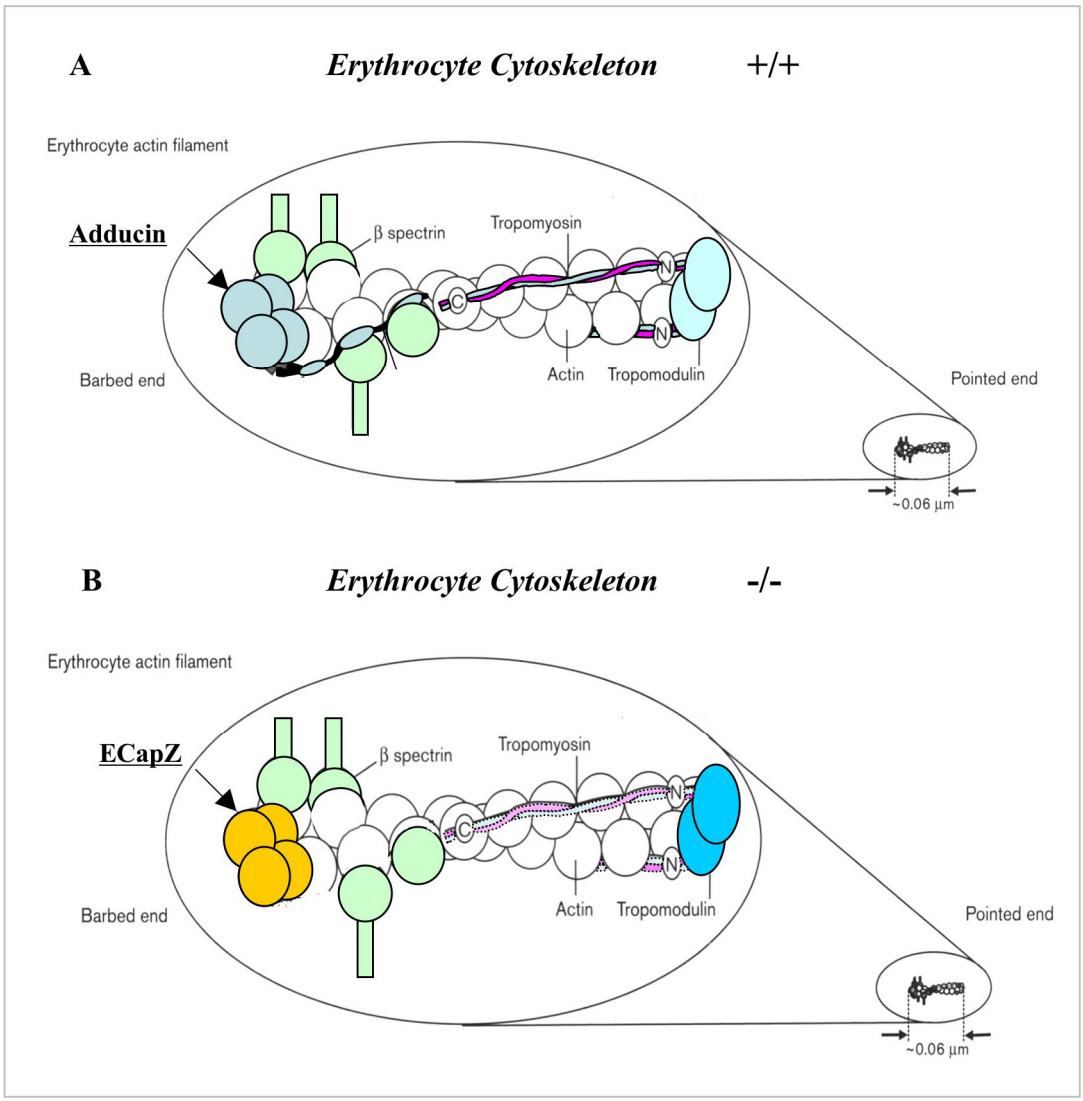

Figure 4.1: Junctional complex components of RBC skeleton of β-adducin mutant and control mice. Panels A and B show a schematic representation of the junctional complex composition of erythrocyte skeletons from wild type and β-adducin deficient mice, respectively. The actin capping proteins at the darbed-end of the protofilament are Adducin and ECapZ in +/+ (Panel A) and -/- skeletons (Panel B), respectively. In Panel B, the reduction in the levels of tropomyosin is indicated by the dotted lines and lighter colours, while the increase in tropomodulin levels is indicated by a darker colour (blue instead of azure, used in Panel A). The Figure was adapted from Fowler, 1996.

4A.1.2- The compensatory mechanism mediated by CapZ is absent in tissues of β-adducin deficient mice -

In contrast to the upregulation of ECapZ in the RBCs skeleton of mutant mice, no differences in the levels of the CapZ subunits were detected analysing either total protein extracts of different tissues (lung, liver, heart, brain, spleen and kidney) or

cytoskeletal preparations of heart and brain of the mutants (Figures 3.9 A and C, and 3.10 A and C, respectively).

CapZ is the major darbed-end capping protein in several non-erythroid cells (muscle and non-muscle cells) (DiNubile et al., 1995; Fowler, 1996), it is therefore conceivable to assume that adducin might have a less relevant role in these cells. In addition, β-adducin expression is mainly restricted to erythroid and brain tissues (Gilligan et al., 1999) and its absence did not influence the gross histology of several non-erythroid tissues (Marro et al., 2000; Muro et al., 2000). The absence of an evident change in the levels of CapZ could also be related to the higher number of components and the more complex organisation of non-erythroid cell skeleton suggesting that the eventual disruptions present in mutants could be compensated by other skeletal proteins. However, functional and electrophysiological studies of the brain showed important alterations in behaviour, learning, long-term potentiation (LTP), and long-term depression (LTD) pointing to an important non-structural role of adducin in the brain [(Rabenstein et al., 2005) and unpublished data from our group].

Our data and the above mentioned evidences indicate that adducin has a less important structural role in the actin-network of non-erythroid cells than in the erythrocyte skeleton. Alternatively, non-erythroid cells have more efficient compensatory mechanisms that minimize the consequences of the absence of β-adducin to maintain a functional membrane skeleton.

4A.1.3- <u>Altered levels of tropomyosin, tropomodulin, actin, adducin subunits indicate an anomalous erythrocyte skeletal architecture in mutant mice</u> -

In addition to ECapZ, altered levels of the key members of the junctional complexes were detected in RBCs skeleton of β-adducin deficient mice. The ~65% reduction in α-tropomyosin, the ~15% decrease in actin levels, and a slight upregulation of tropomodulin suggest important alterations of the mutant erythrocyte skeleton.

The detected opposite trends of tropomyosin and tropomodulin levels in the mutant RBC seem to be in contrast with previous evidence showing that the binding of tropomodulin to the actin filaments pointed-ends is stabilised by tropomyosin and *vice versa* (Weber et al., 1994). In fact, according with Weber's data, a similar trend of the two protein levels in the mutant RBC skeleton should have been observed. There is no clear explanation for the opposite variations we observed. However, overexpression of tropomodulin in mouse cardiomyocytes produced shortened actin filaments inducing

widespread loss of skeleton organisation and degeneration (Sussman et al., 1998; Sussman et al., 1998). The targeted disruption of the α-tropomyosin gene caused embryonic lethality in homozygous null mice (Blanchard et al., 1997; Rethinasamy et al., 1998). In addition, recent *in vitro* experiments demonstrated that selective depletion of tropomyosin from the membrane resulted in decreased membrane mechanical stability due to the weakening and destabilisation of the junctional complexes, an effect that is reversed when tropomyosin is added back (An et al., 2007). These experiments suggest that the downregulation of tropomyosin and increase of tropomodulin that we detected may significantly compromise the structure of the junctional complex affecting, consequently, the stability of the mutant erythrocyte skeleton.

The important decrease in the levels of α-tropomyosin in mutant preparations suggests a new role for adducin in stabilising tropomyosin within the actin filament-complex of erythrocytes. In the case of the targeted inactivation in mice of the anion transporter Band 3, a close interaction of this protein with glycophorin A (GPA) was shown during their biosynthesis as the Band 3 deficient erythrocytes were devoid of GPA (Hassoun et al., 1998). One possible hypothesis could be that, similarly to that proposed for Band 3, adducin (directly, or indirectly via another adducin partner) might play a "chaperon-like" role in the formation of actin filaments, affecting the levels of α-tropomyosin and tropomodulin, a task that seems not to be efficiently performed by ECapZ.

As previously observed (Muro et al., 2000), we also showed a reduction in the levels of actin in the skeleton of mutant erythrocytes. This reduction might be generated by a decrease in the number of protofilaments, in their length and/or stability induced by the lack of the binding and stabilising function of tropomyosin, and by the absence of some of the adducin activities not fully compensated by ECapZ, such as actin filament capping and bundling.

In addition, as formerly evidenced (Gilligan et al., 1999; Muro et al., 2000), an ~75% decrease in α-adducin and a 4-fold increase in the γ subunit were seen in the skeletons of KO erythrocytes (Figures 3.6 A and B). The adducin heterodimers found in erythrocyte skeletons are mainly composed of α and β subunits. The α/γ heterodimers, completely absent in humans, are also found at low levels in RBCs of mice. Thus, the absence of β-adducin in mice seems to trigger a compensatory mechanism aimed to re-establish normal adducin levels by increasing the number of α/γ heterodimers. In fact,

the increase in the γ subunit was probably due to the formation of α/γ dimers caused by the abundance of "free" α-adducin which is not associated with the β-subunit to form α/β heterodimers in the mutant mice.

Therefore, two different compensatory mechanisms seem to be present in β-adducin deficient animals, minimizing the cytoskeletal alterations of the mutant RBCs and justifying the mild phenotypical alterations observed: the partial recruitment of ECapZ at the darbed-ends of the protofilaments and the increased levels of the α/γ adducin oligomers in KO erythrocytes.

Finally, the absence of variations in p55 and Protein 4.1 in the RBC of KO animals (Figure 3.8) suggests that direct or indirect interactions of adducin with these proteins are limited and not affected.

In conclusion, despite of the above-mentioned adaptation mechanisms, these are not sufficient to rescue the phenotype created by the absence of the β subunit in the animal and are therefore not able to attain normal erythrocyte functions. In fact, our results suggest that the described molecular defects probably generate an anomalous skeletal network having altered junctional complexes. Membrane stability mainly derives from the structural and functional integrity of the associations within the spectrin-actin skeleton (horizontal interactions) and the correct assembly of the junctional complexes (Mohandas and Evans, 1994). Thus, alterations of these complexes in the mutant RBCs probably induce the instability of the membrane skeleton and could be the cause of the increased erythrocyte fragility, elliptocytosis and of the consequent presence of the SphHE in mutant mice (Gilligan et al., 1999; Muro et al., 2000).

The increased fragility of the actin network of mutant RBCs could also explain the identification of proteins not associated to spectrin-based network, such as β- and γ–fibrinogen, in skeletal of KO animals by mass spectrometry (Figures 3.1 and 3.3). In fact, the markedly less stable plasma membrane of the β-adducin KO erythrocyte (Muro et al., 2000) could be damaged during microcirculation through small capillaries (whose diameter is 5-10 μm) and undergo an abnormal uptake of plasma proteins by a rupture-resealing mechanism.

It is important to notice that the proteomic analysis indicated differences between the skeleton of erythrocytes of KO and control mice that were not characterised in the present work (Figure 3.3). Therefore, other undetected mechanisms of compensation

could be acting in the erythrocyte skeleton of β-adducin animals. Future mass spectrometry analyses will allow us to further study the composition of the mutant RBC skeleton.

4A.2 Unaltered levels α-tropomyosin indicate a functional skeletal network in the heart of mutant mice

Analysis of α-tropomyosin levels in skeletons purified from mouse heart showed no variations in protein levels, differing from that observed in erythrocytes (Figure 3.5 B). Previous experiments have shown no defects in the heart of KO mice analysing morphological and physiological parameters, such as heart rate, ventricular wall thickness, ventricular muscle volume, m-Mode and Doppler echocardiography and electrocardiogram (Marro et al., 2000).

The absence of morphological, mechanical and electric alterations, and the observed normal levels of α-tropomyosin suggest a normal structure and function of the sarcomeres of mutant mice cardiomyocytes.

These observations may be explained by the fundamental role of α-tropomyosin in cardiac cells. In fact, α-tropomyosin is the predominant isoform expressed in mature heart (α/α homodimers are the preferred association in this tissue) and it is one of the main contractile proteins that compose the skeleton in cardiomyocytes. Tropomyosin is essential to maintain sarcomere structure and the function and, therefore, to activate cardiac muscle myofilaments involved in myocardial contraction (Wolska and Wieczorek, 2003). In addition, as we mentioned (Section 1.5.4), total α-tropomyosin deficiency is incompatible with life, whereas its haploinsufficiency induces the activation of regulatory mechanisms (translational regulation mechanisms sill unknown). These mechanisms maintain the levels of myofibrillar tropomyosin despite the reduction of its mRNA, consequently, heterozygosity produces little or no change in cardiac function or structure (Blanchard et al., 1997; Rethinasamy et al., 1998).

Moreover, the absence of changes in α-tropomyosin levels in cardiac cells could be related to the less crucial role of adducin in maintaining the skeletal structure in cardiomyocytes. Nevertheless, the absence of β-adducin and concomitant downregulation of α- and γ-adducin levels detected in hearts (Marro et al., 2000), highlight the potential presence of some yet undetected variations of the myofilaments or the existence of mechanisms of compensation still unknown.

Further analyses of other contractile and sarcomeric proteins might bring to light additional alterations that could be induced by the lack of β-adducin and/or undetected potential compensatory mechanisms that minimize the effect of its absence in the heart skeleton.

Considering that the precise mechanism of hypertension in our KO mice remains uncertain, future studies could also give us the opportunity to identify molecules and/or processes to shed light on the correlation between adducin and hypertension.

4A.3 The RBC membrane skeleton organisation of dematin deficient mice and adducin-dematin double knock-out mice

The analysis of the protein expression profile of dematin deficient (DKO) and dematin-adducin double mutant mice (DAKO) RBC skeletons, performed in collaboration with Chishti's group, allowed us to gain further insights on the functions and possible interconnected roles of adducin and dematin.

Erythrocyte skeletal samples of dematin headpiece deficient mice showed only a minor reduction in α–adducin levels among the analysed proteins (Figure 3.11). In addition, as previously demonstrated, DKO erythrocytes have a partial loss of spectrin and actin from RBCs membrane skeleton and of GPC from the lipid bilayer (Chen et al., 2007; Khanna et al., 2002). These evidences suggest the presence of a weakened cytoskeleton inadequately anchored to the lipid bilayer, and justifying the increased erythrocyte fragility and mild haemolytic anaemia in dematin mutant animals.

The inactivation of both adducin and dematin increased changes in the levels of the majority of the analysed skeletal proteins. In fact, an almost total absence of the adducin α subunit, a significant downregulation of tropomyosin (~35%) and a strong increase of γ-adducin (~1.5-fold upregulation) and apparently of tropomodulin, were detected in the erythrocyte skeleton of DAKO mice.

We observed some differences between our mutant animals and Gilligan's AKO mice (Gilligan et al., 1999; Muro et al., 2000) that were probably caused by variations in the preparation of the RBCs skeletal samples. Our samples were prepared under more stringent conditions, producing more evident changes in the levels of some of the skeletal proteins. For example, we observed a ~65% decrease of α-tropomyosin levels analyzing skeletal extracts from our mutants, while only a minimal reduction in samples from Chishti's group (Gilligan's AKO) (Figures 3.5 A versus 3.11 F). Since we detected a more important reduction of α-tropomyosin (~35%) in the DAKO skeletons

prepared by Chishti's group, we assume that the reduction would be even higher in our conditions, pointing to an important combined role of adducin and dematin in the stability of actin-tropomyosin interactions. This hypothesis is also supported by the observation that α-adducin levels are also reduced in the DKO and that the decrease in the DAKO is even higher than that observed in the AKO (Figure 3.11 A). In, fact, the strong downregulation of α-tropomyosin and α-adducin and the previously seen reductions of both spectrin and actin (Chen et al., 2007), triggered by the absence of both adducin and dematin, suggest the presence of remarkable defects in actin assembly and in the formation of junctional complexes, and, consequently, reduced stability of RBCs membrane skeleton of the double mutant.

Interestingly, not only the decrease of several skeletal proteins, but also the attempt to minimize the loss of adducin and dematin functions, appears to be amplified in the double mutant when compared to the single mutants. In fact, γ-adducin is significantly increased (Figure 3.11 C) and it seems to partially compensate the absence of β-adducin and the strong decrease in α-subunit in DAKO.

The absence of ECapZ upregulation in DKO erythrocyte skeletal extracts (Figures 3.11 D and E) suggests that adducin is able to cap actin filaments even in the absence of the dematin headpiece domain. It is reasonable to hypothesise that dematin may participate in the recruitment of ECapZ when adducin is absent. In the situation in which the dematin headpiece domain is absent (in both DKO and DAKO), there is no recruitment of ECapZ due to the lack of dematin or, alternatively, because the structure of actin filaments and junctional complexes is altered such that ECapZ cannot cap the actin filaments. The absence of the ECapZ recruitment from the cytoplasm and the consequent lack of all the actin beaded end capping proteins in the erythrocyte junctional complexes of DAKO may justify the fact that the combined mutations, in comparison to single deletions, resulted in a more severe phenotype (Gilligan et al., 1999; Khanna et al., 2002; Muro et al., 2000). However, it is not clear why the decrease in the levels of actin was not higher in DAKO RBC membranes. The presence of an increased level of γ-adducin and the apparent mild upregulation of tropomodulin (Figure 3.11 G) could partially stabilise both the extremity of the RBC actin filaments of the double mutants.

However, the fact that the DAKO animals suffer of a more severe form of haemolytic anaemia and the marked cytoskeletal network damage seen by atomic force microscopy in the double mutant erythrocytes (Chen et al., 2007), strongly support the

idea that adducin and dematin may cooperate in the stabilisation of the junctional complexes, especially in actin-tropomyosin interactions. Moreover, taking into account that DAKO skeletons show a modest decrease in the retention of protein 4.1 (Chen et al., 2007), not only vertical but also horizontal associations of the RBC cytoskeleton appear to be altered in the double KO inducing a reduction of the stress shared between the lipid bilayer and protein skeleton.

In conclusion, the precipitous decrease in the erythrocyte membrane stability, and the inability to regulate cell shape, inducing cell fragility and severe haemolytic anaemia in DAKO animals, are caused by alterations of the cytoskeletal composition and probably by altered linkages between spectrin-actin network and the plasma membrane.

Taken together, these results reveal the essential physiological role of dematin and adducin *in vivo*: they maintain the mechanical properties and structural integrity of erythrocyte membranes by mainly stabilising junctional complexes of the cytoskeleton. Moreover, these data suggest that the two proteins are not completely functionally redundant, as was recently hypothesised by Chishti (Chen et al., 2007). On the contrary, adducin and dematin seem to have similar but distinct roles in the spectrin-based network aimed at the conservation of skeletal structure and function.

Up to now the function of dematin was not completely elucidated and it was assumed that it might be related to its actin-binding activity and/or by unknown binding functions in mature RBCs. Intriguingly, both adducin and dematin have been localised at the junctional complex and their copy number [~3 x 10^4 adducin dimers (Gardner and Bennett, 1986) and ~4.3 x 10^4 dematin trimers (Husain-Chishti et al., 1989; Husain-Chishti et al., 1988)] is consistent with the calculated ~3-4 x 10^4 actin oligomers per erythrocyte (Fowler, 1996; Shen et al., 1986). Based on these and our results, the determination of direct or indirect interactions between dematin and adducin will be of crucial importance to understand the role of both proteins in the red cells skeleton.

4A.4 Lens fibre cells of adducin deficient mice show an altered actin filament based-skeletal organisation

The majority of the alterations in skeletal proteins in β-adducin mutant RBCs were also detected in the actin-skeleton of lens fibre cells of KO mice (Figure 3.13).

Similarly to erythrocytes, the lack of the β subunit produced an important decrease in the levels of α-adducin and an upregulation of the γ subunit in the lens

membrane proteins of KO animals. However, the apparent compensation by γ-adducin was not sufficient to limit the detrimental effects triggered by the lack of adducin in the actin-filament network: a significant downregulation of tropomyosin and a ~20% decrease in actin levels were present in lens membranes extracts from mutants. The amount of CapZ associated to the actin filament was slightly reduced in lens fibres of KO mice (~20%) suggesting the presence of actin-capping mechanisms in the skeleton of lens fibre cells different from those detected in RBC skeletal network. It is important to note that no data about the presence and the subcellular localisation of CapZ dimer in lens fibre is available. We could speculate that the levels of CapZ are very low in eye fibre cells preventing its recruitment to the fast-growing end of actin filaments.

The lack of β-adducin induced an important decrease in the levels of α-tropomyosin in lens membrane proteins of KO animals, as observed RBC skeleton. Considering that tropomyosin and capping proteins like adducin stabilise actin filaments and control their length in almost all cells, their reduction or absence may reduce F-actin stability not only in red cells but also in the lens fibre cells of KO mice. As mentioned in the Introduction (Section 1.6), the lens fibre is characterised by the presence of long actin filaments. The decrease in the level of actin incorporated in the membrane skeleton could be due to a reduction either in filament length and/or in the number of filaments. Alternatively, considering that two distinct pools of actin have been identified in lens cells (membrane-bound and soluble portions) (Woo and Fowler, 1994), the reduced actin skeletal incorporation could also be associated to an increase in cytoplasmatic localisation of the protein in mutant lens. The evaluation of the relative levels of actin in the cytoplasm of lens cells of KO mice will allow us to verify this hypothesis.

We were unable to detect tropomodulin in lens membranes of KO and control mice (data not shown) probably because our lens protein extracts derive mainly from undifferentiated cells (capsule and epithelial cells) and partially differentiated young fibre cells (cortical fibre cells), where tropomodulin is not present. In fact, in contrast to other actin-skeletal components, which are expressed and membrane-associated in all lens cells (both undifferentiated and differentiated lens cells), tropomodulin is expressed concomitantly with lens fibre cell differentiation and assembles onto the membrane skeleton only after fibre cells have begun to elongate (Lee et al., 2000; Sussman et al., 1996).

The molecular organisation of the skeletal network is probably different between RBC and lens fibre cell because despite their similar protein composition deletion of β-adducin results in different skeletal alterations and compensatory processes in the two cell types (Woo et al., 2000).

The observed variations of the levels of membrane proteins in the epithelial and cortical fibre cells of mutant mice could influence the structural organisation of the actin filament based-skeleton and consequently could impair the mechanical stability and the elastic proprieties of the plasma membrane. Considering that the actin-skeleton is the only intact cytoskeletal system remaining in the nuclear fibre cells of aged lenses (Lee et al., 2000; Menko, 2002; Prescott et al., 1996), the presence of the skeletal alterations in the epithelial and cortical fibre cells probably compromise the organisation and function of the actin filament network in the completely differentiated nuclear lens fibre as well. Moreover, the altered composition of the actin-skeleton observed in undifferentiated fibres of KO animals suggests that these cells are not able to undergo proper differentiation. In fact, the reorganisation of actin filaments coordinates most of the events that occur during differentiation of lens epithelial cells into fibre cells, including morphological changes, membrane remodelling, polarization, transcriptional activation, elimination of cellular organelles, and migration (Rao and Maddala, 2006).

In addition, the presence of an anomalous actin–based skeleton could impair some of the optical properties of the lens, like transparency, reflection power and accommodation ability. Lens transparency and reflection power are maintained when skeletal filaments properly organise and distribute the cytosolic and membrane-bound proteins in the lens fibre (Clark et al., 1999), while visual accommodation is principally assured by an adequate lens fibre deformability (Yeh et al., 1986).

The observation that a progressive increase in protein aggregation and lens opacification is associated with the loss of cytoskeletal proteins in some models for cataract, including the selenite model in rat (Matsushima et al., 1997; Mousa et al., 1979; Tagliavini et al., 1986), suggests that the modification in the levels of several skeletal components induced by the absence of adducin could provoke the formation of an abnormal architecture of the actin filaments network and cause opacification in the crystalline lens of the eye and consequently cataract. Differences in the structural organisation of the actin filament have been correlated to variable lens accommodation ability (Rafferty and Scholz, 1985; Rafferty and Scholz, 1991; Yeh et al., 1986). Therefore, the hypothesised variations of the skeletal structure in mutant lens could

reduce the deformability of the membrane, compromise the contractile activity that derives from the interaction between actin and myosin II and finally alter the visual accommodation ability (Kibbelaar et al., 1980; Rafferty et al., 1990).

Future studies on the structural organisation of lens fibre actin-skeleton and on the visual ability of KO mice will give us the opportunity to verify the function of adducin in the fibre cells of lens crystalline.

Chapter B

β-adducin gene structure and its tissue-specific expression

4B.1 β-adducin tissue-specific expression is governed by brain- and spleen-specific promoters in rodents but not in humans

For several years it was known that the β-adducin gene has a pattern of expression restricted to brain and haematopoietic tissues, both in humans and rodents (Gilligan et al., 1995; Muro et al., 2000; Tripodi et al., 1991), but neither the complete gene structure, nor the mechanisms of regulation that are at the basis of this tissue-specific expression have been elucidated.

Our analyses on the expression of β-adducin genes showed that two main distinct promoters are present in rodents: one specific for haematopoietic tissues and the other one specific for neuronal tissues (Figure 3.17 B and C, 3.18 and 3.20 C).

The observations that the homology between the human and rodent brain-specific promoters was only of 47% and that the structure and base compositions were highly different among species (80% and 55% of CG content for humans and rodents, respectively) (Figure 3.19 A) suggested important differences in the transcriptional regulation between humans and rodents. This hypothesis is supported by data on the expression data of the human β-adducin gene promoter (Figure 3.21 C). The presence of a human brain-specific promoter has previously been suggested [M. Bulger, unpublished data; (Yenerel et al., 2005)], but we detected transcription from this promoter not only in brain but also in haematopoietic tissues, such as spleen and bone marrow, and at lower levels in lung (Figure 3.21 C). However, our results were obtained by semiquantitative RT–PCR and need further analysis for their confirmation.

The ubiquitous transcription from the human promoter might be due to the presence of a high CG content and the numerous predicted binding sites for the transcription factor SP1 within its sequence (Figure 3.19 A). In fact, CpG islands are found to be more likely associated to housekeeping genes than to highly regulated ones, even if it was observed that this correlation cannot be applied universally, specially for promoters of central nervous system genes which are CpG-reach (Gustincich et al., 2006; Schug et al., 2005; Smale and Kadonaga, 2003). In addition, SP1 is required for the ubiquitous transcription of several housekeeping genes and plays an important

regulatory role in cellular processes during development and differentiation (Saffer et al., 1991).

In contrast, the rodent brain-specific promoters showed a very tight expression pattern, in fact we detected its activity in the mouse brain of 13.5 day embryos, postnatal 1- and 14-day-old pups, and in adults, but not in other tissues (Figure 3.20 C). No band corresponding to the product of this promoter was detected in the spleen RNA samples by RNase protection experiments (Figure 3.17 C).

Therefore, we propose the name of rodent brain-specific promoters and first exons as mN1 and rN1, to designate the neuronal mouse and rat first exons, respectively. In addition, we suggest that in humans the promoter and first exon are not found exclusively in brain and not tissue-specific (Yenerel et al., 2005).

These conclusions obtained by experimental studies are also supported by *in silico* prediction of transcription binding sites. In fact, a number of predicted binding sites for transcription factors which have been identified to be involved in the expression modulation of several neuronal genes, like NF1, Krox, AP-2, Fos and Jun families (Damberg, 2005; Tamura et al., 1996; Tischmeyer and Grimm, 1999), are conserved between rodents and almost all of them were absent in the human promoter (Figure 3.19 A).

The activities of mouse and rat spleen-specific promoters were mainly detected in erythropoietic tissues such as embryonic liver and placenta, and was also active in other embryonic tissues although at a lower expression level (Figure 20 C, primers pair "c"), similar to what was observed in humans, [Figure 3.21 C and (Yenerel et al., 2005)]. In 14 day-old mice, β-adducin expression in liver and in other tissues seemed to be completely shut down and only active in spleen and bone marrow. These data are in agreement with the evidence that liver and placenta are the sites of fetal haematopoiesis. In fact, in uterus, haematopoiesis initially takes place in the extraembryonic yolk sac, then switches to the fetal liver, thymus and, finally, to bone marrow and spleen during adult life (McGrath and Palis, 2005).

Sequence comparison between the rodent spleen-specific promoter and the first transcribed exon with those of human (Yenerel et al., 2005) showed 43 and 47% homology with rat and mouse, respectively, while the rat and mouse sequences showed higher homology (84%). Moreover, some of the predicted regulatory sites present in the rodent promoters were conserved. Several of them, like GATA-1 (GATA transcription factor 1), EKLF (erythroid kruppel-like factor) and NF-E2 (nuclear factor erythroid-

derived 2), are putative transcription factor binding sites known to be crucial for progression along the erythroid maturation pathway (Ingley et al., 2004). Remarkably, most of the human-predicted transcription binding sites were not conserved in rodents. However, the binding sites of the haematopoietic GATA transcription factor family (Orkin, 1992) and the EKLF transcription factor predicted for the human erythroid promoter (Yenerel et al., 2005) were present in rodents in highly conserved regions, suggesting that the analysed erythroid promoters might be regulated, at least in part, by mechanisms common to all three species. Nevertheless, functional analyses are needed to more precisely determine the *in vivo* regulation of both brain- and spleen-specific β-adducin gene promoters.

Nevertheless, we noticed that despite the fact that β-adducin expression in rodents is clearly regulated by brain and spleen specific promoters, the 5'-sequence also contains some of the features typically associated to housekeeping gene promoters, like the absence of the TATA-box, the presence of Inr sequences and GC rich regions containing multiple SP1 binding sites.

As mentioned in Section 1.13.1, approximately half of the mammalian protein coding genes are known to be regulated by alternative promoters (Carninci et al., 2006; Cooper et al., 2006; Kimura et al., 2006; Landry et al., 2003). A large scale study showed that in 17% of the human alternative promoter-containing loci, tissue-specific use of the alternative promoters was observed and the tissues in which the usage of alternative promoters was most frequently observed were testis and brain (Kimura et al., 2006). The observation that this molecular mechanism occurs more frequently in neuronal tissues could be due to the fact that specific diversification of a large population of genes may be required to create an elaborate system such as the brain. It was also observed that the presence of alternative promoters is enriched in genes encoding erythrocyte membrane proteins and cytoskeletal components (Gallagher, 2003). For instance, the AE1 gene is transcribed by two promoters: the upstream promoter produces erythroid Band 3, whereas the one downstream initiates transcription of the Band 3 isoform in kidneys. Tropomyosin is expressed as large number of isoforms (high and low molecular weight isoforms) some of which are driven by alternative promoters. Many of the these isoforms are tissue- and filament-specific(Lin et al., 1997). Expression of multiple Protein 4.1 isoforms in mature RBCs, erythroid progenitors and in a variety of different tissues results from alternative promoters and pre-mRNA splicing processes. Moreover, alternative tissue-specific promoters direct

the expression of ankyrin isoforms in erythroid, muscle and neuronal cells (Gallagher, 2003).

In all the mentioned cytoskeletal and erythroid membrane proteins, the use of alternative promoters produces isoforms with different N-terminus. On the contrary, the β-adducin transcripts in rodents have alternative initial exons in neuronal and erythroid tissues but a common downstream exon (102 and 99 bp exons in mice and rats, respectively) (Table 3.6) contains the translation start site, therefore the tissue-specific transcripts have the same ORF at the 5'-end and the two protein isoforms have the same N-terminus.

In summary, we demonstrated that β-adducin neuronal and erythroid-specific first exons are generated by the use of tissue-specific alternative promoters in rodents, while a similar control of ADD2 expression seemed not to be present in humans. The observation that *Add2* tissue-specific promoters of rodents are enriched for particular motifs that serve as binding sites for transcription factors able to regulate the tissue-specific expression of several genes suggests that they could induce the assembly of specific pre-initiation complexes allowing the diverse regulation of β-adducin expression in erythroid and neuronal cells.

4B.2 Mouse β-Add63 and β-Add97 mRNA families have a tissue- and developmental-restricted expression

Analysis of the β-Add63 and β-Add97 families of mRNAs during mouse maturation showed that both were expressed in most analysed tissues derived from embryos and new born animals, with higher levels in brain and spleen (Figures 3.14 and 3.15).

On the contrary, previous studies and our analysis showed that the expression of the two families in adult animals is restricted to neuronal and erythroid tissues (Gilligan et al., 1995; Muro et al., 2000; Tripodi et al., 1991) (Figures 3.14 and 3.15). Nevertheless, Northern blot analyses suggested that β-Add63 was mainly expressed in spleen while β-Add97 levels were higher in brain (Figure 3.25 A and B).

These results are to a large extent in agreement with previous observations regarding the pattern of expression of the β-adducin families in human tissues (Gilligan et al., 1999). Dr. Gilligan's group observed that β-Add63 mRNAs are expressed not only in neuronal and haematopoietic tissues, but also in lungs of adult humans. In contrast, we observed very low levels of β-Add63 mRNAs in 14-day old mouse lungs

and an absence of the transcript in adults, due probably to species-specific differences in β-adducin pre-mRNA transcription and processing.

The observed developmental-specific expression of the alternative splicing variants of β-adducin could be also correlated to the differential activity of the *Add2* tissue-specific promoters during mouse growth. Based on the obtained experimental data (Figure 3.20 C), it is possible to hypothesise a progressive deactivation of the erythroid promoter in non-erythroid tissues during the maturation of the animal (as observed in adult heart, kidney, lung and liver) and the conservation of its activity during adult life only in spleen. This phenomenon could be justified by the fact that the basal transcription apparatus can be recruited to the promoter in a developmental-dependent manner, as demonstrated in mouse erythroid cells for the γ-globin gene (Duan et al., 2002). In addition, the idea that alternative promoter usage may provide a mechanism for tissue- and developmental stage-specific activity of genes is supported by a recent global analysis of mammalian promoters. This study concluded that alternative promoters mostly play a role in highly regulated developmental genes, while single-promoter genes are more likely involved in general cellular processes active in a broad range of tissues (Baek et al., 2007). However, further analysis is necessary to prove this hypothesis.

It is relevant to note that the β-Add97 and β-Add63 mRNAs families can be also considered as two groups of transcripts that undergo alternative polyadenylation associated to the presence of a "composite exon" (Edwalds-Gilbert et al., 1997)(Section 1.13.3 and Figure 1.17 B). In fact, the β-Add63 mRNAs are obtained when the 5'-splice site of exon 13a is silent and intron 13 is retained. A polyadenylation site located within intron 13 is used and, consequently, transcription termination occurs downstream of this position. In contrast, in β-Add97 transcripts intron 13 is removed, the downstream exons are also included in the mRNA and polyadenylation and transcription/termination processes take place at the 3'-end of the exon 16 (Figure 1.6) (Gilligan et al., 1997; Tisminetzky et al., 1995).

Considering that the choice of a specific promoter can influence splice site selection (Kornblihtt, 2005; Landry et al., 2003), thus affecting the inclusion pattern of alternatively spliced exons into the mature mRNA, it may be interesting to investigate whether the differential use of the two tissue-specific *Add2* promoters modulates the

pattern of splicing and polyadenylation processes observed in β-Add63 and β-Add97 families.

4B.3 Brain-specific β-adducin pre-mRNA processing uses a distal polyadenylation site generating a 5-6 kb 3'-UTR

Despite the 8–9 kb β-adducin mRNA was detected in human and rat brain instead of the 3.5–4.5 kb spleen transcript about 15 years ago (Joshi et al., 1991; Tripodi et al., 1991) and at least three attempts were made to completely characterise the ADD2 gene structure (Gilligan et al., 1997; Tripodi et al., 1995; Yenerel et al., 2005), the molecular basis of this long brain-specific form remained unknown.

After ruling out the presence of undetected internal exons or a long 5'-UTR that could justify the formation of the 8-9 kb mRNA in brain, we focused our attention on the 3'-UTR.

The presence in the brain of a variety of ESTs that mapped to the region downstream of the polyadenylation sites reported for the ADD2 gene strongly suggested that a distal site could be used in the brain-specific β-adducin mRNA. We confirmed experimentally this hypothesis demonstrating the presence and use of a novel brain-specific polyadenylation site, generating 8262, 7817 and 9286 base long mRNAs in mice, rats and humans, respectively. In contrast, the longest form containing all internal exons of the erythroid-specific transcript was 3664, 3574 and 4631 bases long for mice, rats and humans, respectively (when the A_3 polyadenylation site was used).

These results indicated that the β-adducin pre-mRNA contained four tandem alternative polyadenylation sites that were used in a tissue-specific manner: the A_1 and $A_{2\text{-}3}$ more proximal ones mainly used in erythroid tissues and the distal A_4 site specifically utilized in brain. In fact, in addition to the Northern blot and RT-PCR data of brain RNA (Figure 3.22 to 3.24), almost all of the ESTs and mRNAs found in the databases that corresponded to the distal A_4 polyadenylation site were derived from brain or brain-related tissues. Instead, libraries generated from a variety of tissues including spleen and embryonic liver included RNA sequences containing the other proximal polyadenylation sites (Table 3.8). Additionally, the functionality of all of the proposed polyadenylation sites was supported by the detection of several ESTs and mRNAs containing poly(A) tails, by 3'-RACE-PCR and sequencing analysis of the brain β-adducin mRNA (Figure 3.32).

Many genes are reported to be subjected to alternative 3'-end processing, and several lines of evidence suggest that polyadenylation site selection is modulated developmentally or in a tissue-specific manner (Edwalds-Gilbert et al., 1997; Zhang et al., 2005). Curiously, similarly to β-adducin, the pre-mRNAs of other skeletal proteins undergo cell type-specific alternative polyadenylation (Gallagher, 2003). The erythroid- and muscle/neuronal/lymphoblast-specific isoforms of β-spectrin are generated by the use of two different polyadenylation sites located downstream of two distinct exons. More in general, in approximately 10% of tandem polyadenylation sites the choice of one specific site is related to tissue types (Ara et al., 2006). It is interesting to note that the β-adducin tissue-specific use of differential sites is in accordance with a recent *in silico* study which shows that for tandem polyadenylation sites, distal poly(A) sites are used in the nervous system and brain , whereas proximal sites tend to be used in blood (Zhang et al., 2005).

Our findings suggest that erythroid and neuronal cell types have a defined "program" to produce mature β-adducin mRNAs with 3'-UTRs of different length.

4B.4 Different features of the proximal and distal polyadenylation signals seem to affect tissue-specific 3'-end processing of β-adducin transcripts

Although many genes that posses multiple polyadenylation sites within the 3'-UTR have been reported and characterised, yet the fundamental mechanisms responsible for regulating alternative poly(A) site selection have not been elucidated.

The strength of *cis*-regulatory elements for binding *trans*-acting factors determines the efficiency of the 3'-end processing at specific sites. Commonly, the efficiency of a polyadenylation reaction determines the choice of one of the multiple sites within a transcript undergoing alternative polyadenylation (Weiss et al., 1991).

In the β-adducin gene, the A_1 and A_4 poly(A) regions in mice, rats and humans contain all the basic sequences that define a polyadenylation signal: the hexanucleotide motif, the upstream and downstream elements (USE and DSE) (Zhao et al., 1999). Instead, partial homology with the canonical polyadenylation elements was observed in the $mA_{2\text{-}3}$, $rA_{2\text{-}3}$ and hA_2 regions, even if the activity of these sites was supported by the presence of numerous polyadenylated ESTs corresponding to those regions and by the Northern blot detection of several bands (Figure 3.16). The putative hexamer motif of the brain mRNA form was the variant AGUAAA which was fully conserved in all three

species and is found in about 3% of genes (Beaudoing et al., 2000; Tian et al., 2005). AUUAAA and ACUAAA are the A_1 hexanucleotide motifs detected in rodents and humans, respectively. The presence of the less efficient and more rare ACUAAA variant (its incidence among the transcripts is only less than 1%) could be correlated to the fact that only two ESTs without the poly(A) tail corresponding to the hA_1 region were detected, suggesting that this site is poorly active. The association between the presence of a specific hexanucleotide element having different efficiency and the activity of the site seem not to be valid for A_1 in rodents. In fact, we detected several polyadenylated ESTs corresponding to the rA_1 but none in mouse despite the fact that both have the same AUUAAA variant of the signal, whose activity is comparable to that of the canonical AAUAAA one. Likewise, the non canonical A_4 hexanucleotide motif in all the three species seems to be correlated to a good polyadenylation activity as numerous ESTs containing poly(A) tail were detected in brain.

It is important to take into account that although *in silico* analyses of EST databases improved the understanding of polyadenylation signals and alternative polyadenylation, EST count does not necessarily reflect polyadenylation efficiency for any specific mRNA form of a gene. In fact, the observed poly(A) variants may come from different EST libraries with diverse sizes and amplification protocols. Additionally, the number of EST libraries varies according to the analysed tissue. Therefore, our EST analysis only showed general tendencies: the number ESTs that we detected provided an indication of the efficiency of the different tissue-specific poly(A) sites.

All the above observations confirm that polyadenylation efficiency at one specific site does not strictly depend on the hexameric signal: in fact, it is also affected by the flanking USE, DSE and other auxiliary sequences (Legendre and Gautheret, 2003). The difference between the well-defined and highly-conserved GU-rich element downstream of the brain-specific A_4 poly(A) site and the poorly defined one, located in the proximal polyadenylation regions (A_1, A_2 and A_3 regions) could be related to differences in the efficiency of 3'-end processing among the sites. Remarkably, DSEs are more frequently associated to "strong" poly(A) sites, in fact they seem to act as enhancers and often specify or help to distinguish the most efficient sites in cases of alternative polyadenylation (Legendre and Gautheret, 2003; Prescott and Falck-Pedersen, 1994). The various combinations of *cis*-acting elements observed in the different polyadenylation signals in the β-adducin transcript could also explain why

unique cleavage sites were detected in the brain-specific A_4 region while multiple sites were found in each of the A_1, A_2 and A_3 regions in all three species.

The presence of hexanucleotide motif variants differing from the canonical one in the β-adducin transcript of all three species is in agreement with the evidence that polyadenylation signals with suboptimal hexameric elements are commonly more frequent in transcripts that undergo alternative 3'-end processing and are usually associated with alternative tissue-specific polyadenylation (Beaudoing et al., 2000; Edwalds-Gilbert et al., 1997). In addition, considering that alternative polyadenylation of the pre-mRNAs containing weak signals offers greater regulatory possibilities, as observed in the case of alternative splicing, the presence of presumably weaker non-canonical sites within the β-adducin transcript could favour mechanisms that modulate tissue-specific 3'-end processing.

Our observations indicate that all the putative polyadenylation signals detected in the β-adducin transcript have different features. The peculiarity of each of them could be important for the tissue-specific polyadenylation process: distinct polyadenylation machineries could be able to recognise the different *cis*-acting elements present in each polyadenylation regions.

4B.5 Minigene-derived β-adducin transcripts are polyadenylated at mA_4 brain-specific site in HeLa cells

Northern blot analyses of RNA purified from HeLa cells transfected with chimeric minigenes, which mimic the structure and the arrangement of β-adducin transcript, allowed us to initiate the study of the mechanisms regulating tissue-specific polyadenylation of *Add2* gene.

We observed that the transcripts generated from the pBS SP-BR pA and pBS tot-wt were cleaved and polyadenylated at the brain-specific mA_4 poly(A) site (Figure 3.29). The preferential use of the distal brain-specific mA_4 among all the β-adducin sites in HeLa cells could be associated to the fact that the polyadenylation elements of the A_4 signal are well defined and have higher homology with the canonical polyadenylation *cis*-acting sequences than those of the proximal sites. Moreover, the results are supported by previous data indicating that the sites located furthest downstream are usually the most efficient, and the predominant forms of alternatively polyadenylated mRNAs are usually the longest ones (Beaudoing et al., 2000; Graber et al., 1999; Tian et al., 2005; Yan and Marr, 2005).

The absence of mRNA after transfection of the pBS IN-wt suggests that, in addition to the presence of specific *cis*-acting element sequences, the context in which the polyadenylation signal is introduced might strongly influence its strength and use. However, this result provided a preliminary indication and is not sufficient to draw a definite conclusion about the impact of context or sequences on the use of a specific polyadenylation site. This hypothesis will be tested in the future.

At the same time, the *trans*-acting factors responsible for the 3'-end processing in HeLa cells could be similar to those of the polyadenylation machinery of neuronal cells. In fact, the evidences that comparable levels of CstF-64 were discovered in HeLa and neuronal cells and that this amount is lower than that detected in spleen seem to support the above hypothesis (Wallace et al., 1999). Therefore, similarities between HeLa and neuronal expression of polyadenylation factors or perhaps the absence of some unknown erythroid-specific factors could be associated to the use of the distal A_4 polyadenylation site.

Finally, it is important to take into account that analysis of these polyadenylation signal sequences in artificial constructs may only partially reproduce the conditions present in the genomic sequence, where 3'-end processing is presumably affected by the presence of other functional elements. Considering that polyadenylation is highly coordinated, or coupled, to splicing, the absence of the 15^{th} intron sequence (including the region from the branch point to the 3'-splice site of 16^{th} exon) in the chimeric minigenes could influence the downstream polyadenylation process. In fact, it was been shown that U2AF and U2 snRNP, which are associated with early recognition of the 3'-splice site, are not only involved in 3'-terminal exon definition but also influence the process of polyadenylation (Millevoi et al., 2006) and mutation of the polypyrimidine tract and the 3'-splice site significantly reduces polyadenylation efficiency (Cooke et al., 1999). On the contrary, 5'-splice site mutation had a minimal negative effect on polyadenylation in the presence of unaltered 3'-splice site and polypyrimidine tract. However, other studies suggest that the U1 snRNP binding site (e.g., a 5'-splice site) upstream of the last exon can negatively affect both polyadenylation reactions (Cooke et al., 1999; Gunderson et al., 1998). The fact that our construct lacked binding sites for these splicing factors could have altered the mechanism leading to the selection of a specific poly(A) site among the other alternative sites. Further experiments will allow us to elucidate these questions.

4B.6 An upstream cryptic poly(A) site was used in the absence of the β-adducin mA_4 site hexanucleotide motif in HeLa cells

While analysing the contribution of the core polyadenylation elements to the polyadenylation site selection in the chimeric minigenes by a deletion strategy, we observed that the absence of the highly conserved A_4 hexanucleotide motif provokes the less efficient formation of a slightly shorter polyadenylated mRNA. This shorter transcript was generated by the activation of a cryptic poly(A) site located upstream of the brain-specific site demonstrating the presence and functionality of an additional weak downstream polyadenylation signal 3'-UTR of β-adducin mRNA.

Mutational inactivation of the AAUAAA element of the early upstream poly(A) site (pAE) of human papillomaviruse-16 (HPVs) resulted not only in the activation of cryptic polyadenylation signals located upstream of the pAE, but also in the increase of late mRNA production, generated by the use of the downstream late poly(A) site (Zhao et al., 2005). In contrast, our *in vitro* analyses showed that deletion of the brain AGUAAA motif did not induce a switch to any of the proximal polyadenylation sites nor to the β-globin site introduced downstream.

Despite the fact that the putative hexamer motif of the cryptic site is a rare AAUAUA variant (its frequency is 1.7% in mice), the HeLa polyadenylation machinery used this signal instead of the more conserved and frequent one located in the proximal mA_1, $mA_{2\text{-}3}$ or in the extra β-globin polyadenylation regions. However, the amount of detected mRNA was lower than that obtained with the nonmutated construct, suggesting that the strength of the cryptic site was weaker than the canonical A_4, and the efficiency of the polyadenylation reaction was consequently lower.

The high degree of conservation in the natural mA_4 polyadenylation region among the six analysed species strongly suggests the existence of essential *cis*-acting elements that could be recognised by *trans*-acting factors involved in the definition of the site and participating in the polyadenylation reaction. The AAUAUA motif and the putative USE and DSE of the cryptic site in the six species also show a high degree of conservation, suggesting that they could be recognised by polyadenylation *trans*-acting factors (Figure 3.33). For instance, the putative DSE of the cryptic site could be bound by CstF. Considering that CPSF-160 has only a slight preference for the canonical AAUAAA motif (Murthy and Manley, 1995) and requires cooperation with CstF to bind pre-mRNA templates (Wilusz et al., 1990), the interaction between CstF and the putative DSE could stimulate binding of CPSF to the non canonical AAUAUA hexamer

conferring specificity to the cryptic polyadenylation site. The presence of a flexible set of elements, not one of which is very strongly bound by the protein machinery that is recruited in a cooperative manner, provides another way to modulate gene expression.

4B.7 The lack of USE of the β-adducin mA_4 site decreases the efficiency of pre-mRNA processing

We observed that removal of the U-rich sequence of the USE mA_4 provokes a significant reduction of the polyadenylation efficiency highlighting the functional importance of this element for efficient pre-mRNA processing in brain (Figure 3.31). This result allows us to add the β-adducin gene to the group of cellular genes [such as complement factor C2 (Moreira et al., 1998), collagen (Natalizio et al., 2002), cyclooxygenase isoenzymes-2 (Hall-Pogar et al., 2005), etc.] in which the USE increases polyadenylation signal strength and consequently enhances the polyadenylation process. Functionally, the U-rich sequences improve cleavage efficiency by acting as recognition sites for 3'-end processing factors (Carswell and Alwine, 1989; Hall-Pogar et al., 2007; Moreira et al., 1998). Therefore, the reduced efficiency of the β-adducin polyadenylation process upon deletion of the U-rich region within the USE could be due to a decreased capability of the polyadenylation signal to recruit and enhance the binding of basal polyadenylation factors, such as CPSF and CstF (Brackenridge and Proudfoot, 2000; Moreira et al., 1998). Considering that the mA_4 USE contains consensus sequences for polypyrimidine tract binding protein (PTB) (UUC/GUG) (Figure 3.33), a factor discovered to bind U-rich sequences and known to increase the efficiency of the polyadenylation process for the C2 and COX-2 transcripts (Hall-Pogar et al., 2007; Moreira et al., 1998), the absence of the β-adducin upstream regulatory element of the A_4 region could interfere with the stimulatory effect mediated by PTB. To determine the *trans*-acting factors interacting with the β-adducin USE in detail further experiments will be performed.

The rationale behind the inclusion of the β-globin polyadenylation region downstream of the mA4 one was to add a downstream functional site where polyadenylation could occur after weakening of the mA4 site by the USE deletion. However, no mRNA species using the β-globin polyadenylation site were detected. Instead, the presence of the β-globin site increased the efficiency of 3'-end processing at the mA_4 in the absence of the upstream U-rich sequence (Figure 3.31). We propose that

the β-globin region has a long distance interaction with the β-adducin mA_4 site enhancing the formation of a functional polyadenylation complex. A more detailed study will probably highlight the molecular mechanisms causing this phenomenon.

The results considered in these last two Sections (4B.6 and 4B.7) were aimed to study the mechanisms regulating the tissue-specific polyadenylation of β-adducin gene. The consequences on polyadenylation of the mA_4 U/GU-rich element deletion, together with the analysis of double or multiple deletion mutants will be performed in the future to characterise the effects of the concomitant absence of more than one polyadenylation signal element. Those experiments will be followed by pull-down and mass spectrometry analysis of the purified proteins.

4B.8 β-adducin mRNA tissue-specific polyadenylation could be regulated by specific *trans*-acting factors

Several of the previous observations indicate that the choice of a particular polyadenylation site of the β-adducin gene in erythroid and neuronal cells likely involves not only features of the diverse *cis*-acting elements but also specific *trans*-acting factors taking part in dissimilar 3'-end processing machineries .

It is known that the efficiency of the 3'-end processing reaction, which determines the choice of one of the multiple sites in alternative polyadenylation processes, is also modulated by the presence, concentration and activity of *trans*-acting factors catalyzing and/or promoting the reaction (Weiss et al., 1991). For example, an increase in CstF-64 levels during the transition of resting B cells to proliferating B lymphoblasts causes preferential use of the upstream signal of IgM heavy chain gene (Takagaki et al., 1996). In accordance with previous evidence, the activation of macrophages with lipopolysaccharide (LPS) induce the upregulation of CstF-64 expression and causes an increase in the selection of a weak proximal polyadenylation site within a reporter mini-gene containing two linked poly(A) sites, contributing also to changes in expression and alternative polyadenylation of a number of genes (Shell et al., 2005). In addition, upregulation or overexpression of CstF-64 increases the polyadenylation site selection for the 1 kb mRNA of mouse Testis Brain RNA-Binding Protein, a gene which encodes three mRNAs of 3.0 kb (preferentially expressed in somatic cells), 1.7 kb and 1.0 kb (predominant in testis), differing in their 3'-UTRs. Similarly, the evidence that the levels of CstF-64 are higher in brain than in spleen

(Wallace et al., 1999) suggests that different expression levels of that factor might also influence the choice of the different polyadenylation sites of the β-adducin transcript.

By knocking-down the 25 kDa subunit of the CF I_m it was demonstrated that it participates in alternative selection among tandem arrays of poly(A) signals within a single 3'-UTR. In fact, in some genes that have multiple polyadenylation sites in their 3'-terminal exon the presence of the factor primarily induces the use of the most distal poly(A) site, while in the absence of CF I_m, the most upstream poly(A) sites predominate (Kubo et al., 2006). In this context, the CF I_m may serve a role in the recognition of the most upstream poly(A) site in a terminal exon, we could hypothesise that different concentrations of the factor in the erythroid and neuronal cells may be involved in the selection of the β-adducin tissue-specific polyadenylation sites.

Some studies suggest that tissue-specific forms of core polyadenylation factors might allow the selection of different signals and, consequently, the use of specific polyadenylation sites. For instance, a variant of CstF-64, τCstF-64, is expressed only in a limited number of tissues: at a high levels in male germ cells and to a minor extent in brain (Wallace et al., 1999). The U/GU-rich downstream elements found in the distal A_4 region of β-adducin might be recognised by brain-specific τCstF and/or other tissue-specific factors favouring the binding of CPSF at the AGUAAA motif and prevailing over the use of the proximal poly(A) sites. This hypothetical model could account for the high efficiency of the 3'-end processing at the distal A_4 site in brain even if the signal contains a non-canonical hexanucleotide motif. A strong affinity for the downstream U/GU-rich signal by a tissue-specific CstF could 'override' a relatively weak affinity for the AGUAAA motif by CPSF. Otherwise, the use of the proximal β-adducin sites in spleen may be mediated by spleen-specific expression of other 3'-end processing factors.

Moreover, additional proteins could alter the specificity of the core polyadenylation machinery. A more recent study indicated that four of the 26 factors known to play roles in nuclear polyadenylation showed significantly different levels of expression between brain and other tissues. PTB and U1A were expressed at lower levels in neuronal tissues than in other tissues, whereas the relative expression levels of PC4 and τCstF-64 were higher in brain tissues. In addition, neural PTB (nPTB) was also found to be preferentially expressed in neuronal cells and tissues (Zhang et al., 2005). This suggests that tissue-specific upregulation or downregulation of factors

involved in splicing and transcription may also contribute to the decision to use a specific alternative polyadenylation site. However, *trans*-acting factors clearly involved in tissue-specific polyadenylation process have not been yet characterised.

4B.9 Could the events responsible for the tissue-specific transcript isoforms of β-adducin be coupled?

Numerous data support the evidence that pre-mRNA processing events -capping, splicing and polyadenylation- influence each other and are also tightly linked to transcription (Bentley, 2005; Calvo and Manley, 2003; Cramer et al., 1997; Proudfoot et al., 2002).

Certain polyadenylation factors can interact with the C-terminal domain (CTD) of the RNA Pol II, enhancing polyadenylation efficiency, and this interaction take place at the promoter. The fact that events at the promoter could influence the efficiency of transcription termination and polyadenylation reactions is also suggested by the existence of gene loops, in which the transcription termination region can be physically linked to its promoter (Ansari and Hampsey, 2005; O'Sullivan et al., 2004). Moreover, it was demonstrated that the communication between the 5'-and 3'-ends of the pre-mRNA during processing is mediated by the physical association of the CBC/cap complex with 3'-processing factors bound at the polyadenylation site. These data provide further support for the hypothesis that pre-mRNAs and mRNAs may exist and be functional in the form of "closed-loops," due to interactions between factors bound at their 5'- and 3'-ends (Flaherty et al., 1997).

Our studies showed that the synthesis of different mature forms of the β-adducin transcript results from the tissue-specific use of alternative promoters and alternative polyadenylation sites, and from a complex pattern of alternative splicing events. The hypothetical existence of a coupling between transcription and pre-mRNA processing events of β-adducin pre-mRNA could suggest that at least part of the decision about the alternative polyadenylation and splicing events may occur at the different promoters. Thus, an intriguing possibility is that the transcriptional complexes formed at the brain-specific promoter could direct the polyadenylation machinery to the distal polyadenylation sites, and that present in the spleen-specific promoter to one of the proximal polyadenylation sites.

4B.10 Possible roles of the long 3'-UTR of brain-specific β-adducin mRNA

We showed that the β-adducin brain mRNA form contains an unusually long 3'-UTR. Although the majority of the human and mouse transcripts have a 3'-UTR smaller than 2 kb, with an average size ranging from 600 nt to 1000 nt for human 3'-UTRs (Mignone et al., 2002), several recent studies based on EST analysis have shown the existence of long 3'-UTR (5-10 kb) for a number of genes (Iseli et al., 2002; Lopez et al., 2006; Tian et al., 2005). Moreover, *in silico* studies of genes having tandem poly(A) sites indicated that they may express mRNAs with longer 3'-UTRs in specific tissues (Zhang et al., 2005). The identification of the brain-specific β-adducin 8-9 kb transcript was consistent with the observation that the 3'-polyadenylation sites tend to be preferentially used in brain and in nervous system mRNAs having tandem polyadenylation (Zhang et al., 2005).

Since the 3'-UTR hosts important *cis*-acting regulatory elements, involved in various aspects of mRNA metabolism, such as localisation, translation efficiency, and stability (Mignone et al., 2002), alternative polyadenylation events producing mature transcript forms with 3'-UTRs of variable lengths may strongly influence the fate of the different mRNAs and therefore affect gene function in a tissue- or developmental-specific manner.

The high degree of conservation of the brain-specific polyadenylation region A_4 in all species analysed is striking (Figure 3.26 C and 3.33). We observed a 99.1% homology between mouse and rat A_4 sequences, and a 75% homology among all three species, while the complete coding region of β-adducin has 95.8% homology between rats and mice, and 86.3% among all three species (Muro et al., 2000). The complete last exon showed 81% homology between mice and rats and 57% between rodents and humans (Table 3.6). Therefore, the highly-conserved A_4 polyadenylation region of the β-adducin gene highlights the importance of producing tissue-specific mRNA products and suggests that the brain-specific 3'-UTR could be involved in the regulation of the function of the β-adducin gene by one or more of the mechanisms mentioned above.

4B.10.1 - The 8-9 kb β-adducin mRNA islocalisedm with dendrites -

In situ hybridisation analysis revealed a high expression of the mRNA β-adducin transcript in the hippocampus, especially *Cornu Ammonis* fields CA1-CA3 regions and dentate gyruns, in layer I-II and V of the entorhinal cortex, substantia nigra and medio dorsal nucleus of thalamus (Figure 3.35). These data confirm previous data on the β-

adducin mRNA level of expression. In fact, in human brain, the β-adducin transcript was found to be highly enriched in hippocampus, corpus striatum, cerebral cortex and cerebellum and its expression levels correlate with cellular density (Gilligan et al., 1999; Rabenstein et al., 2005).

Interestingly, higher magnifications of the in situ hybridisation images showed that β-adducin mRNA has a remarkable dendritic localisation.

In many cells, especially in neurons, the targeting of mRNA to distinct compartments is an important protein-sorting mechanism. Neurons have a highly polarized cell structure and typically contain one long, thin filamentous axon and multiple dendrites that differ morphologically and functionally from one another. A great number of mRNAs in neurons are localised either in dendrites or in the synaptic endings of axons (Job and Eberwine, 2001).

It is known that most of the *cis*-acting sequences in transcripts identified as being involved in mRNA dendritic localisation are within the 3'-UTR (Chabanon et al., 2004). Taking into account that brain-specific β-adducin mRNA contains an extremely long 3'-UTR, *in situ* hybridisation results allowed to hypothesise the existence of a correlation between the presence of the brain 5-6 kb 3'-UTR and the observed dendritic localisation of the transcript.

The cytoplasmic polyadenylation element (CPE) is a *cis*- element identified in the 3'-UTRs of specific mRNAs having dendritic localisation which promotes cytoplasmic polyadenylation-induced translation in response to synaptic stimulation. It has been demonstrated that the CPE and its binding protein (CPEB) facilitates mRNA targeting to dendrites (Huang et al., 2003) and triggers "on-site" translation in response to external signals (Wu et al., 1998). Although a perfect consensus sequence for CPEB (UUUUUAU) is not detectable in the region upstream the A_4 hexameric element, two motifs similar to CPE (UUUUAU), highly conserved in all of the six analysed species, are located approximately 250 nt upstream of the hexameric motif of the β-adducin A_4 polyadenylation site (Figure 3.34).

In addition, numerous other proteins that constitute the RNA-granules that carry mRNAs into dendrites have been identified and it has been shown that a subset of these factors, such as heterogeneous nuclear ribonucleoprotein U (hnRNP U), staufen, and pyrimidine tract binding protein-associated splicing factor (PSF), seem to be critical to dendritic RNA transport (Hirokawa, 2006).

It would be interesting to investigate if the CPE-like consensus sequence identified in the 3'-UTR of β-adducin mRNA and CPEB, or other localisation signals and their binding factors are involved in the dendritic localisation of the transcript.

It is known that mRNAs localise to dendrites and the local translation of these mRNAs is regulated in response to neuronal activity (synaptic stimulation). Moreover, recent studies have revealed that protein synthesis derived from mRNAs localised in dendrites contributes to synaptic remodelling and plasticity (Martin and Zukin, 2006).

Previous evidence show that β-adducin transcripts have been found in dendrites of neurons within brain region of high synapse density (such as hippocampus and cortex) and that adducin in neuronal tissues was identified as a constituent of synaptic structures playing a role in the dynamic regulation of spectrin assembly-disassembly processes (Bennett et al., 1988; Seidel et al., 1995). These evidences support the neurophysiologic and behavioural deficiencies observed in β-adducin mutant mice [(Gilligan et al., 1999; Rabenstein et al., 2005; Seidel et al., 1995) and data not shown] and the idea that β-adducin is involved in plastic changes at the synapse that occur as a result of neuronal activity associated with learning and memory.

Further analyses will be focused in the identification of the mechanisms that export β-adducin mRNA to the neuronal processes. In addition, these studies will aim to elucidate the function of this localised transcript in terms of synaptic remodelling and plasticity and on its potential to be translated locally.

3B.10.2 - <u>The different 3'-UTRs could influence the efficiency of translation and the stability of spleen and brain β-adducin mRNA</u> -

The different length of the 3'-UTRs generated by the use of the alternative tissue specific polyadenylation sites could modulate the levels of the spleen and brain-specific β-adducin mRNAs. In fact, the presence or absence of specific regulatory motifs, like AREs or binding sites for regulatory RNAs, in the different forms of the transcripts may influence translation efficiency and stability (Mignone et al., 2002). In addition, the differential concentration of the regulatory binding proteins in different subcellular regions or their different level of expression in the erythroid or neuronal cells could influence the destiny of the same mRNA form in diverse cells or its subcellular location (Derrigo et al., 2000).

The AU-rich elements (AREs) are associated with the regulation of mRNA stability and translation (Barreau et al., 2005). One putative ARE is found

approximately 200 nt upstream the AGUAAA motif of brain-specific polyadenylation signal in a highly-conserved region of all three species, suggesting that it might play a regulatory role in the turnover and/or translation of the β-adducin mRNA in brain.

In addition, bioinformatic analyses using different programs (MiRanda, TargetScan, RegRNA) indicated the presence of several predicted miRNA binding sites in the 3'-UTR of β-adducin of the three species. Target sequences, conserved between humans and rodents, miR34b/c, miR125b, miR149, miR449, were predicted in the 3'-UTR upstream of the proximal spleen poly(A) sites. Binding sites for miR296 and miR342 were detected in the brain-specific 3'-UTR of all the three species. Moreover, brain-specific 3'-UTR predicted target sequences for miR130a/b, miR132, miR324-5p, miR326, miR330, miR331 and 377 were conserved in rodents, while miR337 and miR339 in both mice and humans.

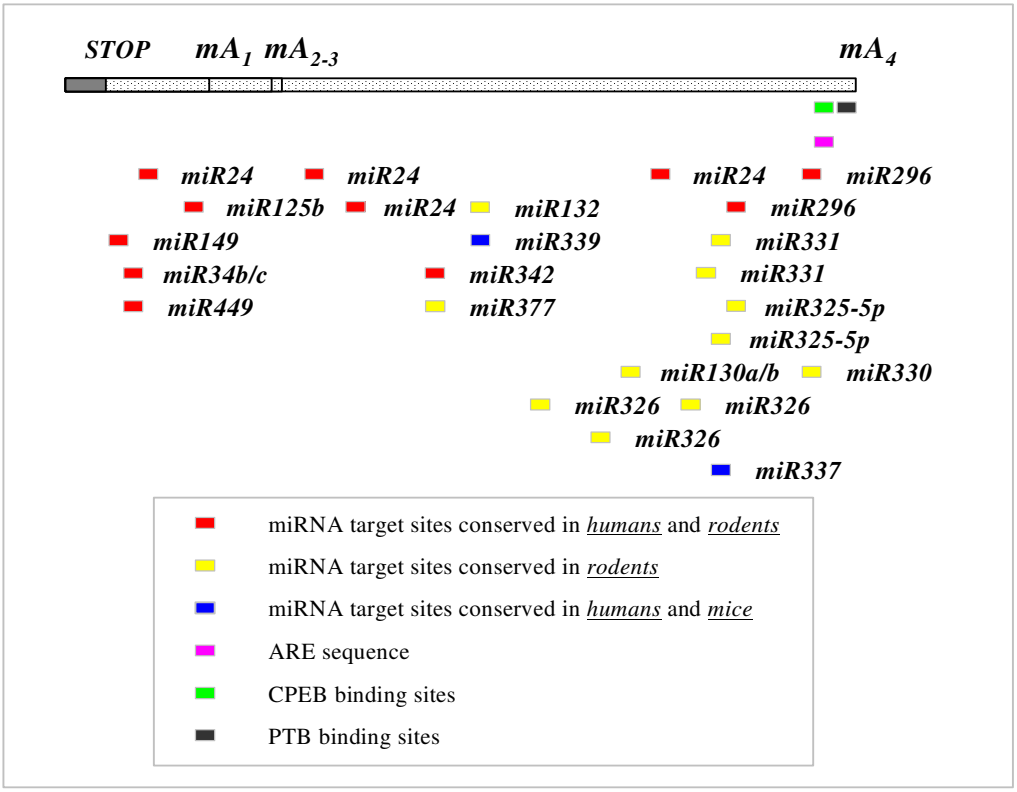

Figure 4.2: Predicted miRNA binding sites within the 3'-UTR of β-adducin. A schematic representation of the last exon (gray box) and the 3'-UTR (dotted box.) of the β-adducin gene indicating the approximate position of the predicted miRNA binding sites (red, yellow and blue boxes). AU-rich element, PTB binding sites and putative consensus sequences for CPEB are indicated with pink, black and green boxes, respectively.

Based on the predicted miRNA target sites we speculate that different concentrations of these regulatory RNAs or their tissue-specific synthesis could lead to a different stability or translational efficiency the spleen and brain β-adducin transcript variants.

The evidence that the miR7 family, miR24, miR34c and miR125b were identified among the miRNA expressed in undifferentiated and mature erythroid cells of mice (Zhan et al., 2007) suggests that they may be able to regulate the metabolism of the spleen-specific forms of β-adducin transcript.

Moreover, miRNAs are abundant in the nervous system, where they play key roles in development and are likely to be important mediators of plasticity (Kosik, 2006). The predicted miR326 and miR331, whose target sites were detected in the brain-specific 3'-UTR of rodents, have been discovered to be expressed in the mouse central nervous system (Tang et al., 2007). In addition, laser capture assays of rat hippocampus cells showed that a large number of the predicted regulatory RNAs (miR7 family, miR24, miR125b, miR130a, miR132, mir296, miR324-5p and miR326) are considered somatodendritic, being localised in both cell body and dendrites of neurons (Kye et al., 2007). These observations suggest that brain-related miRNAs could influence the destiny of the 8-9 kb β-adducin transcript and regulate its expression at the level of dendrites. In fact, mRNAs found in RNA-granules and localised in dendrites exist mainly in a "dormant state" (translational inactive form) and, therefore, an important aspect of mRNA localisation involves the repression of mRNA translation until a specific stimulus activates translation.

Recent studies have uncovered an important role for miRNA-mediated translational regulation in dendrites. Under non-stimulated conditions persistent generation of miRNAs is able to repress translation at the synapse, while neuronal activity leads to the degradation of components of the miRNA processing machinery such that miRNAs are no longer generated, thereby lifting translational repression (Ashraf et al., 2006; Schratt et al., 2006).

These evidences and the *in silico* prediction analysis suggest that the long β-adducin mRNA localised in dendrites, may be maintained in a translationally "dormant form" by the presence of specific miRNAs and activated at synapses in response to a particular stimuli. In addition, activation could be mediated by CPEB binding to the predicted CPE element of the β-adducin 3'-UTR.

The results discussed in this chapter can be considered the starting point of several interesting future experiments aimed to validate or reject the proposed hypotheses regarding the mechanisms that modulate the tissue-specific expression of β-adducin mRNAs, its localisation and function.

REFERENCES

An, X., Salomao, M., Guo, X., Gratzer, W. and Mohandas, N. (2007) Tropomyosin modulates erythrocyte membrane stability. *Blood*, **109**, 1284-1288.

Ansari, A. and Hampsey, M. (2005) A role for the CPF 3'-end processing machinery in RNAP II-dependent gene looping. *Genes Dev*, **19**, 2969-2978.

Ara, T., Lopez, F., Ritchie, W., Benech, P. and Gautheret, D. (2006) Conservation of alternative polyadenylation patterns in mammalian genes. *BMC Genomics*, **7**, 189.

Arhin, G.K., Boots, M., Bagga, P.S., Milcarek, C. and Wilusz, J. (2002) Downstream sequence elements with different affinities for the hnRNP H/H' protein influence the processing efficiency of mammalian polyadenylation signals. *Nucleic Acids Res*, **30**, 1842-1850.

Ashe, M.P., Pearson, L.H. and Proudfoot, N.J. (1997) The HIV-1 5' LTR poly(A) site is inactivated by U1 snRNP interaction with the downstream major splice donor site. *Embo J*, **16**, 5752-5763.

Ashraf, S.I., McLoon, A.L., Sclarsic, S.M. and Kunes, S. (2006) Synaptic protein synthesis associated with memory is regulated by the RISC pathway in Drosophila. *Cell*, **124**, 191-205.

Aster, J.C., Welsh, M.J., Brewer, G.J. and Maisel, H. (1984) Identification of spectrin and protein 4.1-like proteins in mammalian lens. *Biochem Biophys Res Commun*, **119**, 726-734.

Awasthi, S. and Alwine, J.C. (2003) Association of polyadenylation cleavage factor I with U1 snRNP. *Rna*, **9**, 1400-1409.

Azim, A.C., Knoll, J.H., Beggs, A.H. and Chishti, A.H. (1995) Isoform cloning, actin binding, and chromosomal localization of human erythroid dematin, a member of the villin superfamily. *J Biol Chem*, **270**, 17407-17413.

Baek, D., Davis, C., Ewing, B., Gordon, D. and Green, P. (2007) Characterization and predictive discovery of evolutionarily conserved mammalian alternative promoters. *Genome Res*, **17**, 145-155.

Bagga, P.S., Ford, L.P., Chen, F. and Wilusz, J. (1995) The G-rich auxiliary downstream element has distinct sequence and position requirements and mediates efficient 3' end pre-mRNA processing through a trans-acting factor. *Nucleic Acids Res*, **23**, 1625-1631.

Baklouti, F., Huang, S.C., Tang, T.K., Delaunay, J., Marchesi, V.T. and Benz, E.J., Jr. (1996) Asynchronous regulation of splicing events within protein 4.1 pre-mRNA during erythroid differentiation. *Blood*, **87**, 3934-3941.

Barkalow, K., Witke, W., Kwiatkowski, D.J. and Hartwig, J.H. (1996) Coordinated regulation of platelet actin filament barbed ends by gelsolin and capping protein. *J Cell Biol*, **134**, 389-399.

Barreau, C., Paillard, L. and Osborne, H.B. (2005) AU-rich elements and associated factors: are there unifying principles? *Nucleic Acids Res*, **33**, 7138-7150.

Beaudoing, E., Freier, S., Wyatt, J.R., Claverie, J.M. and Gautheret, D. (2000) Patterns of variant polyadenylation signal usage in human genes. *Genome Res*, **10**, 1001-1010.

Beaudoing, E. and Gautheret, D. (2001) Identification of alternate polyadenylation sites and analysis of their tissue distribution using EST data. *Genome Res*, **11**, 1520-1526.

Bennett, V. (1982) The molecular basis for membrane - cytoskeleton association in human erythrocytes. *J Cell Biochem*, **18**, 49-65.

Bennett, V. (1989) The spectrin-actin junction of erythrocyte membrane skeletons. *Biochim Biophys Acta*, **988**, 107-121.

Bennett, V., Gardner, K. and Steiner, J.P. (1988) Brain adducin: a protein kinase C substrate that may mediate site-directed assembly at the spectrin-actin junction. *J Biol Chem*, **263**, 5860-5869.

Bennett, V. and Gilligan, D.M. (1993) The spectrin-based membrane skeleton and micron-scale organization of the plasma membrane. *Annu Rev Cell Biol*, **9**, 27-66.

Bentley, D.L. (2005) Rules of engagement: co-transcriptional recruitment of pre-mRNA processing factors. *Curr Opin Cell Biol*, **17**, 251-256.

Bianchi, G., Ferrari, P. and Staessen, J.A. (2005) Adducin polymorphism: detection and impact on hypertension and related disorders. *Hypertension*, **45**, 331-340.

Birkenmeier, C.S. and Barker, J.E. (2004) Hereditary haemolytic anaemias: unexpected sequelae of mutations in the genes for erythroid membrane skeletal proteins. *J Pathol*, **204**, 450-459.

Black, D.L. (2003) Mechanisms of alternative pre-messenger RNA splicing. *Annu Rev Biochem*, **72**, 291-336.

Blanchard, E.M., Iizuka, K., Christe, M., Conner, D.A., Geisterfer-Lowrance, A., Schoen, F.J., Maughan, D.W., Seidman, C.E. and Seidman, J.G. (1997) Targeted ablation of the murine alpha-tropomyosin gene. *Circ Res*, **81**, 1005-1010.

Brackenridge, S., Ashe, H.L., Giacca, M. and Proudfoot, N.J. (1997) Transcription and polyadenylation in a short human intergenic region. *Nucleic Acids Res*, **25**, 2326-2336.

Brackenridge, S. and Proudfoot, N.J. (2000) Recruitment of a basal polyadenylation factor by the upstream sequence element of the human lamin B2 polyadenylation signal. *Mol Cell Biol*, **20**, 2660-2669.

Calvo, O. and Manley, J.L. (2003) Strange bedfellows: polyadenylation factors at the promoter. *Genes Dev*, **17**, 1321-1327.

Carninci, P. (2007) Constructing the landscape of the mammalian transcriptome. *J Exp Biol*, **210**, 1497-1506.

Carninci, P., Kasukawa, T., Katayama, S., Gough, J., Frith, M.C., Maeda, N., Oyama, R., Ravasi, T., Lenhard, B., Wells, C., Kodzius, R., Shimokawa, K., Bajic, V.B., Brenner, S.E., Batalov, S., Forrest, A.R., Zavolan, M., Davis, M.J., Wilming, L.G., Aidinis, V., Allen, J.E., Ambesi-Impiombato, A., Apweiler, R., Aturaliya, R.N., Bailey, T.L.,

Bansal, M., Baxter, L., Beisel, K.W., Bersano, T., Bono, H., Chalk, A.M., Chiu, K.P., Choudhary, V., Christoffels, A., Clutterbuck, D.R., Crowe, M.L., Dalla, E., Dalrymple, B.P., de Bono, B., Della Gatta, G., di Bernardo, D., Down, T., Engstrom, P., Fagiolini, M., Faulkner, G., Fletcher, C.F., Fukushima, T., Furuno, M., Futaki, S., Gariboldi, M., Georgii-Hemming, P., Gingeras, T.R., Gojobori, T., Green, R.E., Gustincich, S., Harbers, M., Hayashi, Y., Hensch, T.K., Hirokawa, N., Hill, D., Huminiecki, L., Iacono, M., Ikeo, K., Iwama, A., Ishikawa, T., Jakt, M., Kanapin, A., Katoh, M., Kawasawa, Y., Kelso, J., Kitamura, H., Kitano, H., Kollias, G., Krishnan, S.P., Kruger, A., Kummerfeld, S.K., Kurochkin, I.V., Lareau, L.F., Lazarevic, D., Lipovich, L., Liu, J., Liuni, S., McWilliam, S., Madan Babu, M., Madera, M., Marchionni, L., Matsuda, H., Matsuzawa, S., Miki, H., Mignone, F., Miyake, S., Morris, K., Mottagui-Tabar, S., Mulder, N., Nakano, N., Nakauchi, H., Ng, P., Nilsson, R., Nishiguchi, S., Nishikawa, S., Nori, F., Ohara, O., Okazaki, Y., Orlando, V., Pang, K.C., Pavan, W.J., Pavesi, G., Pesole, G., Petrovsky, N., Piazza, S., Reed, J., Reid, J.F., Ring, B.Z., Ringwald, M., Rost, B., Ruan, Y., Salzberg, S.L., Sandelin, A., Schneider, C., Schonbach, C., Sekiguchi, K., Semple, C.A., Seno, S., Sessa, L., Sheng, Y., Shibata, Y., Shimada, H., Shimada, K., Silva, D., Sinclair, B., Sperling, S., Stupka, E., Sugiura, K., Sultana, R., Takenaka, Y., Taki, K., Tammoja, K., Tan, S.L., Tang, S., Taylor, M.S., Tegner, J., Teichmann, S.A., Ueda, H.R., van Nimwegen, E., Verardo, R., Wei, C.L., Yagi, K., Yamanishi, H., Zabarovsky, E., Zhu, S., Zimmer, A., Hide, W., Bult, C., Grimmond, S.M., Teasdale, R.D., Liu, E.T., Brusic, V., Quackenbush, J., Wahlestedt, C., Mattick, J.S., Hume, D.A., Kai, C., Sasaki, D., Tomaru, Y., Fukuda, S., Kanamori-Katayama, M., Suzuki, M., Aoki, J., Arakawa, T., Iida, J., Imamura, K., Itoh, M., Kato, T., Kawaji, H., Kawagashira, N., Kawashima, T., Kojima, M., Kondo, S., Konno, H., Nakano, K., Ninomiya, N., Nishio, T., Okada, M., Plessy, C., Shibata, K., Shiraki, T., Suzuki, S., Tagami, M., Waki, K., Watahiki, A., Okamura-Oho, Y., Suzuki, H., Kawai, J. and Hayashizaki, Y. (2005) The transcriptional landscape of the mammalian genome. *Science*, **309**, 1559-1563.

Carninci, P., Sandelin, A., Lenhard, B., Katayama, S., Shimokawa, K., Ponjavic, J., Semple, C.A., Taylor, M.S., Engstrom, P.G., Frith, M.C., Forrest, A.R., Alkema, W.B., Tan, S.L., Plessy, C., Kodzius, R., Ravasi, T., Kasukawa, T., Fukuda, S., Kanamori-Katayama, M., Kitazume, Y., Kawaji, H., Kai, C., Nakamura, M., Konno, H., Nakano, K., Mottagui-Tabar, S., Arner, P., Chesi, A., Gustincich, S., Persichetti, F., Suzuki, H., Grimmond, S.M., Wells, C.A., Orlando, V., Wahlestedt, C., Liu, E.T., Harbers, M., Kawai, J., Bajic, V.B., Hume, D.A. and Hayashizaki, Y. (2006) Genome-wide analysis of mammalian promoter architecture and evolution. *Nat Genet*, **38**, 626-635.

Carswell, S. and Alwine, J.C. (1989) Efficiency of utilization of the simian virus 40 late polyadenylation site: effects of upstream sequences. *Mol Cell Biol*, **9**, 4248-4258.

Casella, J.F., Maack, D.J. and Lin, S. (1986) Purification and initial characterization of a protein from skeletal muscle that caps the barbed ends of actin filaments. *J Biol Chem*, **261**, 10915-10921.

Casella, J.F. and Torres, M.A. (1994) Interaction of Cap Z with actin. The NH2-terminal domains of the alpha 1 and beta subunits are not required for actin capping, and alpha 1 beta and alpha 2 beta heterodimers bind differentially to actin. *J Biol Chem*, **269**, 6992-6998.

Castelo-Branco, P., Furger, A., Wollerton, M., Smith, C., Moreira, A. and Proudfoot, N. (2004) Polypyrimidine tract binding protein modulates efficiency of polyadenylation. *Mol Cell Biol*, **24**, 4174-4183.

Chabanon, H., Mickleburgh, I. and Hesketh, J. (2004) Zipcodes and postage stamps: mRNA localisation signals and their trans-acting binding proteins. *Brief Funct Genomic Proteomic*, **3**, 240-256.

Chang, S.H. and Low, P.S. (2001) Regulation of the glycophorin C-protein 4.1 membrane-to-skeleton bridge and evaluation of its contribution to erythrocyte membrane stability. *J Biol Chem*, **276**, 22223-22230.

Chasis, J.A., Coulombel, L., McGee, S., Lee, G., Tchernia, G., Conboy, J. and Mohandas, N. (1996) Differential use of protein 4.1 translation initiation sites during erythropoiesis: implications for a mutation-induced stage-specific deficiency of protein 4.1 during erythroid development. *Blood*, **87**, 5324-5331.

Chasis, J.A. and Mohandas, N. (1986) Erythrocyte membrane deformability and stability: two distinct membrane properties that are independently regulated by skeletal protein associations. *J Cell Biol*, **103**, 343-350.

Chasis, J.A. and Mohandas, N. (1992) Red blood cell glycophorins. *Blood*, **80**, 1869-1879.

Chasis, J.A., Prenant, M., Leung, A. and Mohandas, N. (1989) Membrane assembly and remodeling during reticulocyte maturation. *Blood*, **74**, 1112-1120.

Chen, F., MacDonald, C.C. and Wilusz, J. (1995) Cleavage site determinants in the mammalian polyadenylation signal. *Nucleic Acids Res*, **23**, 2614-2620.

Chen, F. and Wilusz, J. (1998) Auxiliary downstream elements are required for efficient polyadenylation of mammalian pre-mRNAs. *Nucleic Acids Res*, **26**, 2891-2898.

Chen, H., Khan, A.A., Liu, F., Gilligan, D.M., Peters, L.L., Messick, J., Haschek-Hock, W.M., Li, X., Ostafin, A.E. and Chishti, A.H. (2007) Combined deletion of mouse dematin-headpiece and beta-adducin exerts a novel effect on the spectrin-actin junctions leading to erythrocyte fragility and hemolytic anemia. *J Biol Chem*, **282**, 4124-4135.

Chen, J.M., Ferec, C. and Cooper, D.N. (2006) A systematic analysis of disease-associated variants in the 3' regulatory regions of human protein-coding genes I: general principles and overview. *Hum Genet*, **120**, 1-21.

Chen, J.M., Ferec, C. and Cooper, D.N. (2006) A systematic analysis of disease-associated variants in the 3' regulatory regions of human protein-coding genes II: the importance of mRNA secondary structure in assessing the functionality of 3' UTR variants. *Hum Genet*, **120**, 301-333.

Chomczynski, P. and Sacchi, N. (1987) Single-step method of RNA isolation by acid guanidinium thiocyanate-phenol-chloroform extraction. *Anal Biochem*, **162**, 156-159.

Chou, Z.F., Chen, F. and Wilusz, J. (1994) Sequence and position requirements for uridylate-rich downstream elements of polyadenylation signals. *Nucleic Acids Res*, **22**, 2525-2531.

Chu, X., Chen, J., Reedy, M.C., Vera, C., Sung, K.L. and Sung, L.A. (2003) E-Tmod capping of actin filaments at the slow-growing end is required to establish mouse embryonic circulation. *Am J Physiol Heart Circ Physiol*, **284**, H1827-1838.

Chung, C.T., Niemela, S.L. and Miller, R.H. (1989) One-step preparation of competent Escherichia coli: transformation and storage of bacterial cells in the same solution. *Proc Natl Acad Sci U S A*, **86**, 2172-2175.

Citterio, L., Azzani, T., Duga, S. and Bianchi, G. (1999) Genomic organization of the human gamma adducin gene. *Biochem Biophys Res Commun*, **266**, 110-114.

Clark, J.I., Matsushima, H., David, L.L. and Clark, J.M. (1999) Lens cytoskeleton and transparency: a model. *Eye*, **13 (Pt 3b)**, 417-424.

Coleman, T.R., Fishkind, D.J., Mooseker, M.S. and Morrow, J.S. (1989) Functional diversity among spectrin isoforms. *Cell Motil Cytoskeleton*, **12**, 225-247.

Conboy, J.G., Chan, J.Y., Chasis, J.A., Kan, Y.W. and Mohandas, N. (1991) Tissue- and development-specific alternative RNA splicing regulates expression of multiple isoforms of erythroid membrane protein 4.1. *J Biol Chem*, **266**, 8273-8280.

Conne, B., Stutz, A. and Vassalli, J.D. (2000) The 3' untranslated region of messenger RNA: A molecular 'hotspot' for pathology? *Nat Med*, **6**, 637-641.

Connelly, S. and Manley, J.L. (1988) A functional mRNA polyadenylation signal is required for transcription termination by RNA polymerase II. *Genes Dev*, **2**, 440-452.

Consortium, I.H.G.S. (2004) Finishing the euchromatic sequence of the human genome. *Nature*, **431**, 931-945.

Conway, L. and Wickens, M. (1987) Analysis of mRNA 3' end formation by modification interference: the only modifications which prevent processing lie in AAUAAA and the poly(A) site. *Embo J*, **6**, 4177-4184.

Cooke, C. and Alwine, J.C. (1996) The cap and the 3' splice site similarly affect polyadenylation efficiency. *Mol Cell Biol*, **16**, 2579-2584.

Cooke, C., Hans, H. and Alwine, J.C. (1999) Utilization of splicing elements and polyadenylation signal elements in the coupling of polyadenylation and last-intron removal. *Mol Cell Biol*, **19**, 4971-4979.

Cooper, J.A. (2002) Actin dynamics: tropomyosin provides stability. *Curr Biol*, **12**, R523-525.

Cooper, S.J., Trinklein, N.D., Anton, E.D., Nguyen, L. and Myers, R.M. (2006) Comprehensive analysis of transcriptional promoter structure and function in 1% of the human genome. *Genome Res*, **16**, 1-10.

Cramer, P., Pesce, C.G., Baralle, F.E. and Kornblihtt, A.R. (1997) Functional association between promoter structure and transcript alternative splicing. *Proc Natl Acad Sci U S A*, **94**, 11456-11460.

Crawford, K., Flick, R., Close, L., Shelly, D., Paul, R., Bove, K., Kumar, A. and Lessard, J. (2002) Mice lacking skeletal muscle actin show reduced muscle strength and growth deficits and die during the neonatal period. *Mol Cell Biol*, **22**, 5887-5896.

Cusi, D., Barlassina, C., Azzani, T., Casari, G., Citterio, L., Devoto, M., Glorioso, N., Lanzani, C., Manunta, P., Righetti, M., Rivera, R., Stella, P., Troffa, C., Zagato, L. and Bianchi, G. (1997) Polymorphisms of alpha-adducin and salt sensitivity in patients with essential hypertension. *Lancet*, **349**, 1353-1357.

Damberg, M. (2005) Transcription factor AP-2 and monoaminergic functions in the central nervous system. *J Neural Transm*, **112**, 1281-1296.

Dantonel, J.C., Murthy, K.G., Manley, J.L. and Tora, L. (1997) Transcription factor TFIID recruits factor CPSF for formation of 3' end of mRNA. *Nature*, **389**, 399-402.

Delaunay, J. (2007) The molecular basis of hereditary red cell membrane disorders. *Blood Rev*, **21**, 1-20.

Derick, L.H., Liu, S.C., Chishti, A.H. and Palek, J. (1992) Protein immunolocalization in the spread erythrocyte membrane skeleton. *Eur J Cell Biol*, **57**, 317-320.

Derrigo, M., Cestelli, A., Savettieri, G. and Di Liegro, I. (2000) RNA-protein interactions in the control of stability and localization of messenger RNA (review). *Int J Mol Med*, **5**, 111-123.

Dichtl, B., Blank, D., Sadowski, M., Hubner, W., Weiser, S. and Keller, W. (2002) Yhh1p/Cft1p directly links poly(A) site recognition and RNA polymerase II transcription termination. *Embo J*, **21**, 4125-4135.

DiNubile, M.J., Cassimeris, L., Joyce, M. and Zigmond, S.H. (1995) Actin filament barbed-end capping activity in neutrophil lysates: the role of capping protein-beta 2. *Mol Biol Cell*, **6**, 1659-1671.

Dong, L., Chapline, C., Mousseau, B., Fowler, L., Ramsay, K., Stevens, J.L. and Jaken, S. (1995) 35H, a sequence isolated as a protein kinase C binding protein, is a novel member of the adducin family. *J Biol Chem*, **270**, 25534-25540.

Duan, Z.J., Fang, X., Rohde, A., Han, H., Stamatoyannopoulos, G. and Li, Q. (2002) Developmental specificity of recruitment of TBP to the TATA box of the human gamma-globin gene. *Proc Natl Acad Sci U S A*, **99**, 5509-5514.

Dye, M.J. and Proudfoot, N.J. (1999) Terminal exon definition occurs cotranscriptionally and promotes termination of RNA polymerase II. *Mol Cell*, **3**, 371-378.

Edwalds-Gilbert, G., Veraldi, K.L. and Milcarek, C. (1997) Alternative poly(A) site selection in complex transcription units: means to an end? *Nucleic Acids Res*, **25**, 2547-2561.

Fairbanks, G., Steck, T.L. and Wallach, D.F. (1971) Electrophoretic analysis of the major polypeptides of the human erythrocyte membrane. *Biochemistry*, **10**, 2606-2617.

Faquin, W.C., Husain, A., Hung, J. and Branton, D. (1988) An immunoreactive form of erythrocyte protein 4.9 is present in non-erythroid cells. *Eur J Cell Biol*, **46**, 168-175.

Flaherty, S.M., Fortes, P., Izaurralde, E., Mattaj, I.W. and Gilmartin, G.M. (1997) Participation of the nuclear cap binding complex in pre-mRNA 3' processing. *Proc Natl Acad Sci U S A*, **94**, 11893-11898.

Fowler, V.M. (1990) Tropomodulin: a cytoskeletal protein that binds to the end of erythrocyte tropomyosin and inhibits tropomyosin binding to actin. *J Cell Biol*, **111**, 471-481.

Fowler, V.M. (1996) Regulation of actin filament length in erythrocytes and striated muscle. *Curr Opin Cell Biol*, **8**, 86-96.

Fowler, V.M. (1997) Capping actin filament growth: tropomodulin in muscle and nonmuscle cells. *Soc Gen Physiol Ser*, **52**, 79-89.

Fowler, V.M. and Bennett, V. (1984) Erythrocyte membrane tropomyosin. Purification and properties. *J Biol Chem*, **259**, 5978-5989.

Fritz-Six, K.L., Cox, P.R., Fischer, R.S., Xu, B., Gregorio, C.C., Zoghbi, H.Y. and Fowler, V.M. (2003) Aberrant myofibril assembly in tropomodulin1 null mice leads to aborted heart development and embryonic lethality. *J Cell Biol*, **163**, 1033-1044.

Gallagher, P.G. (2003) Regulation of erythrocyte membrane protein gene expression. *Curr Opin Hematol*, **10**, 115-122.

Gardner, K. and Bennett, V. (1986) A new erythrocyte membrane-associated protein with calmodulin binding activity. Identification and purification. *J Biol Chem*, **261**, 1339-1348.

Gardner, K. and Bennett, V. (1987) Modulation of spectrin-actin assembly by erythrocyte adducin. *Nature*, **328**, 359-362.

Gautheret, D., Poirot, O., Lopez, F., Audic, S. and Claverie, J.M. (1998) Alternate polyadenylation in human mRNAs: a large-scale analysis by EST clustering. *Genome Res*, **8**, 524-530.

Gershenzon, N.I. and Ioshikhes, I.P. (2005) Synergy of human Pol II core promoter elements revealed by statistical sequence analysis. *Bioinformatics*, **21**, 1295-1300.

Gil, A. and Proudfoot, N.J. (1987) Position-dependent sequence elements downstream of AAUAAA are required for efficient rabbit beta-globin mRNA 3' end formation. *Cell*, **49**, 399-406.

Gilligan, D.M. and Bennett, V. (1993) The junctional complex of the membrane skeleton. *Semin Hematol*, **30**, 74-83.

Gilligan, D.M., Lieman, J. and Bennett, V. (1995) Assignment of the human beta-adducin gene (ADD2) to 2p13-p14 by in situ hybridization. *Genomics*, **28**, 610-612.

Gilligan, D.M., Lozovatsky, L., Gwynn, B., Brugnara, C., Mohandas, N. and Peters, L.L. (1999) Targeted disruption of the beta adducin gene (Add2) causes red blood cell spherocytosis in mice. *Proc Natl Acad Sci U S A*, **96**, 10717-10722.

Gilligan, D.M., Lozovatsky, L. and Silberfein, A. (1997) Organization of the human beta-adducin gene (ADD2). *Genomics*, **43**, 141-148.

Gilmartin, G.M., McDevitt, M.A. and Nevins, J.R. (1988) Multiple factors are required for specific RNA cleavage at a poly(A) addition site. *Genes Dev*, **2**, 578-587.

Gotoh, H., Okumura, N., Yagi, T., Okumura, A., Shima, T. and Nagai, K. (2006) Fyn-induced phosphorylation of beta-adducin at tyrosine 489 and its role in their subcellular localization. *Biochem Biophys Res Commun*, **346**, 600-605.

Graber, J.H., Cantor, C.R., Mohr, S.C. and Smith, T.F. (1999) In silico detection of control signals: mRNA 3'-end-processing sequences in diverse species. *Proc Natl Acad Sci U S A*, **96**, 14055-14060.

Gunderson, S.I., Polycarpou-Schwarz, M. and Mattaj, I.W. (1998) U1 snRNP inhibits pre-mRNA polyadenylation through a direct interaction between U1 70K and poly(A) polymerase. *Mol Cell*, **1**, 255-264.

Gunning, P.W., Schevzov, G., Kee, A.J. and Hardeman, E.C. (2005) Tropomyosin isoforms: divining rods for actin cytoskeleton function. *Trends Cell Biol*, **15**, 333-341.

Gustincich, S., Sandelin, A., Plessy, C., Katayama, S., Simone, R., Lazarevic, D., Hayashizaki, Y. and Carninci, P. (2006) The complexity of the mammalian transcriptome. *J Physiol*, **575**, 321-332.

Haile, D.J. (1999) Regulation of genes of iron metabolism by the iron-response proteins. *Am J Med Sci*, **318**, 230-240.

Hall-Pogar, T., Liang, S., Hague, L.K. and Lutz, C.S. (2007) Specific trans-acting proteins interact with auxiliary RNA polyadenylation elements in the COX-2 3'-UTR. *Rna*, **13**, 1103-1115.

Hall-Pogar, T., Zhang, H., Tian, B. and Lutz, C.S. (2005) Alternative polyadenylation of cyclooxygenase-2. *Nucleic Acids Res*, **33**, 2565-2579.

Hart, R.P., McDevitt, M.A. and Nevins, J.R. (1985) Poly(A) site cleavage in a HeLa nuclear extract is dependent on downstream sequences. *Cell*, **43**, 677-683.

Hassoun, H., Hanada, T., Lutchman, M., Sahr, K.E., Palek, J., Hanspal, M. and Chishti, A.H. (1998) Complete deficiency of glycophorin A in red blood cells from mice with targeted inactivation of the band 3 (AE1) gene. *Blood*, **91**, 2146-2151.

Hirokawa, N. (2006) mRNA transport in dendrites: RNA granules, motors, and tracks. *J Neurosci*, **26**, 7139-7142.

Hirose, Y. and Manley, J.L. (1998) RNA polymerase II is an essential mRNA polyadenylation factor. *Nature*, **395**, 93-96.

Hoffman, R., E. J Benz, S.J Shattil, B.Furie, H.J. Cohel, L.E. Silberstein, and P. PcGlove. (2000) *Hematology. Basic Principle and Practice*. Churchill, Philadelphia.

Hook, J., Lemckert, F., Qin, H., Schevzov, G. and Gunning, P. (2004) Gamma tropomyosin gene products are required for embryonic development. *Mol Cell Biol*, **24**, 2318-2323.

Hsieh, S.Y., Yang, P.Y., Ou, J.T., Chu, C.M. and Liaw, Y.F. (1994) Polyadenylation of the mRNA of hepatitis delta virus is dependent on the structure of the nascent RNA and regulated by the small or large delta antigen. *Nucleic Acids Res*, **22**, 391-396.

Hu, J., Lutz, C.S., Wilusz, J. and Tian, B. (2005) Bioinformatic identification of candidate cis-regulatory elements involved in human mRNA polyadenylation. *Rna*, **11**, 1485-1493.

Huang, Y. and Carmichael, G.G. (1996) Role of polyadenylation in nucleocytoplasmic transport of mRNA. *Mol Cell Biol*, **16**, 1534-1542.

Huang, Y.S., Carson, J.H., Barbarese, E. and Richter, J.D. (2003) Facilitation of dendritic mRNA transport by CPEB. *Genes Dev*, **17**, 638-653.

Hughes, C.A. and Bennett, V. (1995) Adducin: a physical model with implications for function in assembly of spectrin-actin complexes. *J Biol Chem*, **270**, 18990-18996.

Husain-Chishti, A., Faquin, W., Wu, C.C. and Branton, D. (1989) Purification of erythrocyte dematin (protein 4.9) reveals an endogenous protein kinase that modulates actin-bundling activity. *J Biol Chem*, **264**, 8985-8991.

Husain-Chishti, A., Levin, A. and Branton, D. (1988) Abolition of actin-bundling by phosphorylation of human erythrocyte protein 4.9. *Nature*, **334**, 718-721.

Ingley, E., Tilbrook, P.A. and Klinken, S.P. (2004) New insights into the regulation of erythroid cells. *IUBMB Life*, **56**, 177-184.

Ireland, M., Lieska, N. and Maisel, H. (1983) Lens actin: purification and localization. *Exp Eye Res*, **37**, 393-408.

Iseli, C., Stevenson, B.J., de Souza, S.J., Samaia, H.B., Camargo, A.A., Buetow, K.H., Strausberg, R.L., Simpson, A.J., Bucher, P. and Jongeneel, C.V. (2002) Long-range heterogeneity at the 3' ends of human mRNAs. *Genome Res*, **12**, 1068-1074.

Jareborg, N., Birney, E. and Durbin, R. (1999) Comparative analysis of noncoding regions of 77 orthologous mouse and human gene pairs. *Genome Res*, **9**, 815-824.

Jennings, M.L. (1989) Structure and function of the red blood cell anion exchange protein. *Prog Clin Biol Res*, **292**, 327-338.

Job, C. and Eberwine, J. (2001) Localization and translation of mRNA in dendrites and axons. *Nat Rev Neurosci*, **2**, 889-898.

Joshi, R., Gilligan, D.M., Otto, E., McLaughlin, T. and Bennett, V. (1991) Primary structure and domain organization of human alpha and beta adducin. *J Cell Biol*, **115**, 665-675.

Kaiser, H.W., O'Keefe, E. and Bennett, V. (1989) Adducin: Ca++-dependent association with sites of cell-cell contact. *J Cell Biol*, **109**, 557-569.

Khanna, R., Chang, S.H., Andrabi, S., Azam, M., Kim, A., Rivera, A., Brugnara, C., Low, P.S., Liu, S.C. and Chishti, A.H. (2002) Headpiece domain of dematin is required for the stability of the erythrocyte membrane. *Proc Natl Acad Sci U S A*, **99**, 6637-6642.

Kibbelaar, M.A., Ramaekers, F.C., Ringens, P.J., Selten-Versteegen, A.M., Poels, L.G., Jap, P.H., van Rossum, A.L., Feltkamp, T.E. and Bloemendal, H. (1980) Is actin in eye lens a possible factor in visual accomodation? *Nature*, **285**, 506-508.

Kim, A.C., Azim, A.C. and Chishti, A.H. (1998) Alternative splicing and structure of the human erythroid dematin gene. *Biochim Biophys Acta*, **1398**, 382-386.

Kimura, K., Wakamatsu, A., Suzuki, Y., Ota, T., Nishikawa, T., Yamashita, R., Yamamoto, J., Sekine, M., Tsuritani, K., Wakaguri, H., Ishii, S., Sugiyama, T., Saito, K., Isono, Y., Irie, R., Kushida, N., Yoneyama, T., Otsuka, R., Kanda, K., Yokoi, T., Kondo, H., Wagatsuma, M., Murakawa, K., Ishida, S., Ishibashi, T., Takahashi-Fujii, A., Tanase, T., Nagai, K., Kikuchi, H., Nakai, K., Isogai, T. and Sugano, S. (2006) Diversification of transcriptional modulation: large-scale identification and characterization of putative alternative promoters of human genes. *Genome Res*, **16**, 55-65.

Klasens, B.I., Thiesen, M., Virtanen, A. and Berkhout, B. (1999) The ability of the HIV-1 AAUAAA signal to bind polyadenylation factors is controlled by local RNA structure. *Nucleic Acids Res*, **27**, 446-454.

Konarska, M.M. (1998) Recognition of the 5' splice site by the spliceosome. *Acta Biochim Pol*, **45**, 869-881.

Kornblihtt, A.R. (2005) Promoter usage and alternative splicing. *Curr Opin Cell Biol*, **17**, 262-268.

Kosik, K.S. (2006) The neuronal microRNA system. *Nat Rev Neurosci*, **7**, 911-920.

Kostyukova, A.S., Choy, A. and Rapp, B.A. (2006) Tropomodulin binds two tropomyosins: a novel model for actin filament capping. *Biochemistry*, **45**, 12068-12075.

Kreis, T. and Vale, R. (1999) *Guidebook to the cytoskeletal and Motor Proteins*.

Kubo, T., Wada, T., Yamaguchi, Y., Shimizu, A. and Handa, H. (2006) Knock-down of 25 kDa subunit of cleavage factor Im in Hela cells alters alternative polyadenylation within 3'-UTRs. *Nucleic Acids Res*, **34**, 6264-6271.

Kuhlman, P.A. and Fowler, V.M. (1997) Purification and characterization of an alpha 1 beta 2 isoform of CapZ from human erythrocytes: cytosolic location and inability to bind to Mg2+ ghosts suggest that erythrocyte actin filaments are capped by adducin. *Biochemistry*, **36**, 13461-13472.

Kuhlman, P.A., Hughes, C.A., Bennett, V. and Fowler, V.M. (1996) A new function for adducin. Calcium/calmodulin-regulated capping of the barbed ends of actin filaments. *J Biol Chem*, **271**, 7986-7991.

Kumar, A., Crawford, K., Close, L., Madison, M., Lorenz, J., Doetschman, T., Pawlowski, S., Duffy, J., Neumann, J., Robbins, J., Boivin, G.P., O'Toole, B.A. and Lessard, J.L. (1997) Rescue of cardiac alpha-actin-deficient mice by enteric smooth muscle gamma-actin. *Proc Natl Acad Sci U S A*, **94**, 4406-4411.

Kyburz, A., Friedlein, A., Langen, H. and Keller, W. (2006) Direct interactions between subunits of CPSF and the U2 snRNP contribute to the coupling of pre-mRNA 3' end processing and splicing. *Mol Cell*, **23**, 195-205.

Kye, M.J., Liu, T., Levy, S.F., Xu, N.L., Groves, B.B., Bonneau, R., Lao, K. and Kosik, K.S. (2007) Somatodendritic microRNAs identified by laser capture and multiplex RT-PCR. *Rna*, **13**, 1224-1234.

Landry, J.R., Mager, D.L. and Wilhelm, B.T. (2003) Complex controls: the role of alternative promoters in mammalian genomes. *Trends Genet*, **19**, 640-648.

Lee, A., Fischer, R.S. and Fowler, V.M. (2000) Stabilization and remodeling of the membrane skeleton during lens fiber cell differentiation and maturation. *Dev Dyn*, **217**, 257-270.

Legendre, M. and Gautheret, D. (2003) Sequence determinants in human polyadenylation site selection. *BMC Genomics*, **4**, 7.

Liang, F., Holt, I., Pertea, G., Karamycheva, S., Salzberg, S.L. and Quackenbush, J. (2000) Gene index analysis of the human genome estimates approximately 120,000 genes. *Nat Genet*, **25**, 239-240.

Lin, B., Nasir, J., McDonald, H., Graham, R., Rommens, J.M., Goldberg, Y.P. and Hayden, M.R. (1995) Genomic organization of the human alpha-adducin gene and its alternately spliced isoforms. *Genomics*, **25**, 93-99.

Lin, J.J., Chou, C.S. and Lin, J.L. (1985) Monoclonal antibodies against chicken tropomyosin isoforms: production, characterization, and application. *Hybridoma*, **4**, 223-242.

Lin, J.J., Warren, K.S., Wamboldt, D.D., Wang, T. and Lin, J.L. (1997) Tropomyosin isoforms in nonmuscle cells. *Int Rev Cytol*, **170**, 1-38.

Liu, S.C., Derick, L.H. and Palek, J. (1987) Visualization of the hexagonal lattice in the erythrocyte membrane skeleton. *J Cell Biol*, **104**, 527-536.

Lo, W.K., Wen, X.J. and Zhou, C.J. (2003) Microtubule configuration and membranous vesicle transport in elongating fiber cells of the rat lens. *Exp Eye Res*, **77**, 615-626.

Lodish, H., Berk A., Matsudaira P, Kaiser C. A., Krieger M. Scott M. P, Zipursky L., and Darnell J. (2003) *Molecular Cell Biology*. W.H. Freeman Company.

Logan, J., Falck-Pedersen, E., Darnell, J.E., Jr. and Shenk, T. (1987) A poly(A) addition site and a downstream termination region are required for efficient cessation of transcription by RNA polymerase II in the mouse beta maj-globin gene. *Proc Natl Acad Sci U S A*, **84**, 8306-8310.

Logette, E., Wotawa, A., Solier, S., Desoche, L., Solary, E. and Corcos, L. (2003) The human caspase-2 gene: alternative promoters, pre-mRNA splicing and AUG usage direct isoform-specific expression. *Oncogene*, **22**, 935-946.

Lopez, F., Granjeaud, S., Ara, T., Ghattas, B. and Gautheret, D. (2006) The disparate nature of "intergenic" polyadenylation sites. *Rna*, **12**, 1794-1801.

Low, T.Y., Seow, T.K. and Chung, M.C. (2002) Separation of human erythrocyte membrane associated proteins with one-dimensional and two-dimensional gel electrophoresis followed by identification with matrix-assisted laser desorption/ionization-time of flight mass spectrometry. *Proteomics*, **2**, 1229-1239.

Lutz, C.S. and Alwine, J.C. (1994) Direct interaction of the U1 snRNP-A protein with the upstream efficiency element of the SV40 late polyadenylation signal. *Genes Dev*, **8**, 576-586.

Lutz, C.S., Cooke, C., O'Connor, J.P., Kobayashi, R. and Alwine, J.C. (1998) The snRNP-free U1A (SF-A) complex(es): identification of the largest subunit as PSF, the polypyrimidine-tract binding protein-associated splicing factor. *Rna*, **4**, 1493-1499.

Lutz, C.S., Murthy, K.G., Schek, N., O'Connor, J.P., Manley, J.L. and Alwine, J.C. (1996) Interaction between the U1 snRNP-A protein and the 160-kD subunit of cleavage-polyadenylation specificity factor increases polyadenylation efficiency in vitro. *Genes Dev*, **10**, 325-337.

Makalowski, W. and Boguski, M.S. (1998) Evolutionary parameters of the transcribed mammalian genome: an analysis of 2,820 orthologous rodent and human sequences. *Proc Natl Acad Sci U S A*, **95**, 9407-9412.

Mangus, D.A., Evans, M.C. and Jacobson, A. (2003) Poly(A)-binding proteins: multifunctional scaffolds for the post-transcriptional control of gene expression. *Genome Biol*, **4**, 223.

Manley, J.L. (1988) Polyadenylation of mRNA precursors. *Biochim Biophys Acta*, **950**, 1-12.

Marfatia, S.M., Leu, R.A., Branton, D. and Chishti, A.H. (1995) Identification of the protein 4.1 binding interface on glycophorin C and p55, a homologue of the Drosophila discs-large tumor suppressor protein. *J Biol Chem*, **270**, 715-719.

Marfatia, S.M., Lue, R.A., Branton, D. and Chishti, A.H. (1994) In vitro binding studies suggest a membrane-associated complex between erythroid p55, protein 4.1, and glycophorin C. *J Biol Chem*, **269**, 8631-8634.

Marfatia, S.M., Morais-Cabral, J.H., Kim, A.C., Byron, O. and Chishti, A.H. (1997) The PDZ domain of human erythrocyte p55 mediates its binding to the cytoplasmic carboxyl

terminus of glycophorin C. Analysis of the binding interface by in vitro mutagenesis. *J Biol Chem*, **272**, 24191-24197.

Marro, M.L., Scremin, O.U., Jordan, M.C., Huynh, L., Porro, F., Roos, K.P., Gajovic, S., Baralle, F.E. and Muro, A.F. (2000) Hypertension in beta-adducin deficient mice. *Hypertension*, **36**, 449-453.

Martin, K.C. (2004) Local protein synthesis during axon guidance and synaptic plasticity. *Curr Opin Neurobiol*, **14**, 305-310.

Martin, K.C. and Zukin, R.S. (2006) RNA trafficking and local protein synthesis in dendrites: an overview. *J Neurosci*, **26**, 7131-7134.

Mason, P.J., Elkington, J.A., Lloyd, M.M., Jones, M.B. and Williams, J.G. (1986) Mutations downstream of the polyadenylation site of a Xenopus beta-globin mRNA affect the position but not the efficiency of 3' processing. *Cell*, **46**, 263-270.

Matsuoka, Y., Li, X. and Bennett, V. (1998) Adducin is an in vivo substrate for protein kinase C: phosphorylation in the MARCKS-related domain inhibits activity in promoting spectrin-actin complexes and occurs in many cells, including dendritic spines of neurons. *J Cell Biol*, **142**, 485-497.

Matsuoka, Y., Li, X. and Bennett, V. (2000) Adducin: structure, function and regulation. *Cell Mol Life Sci*, **57**, 884-895.

Matsushima, H., David, L.L., Hiraoka, T. and Clark, J.I. (1997) Loss of cytoskeletal proteins and lens cell opacification in the selenite cataract model. *Exp Eye Res*, **64**, 387-395.

McCracken, S., Fong, N., Yankulov, K., Ballantyne, S., Pan, G., Greenblatt, J., Patterson, S.D., Wickens, M. and Bentley, D.L. (1997) The C-terminal domain of RNA polymerase II couples mRNA processing to transcription. *Nature*, **385**, 357-361.

McDevitt, M.A., Hart, R.P., Wong, W.W. and Nevins, J.R. (1986) Sequences capable of restoring poly(A) site function define two distinct downstream elements. *Embo J*, **5**, 2907-2913.

McGrath, K.E. and Palis, J. (2005) Hematopoiesis in the yolk sac: more than meets the eye. *Exp Hematol*, **33**, 1021-1028.

McLauchlan, J., Gaffney, D., Whitton, J.L. and Clements, J.B. (1985) The consensus sequence YGTGTTYY located downstream from the AATAAA signal is required for efficient formation of mRNA 3' termini. *Nucleic Acids Res*, **13**, 1347-1368.

Menko, S.A. (2002) Lens ephitelial cell differentiation. *Experimental Eye Research*, **75**, 485-490.

Meyer, S., Temme, C. and Wahle, E. (2004) Messenger RNA turnover in eukaryotes: pathways and enzymes. *Crit Rev Biochem Mol Biol*, **39**, 197-216.

Mignone, F., Gissi, C., Liuni, S. and Pesole, G. (2002) Untranslated regions of mRNAs. *Genome Biol*, **3**, REVIEWS0004.

Millevoi, S., Loulergue, C., Dettwiler, S., Karaa, S.Z., Keller, W., Antoniou, M. and Vagner, S. (2006) An interaction between U2AF 65 and CF I(m) links the splicing and 3' end processing machineries. *Embo J*, **25**, 4854-4864.

Mische, S.M., Mooseker, M.S. and Morrow, J.S. (1987) Erythrocyte adducin: a calmodulin-regulated actin-bundling protein that stimulates spectrin-actin binding. *J Cell Biol*, **105**, 2837-2845.

Mohandas, N. and Chasis, J.A. (1993) Red blood cell deformability, membrane material properties and shape: regulation by transmembrane, skeletal and cytosolic proteins and lipids. *Semin Hematol*, **30**, 171-192.

Mohandas, N. and Evans, E. (1994) Mechanical properties of the red cell membrane in relation to molecular structure and genetic defects. *Annu Rev Biophys Biomol Struct*, **23**, 787-818.

Mohandas, N. and Gascard, P. (1999) What do mouse gene knockouts tell us about the structure and function of the red cell membrane? *Baillieres Best Pract Res Clin Haematol*, **12**, 605-620.

Moore, C.L., Skolnik-David, H. and Sharp, P.A. (1986) Analysis of RNA cleavage at the adenovirus-2 L3 polyadenylation site. *Embo J*, **5**, 1929-1938.

Moreira, A., Takagaki, Y., Brackenridge, S., Wollerton, M., Manley, J.L. and Proudfoot, N.J. (1998) The upstream sequence element of the C2 complement poly(A) signal activates mRNA 3' end formation by two distinct mechanisms. *Genes Dev*, **12**, 2522-2534.

Moreira, A., Wollerton, M., Monks, J. and Proudfoot, N.J. (1995) Upstream sequence elements enhance poly(A) site efficiency of the C2 complement gene and are phylogenetically conserved. *Embo J*, **14**, 3809-3819.

Mortz, E., Krogh, T.N., Vorum, H. and Gorg, A. (2001) Improved silver staining protocols for high sensitivity protein identification using matrix-assisted laser desorption/ionization-time of flight analysis. *Proteomics*, **1**, 1359-1363.

Mousa, G.Y., Creighton, M.O. and Trevithick, J.R. (1979) Eye lens opacity in cortical cataracts associated with actin-related globular degeneration. *Exp Eye Res*, **29**, 379-391.

Muro, A.F., Marro, M.L., Gajovic, S., Porro, F., Luzzatto, L. and Baralle, F.E. (2000) Mild spherocytic hereditary elliptocytosis and altered levels of alpha- and gamma-adducins in beta-adducin deficient mice. *Blood*, **95**, 3978-3985.

Murthy, K.G. and Manley, J.L. (1995) The 160-kD subunit of human cleavage-polyadenylation specificity factor coordinates pre-mRNA 3'-end formation. *Genes Dev*, **9**, 2672-2683.

Nag, A., Narsinh, K. and Martinson, H.G. (2007) The poly(A)-dependent transcriptional pause is mediated by CPSF acting on the body of the polymerase. *Nat Struct Mol Biol*, **14**, 662-669.

Nagasaki, H., Arita, M., Nishizawa, T., Suwa, M. and Gotoh, O. (2005) Species-specific variation of alternative splicing and transcriptional initiation in six eukaryotes. *Gene*, **364**, 53-62.

Natalizio, B.J., Muniz, L.C., Arhin, G.K., Wilusz, J. and Lutz, C.S. (2002) Upstream elements present in the 3'-untranslated region of collagen genes influence the processing efficiency of overlapping polyadenylation signals. *J Biol Chem*, **277**, 42733-42740.

Nehls, V., Drenckhahn, D., Joshi, R. and Bennett, V. (1991) Adducin in erythrocyte precursor cells of rats and humans: expression and compartmentalization. *Blood*, **78**, 1692-1696.

Niwa, M., MacDonald, C.C. and Berget, S.M. (1992) Are vertebrate exons scanned during splice-site selection? *Nature*, **360**, 277-280.

Nomoto, S., Tatematsu, Y., Takahashi, T. and Osada, H. (1999) Cloning and characterization of the alternative promoter regions of the human LIMK2 gene responsible for alternative transcripts with tissue-specific expression. *Gene*, **236**, 259-271.

Nunomura, W., Takakuwa, Y., Parra, M., Conboy, J. and Mohandas, N. (2000) Regulation of protein 4.1R, p55, and glycophorin C ternary complex in human erythrocyte membrane. *J Biol Chem*, **275**, 24540-24546.

O'Sullivan, J.M., Tan-Wong, S.M., Morillon, A., Lee, B., Coles, J., Mellor, J. and Proudfoot, N.J. (2004) Gene loops juxtapose promoters and terminators in yeast. *Nat Genet*, **36**, 1014-1018.

Orkin, S.H. (1992) GATA-binding transcription factors in hematopoietic cells. *Blood*, **80**, 575-581.

Orozco, I.J., Kim, S.J. and Martinson, H.G. (2002) The poly(A) signal, without the assistance of any downstream element, directs RNA polymerase II to pause in vivo and then to release stochastically from the template. *J Biol Chem*, **277**, 42899-42911.

Osheim, Y.N., Proudfoot, N.J. and Beyer, A.L. (1999) EM visualization of transcription by RNA polymerase II: downstream termination requires a poly(A) signal but not transcript cleavage. *Mol Cell*, **3**, 379-387.

Oyama, M., Itagaki, C., Hata, H., Suzuki, Y., Izumi, T., Natsume, T., Isobe, T. and Sugano, S. (2004) Analysis of small human proteins reveals the translation of upstream open reading frames of mRNAs. *Genome Res*, **14**, 2048-2052.

Pecci, A., Viegas, L.R., Baranao, J.L. and Beato, M. (2001) Promoter choice influences alternative splicing and determines the balance of isoforms expressed from the mouse bcl-X gene. *J Biol Chem*, **276**, 21062-21069.

Perng, M.D. and Quinlan, R.A. (2005) Seeing is believing! The optical properties of the eye lens are dependent upon a functional intermediate filament cytoskeleton. *Exp Cell Res*, **305**, 1-9.

Pesole, G., Bernardi, G. and Saccone, C. (1999) Isochore specificity of AUG initiator context of human genes. *FEBS Lett*, **464**, 60-62.

Pesole, G., Liuni, S., Grillo, G., Licciulli, F., Larizza, A., Makalowski, W. and Saccone, C. (2000) UTRdb and UTRsite: specialized databases of sequences and functional elements of 5' and 3' untranslated regions of eukaryotic mRNAs. *Nucleic Acids Res*, **28**, 193-196.

Pesole, G., Mignone, F., Gissi, C., Grillo, G., Licciulli, F. and Liuni, S. (2001) Structural and functional features of eukaryotic mRNA untranslated regions. *Gene*, **276**, 73-81.

Peters, L.L., Jindel, H.K., Gwynn, B., Korsgren, C., John, K.M., Lux, S.E., Mohandas, N., Cohen, C.M., Cho, M.R., Golan, D.E. and Brugnara, C. (1999) Mild spherocytosis and altered red cell ion transport in protein 4. 2-null mice. *J Clin Invest*, **103**, 1527-1537.

Peters, L.L., Shivdasani, R.A., Liu, S.C., Hanspal, M., John, K.M., Gonzalez, J.M., Brugnara, C., Gwynn, B., Mohandas, N., Alper, S.L., Orkin, S.H. and Lux, S.E. (1996) Anion

exchanger 1 (band 3) is required to prevent erythrocyte membrane surface loss but not to form the membrane skeleton. *Cell*, **86**, 917-927.

Phillips, C., Kyriakopoulou, C.B. and Virtanen, A. (1999) Identification of a stem-loop structure important for polyadenylation at the murine IgM secretory poly(A) site. *Nucleic Acids Res*, **27**, 429-438.

Pickering, B.M. and Willis, A.E. (2005) The implications of structured 5' untranslated regions on translation and disease. *Semin Cell Dev Biol*, **16**, 39-47.

Pollard, T.D., Blanchoin, L. and Mullins, R.D. (2000) Molecular mechanisms controlling actin filament dynamics in nonmuscle cells. *Annu Rev Biophys Biomol Struct*, **29**, 545-576.

Prescott, A.R., Sandilands, A., Hutcheson, A.M., Carter, J.M. and Quinlan, R.A. (1996) The intermediate filament cytoskeleton of the lens: an ever changing network through development and differentiation. A minireview. *Ophthalmic Res*, **28 Suppl 1**, 58-61.

Prescott, J. and Falck-Pedersen, E. (1994) Sequence elements upstream of the 3' cleavage site confer substrate strength to the adenovirus L1 and L3 polyadenylation sites. *Mol Cell Biol*, **14**, 4682-4693.

Proudfoot, N. (1991) Poly(A) signals. *Cell*, **64**, 671-674.

Proudfoot, N. (1996) Ending the message is not so simple. *Cell*, **87**, 779-781.

Proudfoot, N.J. (1989) How RNA polymerase II terminates transcription in higher eukaryotes. *Trends Biochem Sci*, **14**, 105-110.

Proudfoot, N.J. and Brownlee, G.G. (1976) 3' non-coding region sequences in eukaryotic messenger RNA. *Nature*, **263**, 211-214.

Proudfoot, N.J., Furger, A. and Dye, M.J. (2002) Integrating mRNA processing with transcription. *Cell*, **108**, 501-512.

Rabenstein, R.L., Addy, N.A., Caldarone, B.J., Asaka, Y., Gruenbaum, L.M., Peters, L.L., Gilligan, D.M., Fitzsimonds, R.M. and Picciotto, M.R. (2005) Impaired synaptic plasticity and learning in mice lacking beta-adducin, an actin-regulating protein. *J Neurosci*, **25**, 2138-2145.

Rafferty, N.S. and Scholz, D.L. (1985) Actin in polygonal arrays of microfilaments and sequestered actin bundles (SABs) in lens epithelial cells of rabbits and mice. *Curr Eye Res*, **4**, 713-718.

Rafferty, N.S. and Scholz, D.L. (1991) Development of actin polygonal arrays in rabbit lens epithelial cells. *Curr Eye Res*, **10**, 637-643.

Rafferty, N.S., Scholz, D.L., Goldberg, M. and Lewyckyj, M. (1990) Immunocytochemical evidence for an actin-myosin system in lens epithelial cells. *Exp Eye Res*, **51**, 591-600.

Raju, V.S. and Jacob, S.T. (1988) Association of poly(A) polymerase with U1 RNA. *J Biol Chem*, **263**, 11067-11070.

Rana, A.P., Ruff, P., Maalouf, G.J., Speicher, D.W. and Chishti, A.H. (1993) Cloning of human erythroid dematin reveals another member of the villin family. *Proc Natl Acad Sci U S A*, **90**, 6651-6655.

Rao, P.V. and Maddala, R. (2006) The role of the lens actin cytoskeleton in fiber cell elongation and differentiation. *Semin Cell Dev Biol*, **17**, 698-711.

Repasky, E.A., Granger, B.L. and Lazarides, E. (1982) Widespread occurrence of avian spectrin in nonerythroid cells. *Cell*, **29**, 821-833.

Rethinasamy, P., Muthuchamy, M., Hewett, T., Boivin, G., Wolska, B.M., Evans, C., Solaro, R.J. and Wieczorek, D.F. (1998) Molecular and physiological effects of alpha-tropomyosin ablation in the mouse. *Circ Res*, **82**, 116-123.

Rio, D.C. (1993) Splicing of pre-mRNA: mechanism, regulation and role in development. *Curr Opin Genet Dev*, **3**, 574-584.

Rosenblum, B.B., Hanash, S.M., Yew, N. and Neel, J.V. (1982) Two-dimensional electrophoretic analysis of erythrocyte membranes. *Clin Chem*, **28**, 925-931.

Rosonina, E., Kaneko, S. and Manley, J.L. (2006) Terminating the transcript: breaking up is hard to do. *Genes Dev*, **20**, 1050-1056.

Ruff, P., Speicher, D.W. and Husain-Chishti, A. (1991) Molecular identification of a major palmitoylated erythrocyte membrane protein containing the src homology 3 motif. *Proc Natl Acad Sci U S A*, **88**, 6595-6599.

Rybicki, A.C., Heath, R., Wolf, J.L., Lubin, B. and Schwartz, R.S. (1988) Deficiency of protein 4.2 in erythrocytes from a patient with a Coombs negative hemolytic anemia. Evidence for a role of protein 4.2 in stabilizing ankyrin on the membrane. *J Clin Invest*, **81**, 893-901.

Sachs, A. and Wahle, E. (1993) Poly(A) tail metabolism and function in eucaryotes. *J Biol Chem*, **268**, 22955-22958.

Sachs, A.B., Sarnow, P. and Hentze, M.W. (1997) Starting at the beginning, middle, and end: translation initiation in eukaryotes. *Cell*, **89**, 831-838.

Sadofsky, M. and Alwine, J.C. (1984) Sequences on the 3' side of hexanucleotide AAUAAA affect efficiency of cleavage at the polyadenylation site. *Mol Cell Biol*, **4**, 1460-1468.

Saffer, J.D., Jackson, S.P. and Annarella, M.B. (1991) Developmental expression of Sp1 in the mouse. *Mol Cell Biol*, **11**, 2189-2199.

Sambrook, J., Fritsch, E.F., Maniatis, T. (1989) *Molecular Cloning-A Laboratory Manual, 2nd edn*.

Sandelin, A., Carninci, P., Lenhard, B., Ponjavic, J., Hayashizaki, Y. and Hume, D.A. (2007) Mammalian RNA polymerase II core promoters: insights from genome-wide studies. *Nat Rev Genet*, **8**, 424-436.

Saxonov, S., Berg, P. and Brutlag, D.L. (2006) A genome-wide analysis of CpG dinucleotides in the human genome distinguishes two distinct classes of promoters. *Proc Natl Acad Sci U S A*, **103**, 1412-1417.

Schafer, D.A. and Cooper, J.A. (1995) Control of actin assembly at filament ends. *Annu Rev Cell Dev Biol*, **11**, 497-518.

Schafer, D.A., Korshunova, Y.O., Schroer, T.A. and Cooper, J.A. (1994) Differential localization and sequence analysis of capping protein beta-subunit isoforms of vertebrates. *J Cell Biol*, **127**, 453-465.

Schratt, G.M., Tuebing, F., Nigh, E.A., Kane, C.G., Sabatini, M.E., Kiebler, M. and Greenberg, M.E. (2006) A brain-specific microRNA regulates dendritic spine development. *Nature*, **439**, 283-289.

Schug, J., Schuller, W.P., Kappen, C., Salbaum, J.M., Bucan, M. and Stoeckert, C.J., Jr. (2005) Promoter features related to tissue specificity as measured by Shannon entropy. *Genome Biol*, **6**, R33.

Seidel, B., Zuschratter, W., Wex, H., Garner, C.C. and Gundelfinger, E.D. (1995) Spatial and sub-cellular localization of the membrane cytoskeleton-associated protein alpha-adducin in the rat brain. *Brain Res*, **700**, 13-24.

Shatkin, A.J. and Manley, J.L. (2000) The ends of the affair: capping and polyadenylation. *Nat Struct Biol*, **7**, 838-842.

Sheets, M.D., Ogg, S.C. and Wickens, M.P. (1990) Point mutations in AAUAAA and the poly (A) addition site: effects on the accuracy and efficiency of cleavage and polyadenylation in vitro. *Nucleic Acids Res*, **18**, 5799-5805.

Shell, S.A., Hesse, C., Morris, S.M., Jr. and Milcarek, C. (2005) Elevated levels of the 64-kDa cleavage stimulatory factor (CstF-64) in lipopolysaccharide-stimulated macrophages influence gene expression and induce alternative poly(A) site selection. *J Biol Chem*, **280**, 39950-39961.

Shen, B.W., Josephs, R. and Steck, T.L. (1986) Ultrastructure of the intact skeleton of the human erythrocyte membrane. *J Cell Biol*, **102**, 997-1006.

Shi, Z.T., Afzal, V., Coller, B., Patel, D., Chasis, J.A., Parra, M., Lee, G., Paszty, C., Stevens, M., Walensky, L., Peters, L.L., Mohandas, N., Rubin, E. and Conboy, J.G. (1999) Protein 4.1R-deficient mice are viable but have erythroid membrane skeleton abnormalities. *J Clin Invest*, **103**, 331-340.

Siegel, D.L. and Branton, D. (1985) Partial purification and characterization of an actin-bundling protein, band 4.9, from human erythrocytes. *J Cell Biol*, **100**, 775-785.

Sinard, J.H., Stewart, G.W., Stabach, P.R., Argent, A.C., Gilligan, D.M. and Morrow, J.S. (1998) Utilization of an 86 bp exon generates a novel adducin isoform (beta 4) lacking the MARCKS homology domain. *Biochim Biophys Acta*, **1396**, 57-66.

Sittler, A., Gallinaro, H. and Jacob, M. (1994) Upstream and downstream cis-acting elements for cleavage at the L4 polyadenylation site of adenovirus-2. *Nucleic Acids Res*, **22**, 222-231.

Smale, S.T. and Kadonaga, J.T. (2003) The RNA polymerase II core promoter. *Annu Rev Biochem*, **72**, 449-479.

Sonenberg, N. and Dever, T.E. (2003) Eukaryotic translation initiation factors and regulators. *Curr Opin Struct Biol*, **13**, 56-63.

Southgate, C.D., Chishti, A.H., Mitchell, B., Yi, S.J. and Palek, J. (1996) Targeted disruption of the murine erythroid band 3 gene results in spherocytosis and severe haemolytic anaemia despite a normal membrane skeleton. *Nat Genet*, **14**, 227-230.

St Johnston, D. (2005) Moving messages: the intracellular localization of mRNAs. *Nat Rev Mol Cell Biol*, **6**, 363-375.

Storz, G., Altuvia, S. and Wassarman, K.M. (2005) An abundance of RNA regulators. *Annu Rev Biochem*, **74**, 199-217.

Sun, M., Hurst, L.D., Carmichael, G.G. and Chen, J. (2005) Evidence for a preferential targeting of 3'-UTRs by cis-encoded natural antisense transcripts. *Nucleic Acids Res*, **33**, 5533-5543.

Sung, L.A., Gao, K.M., Yee, L.J., Temm-Grove, C.J., Helfman, D.M., Lin, J.J. and Mehrpouryan, M. (2000) Tropomyosin isoform 5b is expressed in human erythrocytes: implications of tropomodulin-TM5 or tropomodulin-TM5b complexes in the protofilament and hexagonal organization of membrane skeletons. *Blood*, **95**, 1473-1480.

Sung, L.A. and Lin, J.J. (1994) Erythrocyte tropomodulin binds to the N-terminus of hTM5, a tropomyosin isoform encoded by the gamma-tropomyosin gene. *Biochem Biophys Res Commun*, **201**, 627-634.

Sung, L.A. and Vera, C. (2003) Protofilament and hexagon: a three-dimensional mechanical model for the junctional complex in the erythrocyte membrane skeleton. *Ann Biomed Eng*, **31**, 1314-1326.

Sussman, M.A., Baque, S., Uhm, C.S., Daniels, M.P., Price, R.L., Simpson, D., Terracio, L. and Kedes, L. (1998) Altered expression of tropomodulin in cardiomyocytes disrupts the sarcomeric structure of myofibrils. *Circ Res*, **82**, 94-105.

Sussman, M.A., McAvoy, J.W., Rudisill, M., Swanson, B., Lyons, G.E., Kedes, L. and Blanks, J. (1996) Lens tropomodulin: developmental expression during differentiation. *Exp Eye Res*, **63**, 223-232.

Sussman, M.A., Welch, S., Cambon, N., Klevitsky, R., Hewett, T.E., Price, R., Witt, S.A. and Kimball, T.R. (1998) Myofibril degeneration caused by tropomodulin overexpression leads to dilated cardiomyopathy in juvenile mice. *J Clin Invest*, **101**, 51-61.

Tabaska, J.E. and Zhang, M.Q. (1999) Detection of polyadenylation signals in human DNA sequences. *Gene*, **231**, 77-86.

Tagliavini, J., Gandolfi, S.A. and Maraini, G. (1986) Cytoskeleton abnormalities in human senile cataract. *Curr Eye Res*, **5**, 903-910.

Takagaki, Y., Seipelt, R.L., Peterson, M.L. and Manley, J.L. (1996) The polyadenylation factor CstF-64 regulates alternative processing of IgM heavy chain pre-mRNA during B cell differentiation. *Cell*, **87**, 941-952.

Takakuwa, Y. (2000) Protein 4.1, a multifunctional protein of the erythrocyte membrane skeleton: structure and functions in erythrocytes and nonerythroid cells. *Int J Hematol*, **72**, 298-309.

Tamura, T., Konishi, Y., Makino, Y. and Mikoshiba, K. (1996) Mechanisms of transcriptional regulation and neural gene expression. *Neurochem Int*, **29**, 573-581.

Tang, X., Gal, J., Zhuang, X., Wang, W., Zhu, H. and Tang, G. (2007) A simple array platform for microRNA analysis and its application in mouse tissues. *Rna*, **13**, 1803-1822.

Tanguay, R.L. and Gallie, D.R. (1996) Translational efficiency is regulated by the length of the 3' untranslated region. *Mol Cell Biol*, **16**, 146-156.

Tanner, M.J. (1993) The major integral proteins of the human red cell. *Baillieres Clin Haematol*, **6**, 333-356.

Taylor, K.A. and Taylor, D.W. (1994) Formation of two-dimensional complexes of F-actin and crosslinking proteins on lipid monolayers: demonstration of unipolar alpha-actinin-F-actin crosslinking. *Biophys J*, **67**, 1976-1983.

Tian, B., Hu, J., Zhang, H. and Lutz, C.S. (2005) A large-scale analysis of mRNA polyadenylation of human and mouse genes. *Nucleic Acids Res*, **33**, 201-212.

Tischmeyer, W. and Grimm, R. (1999) Activation of immediate early genes and memory formation. *Cell Mol Life Sci*, **55**, 564-574.

Tisminetzky, S., Devescovi, G., Tripodi, G., Muro, A., Bianchi, G., Colombi, M., Moro, L., Barlati, S., Tuteja, R. and Baralle, F.E. (1995) Genomic organisation and chromosomal localisation of the gene encoding human beta adducin. *Gene*, **167**, 313-316.

Tripodi, G., Casari, G., Tisminetzky, S., Bianchi, G., Devescovi, G., Muro, A., Tuteja, R. and Baralle, F.E. (1995) Characterisation and chromosomal localisation of the rat alpha- and beta-adducin-encoding genes. *Gene*, **166**, 307-311.

Tripodi, G., Piscone, A., Borsani, G., Tisminetzky, S., Salardi, S., Sidoli, A., James, P., Pongor, S., Bianchi, G. and Baralle, F.E. (1991) Molecular cloning of an adducin-like protein: evidence of a polymorphism in the normotensive and hypertensive rats of the Milan strain. *Biochem Biophys Res Commun*, **177**, 939-947.

Vagner, S., Vagner, C. and Mattaj, I.W. (2000) The carboxyl terminus of vertebrate poly(A) polymerase interacts with U2AF 65 to couple 3'-end processing and splicing. *Genes Dev*, **14**, 403-413.

Valencia-Sanchez, M.A., Liu, J., Hannon, G.J. and Parker, R. (2006) Control of translation and mRNA degradation by miRNAs and siRNAs. *Genes Dev*, **20**, 515-524.

Vilela, C. and McCarthy, J.E. (2003) Regulation of fungal gene expression via short open reading frames in the mRNA 5'untranslated region. *Mol Microbiol*, **49**, 859-867.

Wahle, E. and Keller, W. (1992) The biochemistry of 3'-end cleavage and polyadenylation of messenger RNA precursors. *Annu Rev Biochem*, **61**, 419-440.

Wahle, E. and Kuhn, U. (1997) The mechanism of 3' cleavage and polyadenylation of eukaryotic pre-mRNA. *Prog Nucleic Acid Res Mol Biol*, **57**, 41-71.

Wahle, E. and Ruegsegger, U. (1999) 3'-End processing of pre-mRNA in eukaryotes. *FEMS Microbiol Rev*, **23**, 277-295.

Wallace, A.M., Dass, B., Ravnik, S.E., Tonk, V., Jenkins, N.A., Gilbert, D.J., Copeland, N.G. and MacDonald, C.C. (1999) Two distinct forms of the 64,000 Mr protein of the cleavage stimulation factor are expressed in mouse male germ cells. *Proc Natl Acad Sci U S A*, **96**, 6763-6768.

Wang, Y., Newton, D.C., Robb, G.B., Kau, C.L., Miller, T.L., Cheung, A.H., Hall, A.V., VanDamme, S., Wilcox, J.N. and Marsden, P.A. (1999) RNA diversity has profound

effects on the translation of neuronal nitric oxide synthase. *Proc Natl Acad Sci U S A*, **96**, 12150-12155.

Weber, A., Pennise, C.R., Babcock, G.G. and Fowler, V.M. (1994) Tropomodulin caps the pointed ends of actin filaments. *J Cell Biol*, **127**, 1627-1635.

Weis, L. and Reinberg, D. (1992) Transcription by RNA polymerase II: initiator-directed formation of transcription-competent complexes. *Faseb J*, **6**, 3300-3309.

Weiss, E.A., Gilmartin, G.M. and Nevins, J.R. (1991) Poly(A) site efficiency reflects the stability of complex formation involving the downstream element. *Embo J*, **10**, 215-219.

Wickens, M. and Stephenson, P. (1984) Role of the conserved AAUAAA sequence: four AAUAAA point mutants prevent messenger RNA 3' end formation. *Science*, **226**, 1045-1051.

Wilusz, J., Pettine, S.M. and Shenk, T. (1989) Functional analysis of point mutations in the AAUAAA motif of the SV40 late polyadenylation signal. *Nucleic Acids Res*, **17**, 3899-3908.

Wilusz, J., Shenk, T., Takagaki, Y. and Manley, J.L. (1990) A multicomponent complex is required for the AAUAAA-dependent cross-linking of a 64-kilodalton protein to polyadenylation substrates. *Mol Cell Biol*, **10**, 1244-1248.

Wolska, B.M. and Wieczorek, D.M. (2003) The role of tropomyosin in the regulation of myocardial contraction and relaxation. *Pflugers Arch*, **446**, 1-8.

Woo, M.K. and Fowler, V.M. (1994) Identification and characterization of tropomodulin and tropomyosin in the adult rat lens. *J Cell Sci*, **107 (Pt 5)**, 1359-1367.

Woo, M.K., Lee, A., Fischer, R.S., Moyer, J. and Fowler, V.M. (2000) The lens membrane skeleton contains structures preferentially enriched in spectrin-actin or tropomodulin-actin complexes. *Cell Motil Cytoskeleton*, **46**, 257-268.

Wu, L., Wells, D., Tay, J., Mendis, D., Abbott, M.A., Barnitt, A., Quinlan, E., Heynen, A., Fallon, J.R. and Richter, J.D. (1998) CPEB-mediated cytoplasmic polyadenylation and the regulation of experience-dependent translation of alpha-CaMKII mRNA at synapses. *Neuron*, **21**, 1129-1139.

Xie, X., Lu, J., Kulbokas, E.J., Golub, T.R., Mootha, V., Lindblad-Toh, K., Lander, E.S. and Kellis, M. (2005) Systematic discovery of regulatory motifs in human promoters and 3' UTRs by comparison of several mammals. *Nature*, **434**, 338-345.

Yan, J. and Marr, T.G. (2005) Computational analysis of 3'-ends of ESTs shows four classes of alternative polyadenylation in human, mouse, and rat. *Genome Res*, **15**, 369-375.

Yang, C., Bolotin, E., Jiang, T., Sladek, F.M. and Martinez, E. (2007) Prevalence of the initiator over the TATA box in human and yeast genes and identification of DNA motifs enriched in human TATA-less core promoters. *Gene*, **389**, 52-65.

Yeh, S., Scholz, D.L., Liou, W. and Rafferty, N.S. (1986) Polygonal arrays of actin filaments in human lens epithelial cells. An aging study. *Invest Ophthalmol Vis Sci*, **27**, 1535-1540.

Yenerel, M.N., Sundell, I.B., Weese, J., Bulger, M. and Gilligan, D.M. (2005) Expression of adducin genes during erythropoiesis: a novel erythroid promoter for ADD2. *Exp Hematol*, **33**, 758-766.

Zarkower, D. and Wickens, M. (1988) A functionally redundant downstream sequence in SV40 late pre-mRNA is required for mRNA 3'-end formation and for assembly of a precleavage complex in vitro. *J Biol Chem*, **263**, 5780-5788.

Zhan, M., Miller, C.P., Papayannopoulou, T., Stamatoyannopoulos, G. and Song, C.Z. (2007) MicroRNA expression dynamics during murine and human erythroid differentiation. *Exp Hematol*, **35**, 1015-1025.

Zhang, H., Lee, J.Y. and Tian, B. (2005) Biased alternative polyadenylation in human tissues. *Genome Biol*, **6**, R100.

Zhao, J., Hyman, L. and Moore, C. (1999) Formation of mRNA 3' ends in eukaryotes: mechanism, regulation, and interrelationships with other steps in mRNA synthesis. *Microbiol Mol Biol Rev*, **63**, 405-445.

Zhao, X., Oberg, D., Rush, M., Fay, J., Lambkin, H. and Schwartz, S. (2005) A 57-nucleotide upstream early polyadenylation element in human papillomavirus type 16 interacts with hFip1, CstF-64, hnRNP C1/C2, and polypyrimidine tract binding protein. *J Virol*, **79**, 4270-4288.

APPENDIX

Part of the work described in this Thesis has been published in the following scientific journals:

Porro F, Costessi L, Marro ML, Baralle FE, Muro AF.

The erythrocyte skeletons of beta-adducin deficient mice have altered levels of tropomyosin, tropomodulin and EcapZ.

FEBS Lett. 2004 Oct 8;576(1-2):36-40.

Costessi L, Devescovi G, Baralle FE, Muro AF.

Brain-specific promoter and polyadenylation sites of the beta-adducin pre-mRNA generate an unusually long 3'-UTR.

Nucleic Acids Res. 2006 Jan 9;34(1):243-53.

Electronic reprints of these two articles can be viewed in the subsequent pages.

FEBS Letters 576 (2004) 36–40 FEBS 28804

The erythrocyte skeletons of β-adducin deficient mice have altered levels of tropomyosin, tropomodulin and EcapZ

Fabiola Porro[1], Luisa Costessi[1], Martín L. Marro[2], Francisco E. Baralle, Andrés F. Muro*

International Centre for Genetic Engineering and Biotechnology, Padriciano 99, I 34012, Trieste, Italy

Received 18 June 2004; revised 23 July 2004; accepted 3 August 2004

Available online 11 September 2004

Edited by Lukas Huber

Abstract The erythrocyte membrane cytoskeleton is organized as a polygonal spectrin network linked to short actin filaments that are capped by adducin at the barbed ends. We have constructed a mouse strain deficient in β-adducin having abnormal erythrocytes. We show here that the levels of several skeletal proteins from β-adducin mutant erythrocytes are altered. In fact, CapZ, the main muscle actin-capping protein of the barbed ends that in the erythrocytes is cytoplasmic, is 9-fold upregulated in mutant skeletons of erythrocytes suggesting a compensatory mechanism. We also detected upregulation of tropomodulin and downregulation of α-tropomyosin and actin. In addition, purified adducin can be re-incorporated into adducin-deficient ghosts.

1. Introduction

The erythrocyte membrane skeleton is a dynamic network of proteins associated with the plasma membrane. The main components are spectrin and actin that are organized as a polygonal spectrin network linked to short actin filaments. The spectrin–actin junctions contain a group of proteins that promote and modulate spectrin–actin interactions, form membrane associations, and regulate the actin filament length. This group includes adducin, tropomodulin (Tmod), tropomyosin (TM), protein 4.1 and dematin [1]. The barbed ends of actin filaments are capped by adducin in erythrocytes [2]. The pointed ends are capped by Tmod [3], while TM stabilizes actin filaments [3–7].

In the muscle, the control of actin filament growth at the barbed ends is achieved by the actin capping protein (CapZ) [8,9] and erythrocytes contain a cytosolic form of CapZ (EcapZ) [10]. Surprisingly, adducin is the erythrocyte actin capping protein despite having a 20–100-fold lower affinity than ECapZ ($K_{\text{cap Add}} \sim 100$ nM vs $K_{\text{cap EcapZ}} \sim 1$–5 nM) [2,10].

The adducin protein family is composed of 3 members encoded by closely related genes: α-, β- and γ-adducin [11,12]. Adducin is present in human erythrocytes as a mixture of α/β heterodimers and heterotetramers [13], whereas the γ-subunit is also found at low levels in mouse red cells [14,15] and combinations of α/β and α/γ oligomers are found in other cells [11,13]. Adducin function is modulated by phosphorylation of several kinases (Rho kinase, PKA, PKC and casein kinase II (CKII)) in different sites [16–22]. Mice bearing a targeted mutation in the β-adducin gene develop mild spherocytic hereditary elliptocytosis (SphHE) [14,15] in addition to hypertension [23].

SphHE is a phenotypical hybrid of mild hereditary elliptocytosis and hereditary spherocytosis: red cells are osmotically fragile, elliptocytes are less pronounced and somewhat rounded, but no poikilocytes or fragmented forms are present [24]. Some patients presented mutations in β-spectrin [25] and protein 4.1 deficiency [26,27], but the molecular basis is poorly understood. Therefore, further dissection of the SphHE molecular pathology was needed and the presence of red cell abnormalities in the β-adducin deficient mice similar to those found in SphHE patients highlights the importance of adducin in the maintenance of the shape and mechanical properties of the erythrocyte membrane skeleton. On the other hand, it raises the possibility that compensatory mechanisms might be activated by the absence of the β-adducin subunit, preventing the manifestation of a more severe phenotype in the KO mice.

In this report, we have analyzed the molecular changes present in the membrane CK of erythrocytes triggered by the absence of β-adducin in mice.

2. Materials and methods

2.1. Mice and antibodies

β-Adducin deficient mice having C57Bl/6 genetic background and the anti α- and β-adducin antibodies have been described previously [15]. To transfer the β-adducin gene mutation to a C3H genetic background, the mutant mice were backcrossed with C3H mice (Harlan, Italy) for six additional generations. Monoclonal antibodies anti-CapZ-α and -β (5B12.3 and 3F2.3, respectively) and anti-α-TM (CH1) were from Developmental Studies Hybridoma Bank at the University of Iowa. The CH1 monoclonal antibody was generated using adult heart TM (mainly α-TM isoform) as antigen [28]. Anti protein 4.1 was a gift from Dirk Hofer, Anatom. Institut, Wurzburg, Germany, anti-p55 (sc-13603) and anti-Tmod (sc-19206) were from Santa Cruz Biotechnology, anti-dematin (D77620) was from BD Transduction Laboratories, and anti-actin (A2066) was from Sigma.

2.2. Preparation of ghosts and skeletal proteins and Western blot analysis

Regarding the experiments described in Fig. 1, skeletal fractions were prepared as previously described in the absence of Mg^{2+} [15].

* Corresponding author. Fax: +39-040-2265 55.
E-mail address: muro@icgeb.org (A.F. Muro).

[1] Both authors contributed equally to the work and should be considered joint first authors.

[2] Present address: Wolfson Institute for Biomedical Research, University College London, Cruciform Building, Gower Street, London WC1E 6AE, UK.

0014-5793/$22.00
doi:10.1016/j.febslet.2004.08.057

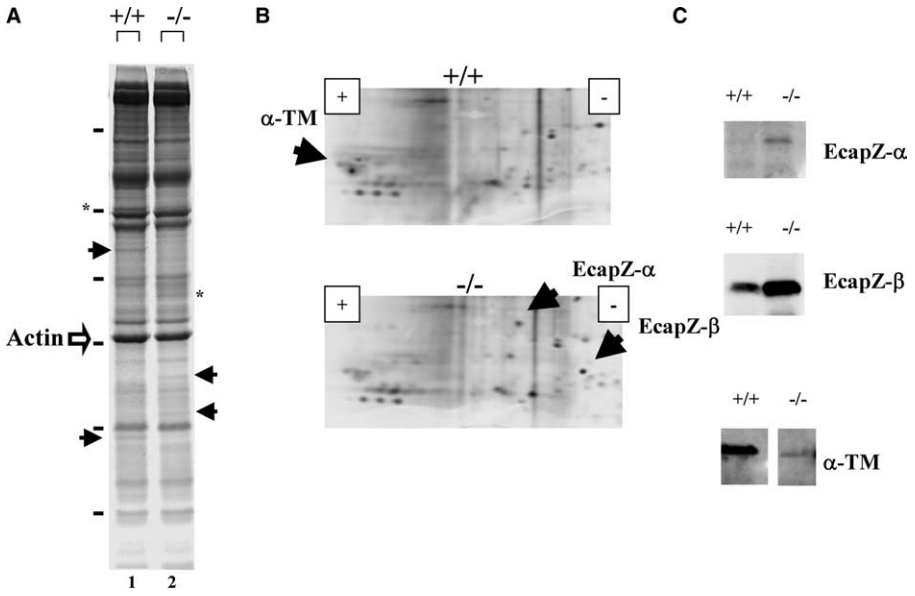

Fig. 1. Mutant erythrocytes have an increase in erythrocyte actin capping protein EcapZ-α and -β, and a decrease in α-TM levels. Panel A. Control (lane 1) and mutant (lane 2) erythrocyte membrane cytoskeleton (80 μg) were separated by SDS–PAGE (8%) and coomassie blue stained. The black arrows indicate proteins that show different levels between control and mutant preparations. The asterisks correspond to degradation products of higher molecular weight proteins. The band corresponding to actin is indicated. A 14% decrease in actin levels was observed in the extracts form mutant erythrocytes. Molecular weight markers are indicated on the left as black bars (175, 83, 62, 47.5, 32.5 and 25 kDa from top to bottom). Panel B. The same extracts from Panel A were analyzed in a silver stained 2D gels. The acidic and basic sides are indicated by the symbols "+" and "−", respectively. α-TM, EcapZ-α and EcapZ-β spots are indicated by arrows. Panel C. Western blot analyses were performed using anti α-TM, anti EcapZ-α and anti EcapZ-β antibodies. +/+ and −/− depict wild type and β-adducin deficient mice, respectively, of the same extracts utilized in Panel A. The same extracts used in Panel A were used for the Western Blot analysis and the same amount of protein was loaded for +/+ and −/− extracts.

Concerning the rest of the manuscript, erythrocyte ghosts and skeletal fractions were prepared in the presence of Mg^{2+} as described [29]. Briefly, red cells were separated from freshly drawn blood anticoagulated with acid citrate-dextrose by sedimentation at 1×*g* through 4 volumes of sedimentation buffer [150 mM NaCl, 5 mM sodium phosphate, pH 7.5, and 0.75% (w/v) Dextrane 500-Pharmacia] at 4 °C. Erythrocytes were then washed three times with 4–10 volumes of PBS (10 mM sodium phosphate pH 7.5, 150 mM NaCl) and centrifuged at 6000 rpm. Pellets were resuspended in lysis buffer (5 mM sodium phosphate, pH 8, 1 mM DTT, 40 μg/μl PMSF and protease inhibitors cocktail, Roche) containing or not 2 mM $MgCl_2$ and frozen at −80 °C. The lyzed cells were frozen/thawed twice in dry-ice and cold water and centrifuged at 40 000×*g* for 10 min in a Ti60-rotor. The cytoplasmic fractions were separated and stored at −80 °C, while the pellets were washed three times with cold lysis buffer (with or without $MgCl_2$) and centrifuged at 40 000×*g*. The final ghost pellets were resuspended in the same buffer at 1/15 of starting volume, briefly sonicated (3 × 10 s) and stored at −80 °C. For skeletal preparations, the ghost fractions were resuspended with Triton X-100-containing solution (10 mM Tris–HCl, pH 8, 100 mM NaCl, 1 mM EDTA, 2 mM DTT, protease inhibitors containing or not 2 mM $MgCl_2$, and 0.5% v/v Triton-X-100) and centrifuged for 40 min at 16 000 rpm. The pellet was resuspended again in the Triton X-100-containing solution and centrifuged for 50 min at 16000 rpm. The final pellet (skeletons) was resuspended in the same solution without Triton X-100. The protein concentration of cytoplasmic and ghost fractions was measured by triplicate by using the Bradford method (Bio-Rad) and analyzed by SDS–PAGE followed by Coomassie blue staining.

Analysis of the ghosts proteins by Western blot was performed as previously described [15]. The gel images were acquired with the VersaDoc Imaging System (Bio-Rad) and bands (or spots) quantified with the help of the Quantity One or PDQUEST software (Bio-Rad).

2.3. 2D gels and mass spectrometry analysis

The protein extracts were precipitated in acetone:tributylphosphate:methanol (1:12:1) as described [30]. The pellets were resuspended in 2D buffer (7 M urea, 2 M thiourea, 2% CHAPS, 4 mM tributyiphosphine and protease inhibitor cocktail). The first dimension was performed by loading 150–300 μg of protein extract into IPG strips with different pH ranges (3–10, 3–6, 4–7 and 5–8; strips were 17 cm long). The Protean IEF (Bio-Rad) cell was used following the protocol described by the manufacturer. Gradient (8–15%) or non-gradient (12%) SDS–PAGE were used for the second dimension.

The selected bands and spots (from the SDS–PAGE and 2D gels, respectively) were extracted from the acrylamide after digestion with trypsin (Promega). The digestion products were separated by micro-high pressure liquid chromatography and analyzed by electrospray ionization mass spectrometry (Finnigan LCQ DECA, Thermo-Finningan Corp., San Jose, CA). The obtained data were analyzed with MASCOT (Matrix Science) and SWISSPROT software.

2.4. Preparation of purified adducin and complementation assay of mutant ghosts

HPLC-purified human erythrocyte adducin was prepared as previously described [13,29,31]. The binding assay of mutant ghosts with HPLC-purified human adducin was performed as described [10] with minimal modifications. Briefly, ghosts from β-adducin deficient erythrocytes (20 μg) were incubated with increasing amounts of HPLC-purified human adducin (0.7, 1.4 and 2.8 μg) for 30 min at 0 °C. Control reactions were performed by omitting ghosts and adding 20 μg of BSA or by omitting purified adducin. The soluble fraction was separated from the membrane-associated skeletons by centrifugation through a sucrose cushion. The pellets were electrophoresed on 10% SDS–PAGE and blotted onto a PVDF membrane.

3. Results

3.1. Erythrocyte skeletons of mutant mice have increased levels of EcapZ and decreased levels of α-TM

Erythrocyte cytoskeletal protein preparations of control and β-adducin deficient mice showed evident differences in at least four bands of apparent MW of 65 and 30–32 kDa observed only in control mice and 38 and 34 kDa present only in mutant mice (see Muro et al. [15] and Fig. 1A). Two-dimensional gels

followed by silver staining evidenced two spots of 38 and 34 kDa (having an approximated pI of 5.4 and 5.7, respectively) that were visible only in the preparation from mutant mice (Fig. 1B). Mass spectrometry analysis indicated that they were the EcapZ-α and EcapZ-β subunits, respectively. Another spot of approximate pI 4.6 having a relative MW of 30 kDa was visible only in the wild type 2D gel. Mass spectrometry analysis identified this spot as α-TM (Fig. 1A and B).

Western blot analysis with antibodies against both subunits of EcapZ showed a ~9-fold increase of both proteins in the skeletal fractions of mutant animals (Fig. 1C) confirming our observations in the SDS–PAGE gels, 2D gels and mass spectrometry, while we observed a 40–50% reduction in the mutant mice using an antibody against α-TM (Fig. 1C).

The 65 kDa band is probably a degradation product of β-adducin as diverse β-adducin peptides were detected by mass spectrometry. The other bands showing differences between control and mutant preparations (Fig. 1A, 55 and 83 kDa of MW, indicated by asterisks) are probably degradation products of high molecular weight proteins as mass spectrometry analysis revealed mostly the presence of α- and β-spectrin, or protein 4.1 peptides (data not shown). We were unable to identify in the 2D gels the 55, 65 and 83 kDa bands marked with the arrow and asterisks in Fig. 1A.

3.2. Altered levels in other major components of the RBC membrane cytoskeleton from β-adducin deficient mice

To determine variations in other erythrocyte skeletal proteins not evidenced by the SDS–PAGE or the 2D analysis, we performed a Western blot analysis using a set of antibodies directed against the main actin-associated proteins.

The protein extracts were prepared using a protocol that contained 2 mM Mg^{2+} that was different to the one used in Fig. 1 (without Mg^{2+}). This change was aimed to obtain a higher stability in the actin filaments (see Section 2 and [10]). In fact, the levels of some of the actin-associated proteins are reduced in ghosts prepared in the absence of Mg^{2+} in comparison to Mg^{2+}-ghosts indicating a skeleton-stabilizing role of Mg^{2+} during protein preparation [10].

In addition to the variations in EcapZ and α-TM (not shown), we observed changes in Tmod, dematin and actin levels. A mean decrease of 74% in the levels of α-adducin, a 65% decrease in α-TM levels and 9-fold increase in EcapZ-β levels in the skeleton mutant extracts preparations were observed (Fig. 2 and Table 1). We confirmed the previously reported trend of ~15% decrease in the actin levels in the cytoskeletal preparations of mutant erythrocytes [15] (Fig. 2 and Table 1). We were not able to detect in the Western blot analysis the appearance of smaller extra bands in the mutant extracts indicating that the decrease in α-TM and actin could be the consequence of increased proteolytic degradation. To verify whether the observed differences were dependent on the genetic background of the mice, we performed protein preparations from erythrocytes of control and β-adducin deficient mice having a C3H genetic background. We observed similar results to those presented in Fig. 2 and Table 1 in preparations from mice with a C3H genetic background (not shown).

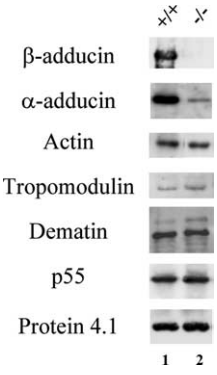

Fig. 2. Differences in the levels of other major skeletal proteins are observed in erythrocyte skeletal preparations of mutant mice. Western blot analysis of erythrocyte skeletal protein preparations of control ("+/+", lane 1) and mutant mice ("–/–", lane 2) using a set of antibodies directed against cytoskeletal proteins (indicated on the left).

Western blot analysis using an anti-Tmod antibody showed a 65% increase in Tmod levels in the mutant preparation (Fig. 2 and Table 1). Dematin showed a minor decrease in the mutant preparations of the main lower band intensity and a 79% increase in the upper band intensity (Fig. 2 and Table 1).

The levels of other cytoskeletal protein (protein 4.1 and p55) showed no significant differences between wild type and KO mice by Western blot analysis (Fig. 2 and Table 1).

No variations were observed in the cytoplasmic levels of α- and β-EcapZ (data not shown). In addition, we were neither able to detect Tmod and α-TM in cytoplasmic preparations from control animals, as reported previously by another group [10], nor from mutant preparations.

3.3. Purified adducin is incorporated into adducin-deficient ghosts

To determine whether purified adducin (as α/β heterodimer) was able to be incorporated into cytoskeletons from β-adducin-deficient mice to eventually replace EcapZ we performed a binding assay utilizing ghosts from KO mice and purified human erythrocyte adducin.

Fig. 3 shows the Western blot analysis of both β-adducin and EcapZ-β after incubation of a fixed amount of mutant ghosts with increasing amounts of purified adducin. We observed that β-adducin was incorporated into adducin-deficient ghosts in a dose-dependent manner (Fig. 3, lanes 2–4). The α-adducin subunit was incorporated in a similar manner to the β-

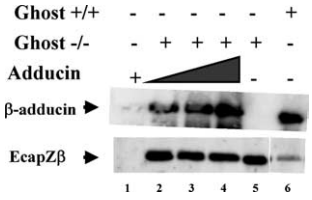

Fig. 3. Purified adducin can be incorporated into adducin-deficient ghosts in vitro. Ghosts from mutant mice were incubated with increasing amounts of purified adducin (0.7, 1.4 and 2.8 μg in lanes 2, 3 and 4, respectively) and the membrane-skeleton (pellet) was separated from the soluble fraction through a sucrose cushion. β-Adducin and EcapZ-β protein levels were detected by Western blot analysis. Lane 1 contains 2.8 μg of adducin plus 20 μg of BSA. Lanes 5 and 6 contain 20 μg of mutant and control ghosts protein preparations, respectively, that underwent the same experimental procedure as the other lanes. Quantification of the bands showed an increase of β-adducin and a decrease of EcapZ-β (relative values of β-adducin: 8, 91, 111, 131, 0 and 100 for lanes 1–6, respectively; relative values of EcapZ-β: 0, 1280, 1069, 985, 1210 and 100 for lanes 1 to 6, respectively; ratio β-adducin/EcapZ-β: 7.1, 10.5 and 13.5 for lanes 2–4, respectively).

Table 1
Altered levels of cytoskeletal proteins in RBC from mutant mice

Band #	Protein	Confirmed by mass spectrometry/WB	Levels in +/+ mice	Levels in −/− mice	*P* value
1	β-Adducin	No/Yes	100[a]	ND	NA
2	α-Adducin	No/Yes	100 ± 6	26 ± 6	⩽0.01
3	EcapZ-α	Yes/Yes	ND	100[a]	NA
4	EcapZ-β	Yes/Yes	100 ± 20	880 ± 153	⩽0.01
5	α-TM	Yes/Yes	100 ± 12	35 ± 9	⩽0.01
6	Actin	No/Yes	100 ± 2	83 ± 8	⩽0.01
7	Tropomodulin	No/Yes	100 ± 13	165 ± 5	⩽0.05
8a	Dematin 52 kDa	No/Yes	100 ± 8	179 ± 20	<0.05
8b	Dematin 48 kDa	No/Yes	100 ± 3	94 ± 4	NS
9	P55	No/Yes	100 ± 2	105 ± 7	NS
10	Protein 4.1	No/Yes	100 ± 9	91 ± 11	NS

The levels of the various cytoskeletal proteins shown in Fig. 2 were quantified as described in Section 2. The numbers indicate relative amounts of each protein in cytoskeleton extracts relative to those found in those control extract (±S.D.). "WB" stands for western blot. ND, not detected; NA, not applicable; NS, non significant.
[a] An arbitrary value of 100 was given as no signal was detected in mutant and control mice, in the case of β-adducin and EcapZ-α, respectively. *P*-value was calculated using the Student *t* test.

subunit (not shown). EcapZ-β levels decreased after the incubation of mutant ghosts with increasing amounts of adducin (Fig. 3, lanes 2–4). The control lane confirmed that the purified adducin did not auto-precipitate (Fig. 3, lane 1) as it included the maximum amount of adducin used in lane 4 (2.8 μg) plus an amount of BSA similar to that of ghosts used in the other lanes (20 μg). Quantification of the bands indicated that the ratio between adducin and EcapZ increases with the addition of higher amounts of adducin supporting the idea that the incorporation of EcapZ is a compensatory mechanism triggered by the absence of β-adducin.

4. Discussion

The β-adducin deficient mice showed a decrease of the α-adducin levels and an up regulation of the γ-subunit in RBC skeletons [14,15]. These adaptations seem not to be sufficient to attain normal erythrocyte function, since β-adducin KO mice have increased erythrocyte fragility and suffer from mild compensated hemolytic anemia [14,15]. We showed now that the levels of some of the actin-associated proteins in mutant mice erythrocytes are different from those found in control animals, suggesting that both the actin filament-complex and actin polymerization activity might be altered.

As previously mentioned, the main capping protein of the actin-filament barbed ends in the muscle is CapZ, while in erythrocyte membrane skeletons this function is performed by adducin [2] and EcapZ remains in the cytoplasm [10]. The affinity of adducin and EcapZ for the actin filaments has been determined in vitro by Dr. Velia Fowler's group using purified proteins [2,3,10]. The fact that adducin is the erythrocyte actin capping protein notwithstanding its lower K_{cap} respect to that of EcapZ strongly suggests that the in vivo affinity is not all and may be other proteins might cooperate in the stabilization of the binding of adducin to the actin-filaments barbed ends [10] as already observed in the case of spectrin–actin complexes [32,33]. In spite of this, we did not observe a complete displacement of EcapZ in the mutant ghosts by exogenously added adducin but increasing amounts of adducin produced a reproducible minor decrease in the EcapZ levels in the ghosts fraction (23% decrease in lane 4 of Fig. 3). Obviously, this is not an in vivo experiment and is far from what really occurs during erythropoiesis, when the cytoskeleton takes its final structure and proteins are synthesized simultaneously and have to compete for a place in the skeleton structure.

However, the increase of the EcapZ levels in the cytoskeleton of mutant erythrocytes did not fully compensate for the absence of β-adducin: variations in α-TM, Tmod and actin, and changes in α- and γ-adducin were observed. Consequently, mice have a change in the shape and mechanical properties of red cells and suffer from mild hemolytic anemia [14,15].

The binding of Tmod to the actin filaments pointed ends is stabilized by TM [34]. The increase in Tmod levels together with the decrease in α-TM and actin suggest that the in vivo interaction among actin, Tmod and TM might be also affected in mutant erythrocytes. In addition, the important decrease in the levels of α-TM in mutant preparations might suggest a new role for adducin in stabilizing α-TM within the actin filament-complex of erythrocytes. In the case of the targeted inactivation in mice of other erythrocyte protein, the anion transporter Band 3 (AE1), it was shown that the close interaction of AE1 with glycophorin A (GPA) during their biosynthesis as the AE1-deficient erythrocytes were devoid of GPA [35]. One possible hypothesis could be that, similarly to that proposed for Band 3, adducin (or other adducin partner disturbed in the erythrocyte skeletons from mutant mice) might play a "chaperon-like" role in the formation of actin filaments, affecting the levels of α-TM and Tmod, a task that seems not to be correctly performed by EcapZ. On the other hand, the absence of variations in p55 and protein 4.1 might suggest that direct or indirect interactions of adducin with p55 and protein 4.1 are limited.

We have shown here that erythrocytes skeletons from β-adducin deficient mice contain a 9–10-fold upregulation of EcapZ, a 65% decrease in α-TM and an increase in Tmod. This is neither a consequence of the protocol used to prepare the protein extract nor due to the genetic background of the mice. The described molecular defects might generate a reduction in the number, length and/or stability of the actin filaments, probably producing altered junctional complexes that could be the cause of the presence of SphHE in mutant mice [15].

Acknowledgements: Author acknowledges Corrado Guarnaccia for help with adducin purification, Mauro Sturnega for animal care and Youhna Ayala for protein sequencing assistance with the mass spectrometer.

References

[1] Bennett, V. and Gilligan, D.M. (1993) Annu. Rev. Cell Biol. 9, 27–66.
[2] Kuhlman, P.A., Hughes, C.A., Bennett, V. and Fowler, V.M. (1996) J. Biol. Chem. 271, 7986–7991.
[3] Fowler, V.M. (1996) Curr. Opin. Cell Biol. 8, 86–96.
[4] Fowler, V.M. and Bennett, V. (1984) J. Biol. Chem. 259, 5978–5989.
[5] Shen, B.W., Josephs, R. and Steck, T.L. (1986) J. Cell Biol. 102, 997–1006.
[6] Cooper, J.A. (2002) Curr. Biol. 12, R523–R525.
[7] Ono, S. and Ono, K. (2002) J. Cell Biol. 156, 1065–1076.
[8] Schafer, D.A. and Cooper, J.A. (1995) Annu. Rev. Cell Dev. Biol. 11, 497–518.
[9] Casella, J.F., Craig, S.W., Maack, D.J. and Brown, A.E. (1987) J. Cell Biol. 105, 371–379.
[10] Kuhlman, P.A. and Fowler, V.M. (1997) Biochemistry 36, 13461–13472.
[11] Dong, L., Chapline, C., Mousseau, B., Fowler, L., Ramsay, K., Stevens, J.L. and Jaken, S. (1995) J. Biol. Chem. 270, 25534–25540.
[12] Joshi, R., Gilligan, D.M., Otto, E., McLaughlin, T. and Bennett, V. (1991) J. Cell Biol. 115, 665–675.
[13] Gardner, K. and Bennett, V. (1986) J. Biol. Chem. 261, 1339–1348.
[14] Gilligan, D.M., Lozovatsky, L., Gwynn, B., Brugnara, C., Mohandas, N. and Peters, L.L. (1999) Proc. Natl. Acad. Sci. USA 96, 10717–10722.
[15] Muro, A.F., Marro, M.L., Gajovic, S., Porro, F., Luzzatto, L. and Baralle, F.E. (2000) Blood 95, 3978–3985.
[16] Shima, T., Okumura, N., Takao, T., Satomi, Y., Yagi, T., Okada, M. and Nagai, K. (2001) J. Biol. Chem. 276, 42233–42240.
[17] Matsuoka, Y., Li, X. and Bennett, V. (2000) Cell. Mol. Life Sci. 57, 884–895.
[18] Fukata, Y., Oshiro, N., Kinoshita, N., Kawano, Y., Matsuoka, Y., Bennett, V., Matsuura, Y. and Kaibuchi, K. (1999) J. Cell Biol. 145, 347–361.
[19] Matsuoka, Y., Li, X. and Bennett, V. (1998) J. Cell Biol. 142, 485–497.
[20] Matsuoka, Y., Hughes, C.A. and Bennett, V. (1996) J. Biol. Chem. 271, 25157–25166.
[21] Bianchi, G. et al. (1994) Proc. Natl. Acad. Sci. USA 91, 3999–4003.
[22] Waseem, A. and Palfrey, H.C. (1988) Eur. J. Biochem. 178, 563–573.
[23] Marro, M.L. et al. (2000) Hypertension 36, 449–453.
[24] Benz, E.J. (1994) in: The Molecular Basis of Blood Diseases (Stamatoyannopoulos, G., Nienhuis, A.W., Majerus, P. and Varmus, H., Eds.), pp. 257–292, WB Saunders Company, Philadelphia, PA.
[25] Jarolim, P., Wichterle, H., Hanspal, M., Murray, J., Rubin, H.L. and Palek, J. (1995) Br. J. Haematol. 91, 502–510.
[26] Tchernia, G., Mohandas, N. and Shohet, S.B. (1981) J. Clin. Invest. 68, 454–460.
[27] Feo, C.J., Fischer, S., Piau, J.P., Grange, M.J. and Tchernia, G. (1980) Nouv. Rev. Fr. Hematol. 22, 315–325.
[28] Lin, J.J., Chou, C.S. and Lin, J.L. (1985) Hybridoma 4, 223–242.
[29] Bennett, V. (1983) Methods Enzymol. 96, 313–324.
[30] Mastro, R. and Hall, M. (1999) Anal. Biochem. 273, 313–315.
[31] Joshi, R. and Bennett, V. (1990) J. Biol. Chem. 265, 13130–13136.
[32] Gardner, K. and Bennett, V. (1987) Nature 328, 359–362.
[33] Mische, S.M., Mooseker, M.S. and Morrow, J.S. (1987) J. Cell Biol. 105, 2837–2845.
[34] Weber, A., Pennise, C.R., Babcock, G.G. and Fowler, V.M. (1994) J. Cell Biol. 127, 1627–1635.
[35] Hassoun, H., Hanada, T., Lutchman, M., Sahr, K.E., Palek, J., Hanspal, M. and Chishti, A.H. (1998) Blood 91, 2146–2151.

Published online January 9, 2006

Nucleic Acids Research, 2006, Vol. 34, No. 1 ***243–253***
doi:10.1093/nar/gkj425

Brain-specific promoter and polyadenylation sites of the β-adducin pre-mRNA generate an unusually long 3′-UTR

Luisa Costessi, Giulia Devescovi, Francisco E. Baralle and Andrés F. Muro*

International Centre for Genetic Engineering and Biotechnology, Trieste, Italy

Received November 11, 2005; Revised and Accepted December 15, 2005 DDBJ/EMBL/GenBank accession no. DQ231568

ABSTRACT

Adducins are a family of membrane skeleton proteins composed of α-, β- and γ-subunits that promote actin and spectrin association in erythrocytes. The α- and γ-subunits are expressed ubiquitously, while the β-subunit is found in brain and erythropoietic tissues. The brain β-adducin protein is similar in size to that of spleen, but the mRNA transcript is a brain-specific one that has not been yet characterized, having an estimated length of 8–9 kb instead of the 3–4 kb of spleen mRNA. Here, we show the molecular basis for these differences by determining the structure of the brain-specific β-adducin transcript in rats, mice and humans. We identified a brain-specific promoter in rodents that, apparently, was not conserved in humans. In addition, we present evidence that the brain-mRNAs are formed by a common mechanism consisting in the tissue-specific use of alternative polyadenylation sites generating unusually long 3′-untranslated region of up to 6.6 kb. This hypothesis is supported by the presence of highly-conserved regions flanking the brain-specific polyadenylation site that suggest the involvement of these sequences in the translational regulation, stability and/or subcellular localization of the β-adducin transcript in the brain.

INTRODUCTION

Adducins are a family of membrane skeleton proteins encoded by three related genes (ADD1 or α, ADD2 or β and ADD3 or γ). All three members undergo alternative splicing of their pre-mRNA potentially generating a variety of protein isoforms, which have not yet been fully characterized (1–4). Adducin is found as hetero-dimer or hetero-tetramer of α/β or α/γ composition in most tissues. Human erythrocytes exclusively contain α/β heterodimers that promote the association of actin and spectrin in the membrane skeleton (5). Both the α- and γ-adducin are expressed ubiquitously, while the β-adducin gene shows a pattern of expression restricted to brain and hematopoietic tissues such as bone marrow and spleen (6–8), suggesting a different transcriptional regulation and function for all three genes.

In the brain, α- and β-adducin expression is found to be highly enriched in regions with high synapse densities of the hippocampus, corpus striatum, cerebral cortex and cerebellum (9,10), and it was shown recently that β-adducin may play a role in the cellular processes underlying synaptic plasticity associated with learning and memory (10). However, both the gene structure of the β-adducin gene and the molecular characterization of the mRNA isoforms are still incomplete. In fact, the brain β-adducin gene product identified by western blot analysis has roughly 110 kDa, only slightly larger than that of 97 kDa detected in spleen (6,11), but the β-adducin mRNA transcript that codes for this protein form is a brain-specific one that has 8–9 kb instead of the 3–4 kb of that one found in spleen (7,12). Although the long brain-specific β-adducin mRNA has been described about 15 years ago (7,12), the molecular basis of this unusually long brain-specific mRNA have not been characterized (1–3,13).

In the present work we determine the molecular structure of the brain-specific β-adducin transcript in rat, mice and humans. The β-adducin gene is found in chromosome 2, 6 and 4 in humans, mice and rats, respectively, in regions of chromosomal synteny, suggesting a common evolution and similar regulatory mechanisms in all three species. However, the brain-specific promoter in rats and mice is not apparently conserved in humans. We show the presence of an 8–9 kb long β-adducin transcript also in human brains and we present evidence of a common mechanism in all three species consisting in the use of tissue-specific polyadenylation sites. In addition, the regions flanking the brain-specific polyadenylation site are highly conserved supporting the hypothesis of a common mechanism regulating the 3′-untranslated region

*To whom correspondence should be addressed. Tel: +39 040 3757312; Fax: +39 040 226555; Email: muro@icgeb.org

(3′-UTR) in rats, mice and humans and highlighting the importance of these sequences in the translational regulation, stability and/or subcellular localization of the β-adducin transcript in brain.

MATERIALS AND METHODS

Animals

The generation of the mice devoid of β-adducin has been described previously (6), the wild-type mice used were C57BL/6. The rats were Sprague–Dawley. All animals used in the experiments described below were males of 3 months of age and were of nearly the same weight.

Protein preparation and western blot analysis

Protein preparations and western blot of erythrocytes and brain were as described (6).

RNA preparation, RT–PCR and northern blot analysis

Total cellular RNA was prepared basically by the guanidinium thiocyanate method (14) from freshly extracted tissues from rat and mice, quantified by measuring absorbance at 260 and 280 nm, and RNA integrity was confirmed by running the samples on 1% agarose formaldehyde gels. Human RNAs were from two commercial suppliers (Ambion and Clonetech). PCR primers used in the present work were prepared by Sigma Genosis. Their sequence and specific use is detailed in Supplementary Table 3. RT–PCRs were performed for 35 cycles.

For northern blot analysis, 20 μg of RNA was loaded in 1.2% agarose formaldehyde gels, transferred to nylon membranes, and hybridized with the appropriate DNA probe labeled with 32-αP-dCTP.

RNase protection and primer extension assays

For the RNase protection assay, overlapping fragments covering the entire rat β-adducin cDNA sequence were subcloned from a full-length rat cDNA clone into pBS-KS plasmid. The RNase protection assay was performed essentially as described (15,16). Each of the DNA subclones was linearized, the antisense strand synthesized radioactively with either T7 or T4 RNA polymerase and purified through denaturing acrylamide gels. The probe and β-adducin RNA hybrids were digested, run in denaturing acrylamide gels and exposed for autoradiography.

The primer extension assays were performed essentially as described (15). Briefly, the oligonucleotide 5′βNC, complementary to the end of the 99 bases rat exon 2 was annealed to rat spleen and brain RNA and the RT reaction was performed in the presence of radioactive 32-αP-dCTP. The primer extension products were run in denaturing acrylamide gels and exposed for autoradiography.

Database analyses and bioinformatics

The search for alternative exons in the β-adducin gene required analysis of both cDNA and expressed sequence tag (EST) sequences in the Genbank. To identify candidate first exons or alternative internal exons, we used each of the β-adducin exon sequences as probes for BLAST species-specific searches of Genbank. The candidate sequences that were found contiguous to β-adducin exons were checked for proper splicing and their chromosomal location was determined by BLAST analysis against the complete genome using the NCBI browser (http://www.ncbi.nlm.nih.gov/BLAST/). The alignment of the ESTs with the β-adducin genomic sequence and the detection of the ESTs containing poly(A) tails were analyzed manually with the help of the UCSC Genome Browser (http://genome.ucsc.edu/). The coordinates of the chromosomal position of the exons and introns listed in Supplementary Table 1 refer to that used in the ENSEMBL browser (July 2005) developed by the EMBL, EBI and Sanger Institute (http://www.ensembl.org/index.html). In order to confirm experimentally that these sequences were bona fide exons in the β-adducin gene, RT–PCRs were performed from brain and spleen total RNA and the results are shown in Figure 3 and Supplementary Figure 2.

Promoter analysis was performed with both the DNAstar Lasergene program and the TESS browser from the University of Pennsylvania (http://www.cbil.upenn.edu/cgi-bin/tess/tess?RQ=WELCOME). A selection of the predicted transcription factor binding sites that displayed a high score and were present in both analyses is shown in Supplementary Figure 1.

RESULTS

The reported full-length cDNAs for β-adducin (ADD2) in mouse, rat and humans have 3119, 3115 and 3938 bp, respectively and the molecular weight of the encoded proteins [(6,7,12), ENSEMBL and Supplementary Table 1] is on line with the presence of 5′- and 3′-UTR of average length (17). In addition, the β-adducin pre-mRNA undergoes alternative splicing and northern blot analysis of erythropoietic tissues using a β-adducin probe detects the expected β-adducin bands in the range of 3.5–4.5 kb in all three species (Figure 1A, Lanes 2, 4 and 7). In fact, more than one band was seen when spleen RNA was used in the northern blot experiment and it was suggested that they might be the result of alternative splicing of the β-adducin pre-mRNA (1–3) generating the β-add97 and β-add63 families of transcripts.

Interestingly, northern blot studies showed that the β-adducin mRNA from brains of rats and mice had ∼8–9 kb (Figure 1A, Lanes 1 and 3) while the protein band in the same tissue had an apparent molecular weight of 110 kDa, only slightly higher than that of 97 kDa observed in spleen (Figure 1B, Lanes 8 and 9) (6,7,11,12). This is consistent with previous reports that showed that brain adducin cross-reacts immunologically with erythrocyte adducin having at least 50% of antigenic sites in common (11). The size differences between the brain and erythrocyte β-adducins might be due to post-translational modifications, but, to our knowledge, there is no report showing neither the reasons for substantial differences between the mRNA and protein size nor the complete identity of the erythroid and brain subunits.

In addition, we show in Figure 1A that the same size difference between brain and bone marrow mRNA was also present in humans. In fact, an 8–9 kb band was also observed by northern blot analysis of human brain RNA (Figure 1A, Lane 5). It is interesting to note that the bands observed in humans were slightly bigger than those of mice and rats. Regrettably, we were not able to detect a clear signal of

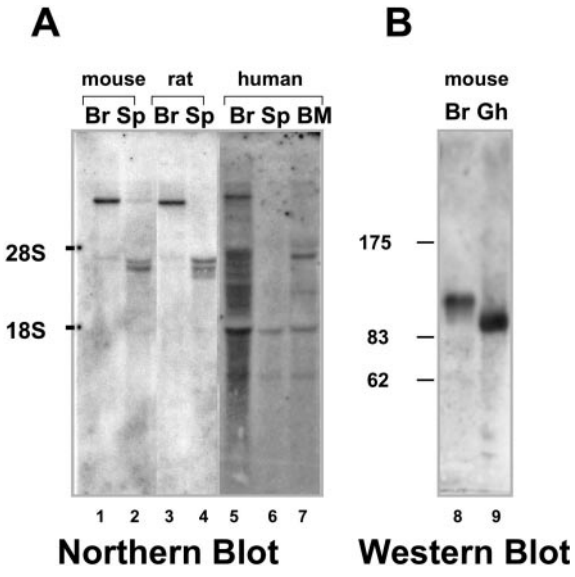

Figure 1. Northern and western blot analysis of brain and spleen β-adducin. (**A**) Northern blot analysis of mouse, rat and human RNAs. RNAs from mouse, rat and human brain and spleen were loaded in lanes 1–6 (25 μg). In lane 7, human bone marrow RNAs was loaded (25 μg). All RNAs were run in the same agarose formaldehyde gel, transferred to Hybond-N and hybridized with the mouse and human β-adducin probes (Lanes 1–4 and 5–7, respectively). The 28S and 18S rRNAs are indicated. (**B**) Brain and ghosts protein extracts (20 μg) were loaded in a 6% SDS–PAGE, blotted onto nitrocellulose, incubated with an anti-β-adducin antibody and visualized by chemioluminiscence. MWMs are indicated on the left. Br, brain; Sp, spleen; BM, bone marrow; Gh, ghosts.

human spleen RNA samples obtained from two different commercial suppliers (Figure 1A, lane 6), which might be due to the fast degradation of the RNA in this tissue before sample preparation. In fact, significant RNA degradation was also observed in human brain and bone marrow samples (Figure 1A, lanes 5–7) and some of the observed bands might be the result of alternative splicing and/or degradation products.

Therefore, the brain β-adducin mRNA contains about 5–6 kb of extra sequences in all three species and, as mentioned above, there is no report describing the molecular characterization of the brain β-adducin mRNA.

A brain-specific exon is present in the 5′-UTR of rats and mice

To identify the molecular basis of the size differences between the brain and spleen β-adducin mRNAs we performed RT–PCR analysis of brain and spleen RNA from mouse, rat and human tissues. The PCRs covered the complete 5′-UTR, coding regions and 3′-UTR of the reported β-adducin sequences in all three species, but produced in all cases the expected products and no extra band appeared that might explain the size difference between brain and spleen β-adducin mRNAs (data not shown).

To rule out that the amplification of a putative longer PCR product could be competed-out by the smaller expected product, we performed RNase protection analysis of rat brain and spleen total RNAs utilizing overlapping antisense riboprobes encompassing the entire reported ADD2 cDNA sequence. Again, no extra bands were observed when probes corresponding to the coding exons were used, indicating the absence of previously undetected exons inserted within the reported β-adducin open reading frame (ORF) (data not shown). In addition, this experiment demonstrated that the ORFs of the erythrocyte and the brain subunits of β-adducin were identical, providing supporting evidence that the size differences between brain and erythrocyte β-adducin observed in the western blot analysis are probably due to post-translational modifications.

Surprisingly, when we used a probe covering the 5′-UTR of the reported rat β-adducin sequence we detected the expected 168 bases protected fragment for the spleen RNA (Figure 2A and B, Lanes 2–3), but a smaller protected fragment of ∼100 bases was present in the brain RNA samples (Figure 2A and B, Lanes 4–5). This indicated the presence of different 5′-UTR in β-adducin mRNAs from brain and spleen tissues.

The 5′ RACE analysis of rat brain RNA led to the cloning and sequencing of a brain-specific exon. The longest clone contained a novel sequence of 258 bases (GenBank accession no. DQ231568, Figure 3). RNase protection analysis using the novel brain exon as probe produced the expected protected fragment of 198 bases in brain RNA samples (Figure 2A and C, Lanes 11–12) while a protected fragment of 104 bases was observed in spleen RNA samples (Figure 2A and C, Lanes 9–10). This result confirmed the exclusive presence of the novel exon in brain β-adducin mRNAs and that of the previously reported 54 bp exon in spleen β-adducin mRNAs.

To determine the transcription initiation site of rat brain and spleen β-adducin mRNAs we performed a primer extension experiment utilizing a primer complementary to the 3′ end of the 99 bases exon, the first exon common to brain and spleen mRNAs (Figure 2D and the scheme of Supplementary Figure 2A). Primer extension analysis of rat brain RNA showed two main bands of about 300 and 320 bases, ending very close to the 5′ end of the longest cDNA clone obtained by RACE–PCR of brain RNA (Figure 2D, Lanes 17–18). Northern blot analysis of RNA samples from mouse cerebellum, brain and spleen with a probe specific for the brain exon is shown in Figure 2E. A band of about 8–9 kb was observed in cerebellum and brain RNA samples (Lanes 19–20) while no band was observed for spleen RNA (Lane 21), confirming the tissue-specific expression of each exon as seen by the RNase protection experiment and suggesting a link between the use of the brain-specific promoter and the 8–9 kb long brain-specific mRNA. In the analysis of the spleen RNA two main bands of 163 and 168 bases were observed by primer extension, the bigger one coinciding with the reported transcription initiation site of the rat β-adducin gene and smaller the one only 5 bases downstream of that site (Figure 2D, Lanes 15–16, and Supplementary Figure 1B).

Structure of brain and spleen-specific promoters

The 5′ end of the human β-adducin mRNA has been determined by RACE analysis of RNA from a neuronal cell line and, using the amplified product as probe, the genomic region containing the putative human β-adducin promoter was cloned (1). However, comparison of the β-adducin exonic architecture and sequences among human, rat and mouse suggested a different genomic structure for the 5′ ends for the murine β-adducin gene. While there was an almost perfect matching

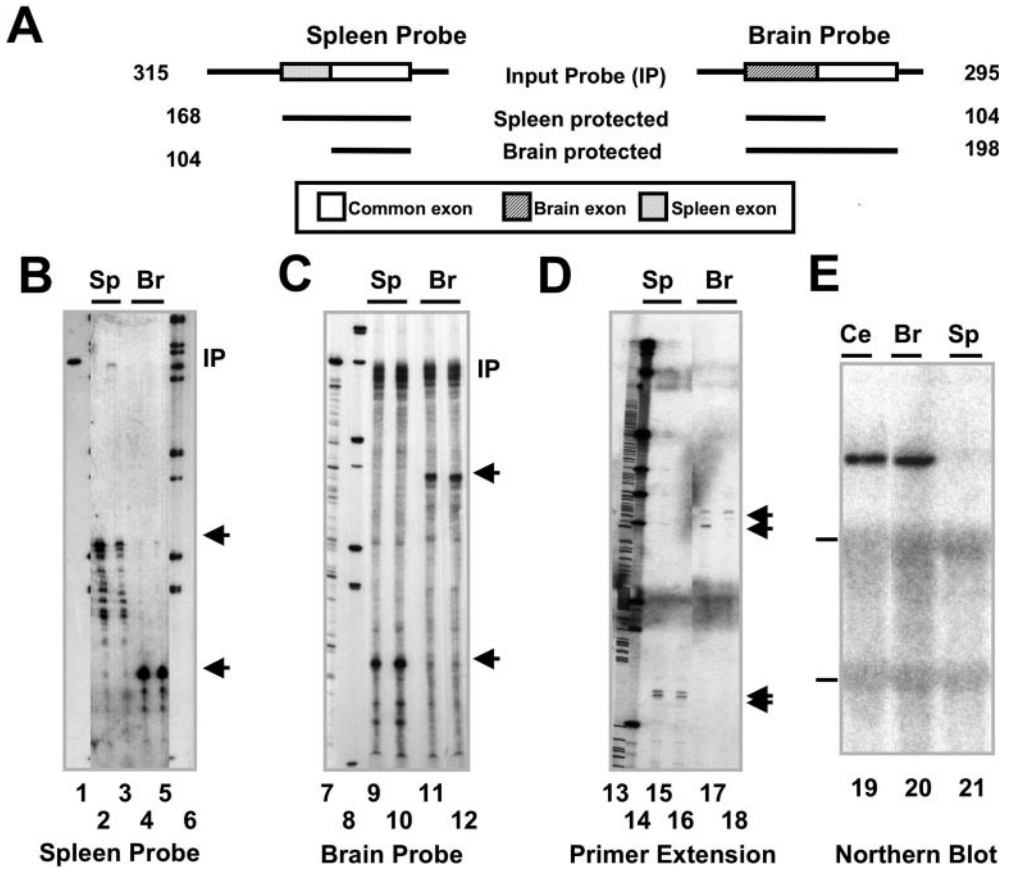

Figure 2. Detection of brain- and spleen-specific β-adducin exons in rats and mice. (**A**) Schematic representation of the riboprobes used in the RNase protection experiment shown in (B and C). The input probe and the size of the protected fragments for each probe and each tissue are indicated. (**B** and **C**) The spleen and brain probes shown in (A) were used in (B and C), respectively. Thirty micrograms of total spleen and brain RNA were annealed to the probe, digested with RNase, run in a polyacrylamide denaturing gel and autoradiographed. Lanes 1 and 7 correspond to the undigested probe (input probe), lanes 6 and 7 are radioactive molecular weight markers, lanes 2–3 and 9–10 spleen RNA, and lanes 4–5 and 11–12 brain RNAs. The arrows indicate the protected fragments. (**D**) Primer extension experiment with a primer annealing in the boundary between the constitutive 99 bp and the 217 bp exons (exons 2 and 3), that are present in both the brain and spleen forms of the β-adducin mRNA. The arrows indicate the primer extension products observed in brain and spleen RNAs. Lanes 15–16 and 17–18 correspond to spleen and brain RNAs, respectively. Lane 14 is a radioactive molecular weight marker, and lane 18 is a one-lane Sanger sequence using the same primer used in the experiment. (**E**) Northern blot experiment of cerebellum, brain and spleen mouse RNA (lanes 19–21, respectively) with a probe corresponding to the mouse brain-specific exon. The position of the 28S and 18S rRNA is indicated.

in the length and a high degree of homology of the protein coding exons among the three species, the conservation and length of the first exon highly differed (Supplementary Table 1). In fact, the human first exon was 312 bp long, while that of mice and rats had 219 bases. In addition, cloning and sequencing of the putative rat brain promoter region showed 90.8 and 94.1% of homology between mouse and rat sequences for the promoter region (up to position −300 bp) and for the brain-specific exon, respectively (Supplementary Figure 1A and Supplementary Table 1). On the contrary, the conservation between the human and rodent promoter region and first exons was only 47 and 53%, respectively.

Promoter prediction analysis of the human, rat and mouse brain-specific promoters showed that the sequences 5′ to the mouse and rat brain-specific exons (mN1 and rN1 exons, respectively) contained a consensus Inr sequence (18) and several potential transcription binding sites (Supplementary Figure 1A). The transcription site determined in rat by the primer extension experiment exactly coincided with that reported for the mouse β-adducin mRNA (ENSEMBL, transcript ENSMUST00000077101, Supplementary Figure 1A). The *in silico* prediction showed that just a few transcription factor sites were common among all three species and in the human promoter numerous SP1 binding sites were predicted, a transcription factor found in many housekeeping genes that binds to GC rich regions, that were not so profuse in the rodent promoter. In fact, the GC value of the human promoter was 79.3% while in the rat and mouse brain rodent promoters it was of 55–60% supporting the observed differences in structure and suggesting a diverse transcriptional regulation of this β-adducin gene promoter.

Sequence comparison of the spleen-specific promoter region and first spleen-transcribed exon of rat and mouse β-adducin erythroid-specific exons (mE1 and rE1, respectively) with the recently reported human erythroid exon (hE1) (13) showed 84% homology between rat and mouse, while the homology between mE1 and rE1 sequences and the hE1 exon were only of 43% and 47%, respectively (Supplementary Figure 1B and Supplementary Table 1). Similarly to that observed for the human erythroid promoter (13), both the rat and mouse spleen promoters contained a conserved Inr sequence (18). In addition, other potential transcription sites

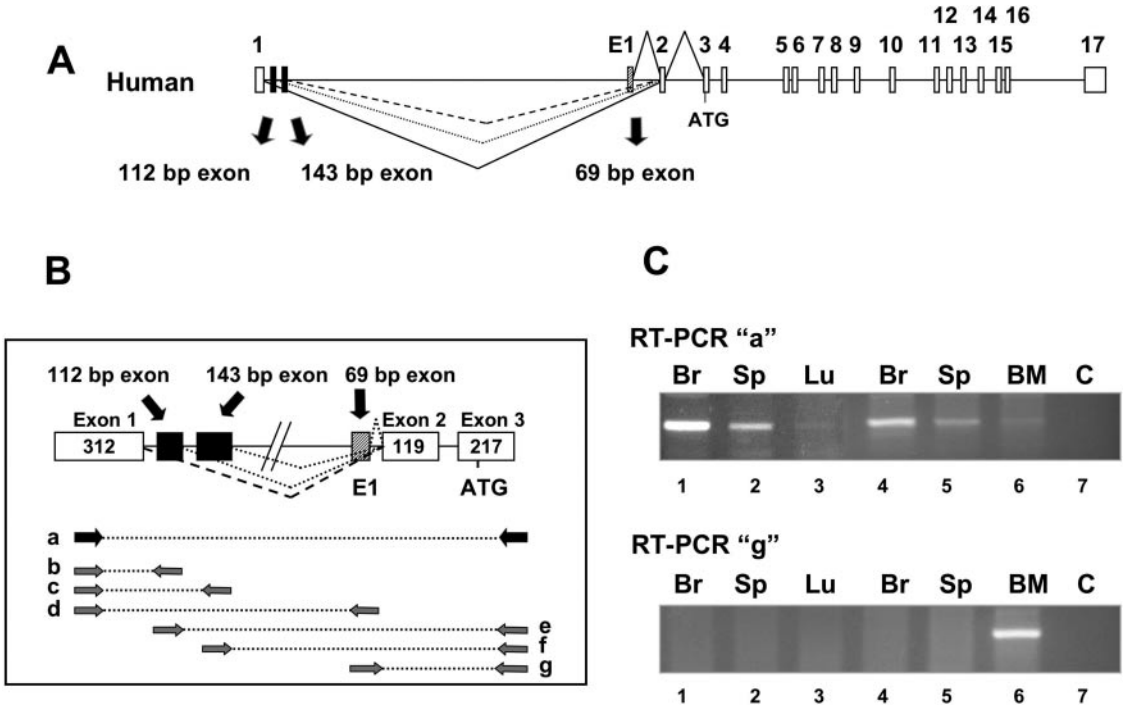

Figure 3. Analysis of new potential β-adducin exons in humans. (**A**) Schematic representation of the human β-adducin gene structure showing the position of the new potential exons composed of novel sequences flanked by known β-adducin exons. The open boxes indicate the exons 1–17; the closed boxes indicate the 112 bp and the 143 bp exons; and the dashed box indicates the erythroid-specific E1 exon. (**B**) Schematic representation shows the position of the oligonucleotides utilized in the RT–PCR to amplify the 112 bp exon (primer pairs 'b' and 'e'), the 143 bp exon (primer pairs 'c' and 'f') and the 69 bp exon (primer pairs 'd' and 'g'). As no product was obtained after the first round of amplification (primer pairs 'b', 'c', 'd', 'e' and 'f'), a nested PCR was performed with negative results (data not shown). (**C**) The primer pairs 'a' and 'g' showed in (B) that amplify a product from exon 1 to exon 3, and from exon E1 to exon 3, respectively, were utilized for an RT–PCR with samples from brain, spleen (two independent preparations, lanes 1–2 and 4–5), bone marrow and lung.

were found within the rat and mouse promoters and are shown in Supplementary Figure 1B. We observed that between rodents and humans most binding sites were not conserved. However, those of the hematopoietic GATA transcription factor family (19) predicted for the human erythroid E1 promoter (13) were present in conserved regions of the rodent promoters.

Tissue-specificity of the β-adducin pre-mRNA transcription

An additional functional difference between human and rodent promoters is their tissue-specificity. In fact, while the mouse and rat β-adducin pre-mRNAs are transcribed from a brain-specific promoter, the human one seems to be active not only in brain but also in spleen and bone marrow, and to a much lesser extent in lung.

We analyzed the pattern of expression of the brain and spleen-specific exons in kidney, liver, brain, lung, heart, placenta, bone marrow and spleen of embryos, newborn and adult mice of different ages. We observed that the mouse brain-specific promoter was active in brain of 13.5 day-embryo, postnatal 1- and 14-day-old animals, and 3-month-old mice (Supplementary Figure 2B, primers pair 'a'). On the contrary, no expression was observed in other tissues. The spleen promoter was active in liver embryo and placenta, and had a low level of expression in other embryonic tissues (Supplementary Figure 2B, primers pair 'c'). In 14-day-old mice and adults, the expression in the liver and other tissues seemed to be completely shutdown and was active only in the spleen and bone marrow.

To determine the expression pattern of the human exon 1 we used the same RNA samples with the pair of primers 'a' shown in Figure 3B and Supplementary Table 3, that amplify the fragment from human exon 1 to exon 3. A specific PCR product was observed for brain, spleen, bone marrow and lung as shown in Figure 3C (primers 'a'), although the amount of RT–PCR product observed in lung was very low. This experiment strongly suggests differences in activity and tissue-specificity between the rodent and human promoter. Those variations might be related to the structural and base composition changes observed among the species, as described above and shown in Supplementary Figures 1 and 2.

The brain-specific β-adducin mRNA has an unusually long 3′-UTR

We showed above the existence of a novel brain-specific first exon and its putative promoter for rats and mice. However, despite that this exon was longer than that used in spleen and other organs, it did not account for the observed size differences between brain and spleen mRNAs (Figure 1 and Supplementary Table 1). Therefore, we focused the search in the 3′-UTR region to determine the molecular basis of the brain 8–9 kb β-adducin mRNA. Database search (UCSC Genome Browser http://genome.ucsc.edu/) showed the presence of ESTs transcripts in mouse, rat and humans in the region downstream to the known β-adducin 3′-UTR, that in all three cases have not been assigned as part of the β-adducin mRNA. A scheme showing the alignment of the genomic

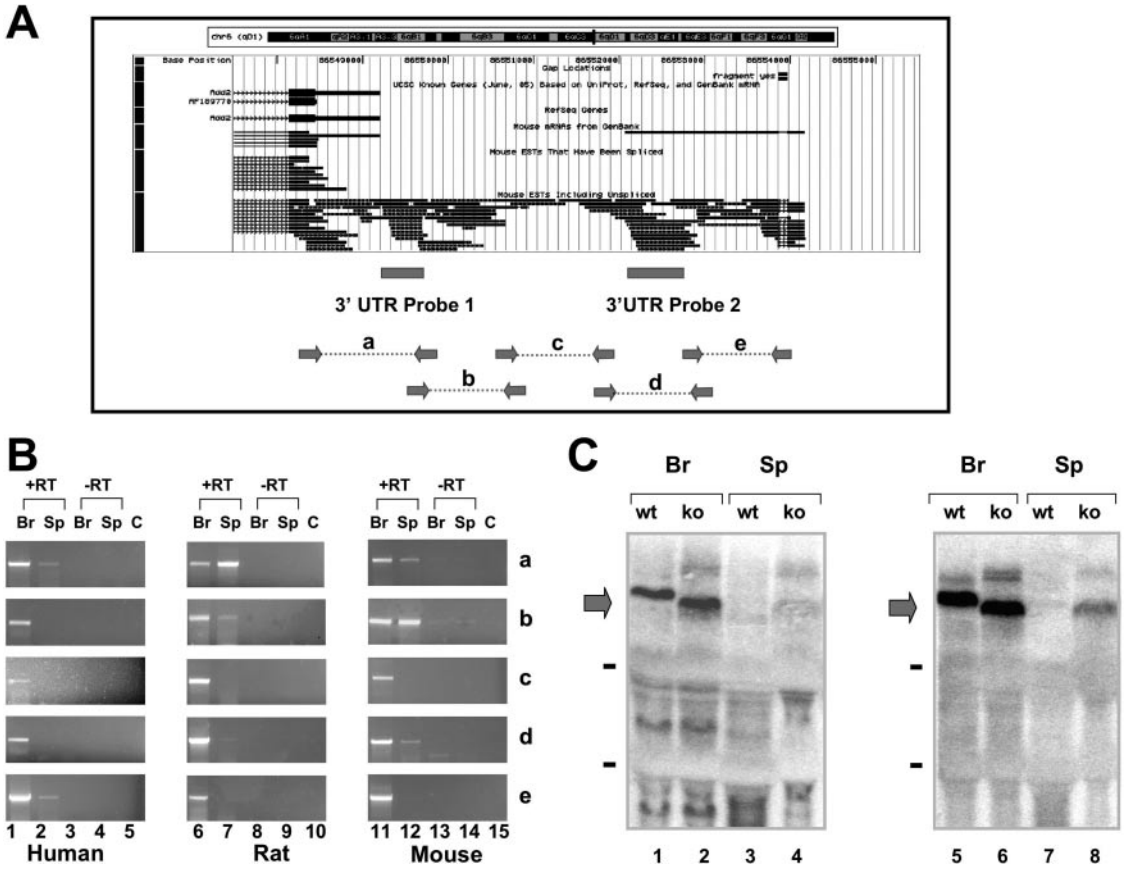

Figure 4. The brain β-adducin mRNA has an unusually long 3′-UTR. (**A**) Schematic representation corresponding to the mouse genomic region downstream of the reported polyadenylation site (UCSC browser). The ESTs corresponding to that region are indicated. The position of the PCR primers used the RT–PCRs shown in (B) are schematically indicated. The probes used in the northern blot experiment of (C) are shown. (**B**) RT–PCRs of brain and spleen RNA, from human (lanes 1–5), rat (lanes 6–10) and mouse (lines 11–15) tissues were performed with different set of primers of the region downstream of the reported β-adducin polyadenylation site. Lanes 3–4, 8–9 and 13–14 were performed with the same RNAs of lanes 1–2, 6–7 and 11–12, respectively, but without the reverse transcriptase reaction. Lanes 5, 10 and 15 correspond to the PCR without the addition of cDNA. (**C**) Northern blot experiment of brain and spleen total RNA (20 μg per lane) from control and β-adducin KO mice (control mice: lanes 1 and 5, brain; lanes 3 and 7, spleen; β-adducin KO mice: lanes 2 and 6, brain; lanes 4 and 8, spleen). Two identical membranes were hybridized with 3′-UTR probes 1 and 2 (Lanes 1–4 and 5–6, respectively). An arrow indicates the detected bands. The size of the band observed in the β-adducin KO brain sample has a lower molecular weight due to the targeted deletion. The position of the 28S and 18S rRNA is indicated.

region downstream of the reported β-adducin gene and the available mouse ESTs is shown in Figure 4A. Human and rat EST distribution covered a similar region to that schematically shown in Figure 4A for mice (data not shown).

To determine whether those ESTs could belong to the β-adducin brain mRNA, a series of overlapping RT–PCR analysis was performed using RNA from brain and spleen, prepared from rat, mouse and human tissues. As schematically shown in Figure 4A, the first pair of primers (called 'a' in Figure 4A and Supplementary Table 3) should amplify a portion of the known β-adducin 3′-UTR and up to 800–1100 bases, depending on the species, of the sequence downstream of the reported 3′-UTR of β-adducin. The other pairs of primers ('b', 'c', 'd' and 'e', Figure 4A and Supplementary Table 3) were complementary to sequences downstream to the known β-adducin 3′-UTR, and were designed in order that each PCR product overlapped the flanking ones covering the entire region up to the most downstream EST shown in Figure 4A.

The RT–PCR analysis showed specific PCR products in brain samples for all primer pairs used (Figure 4B, Lanes 1, 6 and 11). In addition, an RT–PCR using a reverse primer located 80 bases after the last reported EST and the forward one used in pair 'e' produced no product, suggesting that all the β-adducin brain mRNA ends at the same site (Figure 4A and data not shown). These results strongly suggested that the 8–9 kb mRNA transcript observed in brain could be generated by alternative usage of polyadenylation sites. To confirm this hypothesis we performed northern blot analysis of mouse brain and spleen RNAs from control and β-adducin KO mice using two different probes of 600 and 800 bp that mapped downstream of the β-adducin stop codon present in exon 16, in the novel 3′-UTR of brain β-adducin mRNA (starting ∼1400 and 3500 bases downstream of the stop codon, respectively; see scheme of Figure 4A). Both probes showed the presence of a band of similar size to that detected for the mouse brain β-adducin mRNA (Figure 4C, Lanes 1 and 5), confirming that the difference in size of the brain β-adducin mRNA is due to the presence of an extremely long 3′-UTR. In addition, taking advantage of the β-adducin KO mice previously generated in our laboratory (6), we run in the same gel RNA samples prepared from the brain of KO mice and we also observed

a high molecular weight band having a small reduction in size indicating, unambiguously, that the detected band was indeed the product of the β-adducin gene and not the result of unspecific hybridization (Figure 4C, Lanes 2 and 6). The targeted deletion in the β-adducin locus corresponds to a reduction of 744 bases in the β-adducin97 mRNA (exons 9 to 13) (6). A faint band of similar size to that observed in brain RNA samples of KO mice was also observed for spleen RNA samples of KO mice (Figure 4C, Lanes 4 and 8). These bands could be the result of altered polyadenylation regulation in spleen of the β-adducin deficient mice due to the loss of important regulatory sequences by the targeted genomic deletion. In fact, no band is observed in the spleen RNA samples of control mice (Figure 4, Lanes 3 and 7).

In addition, northern blot analysis using an Add63-specific probe showed that the ADD63 family of transcripts also has a long 3′-UTR in brain (Supplementary Data and Supplementary Figure 3). Moreover, hybridization of a parallel membrane with an Add97-specific probe suggested that the relative abundance of the Add63 transcripts is considerably less than the Add97 forms.

A highly-conserved brain-specific polyadenylation site is used in mice, rats and humans

According to the scheme shown in Figure 4A, EST sequences were aligned to genomic sequences of the region downstream of the known β-adducin poly(A) site reported in the last exon and were examined for the presence of poly(A) tails after the alignment. Several EST-containing poly(A) tails were found at chromosomal positions 86 554 176, 120 280 485 and 70 795 572 for mouse chromosome 6q, rat chromosome 4q and human chromosome 2p, respectively (see below and Supplementary Tables 1 and 2), thus generating extremely long brain-specific last exons of 6034, 5592 and 6951 bases and a 3′-UTR of 5831, 5289 and 6642 bases for mouse, rat and human, respectively (Figure 5A and Supplementary Table 1). We will call these distal brain-specific polyadenylation sites mA_4, rA_4 and hA_4 for mice, rats and humans, respectively (Figure 5A and C).

The DNA sequences of the last exon up to the detected poly(A) sites, including the adjacent downstream regions, were retrieved for all three species. Sequence comparison among mouse, rat and human genomic sequences showed a very high degree of conservation of the 3′ end of the 8–9 kb brain β-adducin transcript, specially in the region of the polyadenylation site used in brain. In fact, within the 200 bp region flanking the distal brain polyadenylation signal we observed a 99.1% homology between mouse and rat sequences, and a 75% homology among all three species (Figure 5C).

Analysis of the sequences lead us to the identification in all three species of all elements required for polyadenylation in mammals: a polyadenylation signal, a putative poorly conserved downstream elements (DSE) downstream of the poly(A) site and a putative U-rich region (upstream element, USE) located upstream of the polyadenylation motif (Figure 5B and C). The polyadenylation motif AGTAAA was found as the brain poly(A) signal in all three species. A scheme of the last exon showing the relative position of all the polyadenylation sites found in the last β-adducin exon of all three species is shown in Figure 5A.

In addition, several ESTs containing poly(A) tails were found for all three species, confirming the use of these distal polyadenylation sites (see the scheme of Figure 4A, Supplementary Data and Supplementary Table 2). Other ESTs that mapped nearby upstream to those mentioned above did not contain the characteristic poly(A) tail. The observation that no ESTs mapping downstream of the proposed polyadenylation site were present (Figure 4A) together with the absence of an RT–PCR product with primers at either side of the mA_4 poly(A) site support the hypothesis that the brain β-adducin pre-mRNA is completely polyadenylated at the proposed A_4 site.

Several proximal polyadenylation sites are present in mice, rats and humans

Based on the available deposited sequences and ESTs, we were able to identify two proximal polyadenylation regions in rodents and three in humans that might generate the spleen β-adducin mRNAs. The first one was located between bases 1000 and 1150 relative to the start of the last exon (named mA_1, rA_1 and hA_1, for mice, rats and humans, respectively, see scheme of Figure 5A), should generate a 3′-UTR of about 750–800 bases and showed a high conservation among the three species (Figure 5A and Supplementary Figure 4). The second region was between the bases 1480–1640 (having more than one cleavage site) and coincided with the polyadenylation region observed in humans at position 1600 relative to the start of the last exon (named $mA_{2\text{-}3}$, $rA_{2\text{-}3}$, and hA_2 for mice, rats and humans, respectively). The putative human polyadenylation signal of hA_2 region was not conserved in rodents as they bear a deletion of the region including that element. However, ESTs with a variable position of the poly(A) tail were found in the $mA_{2\text{-}3}$ and $rA_{2\text{-}3}$ regions (Supplementary Table 2) but no consensus polyadenylation signal was identified in this rodent region (Supplementary Figure 4B, underlined region). Another polyadenylation site (hA_3) mapping at position 2532 of the last human exon was detected and its functionality is supported by the presence of numerous EST containing a poly(A) tail (Figure 5A and Supplementary Table 2).

Additional supporting evidence derives from the observation that more than one band is present in the 3.5–4.5 kb region in the northern blot shown in Figure 1A. In fact, we observe two bands in rat and mouse spleen samples that might correspond to the mRNA forms utilizing the A_1 and $A_{2\text{-}3}$ polyadenylation sites. In the human brain, we see three bands that might be the results of the use of the hA_1, hA_2 and hA_3 polyadenylation sites (depicted in Figure 5A). In the bone marrow sample we mainly detected the higher molecular weight band, which might correspond to the use of the A_3 polyadenylation site. The human bands were of higher molecular weight than the rodent ones, which is on line with the expected position of the different polyadenylation sites and, in consequence, the length of the human transcripts (Figures 1A and 5A). Alternatively, these bands might be the consequence of the generation by alternative splicing of the β-Add97 and β-Add63 families of transcripts. However, this possibility is less probable as the Add63 levels are much lower than those detected for the Add97 family of transcripts (Supplementary Figure 3) and we have observed no other major band in the RNase protection experiment of the

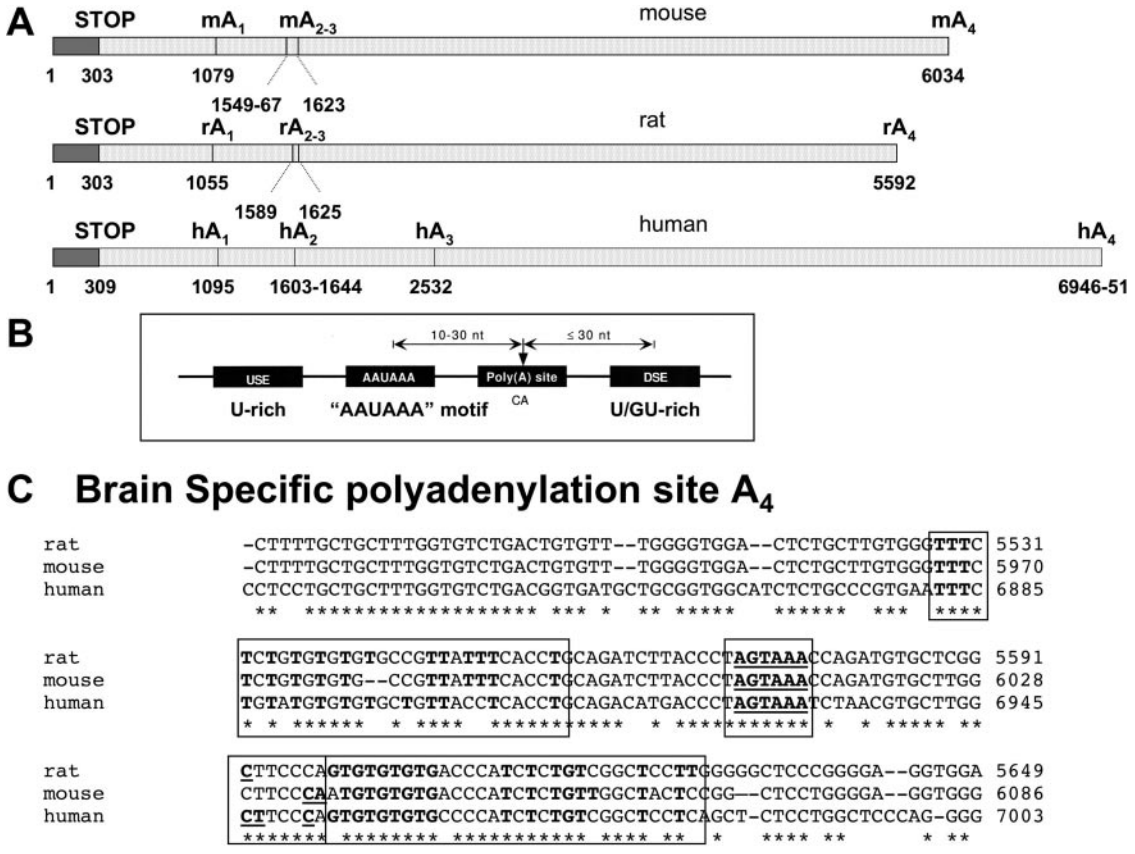

Figure 5. Brain-specific alternative polyadenylation sites. (**A**) A schematic representation of the last exon of the β-adducin gene is shown. The ORF (gray box) and the stop codon are indicated. The positions of the polyadenylation sites used in brain are indicated. The 3′-UTR (5731, 5289 and 6642 bases for mice, rats and humans, respectively) are indicated as a dotted box. (**B**) Schematic representation showing the position of the elements found in the region of the polyadenylation sites of genes. USE, upstream element; DSE, downstream element. (**C**) Sequence comparison among rats, mice and humans of the brain-specific polyadenylation sites. The AGTAAA motifs and the polyadenylation sites are underlined. The U-rich and U/UG-rich elements are indicated. Numbers are relative to the first base of the last exon of each species.

complete β-adducin ORF that might have been produced by alternative splicing.

DISCUSSION

This report describes the complete primary structure of the β-adducin mRNA of brain in humans, rats and mice. We show that the brain mRNA form contains an unusually long 3′-UTR in all three species. Moreover, we present evidence that there is a brain-specific promoter in rodents that was apparently not conserved in humans. Consequently, the architecture of the ADD2 gene is extremely complex with alternative use of tissue-specific promoters and polyadenylation sites, in addition to the intricate alternative splicing pattern of the pre-mRNA already described (2). Moreover, considering the use of the brain-specific mN1 and rN1 exons, the maximum predicted length of the primary transcript of the β-adducin gene in brain was of 96 144 bases, 111 835 bases and 111 412 bases for mice, rats and humans, respectively. We also provide evidence demonstrating the identity between the ORFs of the brain and erythroid β-adducin subunits, suggesting that the observed molecular weight differences in the proteins are the result of post-translational modifications.

Genes encoding intracellular proteins tend to have alternative poly(A) sites (20) and many genes coding for proteins of the membrane skeleton fall within this group having both alternative promoters and polyadenylation sites. For example, the ANK-1 gene has different polyadenylation sites and two promoters that direct its expression to erythroid cells or muscle cells (21,22), protein 4.1 has three promoters that generate distinct N-termini (23) and human band 7.2 gene also utilizes alternative polyadenylation signals (24). In the case of ADD2, we show here that there are two main distinct promoters in rodents, one specific for hematopoietic tissues such as spleen and bone marrow, and the other one specific for neuronal tissues such as brain and cerebellum.

The observations that the homology between the human promoter and rodent brain-specific promoter was only of 48% and that the structure and base composition were highly different among species (80 and 55% of CG content for humans and rodents, respectively) suggested important differences in the regulation of the brain-specific β-adducin transcript in humans and rodents. This hypothesis is supported by the expression data of the human β-adducin gene promoter (Figure 3). The presence of a human brain-specific promoter was previously suggested [M. Bulger, unpublished data; (13)] but we detected transcription from this promoter not only in brain but also in hematopoietic tissues such as spleen and bone

marrow, and at lower levels in lung (Figure 3). However, our observations were performed by RT–PCR and need further analysis for their confirmation. The ubiquitous transcription from the human promoter might be the consequence of the presence of numerous binding sites of the transcription factor SP1, which is required for ubiquitous transcription of multiple housekeeping genes and play an important regulatory role in cellular processes during development and differentiation (25). On the contrary, the rodent brain-specific promoters showed a very tight expression pattern, as we were able to detect its activity only in mouse brain of 13.5 day embryo, postnatal 1- and 14-day-old babies, and adults, but not in other tissues, and no band corresponding to the product of this promoter was detected in the rat spleen sample of the RNase protection experiment. Therefore, we propose the designation of the rodent brain-specific promoters and first exons as mN1 and rN1, standing for neuronal mouse and rat first exons, respectively, but we suggest that the human promoter and first exon are not exclusive to brain (13).

Similarly to that observed in humans, [Figure 3C and (13)], the activity of the mouse and rat spleen-specific promoter was mainly detected in erythropoietic tissues such as liver embryos and placenta, and was also active in other embryonic tissues, although at a lower level of expression (Supplementary Figure 2B, primers pair 'c'). In 14-day-old mice, the expression in the liver and other tissues seemed to be completely shutdown and was active only in the spleen and bone marrow.

Promoter comparison of the rodent spleen-specific promoter with the human E1 promoter (13) showed a 43 and 47% homology with rats and mice, respectively, while the rat and mouse sequences showed a higher homology (91%). Prediction of the regulatory sites present in the rodent promoters showed conservation of some of the sites but most of the human-predicted ones were not conserved. However, the binding sites of the hematopoietic GATA transcription factor family (19) predicted for the human erythroid E1 promoter (13) were present in conserved regions of the rodent promoters suggesting that these erythroid promoters might be regulated, at least in part, by mechanisms common to all three species. Nevertheless, functional analyses are needed to more precisely determine the *in vivo* regulation of both the brain- and spleen-specific ADD2 promoters.

Despite the fact that the 8–9 kb ADD2 mRNA was detected in brain about 15 years ago (7,12) and at least three attempts that were made to completely characterize the ADD2 gene structure (1,2,13), the molecular basis of this long brain-specific form remained unknown. After ruling out the presence of undetected internal exons or a long 5′-UTR in the brain isoform, we focused our attention to the 3′-UTR. We detected the presence of transcripts in the region downstream of the reported ADD2 gene, and we demonstrated that they belong to the brain-specific β-adducin mRNA, generating an 8262, 7817 and 9286 bases long mRNA for mice, rats and humans, respectively. On the contrary, the longest form containing all internal exons of the erythroid-specific transcript was 3664, 3574 and 4631 bases long for mice, rats and humans, respectively, when the A_3 polyadenylation site was used. The functionality of all of the proposed polyadenylation sites is supported by the presence of several ESTs and mRNAs containing poly(A) tails.

We present evidence that the β-adducin pre-mRNA is processed at many alternative polyadenylation sites, with the more proximal ones mainly used in erythroid tissues and the distal site in brain. In fact, in addition to the northern blot data of brain RNA (Figure 4), almost all of the EST and RNAs found in the databases that corresponded to the distal A_4 polyadenylation site were derived from brain or brain-related tissues (Supplementary Table 2). On the contrary, libraries originated from a variety of tissues including spleen and liver embryo were the source of the RNA sequences containing the other polyadenylation sites.

The UTRs of mRNAs regulate the expression of genes by modifying the mRNA stability due to the presence of elements affecting the degradation rate, the efficiency of transcription, the translation efficiency by the presence of binding sites for specific proteins and/or antisense RNAs, and the differential concentration of the corresponding proteins in different subcellular regions (26). It is striking the high degree of conservation of the brain-specific polyadenylation region (A_4) in all three species studied. We observed a 99.1% homology between mouse and rat sequences, and a 75% homology among all three species, while the complete coding region of β-adducin has 95.8% homology between rat and mouse sequences, and 86.3% among all three species (6) and the complete last exon showed 81 and 57% homology between mice and rats, and rodents and humans, respectively (Supplementary Table 1). Therefore, the highly-conserved polyadenylation configuration of mouse, rat and human β-adducin genes highlights the importance of producing tissue-specific mRNA products and suggests that the brain-specific 3′-UTR could be involved in the regulation of the function of the β-adducin gene by one or more of the mechanisms mentioned above. The AU-rich elements (AREs) are associated to the regulation of mRNA stability and translation (17) and one ARE is found 149 bases upstream of the brain-specific polyadenylation signal in a highly-conserved region of all three species, suggesting that it might play a regulatory role in the turnover and/or translation of the β-adducin mRNA in brain. However, the regulatory role of the initiation step of translation by elements at the 3′ end of eukaryotic mRNAs is still controversial (27,28).

Polyadenylation of the pre-mRNA is a process common to the majority of genes transcribed by RNA polymerase II. Three major steps in polyadenylation are (i) recognition of the authentic poly(A) site; (ii) cleavage of the pre-mRNA; and (iii) addition of up to 250 adenosine residues (29). The recognition step is determined by at least two sequences: (i) the polyadenylation signal (AAUAAA or similar) and (ii) the U-rich or GU-rich elements found downstream of the cleavage site. These two sequences are recognized by the cleavage and polyadenylation factor (CPSF) and the cleavage stimulation factor (CstF), respectively. CstF stimulates binding of CPSF to non-AAUAAA sites conferring specificity to polyadenylation site choice (30). In this respect, the poly(A) sites in mice, rats and humans meet all these basic sequence requirements.

The most frequent poly(A) signal is AATAAA that is found in 50–60% of genes (20,31,32), and polyadenylation signals differing with the canonical sequence are usually associated with alternative or tissue-specific polyadenylation (29). Although the consensus sequence for GU- and U-rich elements have been determined (29), some DSE contain no match to either the U- or GU-rich consensus motifs and large deletions are required to abolish its function. The USEs are often U-rich, supporting the idea that those sites are poorly defined and

possible redundant (29). The putative poly(A) signal for the brain mRNA form was AGTAAA was fully conserved in all three species and is found in about 3% of genes (20,31,32). In the brain-specific A_4 region, one polyadenylation site was observed in rodents and two in humans (separated by only 5 bases), while multiple sites were found in each of the A_1, A_2 and A_3 regions in all three species. The reasons for the use of a single poly(A) site in the A_4 region could reside in presence of a well-defined and highly-conserved GU-rich element downstream of the brain-specific A_4 poly(A) site. On the contrary, the GU-rich element was poorly defined in the proximal polyadenylation regions (A_1, A_2 and A_3 regions). The associated elements (U- and GU-rich elements) found in distal brain poly(A) region might be recognized by brain-specific CstF and/or other tissue-specific factors favoring the binding of CPSF, as observed with the tissue-specific tCstF-64 factor found in germ cells (33), and prevailing over the use of the proximal poly(A) sites. However, it is not clear how a distal poly(A) site might influence the use of the upstream proximal poly(A) site (30), but given the coupling between transcription and pre-mRNA processing, it is conceivable that part of the decision may occur at the promoter (29). Recent studies have shown the coupling between the transcriptional processes and pre-mRNA processing including pre-mRNA splicing and polyadenylation (34–36). An intriguing possibility is that the transcriptional complexes formed at the brain-specific promoter could direct the polyadenylation machinery to the distal polyadenylation sites, as already observed in the coupling of transcription to pre-mRNA splicing (37,38).

SUPPLEMENTARY DATA

Supplementary Data are available at NAR Online.

ACKNOWLEDGEMENTS

The authors wish to thank Emanuele Buratti for critical reading of the manuscript and to Kristian Vlahovicek for help with computer analysis. This work was supported by FIRB (contract RBNE01W9PM). Funding to pay the Open Access publication charges for this article was provided by ICGEB Institutional Funding.

Conflict of interest statement. None declared.

REFERENCES

1. Gilligan,D.M., Lozovatsky,L. and Silberfein,A. (1997) Organization of the human beta-adducin gene (ADD2). *Genomics*, **43**, 141–148.
2. Tisminetzky,S., Devescovi,G., Tripodi,G., Muro,A., Bianchi,G., Colombi,M., Moro,L., Barlati,S., Tuteja,R. and Baralle,F.E. (1995) Genomic organisation and chromosomal localisation of the gene encoding human beta adducin. *Gene*, **167**, 313–316.
3. Tripodi,G., Casari,G., Tisminetzky,S., Bianchi,G., Devescovi,G., Muro,A., Tuteja,R. and Baralle,F.E. (1995) Characterisation and chromosomal localisation of the rat alpha- and beta-adducin-encoding genes. *Gene*, **166**, 307–311.
4. Citterio,L., Azzani,T., Duga,S. and Bianchi,G. (1999) Genomic organization of the human gamma adducin gene. *Biochem. Biophys. Res. Commun.*, **266**, 110–114.
5. Gardner,K. and Bennett,V. (1987) Modulation of spectrin–actin assembly by erythrocyte adducin. *Nature*, **328**, 359–362.
6. Muro,A.F., Marro,M.L., Gajovic,S., Porro,F., Luzzatto,L. and Baralle,F.E. (2000) Mild spherocytic hereditary elliptocytosis and altered levels of alpha- and gamma-adducins in beta-adducin-deficient mice. *Blood*, **95**, 3978–3985.
7. Tripodi,G., Piscone,A., Borsani,G., Tisminetzky,S., Salardi,S., Sidoli,A., James,P., Pongor,S., Bianchi,G. and Baralle,F.E. (1991) Molecular cloning of an adducin-like protein: evidence of a polymorphism in the normotensive and hypertensive rats of the Milan strain. *Biochem. Biophys. Res. Commun.*, **177**, 939–947.
8. Gilligan,D.M., Lozovatsky,L., Gwynn,B., Brugnara,C., Mohandas,N. and Peters,L.L. (1999) Targeted disruption of the beta adducin gene (Add2) causes red blood cell spherocytosis in mice. *Proc. Natl Acad. Sci. USA*, **96**, 10717–10722.
9. Seidel,B., Zuschratter,W., Wex,H., Garner,C.C. and Gundelfinger,E.D. (1995) Spatial and sub-cellular localization of the membrane cytoskeleton-associated protein alpha-adducin in the rat brain. *Brain Res.*, **700**, 13–24.
10. Rabenstein,R.L., Addy,N.A., Caldarone,B.J., Asaka,Y., Gruenbaum,L.M., Peters,L.L., Gilligan,D.M., Fitzsimonds,R.M. and Picciotto,M.R. (2005) Impaired synaptic plasticity and learning in mice lacking beta-adducin, an actin-regulating protein. *J. Neurosci.*, **25**, 2138–2145.
11. Bennett,V., Gardner,K. and Steiner,J.P. (1988) Brain adducin: a protein kinase C substrate that may mediate site-directed assembly at the spectrin–actin junction. *J. Biol. Chem.*, **263**, 5860–5869.
12. Joshi,R., Gilligan,D.M., Otto,E., McLaughlin,T. and Bennett,V. (1991) Primary structure and domain organization of human alpha and beta adducin. *J. Cell. Biol.*, **115**, 665–675.
13. Yenerel,M.N., Sundell,I.B., Weese,J., Bulger,M. and Gilligan,D.M. (2005) Expression of adducin genes during erythropoiesis: a novel erythroid promoter for ADD2. *Exp. Hematol.*, **33**, 758–766.
14. Chomczynski,P. and Sacchi,N. (1987) Single-step method of RNA isolation by acid guanidinium thiocyanate-phenol-chloroform extraction. *Anal. Biochem.*, **162**, 156–159.
15. Sambrook,J., Fritsch,E.F. and Maniatis,T. (1989) *Molecular Cloning—A Laboratory Manual, 2nd edn*. Cold Spring Harbor Laboratory Press, NY.
16. Muro,A.F., Chauhan,A.K., Gajovic,S., Iaconcig,A., Porro,F., Stanta,G. and Baralle,F.E. (2003) Regulated splicing of the fibronectin EDA exon is essential for proper skin wound healing and normal lifespan. *J. Cell. Biol.*, **162**, 149–160.
17. Mignone,F., Gissi,C., Liuni,S. and Pesole,G. (2002) Untranslated regions of mRNAs. *Genome Biol.*, **3**, REVIEWS0004.
18. Weis,L. and Reinberg,D. (1992) Transcription by RNA polymerase II: initiator-directed formation of transcription-competent complexes. *FASEB J.*, **6**, 3300–3309.
19. Orkin,S.H. (1992) GATA-binding transcription factors in hematopoietic cells. *Blood*, **80**, 575–581.
20. Tian,B., Hu,J., Zhang,H. and Lutz,C.S. (2005) A large-scale analysis of mRNA polyadenylation of human and mouse genes. *Nucleic Acids Res.*, **33**, 201–212.
21. Gallagher,P.G. and Forget,B.G. (1998) An alternate promoter directs expression of a truncated, muscle-specific isoform of the human ankyrin 1 gene. *J. Biol. Chem.*, **273**, 1339–1348.
22. Gallagher,P.G., Tse,W.T., Scarpa,A.L., Lux,S.E. and Forget,B.G. (1997) Structure and organization of the human ankyrin-1 gene. Basis for complexity of pre-mRNA processing. *J. Biol. Chem.*, **272**, 19220–19228.
23. Parra,M.K., Gee,S.L., Koury,M.J., Mohandas,N. and Conboy,J.G. (2003) Alternative 5′ exons and differential splicing regulate expression of protein 4.1R isoforms with distinct N-termini. *Blood*, **101**, 4164–4171.
24. Gallagher,P.G. and Forget,B.G. (1995) Structure, organization, and expression of the human band 7.2b gene, a candidate gene for hereditary hydrocytosis. *J. Biol. Chem.*, **270**, 26358–26363.
25. Saffer,J.D., Jackson,S.P. and Annarella,M.B. (1991) Developmental expression of Sp1 in the mouse. *Mol. Cell. Biol.*, **11**, 2189–2199.
26. Pesole,G., Liuni,S., Grillo,G. and Saccone,C. (1997) Structural and compositional features of untranslated regions of eukaryotic mRNAs. *Gene*, **205**, 95–102.
27. Kozak,M. (2004) How strong is the case for regulation of the initiation step of translation by elements at the 3′ end of eukaryotic mRNAs? *Gene*, **343**, 41–54.
28. Wells,S.E., Hillner,P.E., Vale,R.D. and Sachs,A.B. (1998) Circularization of mRNA by eukaryotic translation initiation factors. *Mol. Cell*, **2**, 135–140.

29. Zhao,J., Hyman,L. and Moore,C. (1999) Formation of mRNA 3′ ends in eukaryotes: mechanism, regulation, and interrelationships with other steps in mRNA synthesis. *Microbiol. Mol. Biol. Rev.*, **63**, 405–445.
30. MacDonald,C.C. and Redondo,J.L. (2002) Reexamining the polyadenylation signal: were we wrong about AAUAAA? *Mol. Cell. Endocrinol.*, **190**, 1–8.
31. Graber,J.H., Cantor,C.R., Mohr,S.C. and Smith,T.F. (1999) *In silico* detection of control signals: mRNA 3′-end-processing sequences in diverse species. *Proc. Natl Acad. Sci. USA*, **96**, 14055–14060.
32. Beaudoing,E., Freier,S., Wyatt,J.R., Claverie,J.M. and Gautheret,D. (2000) Patterns of variant polyadenylation signal usage in human genes. *Genome Res.*, **10**, 1001–1010.
33. Wallace,A.M., Dass,B., Ravnik,S.E., Tonk,V., Jenkins,N.A., Gilbert,D.J., Copeland,N.G. and MacDonald,C.C. (1999) Two distinct forms of the 64,000 Mr protein of the cleavage stimulation factor are expressed in mouse male germ cells. *Proc. Natl Acad. Sci. USA*, **96**, 6763–6768.
34. Bentley,D. (1999) Coupling RNA polymerase II transcription with pre-mRNA processing. *Curr. Opin. Cell Biol.*, **11**, 347–351.
35. Hirose,Y. and Manley,J.L. (1998) RNA polymerase II is an essential mRNA polyadenylation factor. *Nature*, **395**, 93–96.
36. Proudfoot,N. and O'Sullivan,J. (2002) Polyadenylation: a tail of two complexes. *Curr. Biol.*, **12**, R855–R857.
37. Cramer,P., Caceres,J.F., Cazalla,D., Kadener,S., Muro,A.F., Baralle,F.E. and Kornblihtt,A.R. (1999) Coupling of transcription with alternative splicing: RNA pol II promoters modulate SF2/ASF and 9G8 effects on an exonic splicing enhancer. *Mol. Cell*, **4**, 251–258.
38. Cramer,P., Pesce,C.G., Baralle,F.E. and Kornblihtt,A.R. (1997) Functional association between promoter structure and transcript alternative splicing. *Proc. Natl Acad. Sci. USA*, **94**, 11456–11460.